EFFECT OF FABRIC STRUCTURE ON THE LIQUID TRANSPORT CHARACTERISTICS OF NONWOVEN WOUND DRESSINGS

NINGTAO MAO

BSc., MSc.

Submitted in accordance with the requirements for the degree of
Doctor of Philosophy

The University of Leeds
School of Textile Industries

Dec. 2000

The candidate confirms that the work submitted is his own and that appropriate credit has been given where reference has been made to the work of others

ACKNOWLEDGEMENTS

The author wishes to express his sincere gratitude and appreciation to Dr. Russell for his supervision, consistent advice and invaluable assistance in every area throughout this research.

Thanks are due to Mr. Philips for the assistance in constructing the instruments; and to Dr. Bandara and Mr. Abadi for their assistance in constructing the electronic circuits and commissioning the system; to Mr. Hampshaw, Mr. Rathod and Dr. Ahmed for the assistance in production of fabric samples.

My thanks also are given to Professor Hoyle in Electrical and Electronic Engineering Department for his helpful advice about the capacitance transducer.

The financial support of the ORS scholarship, Tetley and Lupton scholarship and the Departmental Scholarship are gratefully acknowledged.

Special thanks are due to my dear wife, Jieqing, and my lovely son, Sida, for their great support and consistent encouragement during the course of this work. Special thanks are also given to my dear sister for her help. Thanks are also given to my parents, parents-in-law and other family members and my friends for their great support.

ABSTRACT

Nonwoven materials are widely used in medical and hygiene applications, and may demonstrate significant anisotropic characteristics in liquid transport. This study investigates the anisotropic liquid transport in such structures, and establishes a relationship between the structure and anisotropic properties of liquid transport.

A comprehensive literature review is concerned with previous work on liquid transport in general with particular reference to its importance in the function of wound dressings. Preliminary experiments using commercial nonwoven wound dressing fabrics demonstrated the anisotropic nature of liquid absorption. After a review of existing steady state and dynamic methods of measuring the liquid transport in fabrics, a novel computer-integrated instrument is described that measures the in-plane liquid transmission in up to eight different directions. Needle-punched and hydroentangled fabrics with different structural parameters (fibre type, fibre diameter, fabric porosity and fibre orientation) were produced and characterised. The anisotropic liquid transport properties of these fabrics were tested using the new instrument. Unique theoretical models were established to predict the specific directional permeability of nonwoven fabrics based on the main fabric structural parameters (fibre diameter, fabric porosity and fibre orientation distribution).

TABLE OF CONTENTS

LIST OF FIGURES

LIST OF TABLES

SYMBOLS AND NOTATIONS

α ----------Fibre orientation direction (degrees)

α_k ----------the ratio of the directional permeability in the machine direction (k_{MD}) to the machine direction (k_{CD})

α_h ----------the ratio of the maximum wicking height in the machine direction to the cross direction

α_V ----------the ratio of the initial wicking rate in the machine direction to the cross direction

β ----------the angle of angular segment area in the fabric plane (degrees)

δ ----------fibre diameter (μm)

ε ----------volume fraction of solid material in a porous material

ε_1, ε_i --------dielectric constant of first or i_{th} dielectric materials

ε_0 ----------dielectric constant of a vacuum

ε_r ----------relative dielectric constant of materials

ρ ---------- fluid density (kg/m^3)

ρ_{fabric} --------- fabric density (kg/m^3)

ρ_{fibre} ---------- fibre density (kg/m^3)

ϕ ---------- characteristic angle of two dimensional fluid flow in anisotropic structures (degrees)

φ ----------contact angle (degrees)

γ ---------- surface tension of liquid (N/m)

η ---------- viscosity of liquid (N*s/m^2)

π ---------- radius constant (=3.1415926)

θ ---------- direction of fluid flow (degrees)

σ ----------fluid surface tension (N/m)

$\Omega(\alpha)$ ---------- fibre orientation distribution function

ω ----------ratio of the measured permeability in two different directions.

ω_k ----------anisotropy of permeability

ω_a ----------anisotropy of liquid absorption

$\omega(\theta)$ ----------fibre orientation distribution density function

ξ ---------- fibre orientation factor.

ψ ----------capacitance coefficient of capacitance transducer

τ ----------roughness factor

A, B, C---------constants (except in Chapter 3)

A, A_u ---------- area of the capacitance plate (m^2) (Chapter 3 only)

A_x---------- area of fabric holding fluids between capacitance plates (m^2)

C, C_0, C_1, C_2, C_u --------electrical capacitance (F)(Chapter 3 only)

a, b, b_0, b_1, b_2, b_3, b_4------fitted constants

D----------distance between two parallel capacitance plates (m)

D_1, D_2--------thickness of dielectric materials between parallel capacitance plates (m)

d_i ----------thickness of i_{th} dielectric materials between parallel capacitance plates (m)

d, d_u, d', d'' ------fabric thickness (m)

f_1, f_2 --------signal frequency in the electronic circuit (Hz)

f_p----------drag force per unit length acting on a single fibre oriented parallel to the fluid flow (N).

f_v----------drag force per unit length acting on a single fibre oriented perpendicular to the fluid flow (N)

$f(\theta)$--------drag force of fluid flow in the direction θ acting on the fibre (N).

k_0----------Kozeny constant

G_c----------gain of electronic circuit.

g---------- gravity constant (9.8 m/s^2)

h_{max}----------maximum wicking height in the vertical strip test (m)

$h_{\max}^{CD}$ ---------maximum height the liquid reaches in the Cross Direction (m)

$h_{\max}^{MD}$ --------maximum height the liquid reaches in the Machine Direction (m)

K----------permeability coefficient in Darcy's law (m/s)

k----------specific permeability (m^2)

$\vec{k}$ ----------vector of specific permeability in general Darcy's law

∇ ----------differential calculus

k_1, k_2--------two principle permeabilities in Ferrandon's equations (m^2)

$k(\theta)$ --------specific directional permeability in the direction θ in an anisotropic medium (m^2)

$k|_Z$ ---------permeability in the Z direction (which is perpendicular to the fabric plane) (m^2)

k_{0X} , k_{0Y} --- two components in the equation $\frac{1}{k(\theta)} = \frac{1}{k_{0X}} + \frac{1}{k_{0Y}}$

L---------- fluid conduit length in Darcy's law (m)

$M(t)$--------mass of the fluid absorbed by the fabric in the moment t (kg).

m----------relative dielectric constant of water (78-80)

m_v----------mass transmission of liquid absorbed in the strip test (kg).

n----------number of fibres per unit volume in the fabric

P, $P(t)$, p---hydraulic pressure (N/m^2)

P_f----------fabric porosity (%)

P_0 --------- hydraulic pressure at an initial source point in the fabric plane (N/m^2)

ΔP --------difference in hydraulic pressure (N/m^2)

Q----------volumetric flow rate ($m^3/s*m^2$).

R----------radius of advancing fluid front in two-dimensional fluid transmission (m)

R_2, R_3------electrical resistance (Ω).

R_f ---------radius of the advancing fluid front in two-dimensional fluid transmission (m)

$R_f(t)$ ------radius of the advancing fluid front in two-dimensional fluid transmission in time t (m)

R_0 ---------- radius of the fluid source point hole, or radius of the initial advancing fluid front in two-dimensional fluid transmission (m)

Re----------Reynolds number

r_0 ---------- radius of the central capacitance segment of the capacitance transducer (m)

r----------capillary radius (m)

S---------- $S = 2\ln\varepsilon - 4\varepsilon + 3 + \varepsilon^2$

s----------fabric saturation (%)

T, t----------time (s)

T---------- $T = \ln\varepsilon + \frac{1-\varepsilon^2}{1+\varepsilon^2}$ (Chapter 6 only)

V, $V(t)$------Voltage of electrical circuits (V).

v---------- volume of liquid absorbed (m^3)

V_0, V_S--------voltage of elements in the electrical circuit (V)

W---------- fabric mass per unit area (g/m^2)

X----------percentage of fibres aligned in a specific direction (%).

x---------- conduit distance (m)

$x(t)$----------liquid transmission distance in time t (m)

$x_{MD}(t)$ -----wicking height the liquid reaches in time t in the Machine Direction (m)

$x_{CD}(t)$ ------wicking height the liquid reaches in time t in the Cross Direction (m)

z----------fraction of fibres aligned perpendicular to the fabric plane (%).

CD----------Cross Direction

MD---------Machine Direction

CHAPTER 1 INTRODUCTION AND REVIEW OF LITERATURE

1.1 INTRODUCTION

Nonwoven fabrics are widely used in applications such as geotextiles, filtration, medicine and hygiene. In many applications the liquid transport and handling properties of nonwoven materials are very important. Wound dressings, for example, are required to have the ability to absorb the body liquids of the patient and the exudate from the wound to remove unnecessary substances. They are also required to maintain a high humidity under the dressing to promote wound healing[1].

Fabrics used in medicine and hygiene may be required to either distribute liquid uniformly, or to deliver liquid faster in specific directions or to impair liquid transmission completely in specific directions. For example, the ideal coverstock, incontinence pad or diaper must meet the following performance requirements[2]:

1). The rapid entry of liquid through the coverstock, i.e., a short strike-through time and minimum run-off, so as to avoid pooling.

2). The rapid dispersal of liquid in the absorbent layer, i.e., a high wicking rate, or alternatively provision for liquid to flow away from the point of entry.

3). The permeability of a coverstock to liquid would ideally be a maximum in one direction and a minimum in the other direction.

While all the above requirements are related to the general liquid transport properties of a nonwoven fabric, the third requirement implies that so-called anisotropic in-plane liquid transport in fabrics is a desirable feature.

In fact, many nonwoven fabrics demonstrate anisotropic characteristics in liquid transport. It is well-known that liquid transmission in the fabric plane may be much faster than in the transverse plane, and many experiments have demonstrated that the rate of liquid absorption in the machine direction differs greatly from the rate in the cross direction[3].

In order to obtain a systematic understanding of the requirements of wound dressings and the liquid transport in nonwoven structures, this literature review covers general areas related to the liquid handling properties of nonwoven wound dressing fabrics and aspects of liquid transport and absorption in such fabrics as follows:

1). The mechanism of wound healing and the corresponding optimum requirements of an ideal wound dressing.

2). The requirements (identified in 1) above) related to liquid transport in fabrics.

3). The application of nonwovens in various wound dressings and their specific requirements.

4). Previous studies of anisotropic liquid transport in fabrics.

Before studying the fundamental effects of fabric structure on liquid transport properties, it was considered important to establish the property requirements of wound dressings, especially with respect to mechanically bonded wound dressing structures.

1.2 REQUIREMENTS OF AN OPTIMUM WOUND DRESSING AND THE IMPORTANCE OF LIQUID TRANSPORT

1.2.1 Introduction to Wound Healing

In clinical practice, wounds are divided into two types: acute and chronic, and wound healing has two classes referred to as first and second intention. Some examples of typical wounds are given as follows[1]:

1) Donor sites, grazes and abrasions.

2) Incisions and puncture wounds.

3) Deep wounds, where there is extensive loss of sub-epidermal tissue.

4) Burns, caused by scalding, electricity, fire, chemicals or irradiation.

5) Pressure sores.

Throughout history, wounds have been dressed to assist in the healing process. The lint of the 1650s and the cotton and gauze tissue invented by Sampson Gamgee many years ago are still used today. Until the 1960s there was relatively little research and development into wound management products. However, during the decade of the 1960s, three key observations helped physicians think of dressings as pharmacological agents. Odland[4] first observed in 1958 that a blister healed faster if left unbroken. Then, in 1962 a landmark article published by Winter[5] showed that in superficial experimental wounds in pigs, (whose skin properties are thought to be the nearest to human skin), they healed more rapidly under an occlusive dressing composed of polyethylene film as compared with those exposed to air. Finally, Himan and Maibach[6] established the

beneficial effects of occlusion on the resurfacing of experimental wounds in normal volunteers in 1963. Since then, there has been extensive literature describing improved healing when superficial skin wounds are not allowed to desiccate[7]. Epithelialization has been particularly well studied[8]. Until this decade, cell migration, replication and differentiation, and the synthesis of extra cellular matrix (ECM) are common to wound healing, embryonic development and tumour growth. As a result of developments in cellular and molecular biology, the mechanisms of normal wound healing and ways in which this can be manipulated are being elucidated[9].

1.2.2 Wound Healing Under Dressings

1.2.2.1 Mechanism of Wound Healing and the Function of Wound Dressings

When a wound is exposed to air, drying of the wound surface results in the forming of a hard scab, which makes regenerating epithelial cells burrow under or through the dead tissues to a moist lower level before epidermal repair can take place. Since the drying of the wound surface extends healing times, the mechanism of moist wound healing and the use of wound dressing are extensively studied.

The 'moist wound healing' approach, advocated by Winter[5, 7] and Himan[6] using occlusive or semi-permeable occlusive dressings, has resulted in a shortening of the period of healing, and less pain and scarring if infection is well controlled. Moist wound healing allows experimentally induced wounds to resurface up to 40% faster than wounds exposed to air[10].

A proposed explanation for "moist wound healing" has been that epidermal migration is physically facilitated in moist conditions and in the absence of a crust[5, 6]. The studies of

Rovee[11] stressed that greater epidermal cell movement, rather than mitosis, is responsible for the increased rate of epithelialization of occluded wounds. Numerous other investigators have since confirmed the usefulness of various types of occlusive dressings in human non-experimental acute wounds. Barnett et al[12] concluded that split-thickness skin graft donor sites covered with a polyurethane film dressing (Op-Site or Tegaderm) healed nearly twice as fast as those covered with a fine-mesh gauze dressing. Similarly, a positive experience with a polyethylene oxide hydrogel dressing (Vigilon) was reported by Mandy[13], in his studies of wounds made during the process of hair transplantation and demarcation.

The rapid development in the methods of wound healing is attributed to advancements in biology. Recent studies (mainly *in vitro*), with the development of growth factors[9], have shown that cytokines have a role in wound healing[14, 15, 16, 17]. An attractive hypothesis to explain the faster epithelialization under occlusive dressings, (films, hydrocolliods or hydrogel dressings), is that they keep wound fluid in contact with the wound, and certain cytokines, (probably growth factors), present in the wound fluid under the film dressing are thought to modulate connective tissue formation and epidermal migration[18, 19, 20]. Peptides such as interleukin 1, epidermal growth factor, platelet-derived growth factor and transforming growth factor-beta are all likely to be present at the wound site[9]. In fact, Buchan et al[21] reported that the gross chemical and immunoglobulin composition of fluid taken from acute wounds occluded with Op-Site is quite similar to that of serum. Ono et al[22] examined the fluids after five days under a film dressing, and found that the fluids accumulated under the film contained growth factors and cytokines that are thought to promote healing. They found the fluids were

rich in TGF-alfa but contained no EGF or bFGF, which indicates that TGF-alfa plays a major part in promoting local wound healing. Nemeth et al[23] found wound fluid from graft donor sites accelerated epidermal outgrowth from split-thickness swine skin.

Other research of chronic wound healing has shown that the wound fluid present in chronic wounds has, *in vitro*, either increased fibroblast proliferation[24] or enhanced connective tissue synthesis[25]. This may explain the mechanism of occlusive dressings. Thus, according to this hypothesis, the optimum wound dressing should not absorb the exudate containing specific growth factors that are thought to help accelerate wound healing. However, the presence of large amounts of fluid under occluded wounds raises concerns about infection.

In fact, there appears to be no doubt that occluded wounds, (whether acute wounds[26] or chronic wounds[25]), accumulate a greater number of microbial organisms than do air-exposed wounds. Katz[27] found that, within six experimentally commercial occlusive dressings, including Duoderm, none of the dressings prevented clinical infection and all the dressings provided microenvironments that were conducive to the growth of resident and pathogenic bacteria. Also there was no difference in the rates of reepithelialization.

However, in acute wound healing, clinical results showed this increased bacterial colonisation does not prevent occluded wounds from healing at the same rate as[27] or faster than[10, 28] air-exposed wounds. Eaglstein[29] has even proposed that bacteria and their metabolites could conceivably stimulate epidermal migration and healing. Other workers did not find an increased frequency of celluliotis[30] or any infection[31] in occlusive wounds. In chronic wounds, the records are more reassuring. Friedman and Su[32] did not report the development of clinical infection, with the possible exception of

one in thirty one, in the treatment of leg ulcers with a hydrocolloid (Duoderm). Alper et al[33] found that clinical evidence of cellulitis developed in three patients when Op-Site was used in 18 patients with various ulcers, although almost all of the patients had obvious wound contamination with numerous bacterial species, including common pathogens. Only one of twenty-seven patients with decubitus ulcers treated with Duoderm was reported by Gores and Messner[34] to have developed a clinical infection at the wound site. Falanga[25] also found occlusion to be safe even in those chronic wounds with heavy bacterial colonisation.

Some reports showed *in vitro* the ability of a polyurethane film such as Op-Site to kill bacterial pathogens and activate complement[35]. In fact, most manufacturers of commercial wound dressings (such as Duoderm[36] and Sorbsan[36]) claim together with some studies[37], that certain dressings (e.g. Duoderm[36]), but not Op-Site[36] and Vigil[36], may prevent bacterial entry into wounds. Therefore, in chronic wounds, it is claimed that the greatest benefit of occlusive dressings is the painless debridement[38] and that hydro-active dressings facilitated wound management because of the convenience and time saving in dressing changes but did not accelerate healing compared with conventional therapy[39]. Possibly, their effectiveness in debriding wounds is due to proteolytic enzymes released by neotrophils, which have been shown to reach the ulcer surface under occlusion[25].

There are other possible explanations for the effectiveness of moist wound healing and the function of occlusive dressings. One that is often downplayed for lack of better understanding is the role of occlusion in maintaining a normal voltage gradient lateral to the wound. Human skin has measurable transcutaneous potential differences that are

decreased by wounding, and there is evidence that the maintenance of such electrical fields may be important to epidermal cell migration[40]. It has been shown[41] that *in vitro* electrical stimulation leads to an increased expression of receptors for growth factors by human dermal fibroblasts and to a subsequently greater synthesis of collagen after the addition of the growth factor. Some researchers[25] have suggested that a higher receptor number for growth factors available in wound fluid, might be a favourable effect of occlusion.

Eaglstein et al[42], after having examined the effect on epithelialization of delayed application and early removal of a polyurethane dressing (Tegaderm), indicated that from first wounding to six hours later, the application of the dressing will increase the rate of epithelialization. Moreover, keeping the dressing on the wound after the initial twenty-four hours was not necessary to enhance epithelialization.

1.2.2.2 Factors Influencing Wound Healing

Factors such as the partial pressure of oxygen (PO_2), the pH of the wound fluid, and the functioning of cells in the wound are thought to influence the rate of healing[43]. Among these factors, the importance of the permeability to oxygen in wound healing and to infection resistance is controversial[44]. Some research has concluded that high oxygen pressure is one of the key parameters that promotes wound healing and prevents wound infection[45, 46, 47], others have reported that reduced PO_2 promotes *in vitro* growth of fibroblasts and production of angiogenesis factors from tissue macrophages[48, 49, 50, 51]. In addition, epidermal cell growth *in vitro* is inhibited at oxygen pressures that exceed that of ambient air[52]. In contrast, Varghese et al[53] suggested that a low rather than a high PO_2 could enhance the healing process.

In fact, experimental results[53] have indicated that the oxygen pressure under both oxygen-permeable and oxygen-impermeable dressings were very low or zero. Wound fluid was more acidic under the impermeable hydrocolloid dressings than under an oxygen-permeable polyurethane dressing, and bacterial growth was retarded at the more acidic pH similar to that found under the hydrocolloid dressing. It was concluded that all these dressings create hypoxic conditions in which wound healing occurs whether or not they are oxygen-permeable. Traditionally, one of the greatest advantages of absorbent dressings is thought to be their permeability to air (oxygen). Viable and functioning neutrophils have been found under both polyurethane and hydrocolloid dressings with a greater percentage of viable cells under the oxygen-permeable polyurethane film[53].

Many other researchers have studied the effect of water vapour transmission in wound healing[54, 55, 56]. Lame et al[57] found that after thermal injury the evaporative water loss from the wound surface can be twenty times greater than normal skin. Queen et al[58] tested *in vitro* the permeability characteristics of a series of commercially available dressings by using a modified international standard technique[59] to assess the water vapour transmittivity and predict the build-up of wound exudate under film or the strike-through under foam. Also, the British Standard Method[60] was used to assess oxygen and carbon dioxide transmission and by adopting a gas to liquid technique[61, 62, 63], the carbon dioxide transmission rate in hydrogel dressings was assessed.

1.2.3. Types of Wound Dressing

Different wounds have different characteristics, which dictate the design of the dressing. Over many years from studies of the healing pattern of partial thickness wounds,

dressings can be separated into two main groups: (a) absorbent, physically porous dressings which allow free passage of exudate from the surface and (b) non-absorbent, water-proof dressings where the wound exudate is retained at the wound bed. Commercially, available dressings which may be of composite construction are usually classified as either occlusive or absorbent.

1.2.3.1 Occlusive Dressings

Falanga[25] defined dressings that keep a wound moist and prevent crust formation as occlusive or semi-occlusive dressings. There are four basic types of occlusive dressings available in the commercial market[25, 64]:

(i). *Films*: Are typically thin, transparent and adherent polyurethane materials that stick only to dry or non-wounded skin when placed over the wound. Films are not absorbent but allow passage of water vapour, oxygen, and carbon dioxide. Once epithelialization begins, a potential problem with films is the stripping away of newly grown skin on removal of the dressing.

(ii). *Foams*: Are generally made of non-adherent polyurethane materials that are taped in place over the wound. The amount of wound fluid absorbed by these products is relatively small.

(iii). *Hydrocolloids*: Are materials in which a water-impermeable polyurethane outer covering is separated from the wound by a hydrocolloid material whose composition varies with the particular dressing. They are opaque, gas impermeable and absorbent. Eventually, the accumulation of wound fluid causes a gradual separation of the dressing from the wound. Hydrocolloids have

proved to be unsuitable for use as a wound contact layer[25]. It is often difficult to retain liquid, resulting in leakage of odorous exudate and wound dressing gel.

(iv). *Hydrogels:* Are made of polyethylene oxide membranes or other polymers. They are always semi-transparent, non-adhesive and absorbent. Hydrogels are difficult to maintain in position without the use of secondary dressings.

Each of the basic dressing materials mentioned above has its own advantages, and composites of the basic dressing types are frequently found in commercial applications. However, occlusive dressings still have limitations.

One major problem with occlusive dressings is that they may cause a rather alarming accumulation of exudate from the wound. The problem of excess accumulation of wound fluid may be dealt with in two ways. Firstly, the fluid may be absorbed, but as previously mentioned, adherence of the dressing to the wound, infection and impaired healing may result from this approach. Secondly, excess water from wound fluid may be allowed to evaporate. Alper et al[65] advocated aspirating the fluid from under the dressing, thereby avoiding premature dressing removal. It has been clearly shown that early removal of adherent occlusive dressings can lead to stripping of the newly epithelialised surface[66]. However, dehydration leading to adherence and impaired healing may result and controlled evaporation and the maintenance of a layer of fluid at the wound surface is not easy to achieve. To overcome the build up of exudate under conventional plastic film dressings on heavily exudating wounds, a nonwoven composite dressing in which the exudate is absorbed through a perforated film into a nonwoven layer has been used[36].

Dressings containing alginates (described as semi-occlusive wound dressings), have been found to be suitable as a dressing/wound interface, and two layers of flat sheet alginate have been used as a primary dressing which forms a gel providing a moist healing environment and low adherence.

Vapour-permeable film dressings are usually used for securing a secondary dressing. However, the weight of the alginate and the absorbed exudate can pull the film away from the skin surface loosening the sealed edges.

1.2.3.2 Absorbent Dressings[67]

Although moist wound healing requires the wound dressing to have the capability to retain the wound surface at a high humidity level, the absorption of excess fluid in the form of exudate is also necessary. The removal of exudate avoids tissue sloughing, and the exotoxins or cell debris which may retard growth or extend the inflammatory phase is also removed along with the excess exudates[1]. The balance of humidity and liquid absorption is critical. Excessive wicking must be avoided to prevent drying of the wound surface.

Basic absorbent dressings based on gauze and similar textile materials are designed to dry out the wound surface. They are effective in removing blood and exudate from the wound but they are all, to a lesser or greater extent, adherent to the wound surface and may cause considerable pain on removal.

The need for absorbency in dressings is very important but it must be achieved while maintaining non-adherence. Non-adherence may be achieved by:

(a) Preventing dehydration of the exudate.

(b) Reducing absorption of fluids into the dressing.

(c) By treating the dressing surface to render it non-adherent.

Recently introduced dressings incorporate features in an attempt to meet one or more of these requirements. An early attempt to produce a non-adherent dressing involved impregnating gauze with paraffin cream, polyethylene glycol or aluminium stearate, but this was not entirely successful. Other commercially available dressings are composed of an absorbent pad covered with a perforated plastic film that is designed to lie in contact with the wound surface. The plastic film is intended to reduce the amount of absorbed exudate and thus to leave a moist gel at the wound surface. However, these dressings can adhere to the wound surface due to columns of exudate drying in the pores of the film. Subsequently, damage is caused to the healing wound when the dressing is removed[68].

To overcome such problems (associated with traditional dry absorbent-dressings) and to avoid the disadvantages of occlusive dressings, composite dressings have been developed. A new composite dressing has been reported, consisting of a net wound contact layer that allows exudate to pass freely into the absorbent layer but separates the absorbent layer from the wound surface[69].

An absorbent dressing made from polyurethane foam has been developed using the standard wound model[70]. The foam dressings, still widely used in wound care at the present time, have been found to be non-adherent and produce an accelerated rate of healing[70]. This dressing presents both an absorbent layer to the exudate and a smooth surface from which particles will not be shed into the wound. The reduced rate of drying

of the wound surface leads to the formation of a gel of exudate at the wound surface. Migrating epidermis cells were observed to pass through this gel and not through the dermis, which is somewhat similar to the pattern of healing seen under occlusive dressings where no absorption of exudate occurs[70].

Nowadays, there is increasing interest in exploiting other natural biocompatible materials in wound dressings because of the disadvantage of traditional gauze.

1.2.4 The Optimum Wound Dressing

The design features of an optimum wound dressing will vary with the particular wound type but there are certain general performance requirements if the healing rate is to be clinically acceptable. The functions of a wound dressing were first summarised by surgeon Abraham Rees in 1819. The requirements of a dressing were stated as[71]:

1). To stop blood in fresh wounds.

2) To agglutinate and heal wounds

3) To dry wounds and forward the formation of a cicatrix.

4) To keep the tops of wounds at a proper distance so that they do not hastily unite before the bottom is well digested and healed.

5) To prevent the access of air.

Thereafter, the optimum relationship between healing and the design of wound management products has been sought.

In 1972, Winter[7] defined the desirable properties of a wound dressing. Turner[72] also identified the performance characteristics of an ideal wound dressing in 1979 as "those

factors which will produce a microenvironment associated with the wound that will allow healing to proceed at the maximum possible rate commensurate with the age and physiological condition of the patient". In summary, Turner[1, 73] proposed the optimum dressing should:

1) Remove excess exudate and toxic components.

2) Maintain a high humidity at the wound/dressing interface.

3) Allow gaseous exchange.

4) Provide thermal insulation.

5) Be impermeable to micro-organisms.

6) Be free from particulate and toxic wound contaminants.

7) Be removable without causing trauma during dressing changes.

Other researchers have also stated similar general requirements for an optimum dressing[8, 67, 74]. In 1995, Whitby[8] proposed a more systemic list of requirements based on the biology of wound healing as follows:

* To permit gaseous exchange. To maintain PO_2 and pH at appropriate levels.

* To maintain high humidity in the wound (epithelialization proceeds more rapidly in a moist environment).

* To maintain wound temperature close to body core temperature, allowing mitosis and phagocytosis to proceed at optimal levels.

* To aid removal of dead tissue and bacterial, chemical and physical contaminants (excess wound exudate containing cellular debris increases the risk of bacterial infection, and the presence of foreign material prolongs the inflammatory phase).

* To be impermeable to bacteria.

* To be non-adherent, non-allergenic and free from contaminants (adherent dressings that damage new epithelium when they are changed, and toxic and particulate contaminants in the dressing, may prolong the inflammatory phase).

Among the requirements of an optimum wound dressing, the following requirements are influenced by the liquid transport properties of the fabric:

Maintenance of a high humidity in the wound.

Non-adherent, non-allergenic and free from contaminants.

Aid removal of dead tissue and bacteria, chemical and physical contaminants.

Comfort.

Maintenance of wound temperature close to body core temperature.

According to the requirements of optimum wound healing mentioned above, the physical properties of nonwoven fabrics, such as thermal insulation, wettability, liquid transfer and liquid retention, water vapour transfer, and absorption of serum album by fabric and fibres, have a significant influence on wound healing, since these parameters will either affect wound healing or the adherence of the fabric to the wound. Some of the main performance requirements depend on the structure of the fabric and the associated liquid transmission properties.

Absorption of exudate by the dressing is designed to aid the removal of dead tissue bacteria, as well as chemical and physical contaminants so as to prevent wound infection and to prevent the presence of foreign material prolonging the inflammatory phase.

The structure of the fabric will clearly influence the liquid uptake and transport characteristics of the fabric which will in turn have a significant influence on the moisture in the wound and on exudate removal.

1.3 APPLICATION OF NONWOVENS IN WOUND DRESSINGS

1.3.1 Nonwoven Wound Dressing Materials

Nonwovens have specific advantages when used in wound dressing applications. The structure of some nonwoven materials has been likened to the structure of collagen, nonwovens are claimed to have controllable exudate absorbing ability, free from chemical detergents and have ideal thermal insulation[3]. Dressings comprising an absorbent pad covered with nonwoven materials have been widely used[36]. A large number of commercial wound dressing products and patents have appeared that combine nonwoven structures and incorporate materials such as chitin, chitosan, alginate, collagen fibre and superabsorbent fibres[75, 76, 77, 78, 79]. Some articles have described wound dressings containing nonwovens[80] that are designed for absorbing and retaining wound fluids in which an absorbent material has a fluid transfer component.

Some examples of developmental or commercial absorbent and occlusive wound dressings are described in Tables 1.1 and 1.2 respectively. The lists are by no means exhaustive.

Table 1. 1 Example of absorbent nonwoven wound dressings[36, 81, 82]

Name of Manufacturer	Additional Drugs Delivered/ Incorporated	Fibre	Structural Characteristics and Properties
BTTG[83].		Micro-fungus, chitin, chitosan	Microfungal material containing chitin and chitosan. It is claimed that the potential wound healing of micro-fungus is due to the high content of chitin and chitosan in the fungal cell walls[84].
Nova-Sorb Ltd[85]	Therapeutic agents.		Intelligent wound dressing produced by a versatile branched pore-forming technique (VBPT) in which highly absorbent areas take up wound exudate and these are interlaced with low-absorbing sites that release therapeutic agents.
US Patent 5,470,576[86]	Bactericides, fungicide		Exhibit desirable haemostatic properties and are soft, highly pliant and cost-effective to manufacture. The nonwoven absorbent pad is impregnated with 5% (by weight) of calcium alginate or a mixture of calcium and sodium alginate.
US Patent US patent 5,520,925[87]			Contains gently hydrolysing native, insoluble collagen that leaves its fibrillar structure intact to give a substance that is excellent for producing films for use in dressing materials.
US patent 5,465,735[88]			Has a structure that aids healing by inter-changing the position of the low and high density material layers in a multiple-layer absorbent wound dressing.
US patent 5,529,784[89]	Tea tree oil in a gel solution		A multiple-layer nonwoven fabric containing tea tree oil which reduces heat around the wound and provides bacteria-static properties to promote healing and debridement of the wound
Lantor inc. of Veenendaal, Netherlands[76]	Antiseptic agents		A hypoallergenic nonwoven structure that is safe in contact with wounds, abrasion resistant, highly absorbent, and has low moisture retention to reduce skin maceration

Kendall Co.[75]			Comprises of a lower layer of low density absorbent fabric with high absorbency, and an upper layer of high density and a high wicking ability. These two layers are placed between a permeable, non-adherent, bacteria barrier and a lower perforated sheet.
Hypafix (Smith & Nephew)		Polyester	Apertured, nonwoven fabric coated with a layer of an acrylic adhesive.
Kaltostat, Kaltoclude (BritCair)		Sodium:Calcium alginate (20:80)	Nonwoven in which sodium alginate rapidly forms a hydrogel.
MEFIX (Molnlycke)		Polyester nonwoven	Apertured, nonwoven fabric coated with a layer of an acrylic adhesive.
Sorbsan		Calcium alginate	Nonwoven fabrics
Scherisorb (Smith & Nephew)		2% modified Co-polymer (derived from corn starch) with propylene glycol	Hydrogel, for leg and decubitus ulcers, extravasation injuries, especially for dry slough and necrotic wounds.
TELFA (Kendall)		Cotton and Poly(ethylene terephthalate) film	Cotton nonwoven enclosed in the sleeve of a film, for dry sutured wounds, superficial cuts, abrasions and other lightly exuding wounds.

Table 1. 2 Example of occlusive dressings

Name of Manufacture	Additional Drugs Delivered/ Incorporated	Fibre	Structural Characteristics and Properties
BioFILM	Gelatine, pectin		Polyester nonwoven layer with film
Pharma-Plast[77]		Polyurethane film	Within the Polyurethane film is a soluble, controlled-release polymer that contains silver compounds
Seton Healthcare[76] Lyofoam		Hydrophobic polyurethane foam	Gas permeable, but resistant to the penertration of wound exudates
Melolin			Dressing perforated film absorbent. Film of Poly(ethyleneterephthalate) with cellulose nonwoven
Opsite		Polyurethane membrane	
Tegaderm		Polyurethane Membrane	

1.3.2 Trends in Wound Dressing Technology

With the rapid progress in the purification and cloning of numerous growth factors and the expanding understanding of matrix proteins that promote epidermal migration and growth, we have a better understanding of the pathophysiology of diseases and of wound healing. New directions for the design of improved wound care and wound dressing materials are now emerging.

Falanga[25] has predicted the development of the 'growth dressing' that combines occlusion with the timed or pulsed delivery of specific growth factors designed to help a specific clinical problem. He proposed the use of occlusion with an angiogenic growth factor to stimulate granulation tissue and then subsequently the use of an occlusive dressing that will deliver various growth factors to speed up epithelialization

The application of growth factors in a gauze or beneath a watertight film or film chamber has also been proposed[9]. Vehicles include the use of cream such as silver sulphadiazine that releases Growth Factor (GF) slowly for at least twelve hours when applied to wounds[9]. Pluronic acid is a liquid at room temperature that becomes a gel at body temperature, and is being evaluated together with collagen gels that dissolve over time and release growth factors. Other techniques include lipid microencapsulation of growth factors in hydrocolloid dressings such as Duoderm® or Comfeel®, and incorporation of growth factors in a polymer matrix[9]. So far, no vehicles have been reported to be totally successful.

Products that incorporate well with Growth Factors and release Growth Factors slowly, which do not jeopardise the microenvironment at the wound surface are expected to become the wound dressings of the future[9].

1.4 NONWOVEN FABRIC STRUCTURES AND LIQUID TRANSPORT

1.4.1 Mechanically Bonded Nonwoven Structures

Mechanically bonded nonwoven fabrics (e.g. needlepunched and hydroentangled) are widely used in wound-care applications. It is well known that the properties of such nonwoven fabrics depend on their structure. The structure is governed by the way in which the fibres are arranged and the properties of these component fibres[90, 91, 92, 93]. Krcma[94] identifies four major structural parameters dominating the structure of nonwoven fabrics:

1) Constituent fibre properties (fibre dimensions, physical and chemical properties).

2) Geometrical fibre alignment (i.e., fibre orientation).

3) Contact points between fibres in the fabric.

4) Porosity of the fabric.

Therefore, from a fundamental standpoint, the liquid transport and uptake characteristics of nonwoven fabrics may be expected to rely on the above four parameters. The importance of fibre properties are well understood and have been described in many authoritive sources[95].

The basic geometrical arrangement of fibres in nonwoven fabrics is partly determined by the structure of the original fibre web which may be considered as a three-dimensional system. Fabric geometry is also influenced by the manufacturing process and the main factors can be summarised as follows[94]:

1) The nature of the fibre material.

2) The method of assembling the web of fibre, i.e. web formation.

3) The method of bonding the web.

4) The chemical or mechanical finishing processes used (if any).

With respect to mechanically bonded fabrics, there are no chemical substances present in the structure which may stimulate an allergenic reaction when used as a wound dressing (assuming fibre finish is removed). One of the geometrical parameters of a nonwoven fabric is the fibre orientation distribution.

1.4.1.1 The Fibre Orientation Distribution (FOD)

The fibre orientation distribution defines the relative positions of individual fibres in the structure of a fibre web or fabric. The following general relationship is proposed for the distribution of fibre orientations in a web or fabric[90]:

$$\int_{-\frac{\pi}{2}}^{\frac{\pi}{2}} \Omega(\alpha) d\alpha = 1 \qquad (1.1)$$

Where α is the fibre orientation angle, and $\Omega(\alpha)$ is the fibre orientation distribution function in the examined area. The numerical value of the orientation distribution indicates the number of observations that fall in the direction α which is the angle relative to the examined area[92].

It has been shown by many researchers that the FOD influences the physical behaviour of the fabric. Backer and Petterson[92] pioneered a fibre network theory for estimating the tensile properties of a nonwoven fabric based on the fibre orientation, fibre tensile properties and the assumption that fibre segments between bonds were straight. Hearle and Stevenson[90, 91] expanded this theory by taking account of the effects of fibre curl. They indicated that the stress-strain properties of a nonwoven fabric were dictated by the orientation distribution of fibre segments. Later, Hearle and Ozsanlav[96] developed a further theoretical model to incorporate binder deformation into the model. The FOD is an essential parameter in constructing these models. However, little research has been reported on the importance of the FOD on the liquid transport of nonwovens.

1.4.1.2 Porosity, Pore Size Distribution (PSD) and Porosimetry

Both the liquid absorption and liquid transmission of fabrics has been found to be influenced by fabric porosity and pore connectivity. A considerable body of work has been conducted in the area of porosimetry.

The structural variables obtained in porosimetry that define the pore structure of a nonwoven fabric include the pore size, pore size distribution, pore connectivity and the total pore volume. Porosity provides information on the overall pore volume of a porous material. Pore connectivity, which is the geometric pathway in which the pores are inter-related, cannot be easily quantified and described. If the total pore area responsible for liquid transport across any distance along the direction of liquid movement is known, its magnitude and change in magnitude are believed to indicate the combined characteristics of the pore structure and connectivity.

The pore spaces between packed fibres may be calculated. The calculations are based on simplified models of the fabric structure and have been developed in an attempt to explain capillary liquid transport in porous media. Wrotnowski[97] proposed a simple pore size prediction model based on the assumption that the fibres are of circular cross-sectional pattern. This assumption permits a geometric calculation that gives an equation for the circular pore size.

Lambard[98] and Faur[99] applied Poissonian line network theory to establish a theoretical model of the "opening sizing" of nonwoven fabrics. In this model, the fabric thickness is assumed to consist of randomly stacked elementary layers, each layer has a thickness T_e and is simulated by two dimensional straight lines, (a Poissonian line network).

The mass transport data from the simultaneous wetting and wicking test method reported earlier[100] have been used to generate information about the pores in the fabric responsible for liquid transport along direction of wicking. Hsieh[101, 102, 103] conducted a series of experiments to illustrate the use of liquid mass transfer data to quantify the pore area responsible for actual liquid movement, and attempted to probe the significance of fibre properties in determining the liquid wetting and transport properties of fabrics. It is claimed that the pore area profiles generated from the mass transport data provides valuable quantitative data on actual liquid transport at a specific distance from the liquid source. It was found that the pore structure of fibrous materials depends on the fibre type and methods of fabric assembly. Fibre width, length and shape, as well as fibre alignment were believed to influence the quality of the capillary channels. The pore size and the pore size distributions will be determined by the manner in which fibres are assembled into fabric during the manufacturing process.

1.4.2 Liquid Transport Properties in Nonwovens Related to Wound Dressings

1.4.2.1 Liquid Transport and Permeability

Liquid transport is particularly important in wound dressing fabrics. Darcy's law[104] introduces the specific permeability, which depends only on the structure of the porous material, and characterises the liquid flow through the material.

Numerous theoretical models describing the laminar flow through porous media have been proposed to predict the permeability. The two most common models that are thought to be suitable for fibrous porous media are the capillary channel theory and the drag force theory. In models based on the capillary channel theory, the hydraulic radius

models based on the work of Kozeny[105] and Carman[106] treat the flow through a porous medium as a conduit flow. Other modified capillary channel models are also proposed [107, 108, 109]. In Drag force theory, the particles (or fibres) in the porous structure are treated as obstacles to the fluid flow[108], and various permeability equations of this type are demonstrated by Iberall[110], Happel[111] and others[112, 113, 114].

Many methods of measuring the permeability of fabrics have been proposed. Nguyen and Durse[115] used the syphon test to determine the planar permeability of fibre webs. Also the relationship between permeability and saturation was later determined using a semi-empirical relationship, which Gillespie[116] used to find the permeability function for filter paper. After comparing the results of the capillary pressure head as a function of saturation using the column test and the permeability as a function of saturation using the syphon test, in both cotton and polypropylene woven fabrics, Ghali et al[117] suggested a new method using a transient measurement technique to determine the permeability which works well for both samples.

Shen[118] derived a model showing that the water permeability in needle punched nonwoven fabrics is proportional to the square of the fibre diameter and is a function of fabric porosity. After comparing the derived model and other models based on drag force theory, cell theory and empirical equations, he found that the newly derived equation and Happels' model[111] gave the closest agreement with experimental data.

To isolate the effect of assembly structure, the water transport behaviour of single fibres and fibre bundles consisting of a few fibres was investigated by Hiruku and Yoichiro[119]. They measured the water transport along textile fibres by an electrical capacitance technique, which is claimed to have potentially high sensitivity[120, 121].

Some workers have studied the in-plane permeability of fabrics[122, 123, 124]. Adams and Rebenfeld[124] developed a method to quantify the directional specific permeability of anisotropic fabrics using an image analysis apparatus that allowed flow visualisation. Montgomery[125] studied the directional in-plane permeability of geotextiles and gave methods of obtaining the maximum and minimum principal specific permeabilities and the resulting degree of anisotropy in geotextiles. However, this method is very complex.

Sluys and Diericky[126] indicated that all the theoretical models describing laminar flow show little correspondence with experimental data obtained for nonwoven geotextiles. They suggested that the water permeability characteristics of geotextiles should be expressed as a discharge rate at a certain hydraulic loss[127].

1.4.2.2 Wettability and Wickability

To distinguish the terms wettability and wickability, Harnett and Mehta[128] defined wettability as the initial behaviour of the fabric, yarn, or fibre when brought into contact with liquid. They also stated that both wetting and wicking could be described by a single process, i.e., liquid flow in response to capillary pressure. Therefore, the liquid transport related to these processes can be described mathematically by Darcy's Law[104].

According to Kissa[129], the wettability of a fibre refers to its ability to be wetted by liquid. Wetting of a fibre involves the displacement of a solid-air (vapour) interface with a solid-liquid interface. Thus, the wettability of fibres depends on the chemical nature of the fibre surface and the fibre geometry[130], especially surface roughness[131].

The wettability of a fibre is determined by the fibre-liquid contact angles[132], and it is usually evaluated by wetting force measurement using the Wilhelmy technique[133, 134]

and other methods[135, 136, 137, 138]. Wetting of fibrous assemblies is a complex process, involving various wetting mechanisms, such as spreading, immersion, adhesion, and capillary penetration, which may operate simultaneously[139]. Since wetting is determined by the fibre-liquid contact angles, previous research work has been undertaken to measure fibre-liquid and fabric-liquid contact angles, but the difficulty is always to obtain reliable measurements[140].

In 1974, Bruil and Van Aartsen[141] attempted to develop a method of measuring the angle of contact on porous media based on Washburn's Equation[142]. They measured the time taken by benzene, n-hexane, toluene, n-heptane, chloroform, acetone, dimethyl formamide, ethanol, methanol, water and aqueous sodium dodecyl, and sulphate solutions to advance through powdered aluminium, graphite, polyethylene, terephthalate and nylon 11. Many of the angles they obtained were zero and a criticism of their work was that the experimental error was very large[143].

Hsieh and Yu [100] concluded that the wettability of any fabric containing a single fibre type is the same as its constituent single fibres. Additionally, they found that the intrinsic wettability of fabrics depends on the chemical composition of the polymeric materials and that liquid retention is governed by the pore structure as well as the properties of the substrate.

After measuring the advancing and receding angles of contact between water and yarns of polyethylene, nylon6.6, polyester, and the angles between water and the individual fibres by using the vertical rod method, Hollies et al[144] found that all the advancing angles of contact were about the same (83^0) while for the yarns the angles of contact were different (varying between 25^0~108^0). However, they found that the contact angles

with woollen yarns were lower than the corresponding angles of contact for single wool fibres. As a result, they concluded that the movement of water through the yarn is directly related to the contact angle of water with the yarns and not the contact angle of water with the fibres constituting the yarn.

Wicking is a particular mechanism of liquid transport in fabrics and wickability is defined as the ability to sustain capillary flow[128]. Wicking is the spontaneous flow of liquid in a porous substrate driven by capillary forces which is governed by the Laplace equation[130]. Fibre wettability is prerequisite for the occurrence of wicking.

Capillary penetration of a liquid might occur from an infinite (unlimited) or limited (finite) reservoir. Wicking processes from an infinite reservoir include immersion absorption, trans-planar wicking, and longitudinal wicking. Wicking from a limited reservoir is exemplified by a liquid drop placed onto the fabric surface. McLaughlin et al[145] studied immersion absorption in textile processing. Wicking processes can be divided into four categories[129]:

(i). Pure wicking of a liquid without diffusion into the fibre surface.

(ii). Wicking accompanied by diffusion of the liquid into the fibres or into a finish on the fibre.

(iii). Wicking accompanied by adsorption by fibres.

(iv). Wicking involving adsorption and diffusion into fibres.

From a consideration of the laws of hydrodynamic flow through capillary channels, Poiseuille[146] first deduced the relation between the volume flowing through a narrow tube and the difference in pressure across its ends. Based on Poiseuille's equation,

Lucas[147] and Washburn[142] calculated the distance along which turbulence occurs and, by converting the volume-flow in Poiseuille's Equation into linear-flow in uniform cylindrical tubes, they developed the Lucas-Washburn's Equation[142]. Many authors[141], [148, 149, 150] have shown that the flow of liquids through porous structures obeys the Lucas-Washburn Equation. This equation accurately characterises the water penetration in paper materials[151]. Similar analyses have been successful in studies of soil[152] and leather[153]. Lord [154] also considered the theoretical capillary flow in a fibrous assembly to consist of a number of parallel capillaries.

However in reality, the structure of porous media, such as textile fabrics and nonwovens, markedly differ from the simplified model of uniform cylindrical capillary tubes. The Lucas-Washburn equation may be criticised because, arguably it incorrectly assumes a constant advancing contact angle θ_A for the moving meniscus[155, 156]. Also, the equation does not take into account the inertia of the flow[157], and implies that at time 0 and l=0, the flow rate is infinite. Despite these limitations, a variety of liquids have been shown to obey the Lucas-Washburn wicking kinetics[158].

For absorbent fibres, it is believed that the spontaneous flow of liquid within capillary spaces is accompanied by a simultaneous diffusion of the liquid into the interior of the fibre or a film on the fibre surface[159]. The sorption of the liquid into fibres can cause fibre swelling[160, 161, 162], thereby reducing the capillary spaces between fibres, and complicating the kinetics[139].

When the liquid contains surfactants, diffusivity and adsorption of the surfactant on the fibre surface will affect the wicking flow[158]. It has been observed that the wicking rate is

proportional to the effective surface tension at the liquid front, if the fibres are completely wetted by the surfactant solution[158].

After simultaneous measurement of the liquid wetting and retention characteristics in woven fabrics, Hollies et al[144] reported that the rate at which water is transported through yarns by capillary forces is determined by the fibre crimp, fibre denier, yarn size and blend uniformity. They found that water moved more rapidly through fabrics composed of highly hydrophobic synthetic fibres than through all-wool fabrics even though wool is very hydrophilic in nature. This observation was explained by the differences in yarn structure rather than the chemical nature of the fibre surfaces. They also reported[148] that the speed of the water travels in the capillaries could be changed by altering the nature of the fabric structure, and they showed that the transport of water through the yarns obeys Washburn's equation.

Miller et al[132] found changes in liquid/water uptake for fabrics treated with durable press resin or with hydrophobic or hydrophilic polymer. Mamiko[163, 164] reported that the water absorbency of fabrics soiled with various substances, such as oil and proteins, varies depending on the fibres and the composition and amount of soil. Mamiko[165] also studied the correlation between wettability and water absorbency in soiled cellulose and polyester fabrics and found a good relationship between the amount of oil on the soiled surface and the liquid water uptake of the fabrics. However, he did not consider the differences between the real geometric structure of the fabric and the assumed plain surfaces of the fabric.

In 1934, Peek et al[151] studied the movement of organic liquids along filter paper. They converted Poiseuille's equation into linear flow and, like Washburn, inserted the

capillary and gravitational terms to obtain a generalised equation for the fluid flow through porous media. By observing the transport of various liquids along a strip of filter paper, the results demonstrated that Washburn's equation did describe the flow of the liquid through the paper. However, it seems likely that whatever the distribution of the capillary channel sizes, the distribution itself will be reasonably constant for paper from a single batch.

Choi et al[166] studied the oil absorbency of needled cotton nonwovens and found that the oil sorption of cotton fibre was controlled by adsorption on the fibre surface and capillary action through the lumen. In contrast, the main mechanism in polypropylene was through capillary bridges formed between fibres. It was also found that the sorption decreased as the needling density increased.

There have been few systematic studies reported in the literature that elucidate the absorption mechanism of blood and other bodily fluids such as serum. Choksi and *et al* [167] compared the differences between water and blood absorption in spun-laced nonwovens. The expected linearity of the liquid volume absorbed versus time was observed with water while some deviation from this linearity and a generally lower absorption rate was observed when blood was used as the test fluid.

1.4.2.3 Liquid Absorption as Unsteady State Flow

Liquid absorption can be studied as a steady state fluid flow in porous media (as mentioned above), although in many practical situations the liquid is in fact an unsteady state flow where the porous medium is not uniformly and completely saturated. There is

usually a saturation gradient in the medium along the direction of flow and this saturation gradient changes with time as the absorption process continues.

Many quantitative observations of the saturation gradients have been made in studies of capillary liquid transport in filter papers, soil physics and water resources[130]. By combining the law of conservation of mass and the differential form of Darcy's law, a one-dimensional general equation for the saturation rate has been derived[168, 169]:

$$\frac{\partial s}{\partial t} = \frac{\partial}{\partial t}\left[F(s)\frac{\partial s}{\partial x} \right] \qquad (1.2)$$

In this equation the diffusivity factor $F(s)$ is related to the specific permeability k via $F(s) = (k/\eta)(dp/ds)/\phi$ [130]. Where s (%) is fabric saturation, t (seconds) is time, x (mm) is the liquid conduit distance, p (N/m^2) is the hydraulic pressure, and η (N*s/m^2) is the viscosity of the liquid.

Many researchers[168, 169, 130] have studied the constant diffusivity coefficient in the one-dimensional strip test. Semi-infinite boundary and other boundary conditions for one-dimensional diffusivity are also discussed in the literature[170, 171, 172]. Provided s_v is saturation at the visually observed advancing front and x_v is the visually observed advancing distance, and t is time, Rudd[168] pointed out that $\frac{x_v}{\sqrt{t}}$ is a constant and is related to s_v. This agrees qualitatively with the Washburn equation[142] with respect to the proportionality between the wicking distance and $\sqrt{t}$.

For two- and three dimensional radial transport, the radial advancement of the liquid front of saturation will vary in proportion to the square root of the wicking time[130], and

the volumetric absorption rate $\frac{dv}{dt}$ will be proportional to $t^{\frac{n}{2}-1}$ [130]. It is also known that in both two- and three- dimensional flows the rates of liquid absorption decrease with time and reach a constant value[130].

1.5 SUMMARY AND THE OBJECTIVES OF THE PRESENT RESEARCH

The main points from the literature review can be summarised as follows.

(i) The optimum conditions for wound healing are a "moist wound healing environment " which can be achieved by suitably designed wound dressings.

(ii) Further studies of liquid transport in fabrics are required for the proper design of wound dressings to control the liquid flow within the fabric structure.

(iii) The specific permeability of a fabric depends only on the porous structure and is used to characterize the liquid flow through porous media such as nonwovens. Models of permeability have been previously established, but none have been introduced to model the specific permeability of nonwoven fabric structures.

(iv) Wicking is a specific type of liquid transport which is driven by capillary pressure. Wettability is a prerequisite for wicking to occur. It can be described by Darcy's law[104] and the Washburn's equation[142].

(v) An understanding of the relationship between anisotropic liquid transport and the fabric structure is essential to enable improved design of nonwoven structures for use as wound dressings. At present, there is a paucity of work in this area.

Although previous studies have been reported on the liquid transport properties of nonwoven fabrics, most of the results have not elucidated the dynamic absorption behaviour and the anisotropy of liquid absorption, both of which are believed to be directly linked with fabric structure.

In order to improve our understanding of the liquid transport in nonwovens, the objectives of this study may be listed as follows (with particular reference to wound dressings):

1) To identify the structural parameters that influence the liquid uptake in nonwoven fabrics and in particular to establish the importance of fibre orientation on the liquid transport behaviour.
2) To establish a suitable method of measuring the anisotropy of liquid transport in nonwoven fabrics.
3) To establish the relationship between the anisotropy of liquid transport in nonwovens and the structural parameters of the fabric.

CHAPTER 2 PRELIMINARY STUDIES: LIQUID TRANSPORT IN NONWOVEN WOUND DRESSING FABRICS

2.1 INTRODUCTION

As indicated in Chapter 1, section 1.4.2.2, liquid absorption in fibrous structures such as nonwovens is believed to be driven by capillary pressure[130]. In general, the wicking behaviour of a nonwoven fabric depends on the structural architecture of the material which is defined in terms of the pore size, pore size distribution, the shape of the pore, fabric porosity, the chemical constituents of the fabric surface and the surface morphology of the fabric. Also important are the bulk properties of the liquid (e.g., viscosity, surface tension and the wetting angle).

In nonwovens, the absorbency in the fabric plane is widely recognised to be highly directional. Anisotropic liquid absorption in the fabric plane is also frequently observed in paper. The capillary penetration in the machine direction of paper is typically 5-15% higher than in the cross-direction[3].

In this chapter, the basic liquid absorption characteristics of commercial nonwoven wound dressing fabrics is investigated using the standard strip test. This method is frequently used by the commercial manufacturers of wound dressings[173]. An evaluation of the anisotropy of liquid absorption in such fabrics is also presented using Darcy's law.

2.2 THE VERTICAL AND HORIZONTAL STRIP TEST

Numerous tests have been used to characterise the liquid absorbency properties of fabrics. The strip test involves suspending a strip of fabric, vertically or horizontally, with one end dipped in a reservoir of liquid. Either the time for the liquid to reach a certain level or the height of the advancing liquid front as a function of time is recorded[174].

Most nonwoven fabrics used in wound care have high porosity and they also tend to have a high initial absorption rate. Thus, the time for the liquid to reach a certain level by visual judgement is a comparatively simple approach and was adopted here. In this method, the distance that the liquid travels in the porous medium is recorded by visual judgement at predetermined time intervals. It is believed to have a relatively high degree of reproducibility and enables the characterisation of the wicking behaviour of porous media. The Vertical Strip test is described by EDANA[175] (method 10.0-72 part C), BS3424 method 21[176] (Determination of resistance to wicking) and the amended Tappi RC-8 method[177]. The rate of absorption is determined by the height of the fluid head rising in the fabric per unit time. There is no standard for the Horizontal Strip test.

Although distilled water is normally used in the strip test, some researchers[178, 179] have reported the addition of a low percentage (0.05-0.2%) of acid dye in order to permit a clearer indication of the wicking distance from the source. However, Lichstein[179] criticised this method because the dye may not necessarily transport at the same rate as the actual advancing water front. Therefore, distilled water is used in all the experiments of liquid transport in this chapter and thereafter.

It should be noted that the strip test is based on the wicking behaviour of fabrics, but wicking may not occur if the contact angle between the fibre and the liquid is more than 90 degrees[130]. In practice, the surface tension of fibres influences this contact angle and is affected by the chemical composition of the fibre and the finish applied.

2.3. MODELS OF LIQUID ABSORPTION IN NONWOVEN FABRICS DURING THE STRIP TEST

In the vertical strip test, the height of the fluid front in the strip will gradually reach an equilibrium when the capillary pressure, which drives the liquid upwards, is balanced by the mass of water absorbed in the sample. In the horizontal strip test, if the supply of water is unlimited, the rate of liquid penetration into the fabric will gradually become constant.

2.3.1 Theoretical Models of Liquid Absorption in Nonwoven Fabrics

Numerous attempts have been made to elucidate the intricate mechanism of liquid absorption in porous media. Two major theories thought to be appropriate for modelling the liquid absorption in the strip test are the classical hydrodynamic model (the capillary flow model or the Washburn's equation) and the steady state flow model (Darcy's law).

The theory of unsteady state flow (the diffusion analogy) is also available for modelling liquid transport in fabrics, however it depends on complex mathematical methods and assumptions that are difficult to verify in real nonwoven fabrics. Although a method based on the unsteady state flow theory of measuring the liquid density in fabrics has

been previously used for woven fabrics, the apparent unevenness and non-uniformity of nonwoven fabric density makes the method unsuitable for nonwoven materials.

2.3.1.1 The Hydrodynamic Model

This classical approach has long been applied to porous media such as powder[141] and textile materials[148, 149].

2.3.1.1.1 The horizontal strip test

In the hydrodynamic model, the liquid sorption mechanism of a fabric is interpreted as a flow through a system of capillary channels. Poiseuille's equation is concerned with the rate of flow in a tube in laminar, non-turbulent flow conditions and is expressed as follows[149].

$$Q = \frac{dv}{dt} = \frac{\pi r^4}{8\eta}\frac{\Delta p}{x} \qquad (2.1)$$

Where Q = volumetric flow rate [m^3/s],

v = volume of liquid absorbed [m^3],

t = wicking time [s],

r = capillary radius [μ m],

η = viscosity of liquid [Ns/m^2],

x = wicking distance [m],

Δp = the driving force of the fluid flow.

For liquid to transport into the fabric, the driving force, Δp (the capillary pressure), arising from the intrinsic liquid attraction capacity of the fabric itself[130], is described by the Laplace equation[130] as follows:

$$p = \frac{2\gamma \cos\varphi}{r} \qquad (2.2)$$

Where p = pressure drop [N/m^2],

γ = surface tension of liquid [N/m],

r = capillary radius [μ m],

φ = contact angle [degrees]

Washburn's equation[142] assumes that the flow is laminar and that the capillary channels are uniformly cylindrical in shape. It demonstrates the variance of the rate of change of wicking distance with wicking time when the liquid is moving through the fabric. This equation can be expressed as follows[142].

$$x = C_0 t^{\frac{1}{2}} \qquad (2.3)$$

Where x = wicking distance [m],

t = wicking time [s],

C_0 = constant.

In the horizontal strip test, provided the volume of liquid absorbed is linearly proportional to the wicking distance, then according to equations (2.1) and (2.2), an alternative form of equation (2.3) can be written as follows:

$$x = \left\{ \frac{r\gamma \cos\varphi}{2\eta} \right\}^{\frac{1}{2}} t^{\frac{1}{2}} \qquad (2.4)$$

2.3.1.1.2 The vertical strip test

Poiseuille's equation for vertical linear flow through uniform cylindrical capillary channels has been given as[130]:

$$\frac{dx}{dt} = \frac{r\gamma \cos\varphi}{4\eta x} - \frac{r^2 \rho g}{8\eta} \qquad (2.5)$$

Where ρ = the liquid density (g/cm^3)

g = gravity constant (9.8 m/s^2)

When $\cos\varphi = 1$, equation (2.5) can be rewritten as follows[130]:

$$t = -\frac{8\eta x}{r^2 \rho g} - \frac{16\eta\gamma}{r^3 \rho^2 g^2} \log_e \left\{ 1 - \frac{\rho g r x}{2\gamma} \right\} \qquad (2.6)$$

To obtain a simplified form of the relationship between t and x, Laughlin[180] rewrote equation (2.6) as follows:

$$\beta t = -h_m \log_e \left\{ 1 - \frac{x}{h_m} \right\} - x \qquad (2.7)$$

Where $h_m = a/b$ with $a = \frac{r\gamma \cos\varphi}{4\eta}$ and $b = \frac{r^2 \rho g}{8\eta}$ (2.8)

By using Taylor's expansion[181], when $x << h_m$, the equation can be reduced to the form:

$$x = \left\{ \frac{r\gamma \cos\varphi}{2\eta} \right\}^{\frac{1}{2}} t^{\frac{1}{2}} \qquad (2.9)$$

The resulting equation (2.9) for the vertical strip test is the same form as equation (2.4), which is the Washburn equation for horizontal absorption.

In other work, Law[174] developed an equation for the mass transmission of water absorbed during the vertical strip test as follows:

$$m_v t = \int_0^t B_v \left\{ \frac{1}{x(t)} - \frac{1}{h_m} \right\} dt \qquad (2.10)$$

where $B_v = \dfrac{\rho \pi r^3 \gamma \cos\varphi}{4\eta}$ $(Kg \cdot m/s)$

However, there are two persistent problems with the Washburn equations. The first is the value of the time exponent which is 0.5 and the second is the quantitative definition of the capillary radii, *r*.

The proportionality between the wicking distance and the time exponent 0.5 when the wicking distance is plotted against $\sqrt{time}$ has been a subject of controversy for many years. In the paper industry, many researchers [182, 183] have confirmed the proportionality by experimentation; while others[184, 185] have given evidence that the equation is inadequate for describing the flow through porous media.

The difficulty in defining the capillary radii quantitatively was revealed by Chatterjee[130] and Robinson[186]. According to them, the capillary channels in a real fabric:

1. Differ in size and shape. They are inter-connected as well as interdependent to form a three dimensional network system.

2. They do not have circular cross-sections and are not uniform along their lengths.

Any attempt to give an exact analysis of a fabric containing capillary channels on a theoretical basis would be impracticable since in reality it is a much more complex structure. However, most researchers have tended to adopt the average equivalent radius[174] to describe the capillary radius in porous media. The value of the average equivalent radius is that of a cylindrical channel in which the rate of flow will be the same as that in the porous media.

2.3.1.2 Darcy's Law

Darcy's law provides an alternative approach for investigating the wicking mechanism in fabrics. It is an empirical formula that describes laminar and slow, steady-flow through a porous medium in terms of the driving force gradient and the permeability of the medium. This equation is written as follows[170].

$$Q = -\frac{k}{\eta}\frac{\Delta P}{\Delta x} \qquad (2.11)$$

Where Q = volumetric flow rate [$m^3/s* m^2$],

ΔP = pressure difference [N/m^2],

Δx = conduit distance [m],

k =specific permeability of sample [m^2],

η = viscosity of liquid [Ns/m^2].

If the term ΔP in Darcy's law is the capillary driving pressure as represented by the Laplace equation[130], then according to Poiseuille's equation, the term $\frac{k}{\eta}$ is numerically and dimensionally equal to $\frac{\pi r^4}{8\eta}$.

2.3.2 The Empirical Model for the Vertical Strip Test

Garner[187] found that it is impossible to use the negative exponential function of time $x = b_0(1 - e^{-b_1 t})$ to describe the liquid flow in porous media (where b_0 = maximum wicking height). Law[174] found that the empirical equation (2.12) described much of the experimental data of liquid absorption in woven fabrics. The equation is written as follows:

$$x = b_2(1 - (1 + b_3 t)^{-b_4}) \qquad (2.12)$$

Where x= wicking height (m), b_2 = maximum wicking height (m), b_1, b_3, b_4 = fitted constants, t = wicking time (s).

2.4 DETERMINATION OF THE ANISOTROPY OF PERMEABILITY IN NONWOVENS USING THE VERTICAL STRIP TEST

Using the parameters measured in the vertical strip test, a model was established to calculate the permeability of the fabric in the direction of liquid transport.

In the vertical strip test, the velocity and the liquid pressure gradient are not constant. According to Darcy's law[104], the volumetric velocity of liquid transport in the strip of fabric will be:

$$v(x,t) = \frac{dx}{dt} = \frac{k}{\eta} \frac{(P - x(t)\rho g)}{x(t)} \qquad (2.13)$$

When the liquid reaches its maximum height, h_{max}, the capillary force in the fabric will be balanced by the weight of liquid absorbed and therefore the liquid will remain at a constant height, h_{max}. Therefore,

When $x = h_{max}$, $v = 0$ and $P = h_{max}\rho g$ (2.14)

Also, the boundary condition for liquid absorption in a dry fabric at an initial time will be:

When t=0, $x(t = 0) = 0$ (2.15)

Substituting equation (2.14) into equation (2.13), Darcy's Law can be rewritten as follows:

$$v(x,t) = \frac{dx}{dt} = \frac{k}{\eta} \frac{(h_{max} - x(t))}{x(t)} \rho g \qquad (2.16)$$

Substituting the boundary condition (2.15) into equation (2.16), we can obtain the specific permeability of the fabric, k, as follows:

$$k = \frac{\eta}{\rho g} \frac{1}{t} \left[h_{max} \ln\left(\frac{h_{max}}{(h_{max} - x(t))}\right) - x(t) \right] \qquad (2.17)$$

Thus, in the vertical strip test, the ratio of the directional permeability the machine direction (k_{MD}) to in the cross direction (k_{CD}) of the fabric, α_k, can be written as follows[188].

$$\alpha_k = \frac{k_{MD}}{k_{CD}} = \frac{\left[h_{\max}^{MD} \ln\left(\frac{h_{\max}^{MD}}{(h_{\max}^{MD} - x_{MD}(t))}\right) - x_{MD}(t) \right]}{\left[h_{\max}^{CD} \ln\left(\frac{h_{\max}^{CD}}{(h_{\max}^{CD} - x_{CD}(t))}\right) - x_{CD}(t) \right]} \quad (2.18)$$

Where $h_{\max}^{CD}$ is the maximum height the liquid reaches in the Cross Direction (CD) of the fabric.

$h_{\max}^{MD}$ is the maximum height the liquid reaches in the Machine Direction (MD) of the fabric.

$x_{MD}(t)$ is the wicking height the liquid reaches in time t in the Machine Direction (MD) of the fabric.

$x_{CD}(t)$ is the wicking height the liquid reaches in time t in the Cross Direction (CD) of the fabric.

This is a convenient means of expressing the anisotropy and was used in the experimental work that follows.

2.5. PRELIMINARY EXPERIMENTS

2.5.1. Structural Characteristics of Commercial Wound Dressing Fabrics

Initially, four commercially available nonwoven wound dressing fabrics were examined. The specifications of the fabrics are summarised in Table 2.1, in which the fabric thickness, with and without compression, is measured according to the standard INDA method for high loft nonwoven fabrics[189]. All the fabrics were single layer nonwoven structures. Among the four commercial wound dressings, the Soffban Synthetic and Lantor Sythetic products were made from synthetic, non-absorbent fibre.

Soffban Natural is made from cellulosic fibre and Sorbsan is made from calcium alginate fibre.

Table 2. 1(a) Thickness and porosity of commercial nonwoven wound dressing fabrics (no compression)

Fabric Name	Fibre Type	Fibre Density (g/cm^3)	Fabric Thickness (mm)	Fabric Density (g/cm^3)	Calculated Fabric Porosity
Soffban Synthetic	Polyester	1.39	2.00	0.046	0.967
Lantor Synthetic	Polyester	1.39	3.00	0.025	0.982
Sorbsan	Calcium Alginate	1.75	0.80	0.273	0.844
Soffban Natural	Cellulose	1.49	2.50	0.048	0.968

Table 2. 1(b) Thickness and porosity of commercial nonwoven wound dressing fabrics (with compression (105 N/m^2))

Fabric Name	Fibre Type	Fibre Density (g/cm^3)	Fabric Thickness (mm)	Fabric Density (g/cm^3)	Calculated Fabric Porosity
Soffban Synthetic	Polyester	1.39	0.479	0.192	0.862
Lantor Synthetic	Polyester	1.39	0.450	0.169	0.878
Sorbsan	Calcium Alginate	1.75	0.415	0.528	0.695
Soffban Natural	Cellulose	1.49	0.535	0.224	0.849

2.5.2 Liquids Used During Testing

Distilled water was used as the test fluid in the strip tests and the experimental work thereafter. Although it may be assumed that body fluids would be ideal for use as a test

liquid in the experiments, there are some drawbacks. Firstly, real fluids are expensive and secondly, no recipes have been reported which accurately reproduce the properties of such body fluids. Also, there are no reports of an acceptable method for analysing experimental results obtained for non-Newtonian liquids of this type. Distilled water is a Newtonian fluid and has been widely used in previous strip test experiments. Also, commercial manufacturers of wound dressings use distilled water to characterise the performance of fabrics. For these reasons, distilled water was used as the test fluid throughout.

2.5.3. Description of the Experimental Strip Test Procedure

2.5.3.1 The Vertical Strip Test Procedure[190]

Strip tests were carried out using a standard procedure[190]. Coloured lines with a graduated scale of half centimetre intervals were drawn across the width of a strip of fabric (dimensions 30 mm width × 100~120 mm length) by using a pen filled with water-soluble ink. The dry strip of the fabric was suspended vertically in a frame, with one end clamped onto the frame and the other end dipped in distilled water. When the water reached the assigned interval, the wicking distance was recorded accordingly. A ruler with millimetre divisions was placed parallel to the sample strip to enhance the accuracy of the measurements. The wicking heights of water absorbed by the strip were recorded at regular time intervals. Five sample strips were tested for each fabric.

2.5.3.2. The Horizontal Strip Test Procedure

The horizontal strip test is carried out with the strip held horizontally. The sample preparation is the same as in vertical strip test and five sample strips were tested for

each sample fabric. In order to prevent elongation of the nonwoven fabric during testing, the two ends of the fabric were attached to the base of a framework, and then suspended horizontally by several filaments of polyester filament. This approach reduced the slackening effect that resulted when water was absorbed into the strip.

2.5.4 Porosity and Absorbency of Commercial Nonwoven Wound Dressing Fabrics

Liquid absorption in fabrics is driven by capillary pressure which largely relies on the fabric porosity. The porosity of nonwovens will vary with fabric thickness which will differ significantly depending on compression. When the fabric is saturated, voids in the fabric will be filled with liquid. Thus, two porosity values can be obtained. One is the calculated porosity obtained from the fabric thickness measured using the standard test for highloft nonwovens[189]. The second is calculated from the dimensions of the saturated fabric in the standard absorbency test[190, 191]. The porosities of the commercial dressings under different test conditions are shown in Table 2.1. The associated liquid absorptions of the fabrics are listed in Table 2.2.

Table 2. 2 Porosity and absorbency of commercial nonwoven wound dressings

Fabric Name	Fibre Type	Fibre Diameter (μm)	Water Absorption Capacity		Fabric Thickness (mm)	Area Density (g/m^2)
			(g/g)	(g/m^2)		
Soffban Synthetic	Polyester	13.6	23.8	2439.2	0.479	98.2
Lantor Synthetic	Polyester	13.0	28.9	2277.8	0.450	78.9
Sorbsan	Calcium Alginate	12.4	7.1	1549.6	0.415	219.1
Soffban Natural	Cellulose	15.8	55.3	2118.0	0.535	38.3

The relationship between the liquid absorbency and the fabric porosity for the four commercial fabrics is plotted in Figure 2.1.

It is clear from Figure 2.1 that fabrics with the higher porosity, (irrespective of fibre composition), have higher absorption capacities. The fabric containing gelling fibres (Calcium alginate), had the lowest porosity and also has the lowest liquid absorption capacity.

The porosity of a nonwoven fabric characterises the percentage void volume in the fabric. The voids occupied by air will be filled with liquid when the fabric is saturated during liquid absorption. However, if the fabric porosity is too high, it might be difficult to retain the water in the fabric structure. Thus, the liquid absorption capacity of nonwoven fabrics relies mainly on the structural architecture of the fabric. In this work, the absorbency was found to be related to fabric porosity (see Figure 2.1), this is believed to explain why Sorbsan has a unusual low liquid absorbency in Table 2.2.

Figure 2. 1 Liquid absorbency vs. porosity for commercial nonwoven wound dressing fabrics

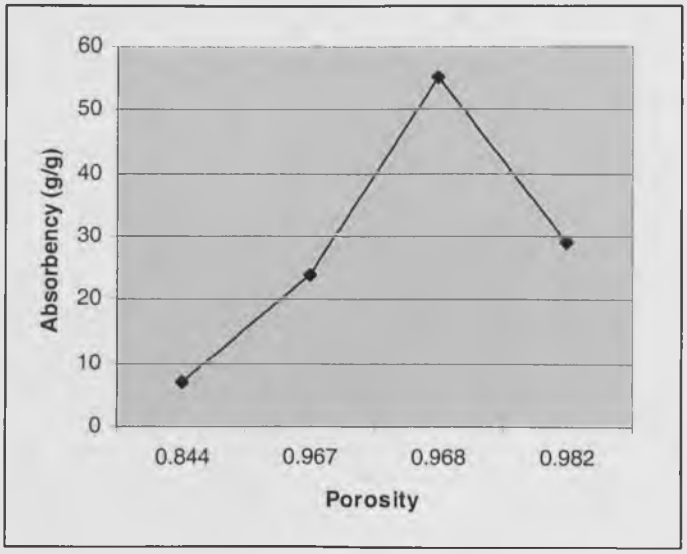

2.5.5 Anisotropy of Liquid Absorption in the Commercial Dressings

Experiments showed that the dressings consisting of synthetic fibres did not wick at all. This is believed to be due to their high water-fibre interface tension. Only the samples composed of absorbent fibres (Cellulose and Calcium Alginate) supported wicking in the strip test. The experimental results are shown in Table 2.3.

The anisotropy of liquid absorption in the fabrics can be expressed in one of the following forms:

1. The ratio of the maximum rise height in the MD to the CD in the vertical strip test (α_h).

$$\alpha_h = \frac{H_{MD}}{H_{CD}}$$

2. The ratio of the initial wicking rate in the MD to the CD in both the vertical and horizontal strip tests (α_V).

$$\alpha_V = \frac{v_{MD}}{v_{CD}}$$

2.5.5.1 Vertical Strip Test Results

The maximum wicking heights in the MD and CD obtained in the vertical strip test for each fabric are shown in Table 2.3. The plots of wicking height versus time in both the CD and MD during the vertical strip test for each fabric are presented in Figures 2.2 and 2.3 respectively.

2.5.5.1.1 Anisotropy of the Wicking Height

In Table 2.3, it may be noted that the liquid rise height in the vertical strip test, for both the cellulosic fabric and the alginate fabric, is generally higher in the machine direction (MD) than in the cross direction (CD).

It was indicated, in section 1.4.2.2 in Chapter 1, that the liquid absorption in nonwoven fabrics is driven by capillary pressure between fibres, which is governed by both the geometrical structure of the fabric and the water-fibre interface properties according to the Laplace Equation. In idealised, homogeneous nonwoven structures, structural parameters such as fibre type, fibre diameter, fibre length and fabric weight will be the

Table 2. 3 Absorption rate and anisotropy of absorption in commercial dressings in the Horizontal and vertical strip tests

Fabric Name	Fibre Type	Vertical test				Horizontal test		Anisotropy of absorption in the vertical Strip test
		h_{max} (cm)		$x(t)$ (cm)				
		MD	CD	MD	CD	MD	CD	
		h_{max}^{MD}	h_{max}^{CD}	$x_{MD}(t)$	$x_{CD}(t)$	$x_{MD}(t)$	$x_{CD}(t)$	
Sorbsan	Calcium Alginate	5.8	4.8	T=90 Sec.		T=35 Sec		1.47
				4.0	3.0	6.0	5.0	
				T=500 Sec.		T=65 Sec.		1.48
				5.0	4.0	9.6	7.2	
Soffban Natural	Cellulose	3.9	2.4	T=150 Sec.		T=80 Sec.		2.18
				2.5	1.2	6.0	5.5	
				T=500 Sec.		T=170 Sec.		2.14
				3.0	1.6	9.0	8.5	

same in all directions. However, this is not the case with respect to the fibre orientation distribution and it may be suggested that the anisotropy of liquid absorption in the plane

of a nonwoven fabric will be largely determined by the anisotropic structure of the fabric. In other words, the anisotropy is thought to reflect differences in the fibre orientation in the MD and CD of the fabric plane.

Referring to Table 2.3, it is apparent that the fabric composed of Calcium Alginate (Sorbsan) has a higher rise height than the fabric consisting of Cellulose (Soffban Natural) in both the MD and CD respectively. In order to compare the anisotropy of the two fabrics, the ratio of the maximum rise heights in the CD and MD for each fabric has been calculated. The anisotropy of the maximum wicking height in the Sorbsan dressing was, $\alpha_h = \frac{6cm}{5cm} = 1.2$, compared to $\alpha_h = \frac{3.8cm}{2.4cm} = 1.583$ in the Soffban Natural dressing.

It is apparent from these results that the Soffban Natural dressing has a greater anisotropy than Sorbsan. The reason for this can only be speculated since there are many differences between the two fabrics with respect to their structure and fibre compositions, e.g., porosity, fibre diameter and fibre orientation distribution. Consequently, it is not clear whether the differences in the anisotropy of liquid absorption in the two fabrics is due to differences in fibre type or due to structural differences in the fabrics.

2.5.5.1.2 Anisotropy of the Wicking Rate

The wicking rate is defined as the time taken for a liquid to rise one inch in the fabric during absorption[190]. Here, it is defined as the wicking height per unit time. As indicated in Figure 2.2, the wicking rate decreased with increases in rise height for the commercial fabrics. Besides differences in the maximum rise height in the machine and

cross directions indicated in section 2.5.5.1.1, it was noted that the absorption rate (shown in Figure 2.2) in the MD was generally higher than that in the CD for both commercial fabrics. Again, this is believed to reflect structural differences in the two fabrics.

Figure 2. 2 Plots of rise height vs. time for commercial wound dressing fabrics
(Vertical Strip Test, test fluid: Distilled Water)

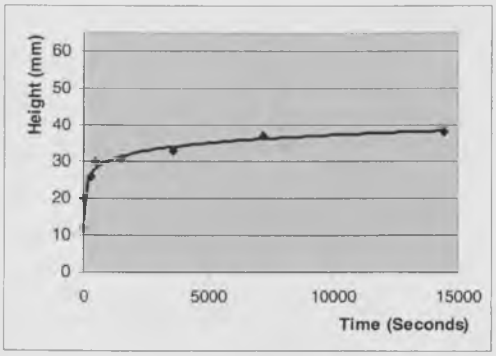

a) Soffban Natural (Machine Direction)

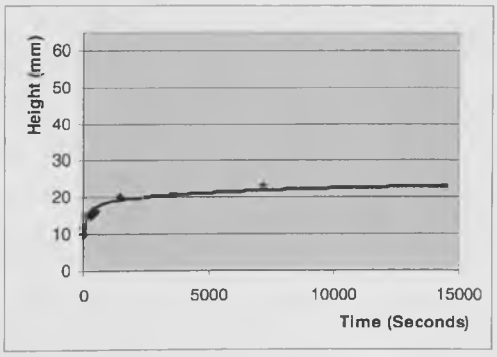

b) Soffban Natural (Cross Direction)

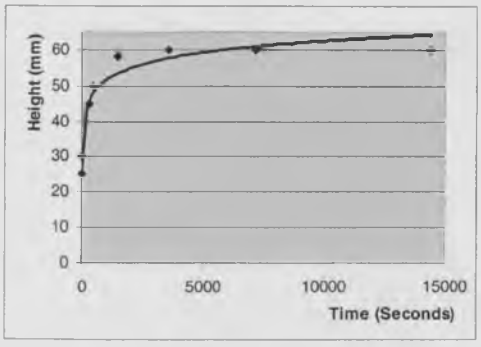

c) Sorbsan (Machine Direction)

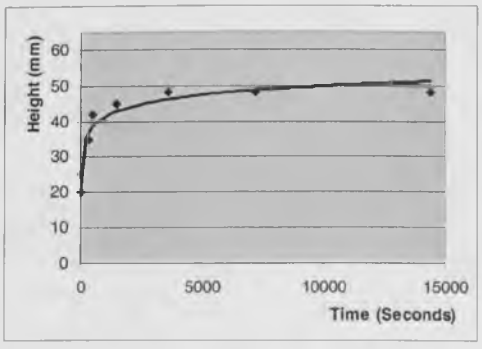

d) Sorbsan (Cross Direction)

Similarly, the fabric composed of alginate (Sorbsan) exhibited a higher liquid absorption rate than Soffban Natural (composed of cellulose fibres) in both the CD and MD. The ratio of the average wicking rate in the MD to the CD (for the first 500 seconds of the test) for Sorbsan and Soffban Natural was measured as indicated in Table 2.4.

Table 2. 4 Anisotropy of the liquid absorption rate in vertical strip tests

Sorbsan	Soffban Natural
$\alpha_V = \frac{5.0cm}{4.0cm} = 1.25$	$\alpha_V = \frac{2.5cm}{1.6cm} = 1.56$

In Table 2.4, it is apparent that Soffban Natural has a greater anisotropy of the average absorption rate than Sorbsan. It is interesting to note that both the anisotropy of the wicking height and the anisotropy of the average absorption rate for the two fabrics follows a similar trend.

2.5.5.2 Horizontal Strip Test Results

In order to exclude the influence of gravity on the liquid absorbed by a fabric, horizontal absorption strip tests may be used. Theoretically, the liquid displacement during wicking is unlimited in the horizontal strip test if the length of the sample strip is also unlimited. Thus, the maximum wicking distance cannot be used to calculate the anisotropy. However, the anisotropy of the average wicking rate in the fabric in both the CD and the MD can be obtained, the experimental results are shown in Figure 2.3.

Table 2. 5 Anisotropy of liquid absorption rate in the horizontal strip tests

Sorbsan	Soffban Natural
$\alpha_V = \frac{200}{175} = 1.14$	$\alpha_V = \frac{115}{65} = 1.77$

It is apparent in Figure 2.3 and Table 2.5 that the absorption rate during the horizontal test is much higher than in the vertical test. For the fabric consisting of calcium alginate fibre (Sorbsan), the anisotropy of the wicking rate in the horizontal strip test was smaller than the anisotropy in the vertical strip test. In contrast, for Soffban Natural, the anisotropy of the wicking rate in the horizontal strip test was obviously greater than in

the vertical strip test. The reasons for this are not clear but it is reasonable to assume that it may be due to differences in the internal structure of the two fabrics.

As in the vertical strip test, the horizontal test indicated that the liquid absorption rates for the Sorbsan fabrics consisting of calcium alginate were markedly higher than for the fabrics containing cellulose fibre (Soffban Natural) in both the MD and CD. It remains unclear if this is due only to differences in fibre type, the fabric structure or to both fibre and fabric structure.

Figure 2. 3 Plots of rise height vs. time for commercial wound dressings
(Horizontal Strip Test, test fluid: Distilled Water)

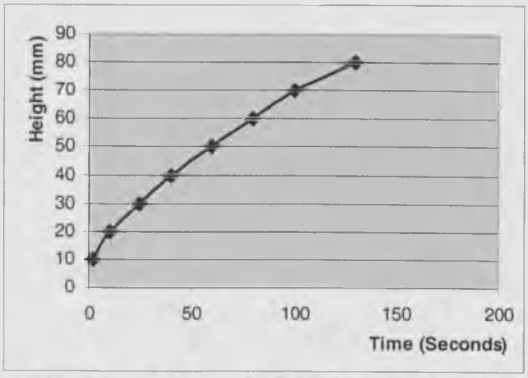

a) Soffban Natural (Machine Direction)

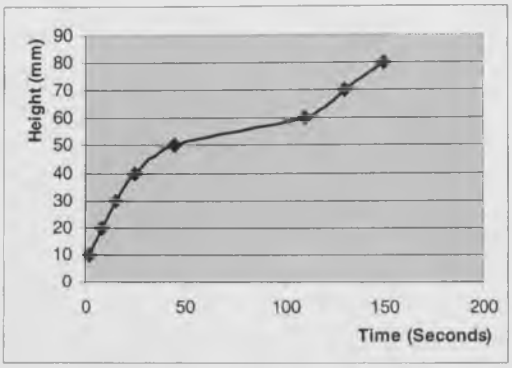

b) Soffban Natural (Cross Direction)

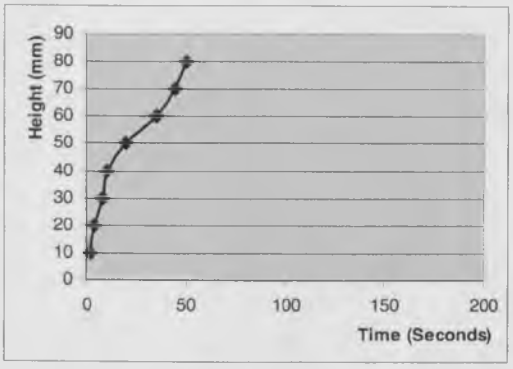

c) Sorbsan (Machine Direction)

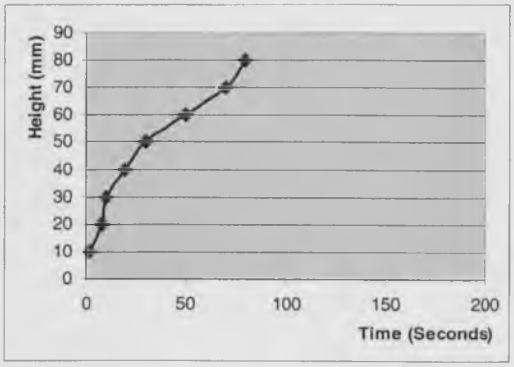

d) Sorbsan (Cross Direction)

2.6 SUMMARY OF PRELIMINARY STUDIES AND CONSIDERATIONS

It has been established that there is significant anisotropy of liquid absorption in commercial nonwoven wound dressing fabrics, and this is evident in both the vertical and the horizontal strip tests. Generally, it is believed that anisotropy in both mechanical and electrical properties are determined by anisotropy of the fabric structure[90, 93]. Although differences in the anisotropy of liquid absorption have been found in fabrics consisting of different fibres, it is not clear whether this difference is caused by the fabric structure or by the liquid handling characteristics of the fibre itself.

Although it may be speculated that the anisotropy of liquid absorption is due to the fibre orientation distribution in the fabric, there is no direct evidence to prove this and there have been few studies demonstrating the relationship between the fibre orientation distribution and the anisotropy of liquid absorption. Furthermore, there is little research available that shows how fabric structural parameters, such as fabric porosity and fibre diameter, influence the anisotropy of liquid absorption. Thus, in order to improve understanding in this area, it is necessary to find an effective way to measure the fibre orientation distribution in nonwoven fabrics and moreover, to establish relationships between fabric structural parameters and the liquid transmission rate.

In the strip test experiments, it was also found that there are limitations in the measuring methods used to assess liquid absorption in nonwovens. Since the wicking height of the liquid in the fabric under test is judged visually and recorded manually, and because the wicking rate in many nonwovens is very high (especially in the initial stages), it is difficult to obtain accurate measurements. Moreover, in the horizontal strip test, measuring error becomes so large that it is impossible to record the correct initial

wicking displacement with time because of the rapid spreading of the liquid in the horizontal plane of the fabric.

As the liquid is absorbed, it spreads in the fabric plane and not necessarily at the same rate in different directions. Furthermore, strip tests only provide a measure of the liquid absorption in one direction at a time during each test and thus are of limited use in any comprehensive study of anisotropic liquid absorption. Therefore, it is necessary to use a method that allows measurement of the anisotropy of in-plane liquid absorption in multiple-directions simultaneously, this is discussed in Chapter 3.

From the preliminary experimental results, it is apparent that the overall absorbent capacities of commercial nonwoven wound dressing fabrics depends mainly on the porosity of the fabric, which in turn depends on other fabric parameters which will influence the variation of fabric porosity.

CHAPTER 3 DEVELOPMENT OF AN INSTRUMENT TO MEASURE THE ANISOTROPY OF LIQUID TRANSPORT IN NONWOVEN DRESSING FABRICS

In Chapter 2, it was demonstrated that anisotropic liquid transport is observed in commercial nonwoven wound dressing fabrics composed of different types of fibre, and it was suggested that this anisotropy is influenced by anisotropy in the structure of the nonwoven fabric itself. Thus, one important focus of this study is to establish the relationship between anisotropic liquid transport and nonwoven fabric structure, and to achieve this it was necessary to find a suitable measurement method for the determination of liquid transport in multiple directions in the fabric plane. Such a method should be capable of measuring liquid transport dynamically. This Chapter is concerned with a comparison of existing methods for the measurement of liquid transport using either steady-state or dynamic measuring approaches. Subsequently, a new computer-integrated apparatus for the real-time measurement of the volumetric flow rate in nonwoven fabrics is described.

3.1 COMPARISON OF MEASUREMENT METHODS FOR THE ASSESSMENT OF LIQUID TRANSPORT IN FABRICS

3.1.1 Definition of Terms

3.1.1.1 Cross-Plane Liquid Flow and In-Plane Liquid Flow

Liquid transport in fabrics may take place in the fabric plane or perpendicular to the fabric plane. The magnitude of liquid transport in fabrics perpendicular to the fabric plane cannot be used to explain the transport characteristics in the fabric plane. Consequently, separate test methods are required to evaluate the two properties.

3.1.1.2 Liquid Absorption and Forced Flow in Fabrics

There are two main types of liquid transport in fabrics[130]. One is referred to as liquid absorption which is assumed to be driven by capillary pressure in the fabric. Here, liquid is taken up by a fabric through a zero or negative hydrostatic pressure gradient. The other type of liquid transport is referred to as forced flow, where liquid is driven through the fabric by an external pressure gradient.

The liquid absorption that takes place when one edge of a fabric is dipped in a liquid so that the liquid is absorbed primarily in the plane of the fabric is called wicking. When the liquid front enters through the face of the fabric, reference is made to demand absorbency or spontaneous uptake. Cary and Sporles[178] compared such test methods in connection with the liquid absorption of paper towels. The measurement methods evaluated included point source and plate source demand wettability tests, wicking measurements (the Cobb[192] and Klemm test[177] and gravimetric absorbency tests[193, 194]). The Cobb test measures the rate of liquid absorption in terms of the amount absorbed,

whereas the Klemm test measures the linear rate of advance of liquid in the paper sample. In practice, they found only a few of these test methods provide useful results[178].

Forced flow through the plane of a fabric can be performed in one of two ways:

(1) The liquid is forced through at a constant velocity and the resistance to passage is measured in some manner, or

(2) The liquid is forced through at a fixed pressure gradient and the resultant flow rate is monitored.

There are also two alternatives for the second case. Either the driving pressure remains constant or alternatively it is systematically increased with time. The latter arrangement is convenient for establishing the critical breakthrough pressure of a fabric barrier. Experimental study of forced flow through fabrics in some cases may also be used to study spontaneous uptake[195].

3.1.1.3 Steady State and Dynamic Measurements

Measurement methods for liquid transport in fabrics can be classified as either 'steady state' or 'dynamic'. In steady state methods the liquid absorption characteristics of a fabric are measured momentarily when the reading is constant, and in dynamic methods, the liquid absorption is continuously measured in real time. Although numerous methods of measuring the liquid transport in fabrics have been proposed, only those methods that are also capable of revealing the anisotropic characteristics of the liquid transport rate in fabrics and which also have the potential to be used for nonwoven fabrics are reviewed in this Chapter.

3.1.2 Steady-State Measurement Methods

Some steady-state methods only allow qualitative assessment of liquid absorption characteristics, and those that give quantitative results are of variable accuracy. The wicking rate, expressed in terms of either wicking displacement or liquid mass, is usually the main parameter measured in steady-state methods to represent the liquid absorption capability of fabrics. Usually, most of these methods provide limited information on the liquid movement in the fabric structure during absorption.

3.1.2.1 The Longitudinal Wicking "Strip" Test

The most widely used method is the vertical strip test of which there are two types. The rate of liquid absorption may be measured in terms of the amount of liquid absorbed, or in terms of the linear rate of advance of the liquid in the sample. The main standard test methods are:

1. BS3424-18, method 21(1988)[176]: Methods for determination of the resistance to wicking and lateral leakage.

2. EDANA method 10.2-96 part C (1996)[175]: Liquid wicking time.

3. INDA, IST10.1 (1995)[190]: Standard test method for absorbency time, absorbency capacity, and wicking rate.

There are some differences in these test procedures. The BS3424-18 (Method 21), specifies a very long test period (24h) and is intended for coated fabrics with very slow wicking rates. In contrast, EDANA 10.2-96 specifies a much shorter test time (maximum 5 min) and applies to fabrics that exhibit rapid wicking. A diagram of this

method is shown in Figure 3.1(a). In this test, the fabric is first conditioned at 20^0C, 65% relative humidity for 24 hours. A strip of the test fabric is suspended vertically with its lower end immersed in a reservoir of distilled water. After a fixed time has elapsed, the height reached by the water in the fabric above the water level in the reservoir is measured. The height is taken as a direct indication of the wickability of the test fabric.

Figure 3. 1 Steady-state testing methods[128]

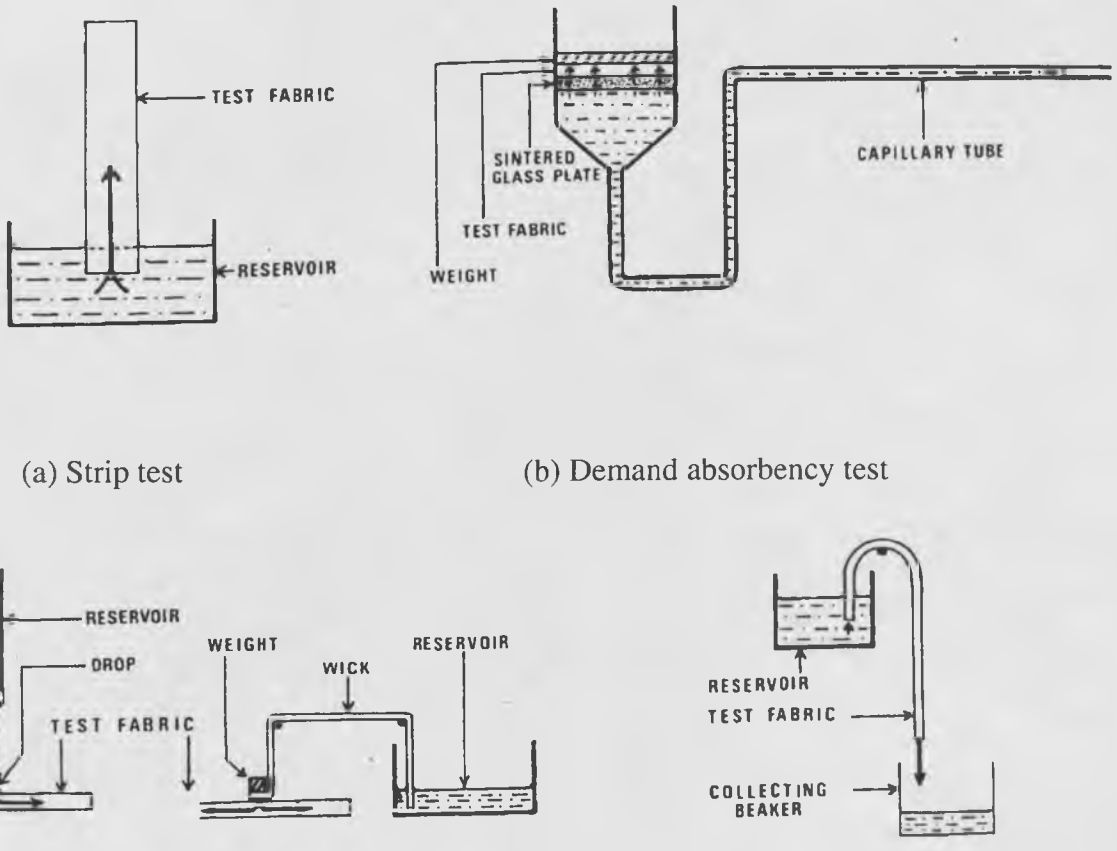

(a) Strip test

(b) Demand absorbency test

(c) Drop test

(d) Syphon test

This strip test method is useful for determining the rate of advance of the liquid front, and it can be used either in fabrics that exhibit rapid or slow wicking. Samples for testing can be taken in different directions in the fabric and therefore it can be used to

determine differences in the liquid absorption rate in different directions in the fabric plane. Also, the method can be modified to measure horizontal wicking by measuring the rate of advance of the liquid front[148].

However, strip test methods involve measuring the position of the advancing front and comparing the heights of the rise in different fabrics. They do not allow a comparison of the mass transfer rates unless the fabrics are of a similar structure and thickness. Another disadvantage of the method is that there is no provision for measuring the mass of liquid that is wicked in a given time.

3.1.2.2 Demand Absorbency Test [196]

The Demand Absorbency Test is sometimes referred to as the demand wettability test, or the transverse wicking "plate" test (see Figure 3.1(b)). In demand tests, the liquid will only enter into the fabric when the sample demands it. These tests involve contacting the dry sample with a liquid in such a way that absorption occurs under a zero or slightly negative hydrostatic head. The method has been used by Buras et al[196] on cotton fabrics and Korner et al[197] on porous acrylic fabrics (or fabrics produced from other fibre types). No test standards for this method are currently available.

If the liquid is introduced from a point source in the fabric, it becomes a dynamic measurement method known as the Point Source Demand Wettability Test[179]. This method is effectively a two-dimensional radial wicking test and may be more useful in measuring the rate of fluid uptake than the strip test.

A classic example of this type of tester[196] is shown in Fig. 3.2. The device consists of a filter funnel fitted with a glass plate that is connected to flexible tubing and to a

horizontal length of capillary glass tube. The horizontal sintered glass plate is fed from below with water from a horizontal capillary tube, the level of which can be set so that the upper surface of the plate is filled with an uninterrupted column of test liquid and kept damp. This is often used to simulate a sweating skin surface. A disk of the test fabric is placed on the plate and held in contact with it under a defined pressure applied by placing weights on top of it. The position of the meniscus along the capillary tube is recorded at various time intervals as water is wicked along the fabric layer. Given the diameter of the capillary tube, the recorded data can be used to calculate the mass transfer rate of water into the fabric.

Figure 3. 2 Instrument for measuring demand wettability[196]

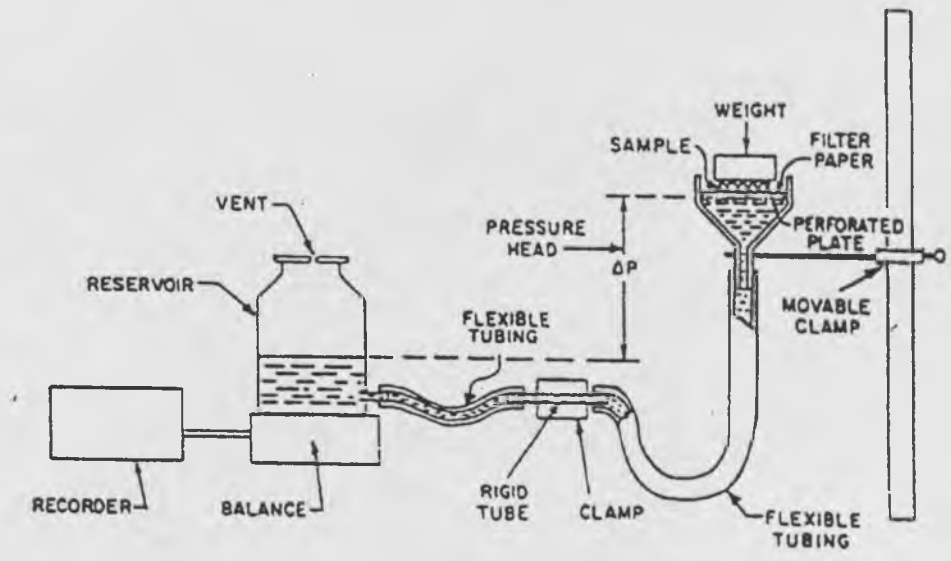

The strength of the porous plate technique lies in its ability to provide fundamental information on the absorbency and structure-property relationships of absorbent systems as well as its high degree of sensitivity. The limitations of this method are its inability to measure the liquid absorbency in the fabric plane and there is a tendency for the porous

plate to clog, creating a reproducibility problem. A further problem with this method is that the mass transfer rate is strongly dependent on the applied pressure, particularly for bulky fabrics. The structure of bulky fabrics may change considerably under greater compression, and low compression may not give uniform perforated plate--fabric contact. Another criticism of the method is that the resistance to flow imposed by the capillary tube decreases during the course of the test, as water is withdrawn from the tube, although this can be improved by replacing the capillary tube by an air bleed system[179]. A further limitation is that the hydrostatic head in the system, which is set a low level at the start of the experiment, decreases during the test as water wicks up through the fabric sample. This could be a particular problem with thick fabrics.

Although the method is complex, if the device is properly maintained, and the limitations of the method are recognized, it has potential as a research tool for the study of liquid absorption.

3.1.2.3 Areal Wicking "Spot" Test

This method is based on modification of the following standard test methods:

(i). BS3554 (1970): Determination of wettability of textile fabrics.

(ii). AATCC method (39-1977): Evaluation of wettability, the "Spot" test attempt to measure the in-plane wickability, or the capability of a liquid drop to spread over the fabric.

As shown in Figure 3.1(c), a drop of liquid (either distilled water, or, for highly wettable fabrics, a 50% sugar solution) is delivered from a height of approximately 6 mm onto a horizontal specimen of the test fabric (preconditioned at 20^0C, 65%RH). The region of

the fabric on to which the drop falls is illuminated by a beam of light to create bright reflection from the liquid surface, and the elapsed time between the drop reaching the fabric surface and the disappearance of the reflection from the liquid surface is measured. The disappearance of the reflection is assumed to indicate that the liquid has spread over and wetted the fabric surface. The elapsed time is taken as a direct measure of the fabric wettability. The shorter the time, the more wettable the fabric.

There are two ways to express the results. One is to measure the area of the wetted region of the fabric at the moment reflection ceases, or to record the mass of the liquid absorbed as a percentage of the dry weight of an area of fabric equal to the area of the wetted region[198]. The other approach is to replace the drop by a continuous supply of liquid (delivered by a capillary tube or a saturated fabric 'wick' in contact with the test specimen) and to measure the rate of increase in diameter of the wetted region[199].

However, the results of this method are relatively inaccurate because only indirect readings are possible. For the single drop test, the results are dependent on the local fabric structure, and therefore the measurements are subject to marked variation even within the same fabric.

3.1.2.4 Syphon Test

The Syphon test (as shown in Figure 3.1(d)) measures the rate of drainage rather than the wicking rate. No standard for this test exists. The method has been reported by Lennox-Kerr[199] on acrylic and porous acrylic polymers, by Tanner[200] (on cotton, polyester/cotton, and polyester/acrylic blends), and by Hardman[128] on polypropylene, wool, polyvinyl-chloride, and blends.

A rectangular strip of the test fabric is used as a syphon, by immersing one end in a reservoir of water or saline solution and allowing the liquid to drain from the other end which is placed at a lower lever, into a collecting beaker. The amount of liquid transmission at successive time intervals can be determined by weighing the collecting beaker[199].

This method measures the rate of liquid transport under external pressure not the volume of liquid absorption. Because the fabric has been saturated, it has a lower resistance to flow than dry fabric and therefore the test results do not indicate the true wicking rate. Also, a comparison of the results provided by this method have shown that the method is not appropriate for measuring wicking properties[128].

In all the steady state measurements methods discussed above, the spot test (continuous supply) or strip test are suitable for measuring liquid absorption in the fabric plane, while the transverse plate test is suitable for measuring liquid absorption perpendicular to the fabric plane.

3.1.3 Dynamic Measurement Methods

Dynamic liquid transport measurements are obtained either from volumetric flow rate data or from qualitative observations of the advancing fluid front in fabrics[149, 201]. The latter case does not yield accurate results, since the position of the advancing front is not obvious in all cases, especially for nonwoven structures of high porosity because of the so-called finger-effect[202]. Local variations in fabric density and therefore pore size may cause substantial deviations from the average velocity value obtained from the volumetric flow rate data. Other dynamic techniques yield only overall values and do

not provide detailed directional quantitative information about the actual dynamic transport process occurring in the fibrous assembly[121, 203, 204, 205]. Thus, it is apparent that only some dynamic techniques can provide detailed directional quantitative information about the actual dynamic liquid transmission process in fibrous assemblies.

The major test methods used in industry for dynamic measurement of the liquid transport properties of fabrics are now summarised.

3.1.3.1 Modified Laser-Doppler Anemometry (MLDA)

MLDA is based on the Doppler principle[203]. One example of the method is shown in Figure 3.3. When a laser beam is passed through a flowing liquid, light is scattered by the particles suspended in the liquid. The scattered light is subject to a frequency shift and contains information about the velocity of the particles which can then be examined by electro-optical techniques. This measurement therefore requires that the flow medium be partly transparent and contain particles that scatter light. Howald and Yoganathan[203] used this method to obtain the local velocity of liquid flow in a nonwoven fabric. MLDA has the following advantages:

(i). No probes need to be inserted into the flow field of interest.

(ii). No calibration is required.

(iii). It has a high signal-to-noise ratio and can therefore be used with good accuracy to measure velocities in highly disturbed flow fields.

(iv). Good accuracy is achieved in measuring velocities close to surfaces.

(v). It has a high-frequency response (at least 10^5Hz).

(vi). It can distinguish between forward and reverse flow directions.

One problem with MLDA is that it requires the flow medium to be transparent and to contain particles that can scatter light. These requirements limit its uses. Furthermore, the equipment needed is very complex and expensive.

Figure 3. 3 Block diagram of Modified Laser Doppler Anemomter (MLDA)[203]

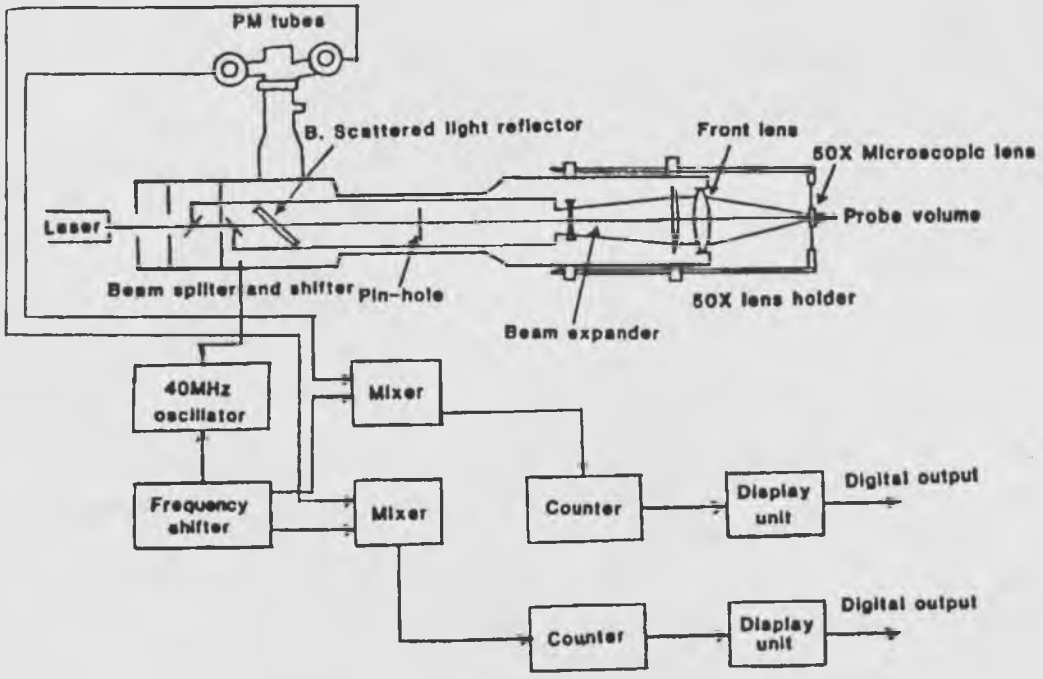

3.1.3.2 Electrical Capacitance Techniques

An electrical capacitance technique was adopted by Ito and Yoichiro[119] to investigate the effect of fibre properties on liquid transport behaviour in unidirectional fibre bundles. Tagaya et al[121] also developed a similar apparatus to measure relatively large volumes of water transport through fabrics, as shown in Figure 3.4.

The principle of the method is based on the fact that the dielectric constant of water is about fifteen to forty times higher than that of normal fibres and fabrics, and therefore

the capacitance of a transducer in a measuring system will be very sensitive to the amount of liquid absorbed by a fabric. The measuring technique can be used in both vertical wicking and horizontal wicking tests and it is easy to use. Furthermore, the measurement data can be imported into a computer for processing. The method can provide both local and dynamic (real time) measurements of the wicking rate in terms of the volume of liquid absorbed.

Problems in testing nonwovens may arise because in saturated fabrics significant geometric deformations may influence the capacitance values. Also, different types of fibrous material may have different dielectric constants, which can lead to difficulties when comparing different materials.

Figure 3. 4 Block diagram of electrical capacitance technique[121]

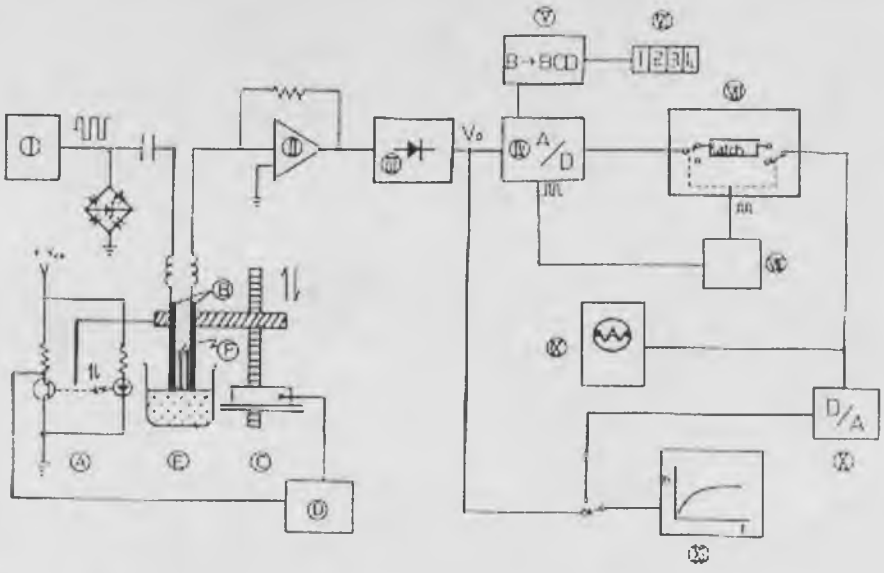

Key,

(I) Square wave generator, (II) I/V converter, (III) Full wave rectifier, (IV) Binary A/D converter, (V) Binary BCD converter, (VI) Digital display, (VII) RAM, (VIII) Timing control circuit. (IX) Monitoring oscilloscope, (X) D/A converter, (XI)

Recorder, (A) Photosensor (Led and Phototransistor), (B) Capacitance electrode, (C) Stepping motor and linear head, (D) Driver and controller circuit for stepping motor, (E) Vessel, (F) Sample.

3.1.3.3 Electronic Micro-balance Method

There are two types of micro-balance method in use. One method is an extension of the vertical strip test and measures the mass of liquid absorbed in the fabric plane[204]. The other method originated from the demand wettability transverse plate method[206] and measures the liquid absorbed perpendicular to the fabric plane.

An electronic micro-balance is used in the vertical strip test to measure the liquid wetting, transmission and retention properties in vertically suspended woven fabrics (see Figure 3.5). The device[204] is perhaps the most convenient to use among all the dynamic test methods. The test values are not influenced by environmental conditions, but it can only be used in vertical wicking tests.

The results from this method have been criticized because it is very difficult to maintain the fabric ends in an accurate position to obtain the correct critical contacts with the liquid reservoir.

One dynamic method modified from the transverse porous plate method and combined with the electronic balance method is called the Gravimetric Absorbency Testing System (GATS) (see Figure 3.6) developed by TRI[194]. The GATS system is based on the principles of a Swedish standard method where the amount of liquid absorbed is determined gravimetrically. This method is a more sophisticated instrument than the plate demand wettability method as shown in Figure 3.6. Instead of horizontal tubing or

a burette with an air bleed, the liquid source is a relatively large vessel resting on top of an electronic balance via a coil spring. The coil spring has a predetermined Hooke constant[207] and is capable of compensating the weight loss (due to absorption of liquid by the fabric) or weight gain (due to exsorption) of liquid in the vessel such that the liquid level can be maintained constant.

Figure 3. 5 Electrical micro-balance method for measuring liquid absorption[204]

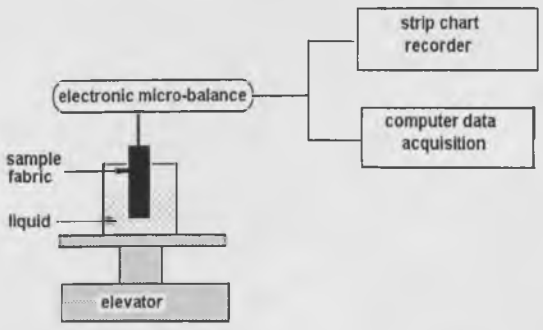

The amount of liquid absorbed is measured continuously by the electronic balance. The amount absorbed as a function of time can be recorded continuously via a strip chart recorder (or digitally via a computer). The advantage of this design, other than its ability to record infinite signal changes, is its flexibility in removing or returning the liquid and the application of a large amount of liquid for test. A wide variety of test cells allowing different modes of contacting the absorbent sample and the liquid, (including the porous plate and a point source), can be used with this equipment. Also, the system may incorporate a sample thickness measuring device which allows continuous monitoring of the change in bulk volume under a constant load. The load can be programmed to allow cyclic loading tests.

Figure 3. 6 Block diagram of GATS technique[194]

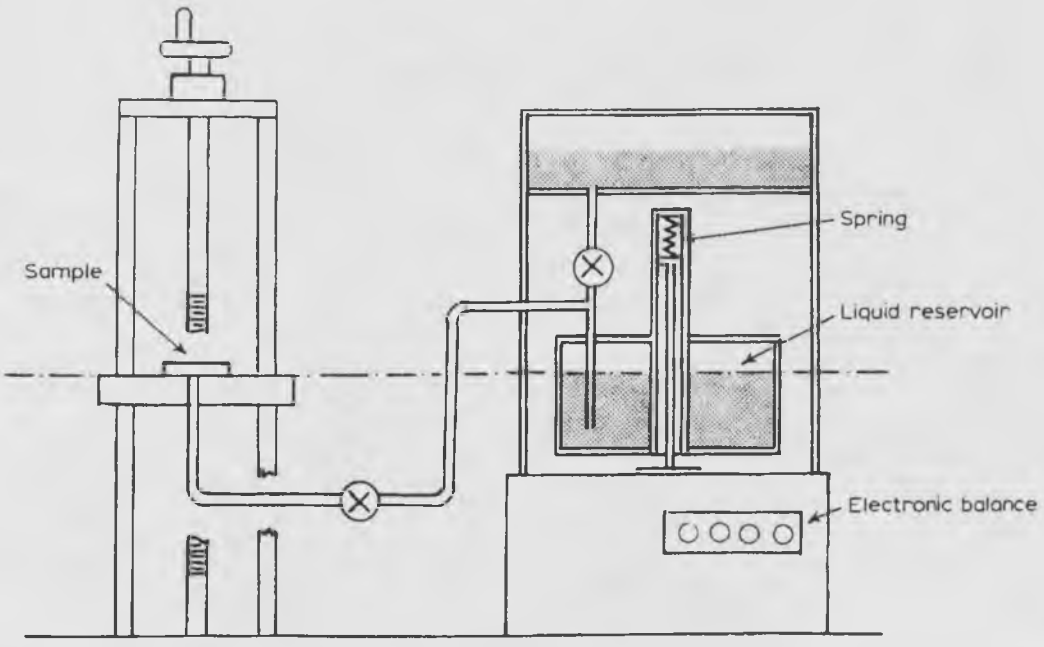

Figure 3. 7 Demand wettability test[206]

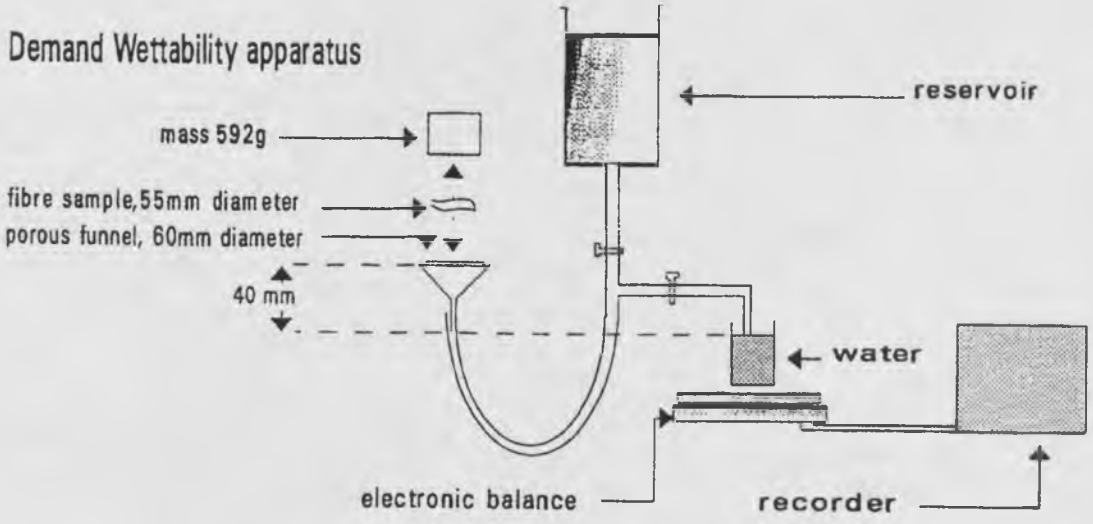

However, the method does not allow measurement of the anisotropy of liquid uptake by fabrics.

Figure 3.7 illustrates another instrument that uses an electronic balance and a computer to record and process the measurement data[206]. It indicates the dynamic variance of the liquid uptake process vs. time.

3.1.3.4 Measurement Using Image Analysis

Image analysis can be used to track the advancing fluid front. Two types of image analysis method have been reported. One is used in conjunction with the vertical strip test, the other is used for determining the in-plane radial liquid transport in the fabric plane. It has been used to measure the anisotropy of liquid transport in the fabric plane[124].

Figure 3. 8 Simple imaging method for liquid drop detection[205]

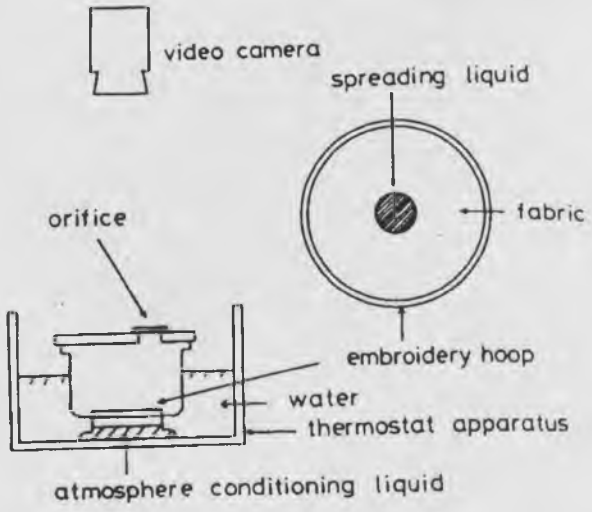

Kawase et al[205] used a simple image analyzer to determine the capillary spreading of liquids in the fabric plane (see Figure 3.8). The apparatus used in his studies comprised a desiccator with a 200 mm diameter. The cover had an orifice for inserting a micropipette. The liquid used was n-decane which was placed at the bottom of the desicator to minimize volatilization of the liquid spreading in the fabrics. To aid

observation of the liquid spreading in test fabrics, the n-decane was dyed with a 0.1% solution of Sudan IV or acid blue 9. The fabric was mounted on a 12.0 cm wooden ring (embroidery hoop) and placed into the desicator along with a stopwatch. The cell was covered and the fabric was left for at least 2 hours. A measured amount (0.05 to 0.20ml) of liquid was introduced onto the fabric by a micropipette. The area of the spreading liquid and the reading on the stopwatch were recorded simultaneously using a video camera (see Figure 3.8). The temperature of the apparatus was maintained at 25^0C during the experiment.

The spreading area was copied on to film, cut out, and weighed. A calibration curve was determined by recording areas of several known sizes and weighing the copied film in every experiment in order to determine the actual spreading area. The correlation coefficients of the calibration curves were reported to be higher than 0.999.

Image analysis allows capillary spreading in the fabric to be represented as a distribution of brightness levels. The profile of the distribution of the liquid concentration in the fabric could be obtained by calibrating the brightness or intensity values with liquid concentration levels in a fabric.

Image analysis is a convenient method and the results partially reflect the anisotropy of liquid transport through fabrics. However, it cannot be used to detect the liquid movement inside the fabric and its results do not indicate the weight of absorbed liquid either locally or over the total area of a fabric.

Other image analysis measuring methods involve in-plane radial flow measurement [124] (see Figure 3.9). The in-plane radial flow apparatus and the method of quantifying the

directional in-plane specific permeabilities of fabrics were introduced by Adams et al[124] and other researchers[125]. It is essentially a modified demand wettability method, where the porous plate method of introducing liquid has been changed to a point source supply. Arguably, it is the only existing method capable of measuring the dynamic anisotropy of liquid flow in fabric structures.

Figure 3. 9 Apparatus for measuring the liquid front in radial in-plane flow[124]

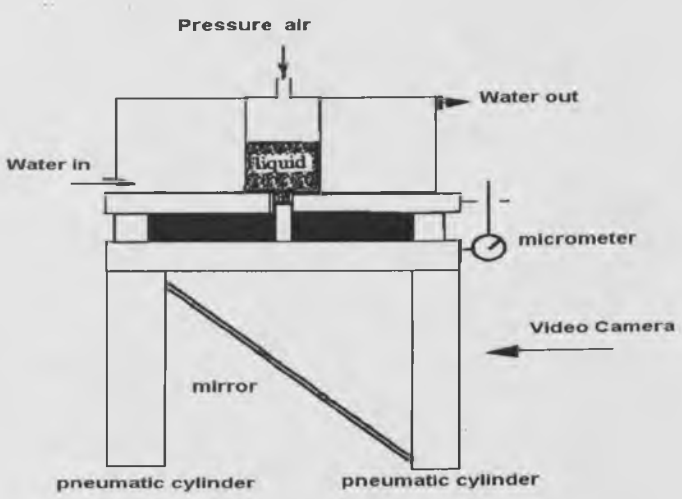

Figure 3. 10 Anticipated liquid front in radial in-plane flow measurement[124]

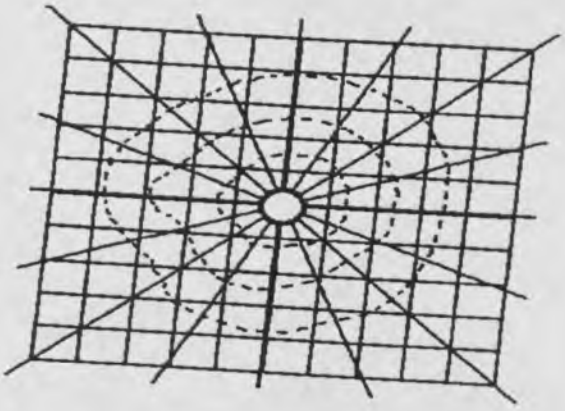

In the test, viscous liquid is forced by gas pressure to flow within a fabric sample. A mirror is positioned just below the apparatus so that the shape and the position of the radially advancing liquid front can be measured using an image analysis system (see Figure 3.10). In this way, the local and dynamic anisotropy of liquid transport through a fabric can be evaluated and the specific permeabilities can be calculated.

However, the method is unable to measure the liquid absorption since the results do not indicate the absolute fabric absorbency in terms of liquid weight or volume. The need to use high viscosity liquids rather than water and other low viscosity liquid is one shortcoming of this method. Adams et al[123, 124] did not establish if there is a difference between water and more viscous fluids when obtaining the specific permeability, although it was claimed that the directional permeabilities are independent of driving pressure, fluid viscosity and the number of fabric layers.

A further limitation of the method is that not all the liquid moving inside the fabric can be recorded by the method. This is particularly problematic for thick or uneven fabrics such as many nonwovens. Furthermore, the contact surfaces between the supporting plates and the fabric risks the formation of a long, wide capillary gap, along which liquid can move more rapidly than the liquid inside the fabric. This may lead to a false impression of the position of the advancing fluid front and its geometric shape with time.

3.1.4 Summary of the Requirements of a New Method for the Measurement of Liquid Transport in Nonwoven Fabrics

The dynamic measuring methods outlined in section 3.1.3 allow measurement of the variation in the liquid up-take by fabrics with time elapsed and they generally give more information about liquid transport through fabrics than steady-state measurements. However, none allow the determination of the anisotropy of liquid transmission in multiple directions simultaneously in terms of the uptake of fluid volume. This is required if comprehensive understanding of the liquid transport in nonwoven wound dressings is to be obtained. A device for the measurement of the anisotropy of liquid transport in this work should meet the following requirements:

1. Liquid transport in the fabric plane should be detected.
2. Real time measurement should be facilitated, i.e., dynamic monitoring of the liquid transport.
3. The measurements should be based on assessment of the variation in the volume of liquid transport (i.e., direct measurement).
4. Measurements of the liquid transport should be possible in multiple directions in the fabric simultaneously.
5. The system should be computer integrated.

In this work, a new computer-integrated apparatus for the real-time measurement of the volumetric flow rate in nonwoven fabrics was developed that meets these requirements and will now be described.

3.2 DESIGN OF THE SYSTEM

3.2.1 Description of the Capacitance Transducers

A photograph of the new system is shown in Figure 3.11 and a schematic diagram of the apparatus is shown in Figure 3.12.

Figure 3. 11 The capacitance measuring system for liquid transport in wound dressings

(a) Capacitance transducer system (mounted in the tube)

(b) The electronic circuit unit for signal conditioning

(c) An overview of the entire measuring system

The operation of the system is based on the principle that as liquid absorption by a fabric proceeds between two capacitance transducer plates there will be an increase in the capacitance of the transducer. The capacitance between each pair of capacitance transducer plates will be largely dependent on the dielectric constants of the materials between the two plates.

Essentially, an electrical capacitance field is created between two capacitance plates UP and LP (upper and lower plates) as shown in Figure 3.12(a).

Figure 3. 12 A schematic diagram of the capacitance transducers

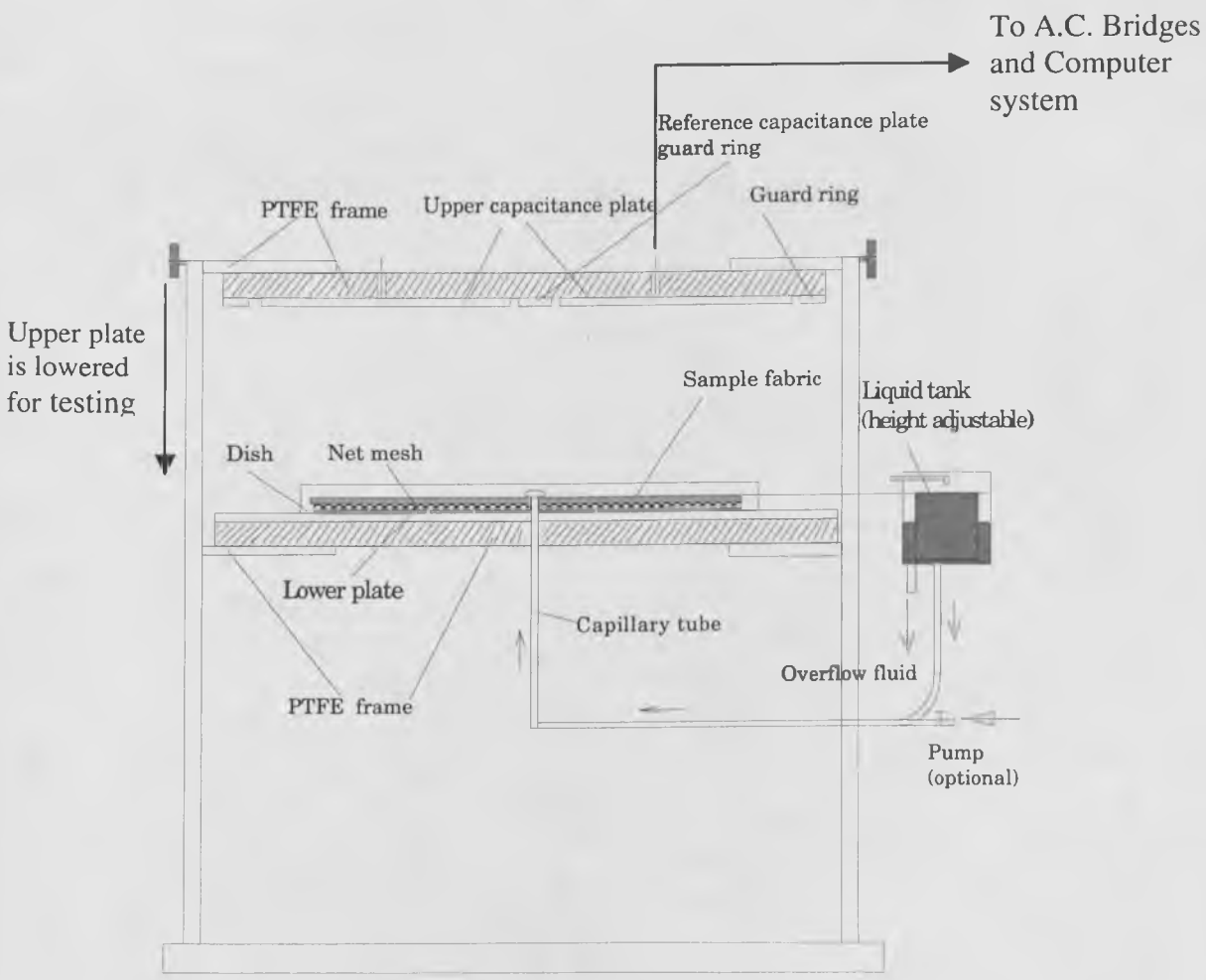

(a). Schematic diagram of the measuring instrument

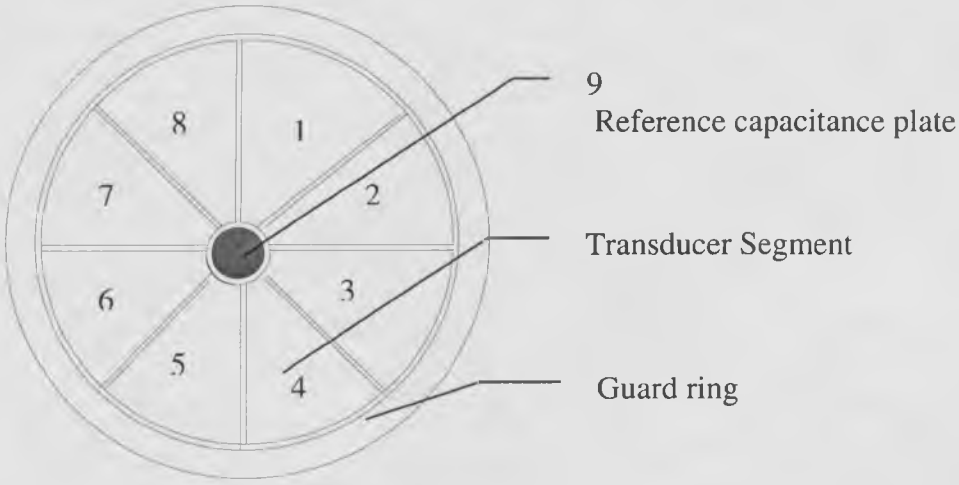

(b) Alignment of transducer segments in the upper plate of the capacitance system

The upper plate (UP) is made of stainless steel and is segmented. It consists of eight separate, equidistantly spaced transducers as shown in Figure 3.12(b). The lower plate (LP) is not segmented and also consists of thin stainless steel coated with Polytetrafluroethylene (PTFE). There are therefore eight points of measurement from the capacitance transducers in the system. Additionally, a circular plate is placed at the centre of the upper plate which is surrounded by the eight segments (see Figure 3.12(b)). Variations in the dielectric between the upper and lower plates (resulting from the absorption of water by the fabric) changes the capacitance value of the plates.

A plastic mesh is placed in a plastic dish located at the centre of the lower plate. A circular sample of fabric the same size as the dish is placed on the top of this mesh. In the centre of the dish is the liquid feed point. This consists of a fine metal tube on top of which is fitted a tiny perforated cap which is designed to allow uniform distribution of

the incoming liquid in all directions. Once the liquid is gradiually introduced into the fabric, it will spread radially from the point of liquid contact into the fabric.

In addition to water, the capacitance value is sensitive to external effects (e.g., air humidity). This is discussed and considered in section 3.7. In order to ensure stability of the capacitance value, the entire measuring system was mounted in a tube to eliminate the fugitive effects of external airflows. All testing was performed in a standard environment (20^0C, 65%RH).

3.2.2 Alignment of the Capacitance Segments

In the system, eight segments are arranged around a central point in eight different directions in the upper plate (see Figure 3.12(b)). Each segment comprises a thin stainless steel plate coated with a continuous layer of PTFE. The central circular transducer in the upper plate provides a reference signal during testing.

When the liquid transport in the fabric structure varies with the direction of the flow, the dielectrics of the fabric between the capacitance transducer aligned in that direction will be determined by the increase in the amount of the liquid retained in the same direction by the fabric. Accordingly, the capacitance of the transducer changes and this can be recorded.

3.2.3 Guard Ring Surrounding the Electrical Field

Guard rings were used to regulate the electrical field of the transducer segments so that the field flux was perpendicular to the lower plate at the extreme edges of the segments. To ensure that the electrical field between the two capacitance plates is perpendicular to

the surface of the plate at the edge of the plates, it was necessary to use a guard ring to transfer the fringing field of the capacitance plate to the edges of the guard ring[208].

The guard ring used in the system was made of a metallic ring of the same thickness as that of the capacitance segments, and was designed to surround the outside ends of the eight capacitance segments. The guard ring used was the same diameter as the bottom plate. The central segment (see Figure 3.12(b)) functions as another guard ring for the inner ends of the eight segments and diminishes fringing effects at the edge of the capacitance segments.

The guard ring had a similar potential voltage as the capacitance segments which it surrounded[208, 209]. The width of the outside guard ring was also found to be very important and it is believed that the outside dimensions of the guard ring should be around three times the radius of the working segments for operating efficiently[210, 211].

The straight sides of each adjacent segment were parallel and each segment was separated by a narrow and uniform air gap. The air gaps between each segment had to be as small as possible to eliminate the capacitance due to the thickness of the plates. The influence of the gap between two capacitance plates on the overall capacitance value has been explained by Maxwell and Kirchhoff[213].

3.2.4 Method of Introducing Liquid to the Fabric

The system can be used to measure two types of dynamic liquid transport in fabrics in up to eight different directions:

1. Liquid absorption (demand wettability).
2. Forced liquid transport under low hydraulic pressure.

There are four types of measurement that can be performed using the new system:

1. Real time liquid volumetric flow rate in eight different directions.
2. Anisotropy of the flow rate in forced flow (at a constant flow rate) in eight directions
3. Anisotropy of the specific permeability.
4. In-plane permeability in eight different directions in fabrics if the initial hydraulic pressure is known.

The liquid is introduced from a reservoir tank (which maintains a constant liquid head) into the fabric through a capillary tube. As shown in Figure 3.12 in the reservoir, there is an overflow section in which two cylindrical tanks are fitted concentrically on a vertical post. The use of two tanks allows the liquid pressure (fed to the fabric) to remain constant as the reservoir level decreases. These tanks can be set to the required level in order to maintain a constant liquid pressure. The amount of liquid absorbed by the fabric is then measured continuously by the capacitance transducers in eight directions simultaneously.

The rate at which liquid is introduced can be varied by changing the vertical position of the reservoir tank or alternatively, by the use of a peristaltic pump. The measuring system can be operated with flow rates in the range of 4 ml/min to 40 ml/min. The pump also allows the continuity of the flow to be varied as required.

3.2.5 Fabric Support Mesh

In order to eliminate the capillary gap that can exist between a wetted fabric and the face of the tray that supports it, a low surface-tension plain woven mesh fabric made of

hydrophobic continuous filament was placed between the test sample and the tray to isolate it from the tray.

3.3 ELECTRONIC COMPONENTS USED IN THE SYSTEM

3.3.1 Signal Conditioning Unit

Signal conditioning is concerned with converting the output from a sensor into a suitable form for signal processing so that it can be displayed or handled by the system. Some of its functionality may be summarised as follows[212]:

1. Transformation of the signal from the sensor into a suitable form for processing.
2. Adjustment of the signal amplitude and frequency.
3. Elimination or reduction of noise.

Several signal conditioning circuits were used and each had a different function. An A.C. bridge was used to convert the capacitance value coming from the capacitance transducer into voltage signals. Several analogue circuits were then adopted to decrease the noise and enhance the ratio of signal to noise, or to convert the A. C. signal to an analogue D. C. signal. The analogue signal was then converted to a digital signal suitable for computer processing.

3.3.1.1 Signal Amplitude Modulation and the Resistance-Capacitance A. C. Bridge

In the process of amplitude modulation, the signal from a transducer is multiplied by a carrier signal of constant frequency and amplitude. It offers several advantages in data transmission (stability, low power and noise suppression) compared to frequency

modulation. The carrier signal can have any periodic form, such as a sinusoid, square wave, saw-tooth or triangle. The only requirements for mixing the carrier and transducer signals is that the frequency ω_c of the carrier signal must be much higher than the frequency ω_i of the transducer signal. The transmission at high frequency permits the use of high-pass filters to eliminate noise signals that usually occur at much lower frequencies.

An A.C. bridge was adopted and proved to be an excellent signal deflection method with amplitude modulation to pick up the resulting voltage signal from the change in capacitance. The variation of the transducer capacitance due to changes in the amount of liquid absorbed by the fabric was initially a weak low frequency signal while the background noise was strong and had low frequency. It was necessary for the amplitude of the signal to be larger so that it could be distinguished from the noise. A high voltage carrier signal of high frequency was needed to carry the weak signal to the next stage.

The basic bridge used (shown in Figure 3.13) was a resistor-capacitance AC bridge consisting of two resistors and two capacitors. The output of the bridge varied with changes in the measured capacitance, and the frequency of the output was a combination of the carrier signal and the frequency of the change in the capacitance itself. Since there were nine individual signal channels to be transmitted, the bridges in the system were constructed as indicated in Figure 3.14.

Figure 3. 13 Schematic diagram of a basic A.C. bridge

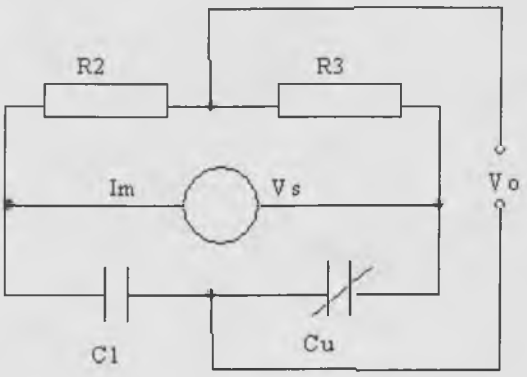

Analysis of the circuit to find the relationship between the output voltage of the bridge, V_0, and the capacitance value of the transducer, C_u, is greatly simplified if it is assumed that the current I_m is very small. The output voltage of the bridge, V_0 in the capacitance bridge will be[213]:

$$V_0 = Vs\left(\frac{C_1}{C_1 + C_u} - \frac{R_3}{R_2 + R_3}\right) \qquad (3.3.1)$$

Where, C_1, R_2 and R_3 are the values of the known standard capacitances and resistances in the bridge, V_s and V_0 are the voltage of signal generator and the output voltage of the bridge respectively. I_m is the current as shown in Figure 3.13.

In Figure 3.14, two standard resistors and two standard capacitors were used to form an A.C. bridge, and the capacitance transducers were then each paralleled with standard 10 pF capacitors. A signal generator was used to provide an input signal to the bridge of 10 kHz, through which the output signal from the capacitance transducers was conditioned and converted into a voltage signal. Since the capacitance values of the transducers varied with the amount of liquid retained in the fabric and the output voltage of the

bridges was approximately linearly proportional to the capacitance value of the transducers, the outputs of the bridges were linearly proportional to the liquid absorption.

Figure 3. 14 Schematic of the A.C. bridge used in the system

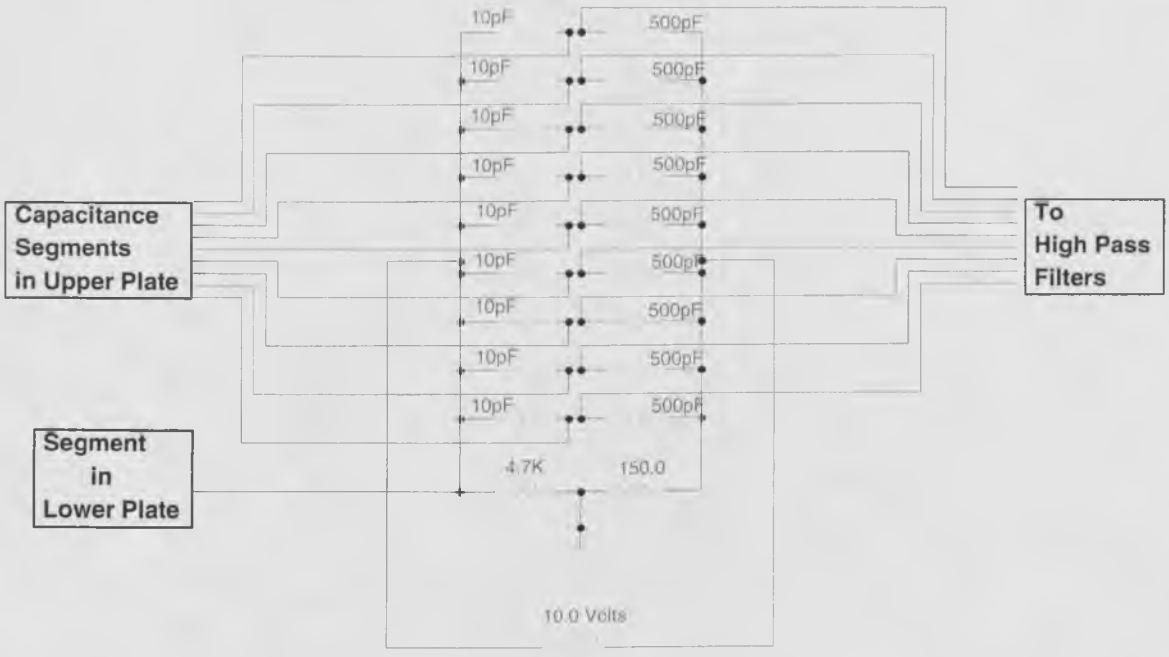

Because the carrier frequencies of 10 to 100 times the signal frequencies were required in demodulation to eliminate the carrier signal, the frequency of the carrier signal, (which is from the signal generator), was set as high as 10 kHz, while the frequency of the variance of the capacitance value due to liquid absorption by the fabric was lower than 10 Hz. Another reason for using high frequency for the bridge was the necessity to generate a sufficiently large signal voltage while the value of the capacitance transducer is small (about 10 pF).

3.3.1.2 From Signals to Digital Data[212, 213]

The signal from the transducer may be combined with noise or other parasitic signals, and these unwanted signals need to be eliminated with an appropriate filter. At the same time it is important to transmit the transducer signal without significant attenuation or distortion. Then the amplified analogue data is obtained after output signals from each bridge being amplified, demodulated and the noise associated with it being filtered in signal conditioning. The electronic set-up is shown in Figure 3.15 and Appendix II.

Figure 3. 15 Schematic of the electronic components used in the system

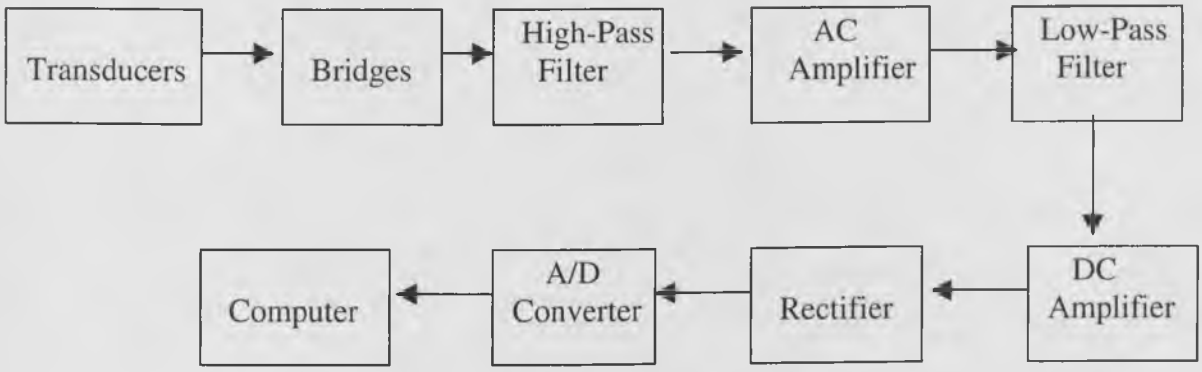

The analogue data of the results from the nine channels in the system was then converted into digital data and collected by a computer via a data acquisition board, PC30F/G[214]. The data acquisition board specification for the analogue inputs included[214]:

1. A maximum sampling rate for analogue inputs of 100 kHz.

2. Multiple data channels and multiplexing to perform simultaneous sampling from 1 to 16 input.

3. Resolution is often specified as the number of bits that the analogue to digital converter uses to represent the analogue signal or the fraction of the analogue signal that represents a change of 1 bit. The resolution of the board was specified as 12 bits, or 1 in 4096.

4. The voltage range in this board were software selectable from $\pm 5V$, $\pm 10V$ and $0 \sim 10V$.

5. The gain available from the amplifier on the board was also selectable and this determined the smallest detectable change in the input analogue voltage. If the gain is 10 and the range is 0 to 10 V for the 12 bit board, the smallest detectable input voltage would be $10/(10*2^{12})=23.4\ \mu V$.

3.4 SOFTWARE FLOW CHART

The F/G series boards can be programmed in most DOS and Windows programming languages, and they can also be controlled using high-level function calls[215]. The software flow chart for the system is given in Figure 3.18.

The major modules of the system are: Board Initialisation, Data Acquisition, Data Processing, Display, and Human/Machine Interfacing.

Figure 3. 16 Software flow chart for the system

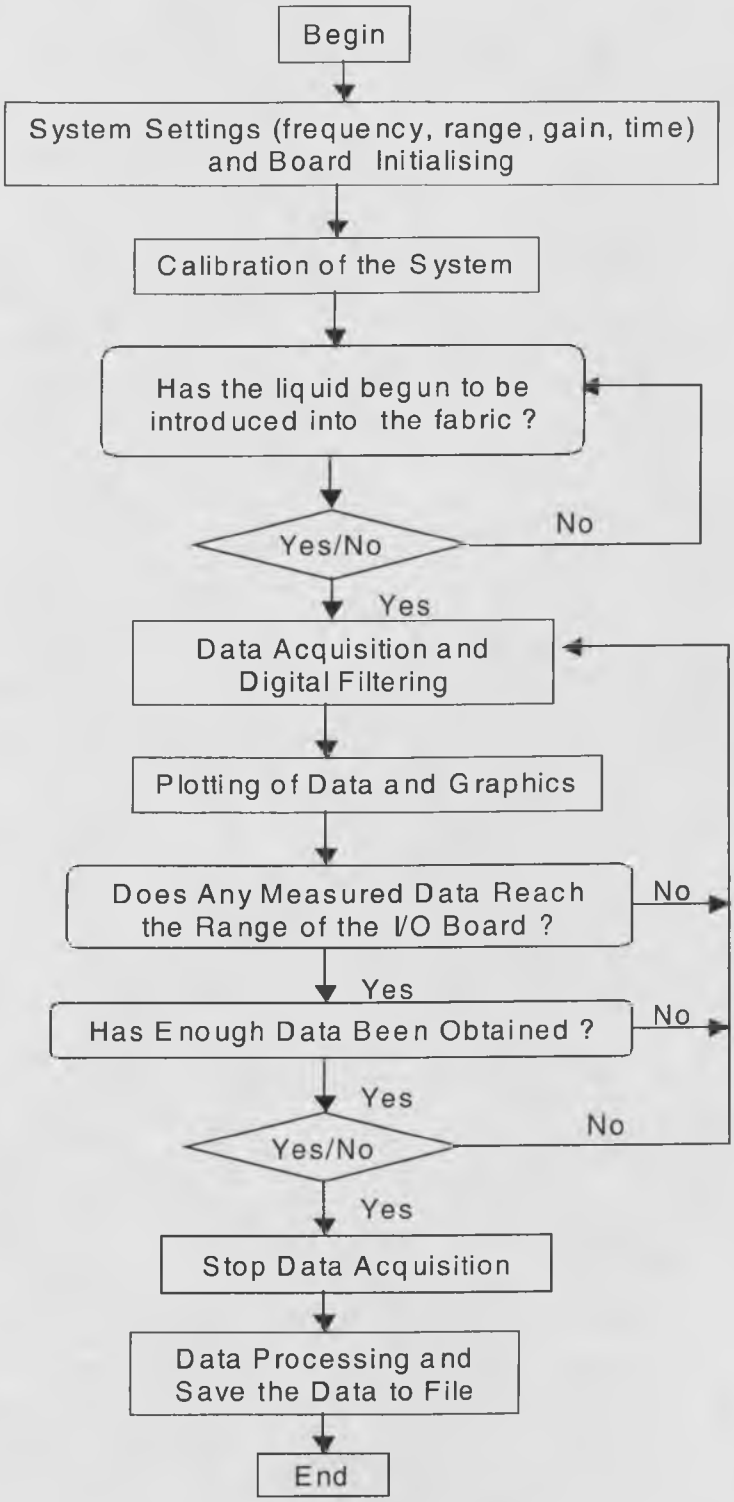

3.5 OPERATING PRINCIPLES OF THE SYSTEM[216]

3.5.1 Capacitance and Dielectric Constant of Materials

It is well known that there is a large difference between the dielectric constants of air (ε_r=1), commonly used textile polymers (ε_r=2-6) and water (ε_r=70-80). The electrical capacitance of a system is dependent on the dielectric constant of the material. The present system consists of two parallel capacitance plates spaced equidistantly along their length. When the space between the two parallel capacitance plates contains nonwoven material, the value of the capacitance, C, will be[208]:

$$C = \varepsilon_0 \varepsilon_r A / D \qquad (3.5.1)$$

Where,

$\varepsilon_0 = 8.854 * 10^{-12}$ (F/m) = the dielectric constant of a vacuum.

ε_r = relative dielectric constant of the dielectric material.

A = area of the capacitance plate.

D = distance between the two capacitance plates.

If, in addition to fibre and air, there are other materials in the field between the two capacitance plates, the capacitance value of the system, C, will be[208]:-

$$C = \frac{A\varepsilon_0}{\left(\frac{d_1}{\varepsilon_1} + \frac{d_2}{\varepsilon_2} + \frac{d_3}{\varepsilon_3} + \ldots + \frac{d_n}{\varepsilon_n}\right)} \qquad (3.5.2)$$

where, d_1 d_2, d_3 and d_n are the thicknesses of the first, second, third, and n_{th} dielectric materials respectively. The terms ε_1, ε_2, ε_3 and ε_n are the relative dielectric constants of these dielectric materials respectively.

If a nonwoven fabric is placed between the two capacitance plates, assuming its area, A, is equal to the area of the capacitance plate, the resulting capacitance, C_0, of the transducer, will be[208]:

$$C_0 = \frac{A\varepsilon_0}{\left(D - d(1 - \frac{1}{\varepsilon_r}) - d_1(1 - \frac{1}{\varepsilon_1}) \right)} \qquad (3.5.3)$$

$$D = d + d_0 + d_1$$

Where,

D = distance between the two capacitance plates.

d = thickness of the fabric.

d_0 = thickness of the air layer.

d_1 = thickness of any other materials in the field between the two plates.

ε_r = dielectric constant of the fabric.

ε_1 = dielectric constant of any other material in the field between the two plates.

If water is gradually introduced into the fabric (assuming the area of the fabric holding water is A_X), because of the effect of polarization of water on the fibre, the dielectric constant of the completely saturated fabric (which is a mixture of wetted fibre and water) may be taken to be nearly the same as the dielectric constant of water, m[95]. The liquid

transport in the z-direction of the fabric is ignored because the fabric is thin. Thus, the capacitance value of the transducer (containing wet fabric), C_X, will be as follows:-

$$C_X = \frac{A_X \varepsilon_0}{\left(D - d(1-\frac{1}{m}) - d_1(1-\frac{1}{\varepsilon_1})\right)} + \frac{(A - A_X)\varepsilon_0}{\left(D - d(1-\frac{1}{\varepsilon_r}) - d_1(1-\frac{1}{\varepsilon_1})\right)}$$

$$= C_0 + A_X\left(\frac{1}{a} - \frac{1}{b}\right) \qquad (3.5.4)$$

Where a and b are constants depending on the particular fabric sample.

$$a = \frac{\varepsilon_0}{\left(D - d(1-\frac{1}{m}) - d_1(1-\frac{1}{\varepsilon_1})\right)} \qquad (3.5.5)$$

$$b = \frac{\varepsilon_0}{\left(D - d(1-\frac{1}{\varepsilon_r}) - d_1(1-\frac{1}{\varepsilon_1})\right)} \qquad (3.5.6)$$

Therefore, the change in the capacitance value, ΔC_X, due to the introduction of water may be given as follows:-

$$\Delta C_X = C_X - C_0 = \Delta A_X\left(\frac{1}{a} - \frac{1}{b}\right) \qquad (3.5.7)$$

If $\psi = \left(\frac{1}{a} - \frac{1}{b}\right)$ Equation (3.5.7) can be rewritten as:

$$\Delta C_X = \Delta A_X * \psi \qquad (3.5.8)$$

From equation (3.5.8), it is clear that the capacitance value varies only with wetting and it is linearly related to the wetted area of the fabric. Changes in the capacitance value can therefore be used as a basis to study the liquid transmission in fabrics. This is a

simple approach that avoids the difficulty of selecting an appropriate model for a specific fabric in order to determine the dielectric constant[95]. In this approach, the relative changes in capacitance are used to study the liquid transport. Using the new system, it is possible to do this in different in-plane directions simultaneously.

3.5.2 Calculated Capacitance of the Transducer

Substituting the particular structural parameters of the transducers in the new system into equation (3.5.4), the capacitance of the transducer (as liquid is introduced) can be calculated as follows:-

$$C = (8.854 * 10^{-12}) \left[\frac{\pi (X^2 - R_0^2)}{\left((D - d) + \frac{d}{m} \right)} + \frac{\pi (R_f^2 - X^2)}{\left((D - d) + \frac{d}{\varepsilon_r} \right)} \right] \qquad (3.5.9)$$

This assumes that the system contains only air and the test fabric. Where D is the distance between the two capacitance plates, d is the thickness of the fabric, X is the radius of the circle of the liquid advancing front, R_0 and R_f are the liquid source point radius and the fluid advancing front radius respectively. The dielectric of water is denoted as m, and the terms ε_0 and ε_r are the dielectric constants of the air layer and the fabric respectively.

In the new measuring system, if d= 2mm, $\varepsilon_0 = 1$, $m = 80$, $\varepsilon_{fibre} = 5$, $\varepsilon_r = 1.5$, R_f= 35mm and R_0 = 5.5mm, then the corresponding capacitance values of the transducers are shown in Table 3.1.

Table 3. 1 Calculated capacitance of the transducers in the system

C (pF)		*X* (mm)			
		5.5	11	21	31
D (mm)	10	0.445	0.450	0.470	0.5031
	5	0.958	0.990	1.105	1.290
	3	1.779	1.960	2.596	3.628

3.6 CALIBRATION OF THE SYSTEM

In the process of calibrating the signal from the segmented transducers, the differences in the signals were first determined. To achieve this, the liquid transport in an isotropic (or nearly isotropic) structure was measured using the system. The data from each transducer was then used to obtain the ratio of gain of each transducer channel to the first transducer channel.

Glass filter paper is a comparatively uniform fibrous porous structure. The maximum differences of radius in the radius of the advancing liquid front circle in such fabrics in each direction is reported to be less than 10%, and this may be taken to be nearly isotropic structure[201]. The specification of the paper used for calibrating the system is given in Table 3.2.

Table 3. 2 Whatman® filter paper properties used in the calibration[217]

Type	Grade Number	Filter Speed	Thickness (mm)	Weight (g/m^2)
Qualitative Paper	1	Medium Fast	0.18	87

3.7 FACTORS AFFECTING THE MEASURED RESULTS AND SENSITIVITY OF THE SYSTEM

There are structural heterogeneities in nonwoven fabrics, such as spatial variations in the arrangement of fibres. This variation is evident in areal density, fibre orientation, fibre crimp, and in the degree of fibre entanglement. In this section, only the uniformity of the fabric density or the variations in the fabric thickness are considered.

3.7.1 Fabric Thickness

The influence of fabric thickness on the capacitance of the transducer can be obtained from Equation (3.5.4). If D=5mm, A=64 cm^2, d_0=1mm, d_1=1mm, m=80, $\varepsilon_0 = 8.854\times10^{-12}$, $\varepsilon_r = 2.5$, $\varepsilon_1 = 3$, when the fabric thickness is either d_3 =2mm or d_4 =4mm, the capacitance of the transducer will be as indicated in Table 3.3.

Table 3. 3 Capacitance value of transducers for fabrics of different thickness

A_X (cm^2)	C_1 (d_3=2mm) (pF)	C_2 (d_4=4mm) (pF)	C_1/C_2
5	0.89	1.20	1.35
10	0.90	1.26	1.40
20	0.93	1.38	1.49
40	0.98	1.61	1.65
60	1.02	1.85	1.80

From Table 3.3, it is clear how variations in fabric thickness lead to a change in capacitance. To avoid problems in testing, the new instrument is designed such that the distance between the two capacitance plates can be adjusted for different fabric thickness in the range 1 to 6 mm.

3.7.2 Uniformity of Fabric Thickness

If the nonwoven fabric varies in weight uniformity, the resulting change in the capacitance of the transducer can be calculated from Equation (3.5.3). If the thickness of a small area A_u is d_u and the thickness of the other area in the fabric plane is d ($d \neq d_u$), (where the whole area of the fabric is assumed to be saturated), the change in capacitance resulting from this change in fabric area and fabric thickness, C_u, can be deduced from Equation (3.5.3) as follows:-

$$C_u = \frac{A_u \varepsilon_0}{\left(D - d_u(1 - \frac{1}{m})\right)} \qquad (3.7.1)$$

Where m is the dielectric constant of the wetted fabric.

The total capacity of the transducer, C, can also be deduced from Equation (3.5.3):-

$$C = \frac{A_u}{\left(D - d_u(1 - \frac{1}{m})\right)} + \frac{A - A_u}{\left(D - d(1 - \frac{1}{m})\right)} \qquad (3.7.2)$$

Thus,

$$\frac{C_u}{C} = \frac{1}{1 + (\frac{A}{A_u} - 1)\frac{(1 - \frac{d_u}{D}) + \frac{d_u}{D}\frac{1}{m}}{(1 - \frac{d}{D}) + \frac{d}{D}\frac{1}{m}}} \qquad (3.7.3)$$

Examples of the effect of fabric thickness uniformity on the capacitance values are shown in Table 3.4. Usually in practice, the ratio between the maximum thickness and the average thickness of the fabric $\frac{d_u}{d}$ does not exceed $\frac{3}{2}$, and therefore, in order to

limit the error resulting from unevenness in fabric thickness, it is very important to ensure the ratio remains within this limit.

Table 3. 4 The effect of uniformity of fabric thickness on the capacitance of the transducers

Distance $D\ (mm)$	Fabric thickness variation $d_u\ (mm)$	Small area in fabric A_u	Dielectric constant of Water	Capacitance variation $\frac{C_u}{C}(\%)$
$d=\frac{1}{2}D$	$d_u=\frac{2}{3}D$	$A_u=10\%A$		13.3%
$d=\frac{1}{3}D$	$d_u\approx D$			75.0%
	$d_u=\frac{1}{2}D$		$m=80$	6.9%

3.7.3 Fabric Placement in the System

A further source of potential error in capacitance measurements arises if there is an uneven distribution of the sample in the field of the condenser. This has been considered by Moorhouse[218]. Figure 3.17 represents an extreme condition in which one end of a damp material lies close to the upper plate, and the other end of the fabric lies close to the lower plate. In practice, such an arrangement would behave like two capacitances, C_1 and C_2 in series. The section of material, x-y, would have high resistance with R joining the two capacitances. The capacitance, C_1, is formed by half the material and the upper plate, and the capacitance, C_2, by the rest of the material and the lower plate (assuming that the material is sufficiently damp to act as a conductor of low resistance).

In this case, the capacitance value can be many times (>10) higher than that obtained when the fabric is arranged totally flat[218].

Figure 3. 17 Extreme placement of wetted fabric between capacitance plates

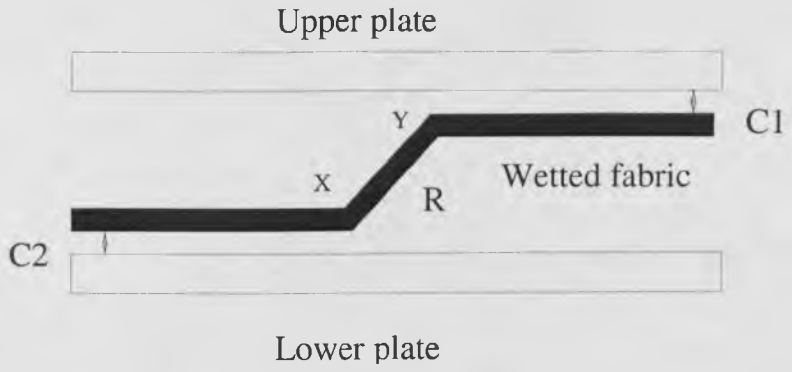

3.8 MEASUREMENT OF THE ANISOTROPY OF LIQUID TRANSPORT IN FABRICS USING THE SYSTEM

3.8.1 Measurement Procedure

The system is first pre-warmed for about thirty minutes before testing begins. The preconditioned sample fabric is then placed on the plastic mesh between the transducers. The liquid pressure is then set to the required level by fixing the height of the water tank.

After completing the calibration and pre-setting the test parameters in the system (data acquisition frequency, testing duration, sample specifications and liquid properties), the capacitance of the dry fabric is automatically measured. Firstly, the system monitors the variation of the capacitance value of the central capacitance transducer before the liquid

is introduced into the fabric. As liquid is introduced into the fabric from the central point, the capacitance value of the central capacitance transducer increases (which is

Figure 3. 18 Screen shot of the new measurement system

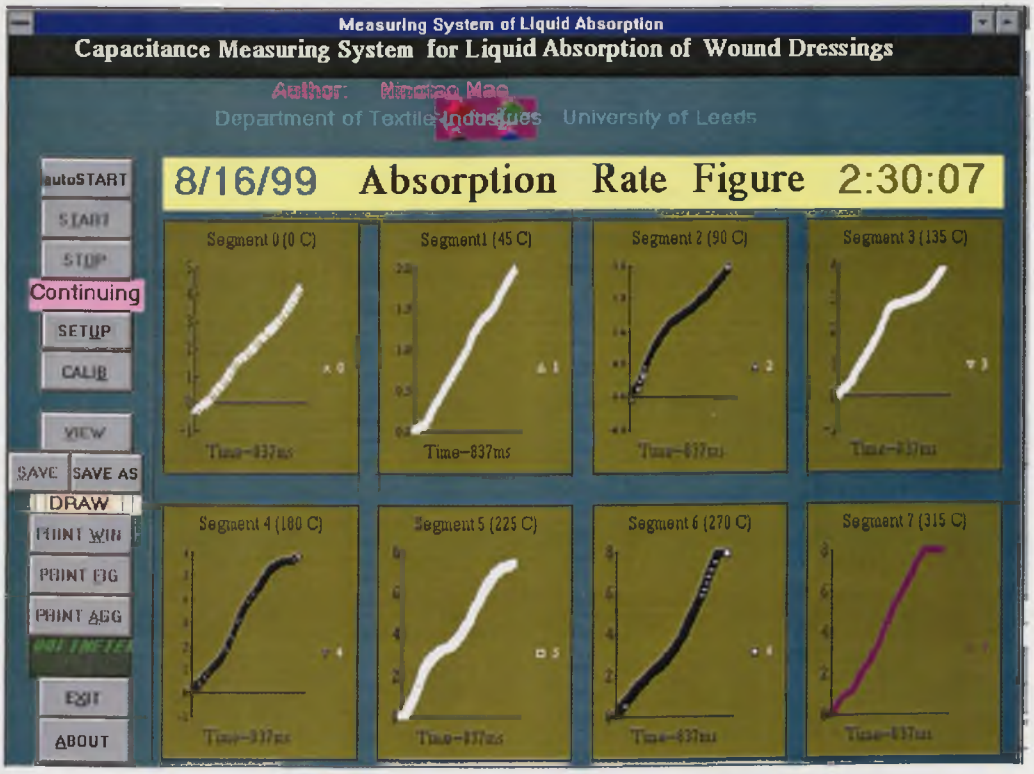

detected by the computer), and the data acquisition process begins. The data in each data channel (representing the variation of each capacitance transducer) is sequentially collected, and the amount of liquid transport in different directions in the fabric plane can then be monitored in real time and is shown on the monitor. When the preset testing time is reached, the data acquisition process is automatically stopped and the introduction of liquid is stopped manually. If needed, the wetted fabric and the dry fabric are weighed using an electronic balance and the weight of the liquid retained by the fabric is obtained. All the measured results of liquid transport in different directions

in the fabric are saved in a file and the results are displayed graphically (see Figure 3.18).

3.8.2 Description of the Measured Results

Using the new system it is possible to measure the change in volume of liquid retained by fabrics in different planar directions and therefore it is possible to characterise the anisotropy of liquid transport. Extensive testing has been carried out to validate the method and typical results are shown in Figure 3.19(a) which illustrate the detailed information that may be obtained. In this particular example, the results refer to a current commercially available wound dressing fabric composed of 100% viscose rayon in a monolithic needle punched structure. In Figure 3.19(b) the absolute liquid absorption and the rate of change in the liquid absorption versus time have been obtained in each direction in the fabric. Also, the rate of change in the liquid transport under external hydraulic pressure versus time in each direction in the fabric can be measured (see Figure 3.19(c)). In Figure 3.19, it should be noted that the rate of absorption in each direction is not identical. The plot (labelled number 9) is the measured change in absorption with time for the reference transducer located immediately above the fabric at the introduction point of the liquid. With reference to Figure 3.19(a), it is apparent that there are two phases in the central area of the fabric. Initially, when the liquid is introduced into the fabric from the source point, the central area of the fabric is not saturated and the absorbency of the fabric continuously increases with time. After a certain period of time, when the fabric in this central area is saturated, the volume of liquid in the fabric in the central area remains constant as a

Figure 3. 1 Example of the measured results from the dynamic testing system for a commercial nonwoven wound dressing fabric

(Sample fabric: 100% viscose rayon, needlepunched, fabric weight =120g/m^2)

(a) Dynamic liquid absorption in a polar system

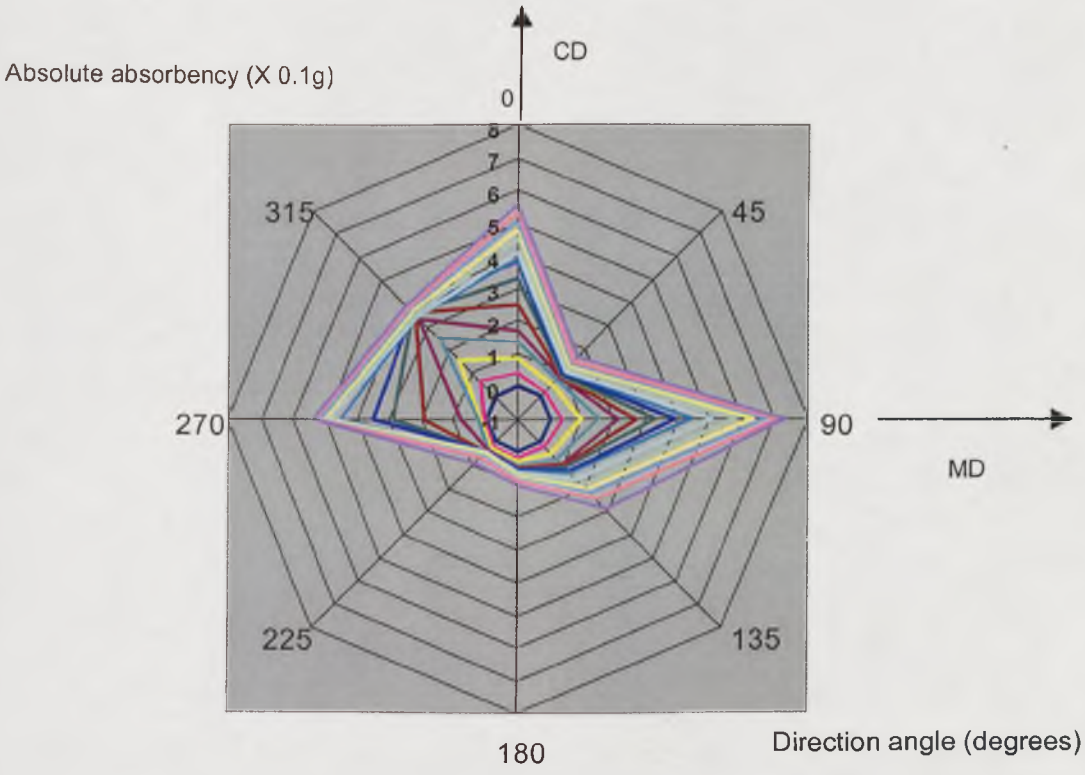

(b) Dynamic liquid absorption in a Cartesian system

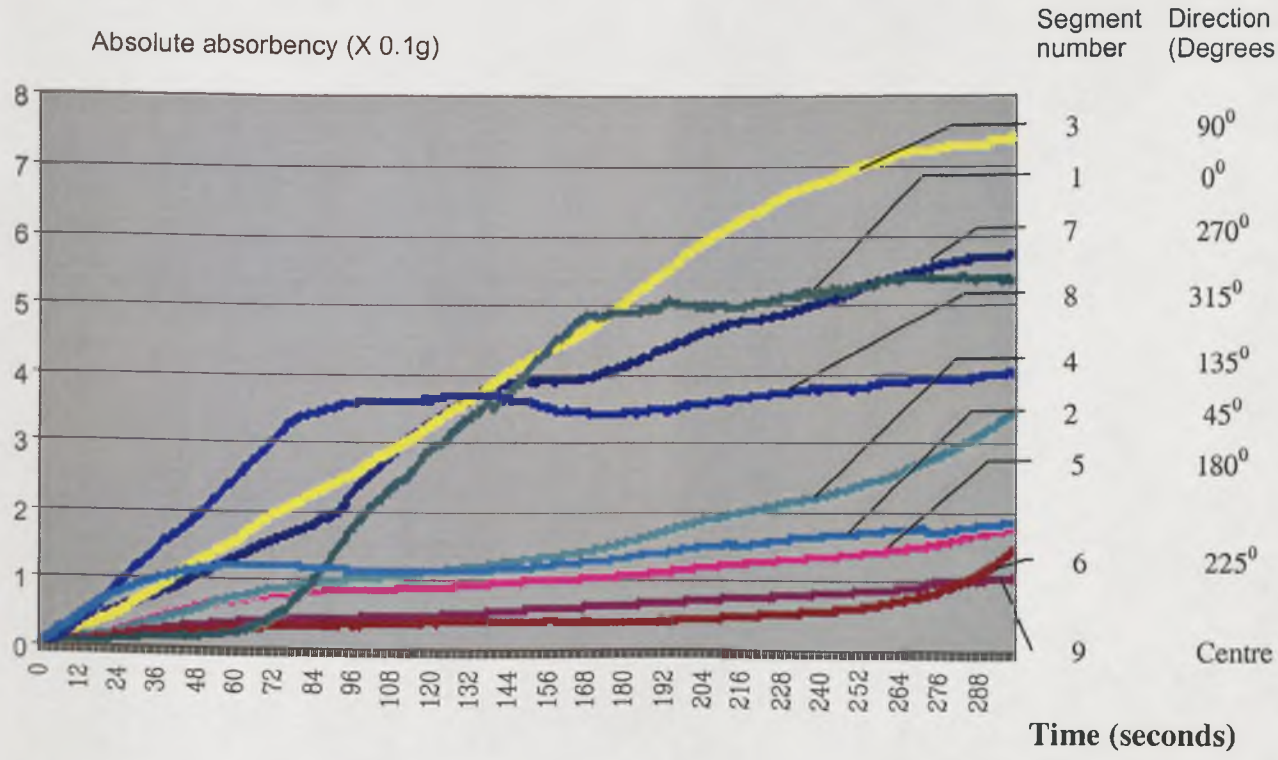

(c) Dynamic results of forced liquid flow in a Cartesian system

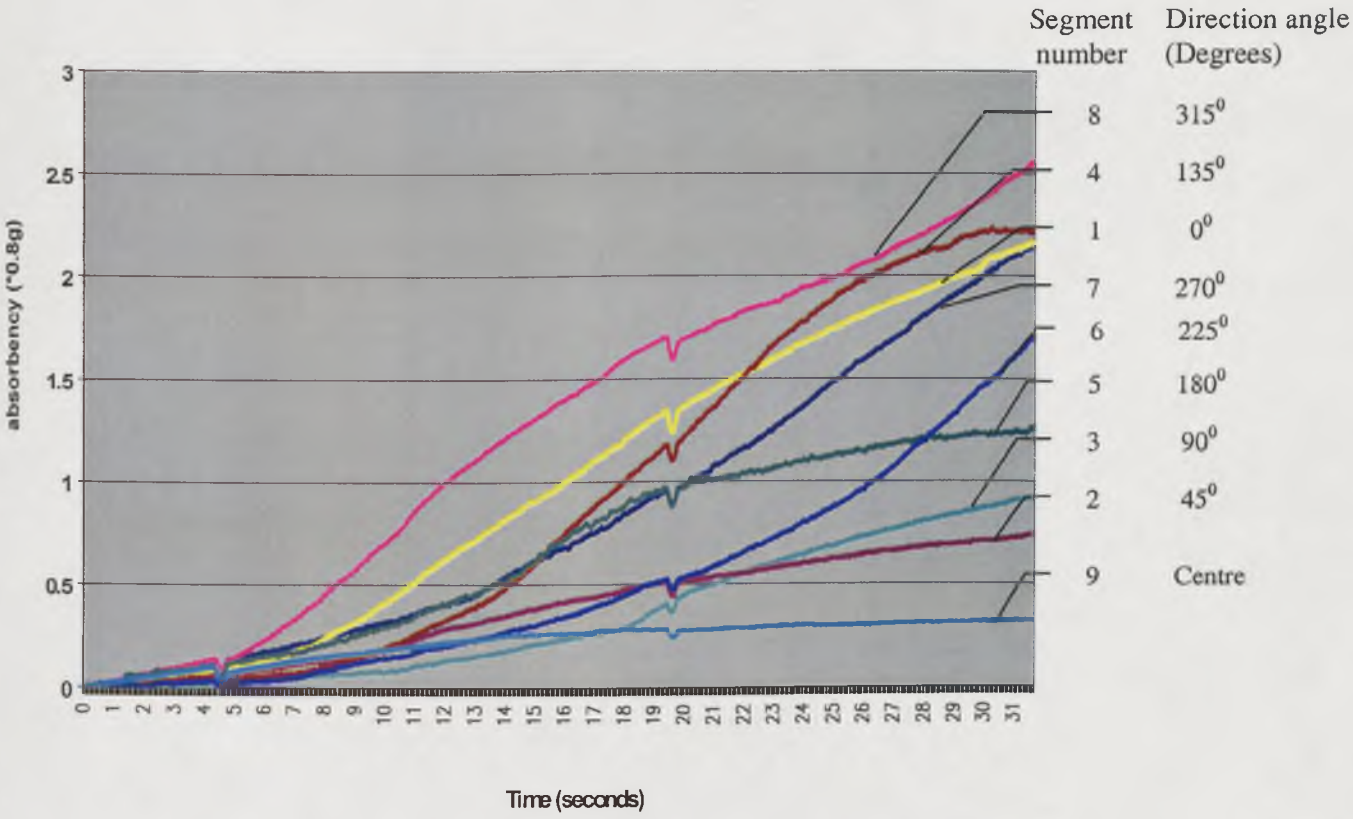

function of time. In combination with an electronic balance, the measured results from the new system can be used to obtain the true fabric absorbency, the fabric absorption rate, the anisotropy of the fabric absorption rate, and the saturation time. In forced liquid flow conditions, the permeability and anisotropy of permeability of the fabric can also be obtained.

3.8.3 Measurement of the Anisotropy of Permeability and Liquid Absorption

The anisotropy of permeability can be determined using data from the new system when liquid is forced by external pressure through the fabrics. The anisotropy of liquid absorption can be determined when the liquid is absorbed on-demand and spreads through the fabric by means of capillary pressure. All measurements were conducted using standard conditions (temperature $=20^0C \pm 2^0C$, humidity $=65\% \pm 2\%$).

When measuring the anisotropy of permeability, the forced flow through the fabric was maintained at a constant volumetric feeding rate. The liquid feed rate (ml/min) should be several times higher than the absorption rate of the fabric in order to maintain an external hydraulic pressure high enough to eliminate the effect of capillary pressure[124]. The liquid feed rate in the experiments ranged from 15 to 30 ml/min.

When measuring the anisotropy of liquid absorption, the external hydraulic pressure produced by differences in the height between the water level and the fabric plane was reduced to zero or to slightly negative by adjusting the height of the water tank in the system.

3.9 ANALYSIS OF DATA PRODUCED BY THE NEW SYSTEM

3.9.1 Two-Dimensional Liquid Flow in Isotropic Structures

The in-plane permeabilities of a two-dimensional isotropic porous medium are identical in all directions. A general analysis of two-dimensional liquid flow in isotropic porous structures under constant pressure and constant volumetric flow rate has been given by many researchers[124, 170, 219, 220, 221].

3.9.1.1 Liquid Flow Under Constant Pressure

The boundary conditions for liquid flow under constant pressure (P_0) are as follows:

$$P = P_0 \text{ at } R = R_0 \text{ and } P = 0 \text{ at } R = R_f \qquad (3.9.1.1)$$

Where P_0 is the constant inlet pressure, R is the advancing liquid front radius, R_0 is the inlet hole radius, and R_f is the flow front radius. The solutions for the pressure gradient and pressure fields are[170]:

$$\left(\frac{dP}{dR}\right)_{R=R} = -\frac{P_0}{R\ln\left(\frac{R_f}{R_0}\right)} \qquad (3.9.1.2)$$

$$\text{or } \frac{P}{P_0} = 1 - \frac{\ln\left(\frac{R}{R_0}\right)}{\ln\left(\frac{R_f}{R_0}\right)} \qquad (3.9.1.3)$$

$$\text{and } P_f - P_0 = -\frac{Q\eta}{2\pi dk}\ln\left(\frac{R_f}{R_0}\right) \qquad (3.9.1.4)$$

Where Q is the volumetric flow rate, d is the fabric thickness, k is the specific permeability, and η is the fluid viscosity.

The relationship between time, t, and the position of the liquid front, R_f, can be obtained from the following mass balance equation[221]:-

$$\int_{t_1}^{t_2} Q(t)dt = (1-\varepsilon)\pi(R_f^2 - R_0^2)d \qquad (3.9.1.5)$$

where t is time and $Q(t)$ is the volumetric flow rate (g/s*m^3) at the moment t.

The superficial velocity of the advancing liquid front with the boundary conditions shown in (3.9.1.1) is given by Adams[124], Scheidegger[170], Collins[219], Muskat[220] and Chan et al[221] as follows:-

$$\frac{dR_f}{dt} = \frac{k}{(1-\varepsilon)\eta}\frac{P_0}{R_f\ln\left(\frac{R_f}{R_0}\right)} \qquad (3.9.1.6)$$

Where $P = P_0$ at $R = R_0$ and $P = 0$ at $R = R_f$.

3.9.1.2 Liquid Flow at a Constant Volumetric Flow Rate at the Liquid Source Point

The boundary conditions at a constant volumetric flow rate are as follows[221]:-

$$\left(\frac{dP}{dR}\right)_{R_0} = -\frac{Q\eta}{2\pi R_0 dk} \quad \text{at } R = R_0 \text{ and}$$

$$P = 0 \quad \text{at } R = R_f \qquad (3.9.1.7)$$

Where Q is the inlet volumetric flow rate and d is the fabric thickness. The pressure gradient, $\left(\frac{dP}{dR}\right)$, and the pressure fields, $(P_f - P_0)$, for liquid flow at a constant volumetric flow rate are[221]:-

$$\left(\frac{dP}{dR}\right)_R = -\frac{Q\eta}{2\pi R dk} \quad \text{or} \quad P = \frac{Q\eta}{2\pi dk}\ln\left(\frac{R_f}{R}\right) \qquad (3.9.1.8)$$

$$\text{and } P_f - P_0 = \frac{Q\eta}{2\pi dk}\ln\left(\frac{R_f}{R_0}\right) \qquad (3.9.1.9)$$

The relationship between time, t, and the position of the liquid flow front, R_f, obtained from the mass balance analysis is:-

$$t = \frac{(1-\varepsilon)\pi(R_f^2 - R_0^2)d}{Q} \qquad (3.9.1.10)$$

3.9.2 Two-Dimensional Liquid Flow in Anisotropic Structures

Compared to isotropic structures, two-dimensional liquid flow in anisotropic structures is more complex. A general description of liquid flow through a thin anisotropic nonwoven fabric (shown in Figure 3.22) can be envisaged as a laminar, pseudo-steady

state process in which liquid radially spreads through a homogenous fibrous medium. Initially, liquid enters the fabric from a small point source. In anisotropic structures, the shape of the advancing front of the liquid will be elliptical in shape[202]. This shape is governed by the principle permeabilities of the fabric and the characteristic angle ϕ. The liquid flow is assumed to be steady-state and the distribution of the liquid driving pressure is independent of time.

Such laminar, incompressible liquid flows through porous materials can also be described by two-dimensional Darcy's law and the general equation of continuity[170]. The general form of Darcy's law and the equation of continuity are shown as follows:-

$$v = -\frac{k}{\eta}\nabla p \qquad (3.9.2.1)$$

$$\nabla v = \nabla(k\nabla p) = 0 \qquad (3.9.2.2)$$

Figure 3. 20 In-plane radial liquid flow and the direction of principal permeabilities in a thin nonwoven fabric

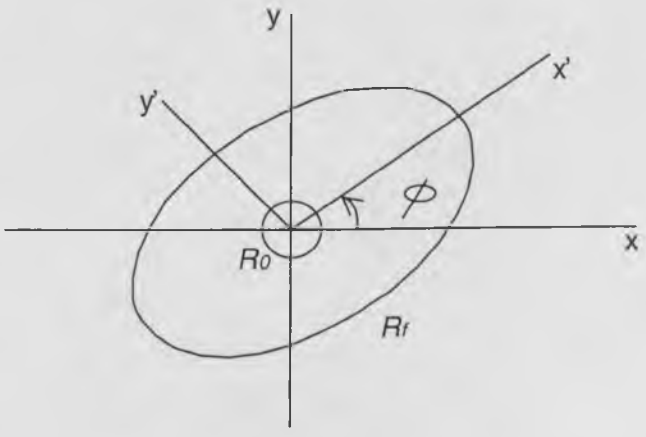

Where, R_0, R_f are the inlet hole radius and liquid flow front radius respectively; ϕ is the characteristic angle, and x', y' are the directions of two principle permeabilities respectively.

There are two existing methods of measuring the anisotropic permeability of porous fabrics. One is to obtain the analytical solution from a combination of the equations (3.9.2.1) and (3.9.2.2)[124, 125] to obtain the directional permeabilities. The second method is to use the existing analytical solution of liquid flow in isotropic structures presented in this thesis to obtain the directional permeabilities[202]. In the second method, the anisotropic structure is treated as several angular sections divided by radial lines emanating from the entrance hole (as shown in Figure 3.23), and each section is treated as an isotropic medium. The first method is very complicated and requires additional data (i.e., the pressure gradient in the liquid flow). In contrast, the second method is relatively simple and is convenient to use. The second method has therefore been adopted in this approach.

In this approach, the capacitance unit is divided into eight angular sections by radial lines emanating from the liquid entrance point, and each segment allows measurement of the volumetric flow rate in each direction (see Figure 3.23). Within each section, the liquid passing through the angular sections can be viewed as two-dimensional liquid flow in an isotropic material. Each radial line serves as the centreline of a sector. Figure 3.24 shows a typical sector used by the capacitance transducer system.

In calculations of the anisotropic permeabilities of a fabric, eight temporal radial data sets are used, and each sector spans 45^0. Each section is analysed to obtain the permeability based on the centreline temporal radial data. From the experimental data,

Figure 3. 21 Liquid flow in the fabric and the calculated dynamic liquid flow front in eight transducer field sectors

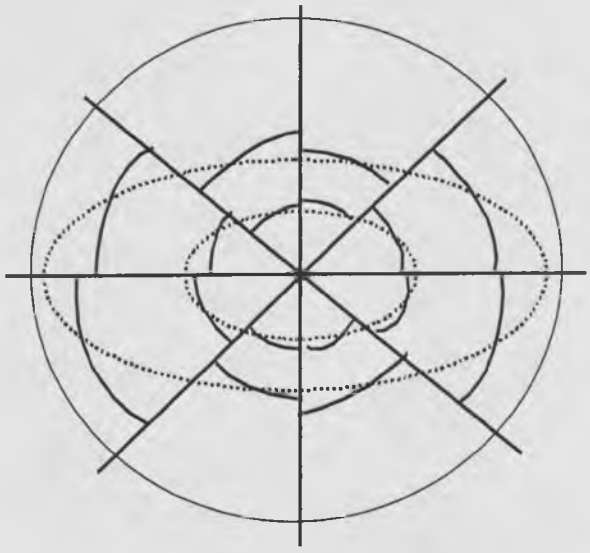

Figure 3. 22 Typical sector showing the development of the liquid flow advancing front

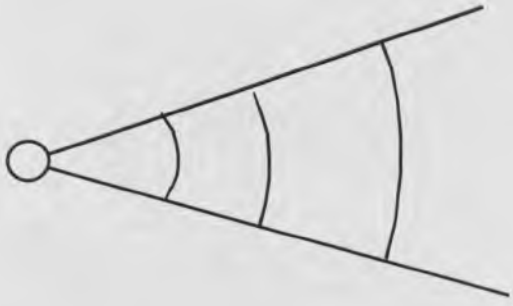

the calculated radial extent along the centreline at time t_i, defined as $r(t_i)$, can be calculated from the measured voltage values from the capacitance transducer. Equations (3.9.1.7~10) are used to calculate the anisotropy of permeability for all sectors using all sets of the radial extent data.

3.9.3 Measurement of the Anisotropy of the Liquid Flow in Anisotropic Fabric Structures Using Data from the Capacitance Transducers

As shown in section 3.5, if the liquid enters a dry dielectric material placed in an electrical field, variation of the capacitance value will be linearly proportional to changes in the area of the wetted fabric.

Initially, if an angular area with an angle β (as shown in Figure 3.24), and diameter r_0 is the radius of the central capacitance segment, from equation (3.5.8) we know that the linearly proportional ratio of the voltage value to the wetted fabric area is ψ. Thus, in time, t, the relationship between the measured voltage in the system, $V(t)$, and the wetted fabric area can also be defined as follows:-

$$V(t) = \psi \frac{\beta}{2}(R_f^2(t) - r_0^2) \qquad (3.9.3.1)$$

If it is assumed that all the liquid is held in the wetted area of the fabric, the mass of the liquid held by the fabric at time t, $M(t)$, will be:-

$$M(t) = \frac{\beta}{2}(R_f^2(t) - R_0^2)\rho d \qquad (3.9.3.2)$$

$$\text{Therefore, } R_f^2(t) = \frac{2V(t)}{\beta\psi} + r_0^2 \qquad (3.9.3.3)$$

Where:- $$\psi = \frac{V(t)}{\left(M(t) - \frac{\beta}{2}(r_0^2 - R_0^2)\rho d \right)} \qquad (3.9.3.4)$$

Rewriting equation (3.9.1.9) for an angular area and substituting Equation (3.9.3.2) into equation (3.9.1.9), we obtain:-

$$k = \frac{Q(t)}{\beta d P_0(t)} \ln\left(\frac{R_f(t)}{R_0} \right), \text{ or} \qquad (3.9.3.5)$$

$$k = \frac{Q(t)}{\beta d P_0(t)} \ln\left(\frac{2V(t)}{\psi \beta R_0^2} + \frac{r_0^2}{R_0^2} \right) \qquad (3.9.3.6)$$

3.9.3.1 Liquid Flow in Anisotropic Structures Under Constant Pressure

At constant pressure conditions $P_0(t) = P_0$, equation (3.9.3.6) will be as follows:-

$$k = \frac{Q(t)}{\beta d P_0} \ln\left(\frac{2V(t)}{\psi \beta R_0^2} + \frac{r_0^2}{R_0^2} \right) \qquad (3.9.3.7)$$

From the mass balance equation (3.9.1.10), the volumetric flow rate, $Q(t)$, can be written as follows:-

$$\overline{Q(t)}\Big|_{t=t_1} = \frac{\beta\left(R_f^2(t_1 + \frac{\Delta t}{2}) - R_f^2(t_1 - \frac{\Delta t}{2}) \right)(1-\varepsilon)d\rho}{2\Delta t} \qquad (3.9.3.8)$$

Substituting equation (3.9.3.3) into Equation (3.9.3.8), we have:-

$$\overline{Q(t)}\Big|_{t=t_1} = \frac{\beta\left(V(t_1 + \frac{\Delta t}{2}) - V(t_1 - \frac{\Delta t}{2}) \right)(1-\varepsilon)d\rho}{2\Delta t} \qquad (3.9.3.9)$$

Substituting equation (3.9.3.9) into (3.9.3.7), we have:-

$$k = \frac{\left(V(t_1 + \frac{\Delta t}{2}) - V(t_1 - \frac{\Delta t}{2})\right)(1-\varepsilon)d\rho}{4dP_0\psi\Delta t} \ln\left(\frac{2V(t_1)}{\psi\beta R_0^2} + \frac{r_0^2}{R_0^2}\right) \qquad (3.9.3.10)$$

Thus, the ratio of permeability between the i_{th} segment and the j_{th} segment will be:-

$$\omega = \frac{k_i}{k_j} = \frac{\left(V_i(t_1 + \frac{\Delta t}{2}) - V(t_1 - \frac{\Delta t}{2})\right)\ln\left(\frac{2V_i(t_1)}{\psi\beta R_0^2} + \frac{r_0^2}{R_0^2}\right)}{\left(V_j(t_1 + \frac{\Delta t}{2}) - V(t_1 - \frac{\Delta t}{2})\right)\ln\left(\frac{2V_j(t_1)}{\psi\beta R_0^2} + \frac{r_0^2}{R_0^2}\right)} \qquad (3.9.3.11)$$

3.9.3.2 Liquid Flow in Anisotropic Structures at a Constant Volumetric Flow Rate

For liquid flow in an angular area at boundary condition $Q(t) = Q$ as shown in Figure 3.24, we also have $M(t) = Q * t$. Thus, Equation (3.9.3.6) can be rewritten as:-

$$k = \frac{M(t)}{\beta dt P_0(t)} \ln\left(\frac{2V(t)}{\psi\beta R_0^2} + \frac{r_0^2}{R_0^2}\right) \qquad (3.9.3.12)$$

Since the permeability of the fabric is independent of time, that is, $k\big|_{t=t_1} = k\big|_{t=t_0}$, from Equation (3.9.3.12) we have:-

$$\frac{P_0(t_1)}{P_0(t_0)} = \frac{\ln\left(\frac{2V(t_1)}{\psi\beta R_0^2} + \frac{r_0^2}{R_0^2}\right)}{\ln\left(\frac{2V(t_0)}{\psi\beta R_0^2} + \frac{r_0^2}{R_0^2}\right)} \qquad (3.9.3.13)$$

Since the liquid travelled in the i_{th} segment and in the j_{th} segment is from the same source point, the pressure at the source point at time t for the i_{th} segment, $P_0^i(t)$, and for the j_{th} segment, $P_0^j(t)$, is identical, that is: $P_0^i(t) = P_0^j(t)$.

Thus, the ratio of permeability between the i_{th} segment and the j_{th} segment can be obtained from equations (3.9.3.12) and (3.9.3.13) as follows:-

$$\omega = \frac{k_i}{k_j} = \frac{Q_i \ln\left(\frac{2V_i(t)}{\psi\beta R_0^2} + \frac{r_0^2}{R_0^2}\right)}{Q_j \ln\left(\frac{2V_j(t)}{\psi\beta R_0^2} + \frac{r_0^2}{R_0^2}\right)} \qquad (3.9.3.14)$$

where Q_i and Q_j are the volumetric flow rates in the fabric along the direction of segment i_{th} and segment j_{th} respectively; $V_i(t)$ and $V_j(t)$ are the voltage data measured in the i_{th} segment and j_{th} segment transducers respectively.

3.9.4 Anisotropy of Liquid Transport in Nonwoven Fabric Structures Measured Using the New System

The directional permeability in a porous material, $k(\theta)$, can be obtained from Ferrandon's equation[170] as follows:-

$$\frac{1}{k(\theta)} = \frac{\cos^2\theta}{k_1} + \frac{\sin^2\theta}{k_2} \qquad (3.9.4.1)$$

Where k_1 and k_2 are the principle permeabilities in the fabric plane in a Cartesian coordinate system x_1 and x_2 respectively.

For flow through anisotropic structures as shown in Figure 3.23, Ferrandon's Equation can be rewritten as equation (3.9.4.2):-

$$\frac{1}{k(\theta)} = \frac{\cos^2(\theta-\phi)}{k_1} + \frac{\sin^2(\theta-\phi)}{k_2} \qquad (3.9.4.2)$$

Where the principle permeabilities are in the direction ϕ and $(\phi+\frac{\pi}{2})$ respectively and the angle ϕ is the characteristic angle. Therefore, Equation (3.9.4.2) can be used to calculate the principle permeabilities and its characteristic angle ϕ.

In order to calculate the principle permeabilities and its characteristic angle ϕ, the measured data and the corresponding flow directions for each of the eight individual capacitance transducers in the system (respectively) can be substituted into equation (3.9.4.2) to obtain a set of non-linear equations as follows:-

$$\frac{1}{k(\theta_i)} = \frac{\cos^2(\theta_i - \phi)}{k_1} + \frac{\sin^2(\theta_i - \phi)}{k_2} \qquad (i=1,2,3,....8) \qquad (3.9.4.3)$$

The equations are solved using the Least Square Residual algorithm[222], to obtain the principle permeabilities, k_1 and k_2, and the characteristic angle, ϕ. The anisotropy of the fabric permeability, ω_k, is defined as the ratio of the two principle permeabilities as follows:-

$$\omega_k = \frac{k_2}{k_1} \qquad (3.9.4.4)$$

According to equations (3.9.4.3) and (3.9.4.4), the anisotropy of permeability can be obtained, and the application of this method in the experimental results will be presented in Chapter 5.

CHAPTER 4 THE PREPARATION OF NONWOVEN FABRIC SAMPLES AND THE CHARACTERISATION OF THE FABRIC STRUCTURE

In order to investigate the influences of individual fabric structural parameters on the anisotropy of liquid transport in nonwoven wound dressing fabrics, unbonded webs, needle-punched and hydroentangled nonwoven fabrics with different structural parameters with respect to fibre type, fibre diameter, fibre orientation distribution and fabric porosity were produced under controlled conditions.

The liquid absorbency and porosity of these materials were obtained using standard measurement methods and the fibre orientation distribution was examined using image analysis. The structural properties of the commercial nonwoven wound dressings reported in Chapter 2, composed of cellulose and calcium alginate fibres, were also measured.

4.1 PURPOSE OF THE EXPERIMENTAL WORK

It is known that the structural characteristics of nonwoven fabric are key to understanding the anisotropy of mechanical properties of nonwoven structures[90]. Previous research on the liquid absorption demonstrates that the liquid transport properties of fibrous materials depends both on the properties of the constituent fibres and on the spatial arrangement of the fibres in the assembly. However, there has been little systematic work on how the structure of nonwovens influences the anisotropy of liquid transport in the fabric. Accordingly, the purpose of the experimental work was to

systematically investigate the influence of fabric structural parameters on the anisotropy of liquid transport in experimental nonwoven wound dressing fabrics.

4.2 THE EXPERIMENTAL PLAN

In the experimental work, five parameters were considered as follows:-

(i) Fibre type (polypropylene, viscose).

(ii) Fibre fineness (1.7dtex, 3.3 dtex).

(iii) Fibre orientation distribution (parallel-laid, cross-laid).

(iv) Fabric porosity (high porosity and low porosity).

(v) Fabric bonding methods (unbonded web, needled and hydroentangled fabrics).

In total, forty-three different fabrics were produced with different combinations of structural characteristics. The experimental plan is presented in Tables 4.2. The symbols used to denote the fabrics in the experimental plan are shown in Table 4.1.

Table 4. 1 Symbols used in the experimental plan to designate samples

Symbol Sequences	Meaning	Symbol
1st Symbol	Fibre type.	V = Viscose fibre P = Polypropylene
2nd Symbol	Fibre fineness.	A = 1.7 dtex B = 3.3 dtex
3rd Symbol	Fibre orientation in web.	1 = Parallel laid 2 = Cross laid
4th Symbol	Bonding method.	PP, VV = Hydroentangled N = Needlepunched WEB = Unbonded web
5th Symbol and after	Fabric porosity.	Different porosity from different fabric density or fabric thickness.

Table 4. 2(a) Experimental plan (polypropylene fibre)

Sample NO.	Fibre Type	Fibre Fineness (linear density)	Type of Fibre Orientation Distribution	Bonding Method	Porosity Change
PA1PP PA1VV1 PA1VV2	Polypropylene	1.7 dtex	Parallel Laid (Single peak)	Hydroentangled	Original
PA1N 1 PA1N 2				Needlepunched	Original Compressed
PA2H			Cross Laid (Bi-modal)	Hydroentangled	Original
PA2N1 PA2N2				Needlepunched	Original Compressed
PB1PP PB1VV1 PB1VV2		3.3 dtex	Parallel Laid (Single peak)	Hydroentangled	Original
PB1N 1 PB1N2				Needlepunched	Original Compressed
PB2H			Cross Laid (Bi-modal)	Hydroentangled	Original
PB2N1_1 PB2N1_1 PB2N2_1 PB2N2_2 PB2N3				Needlepunched	Original Compressed Original Compressed Original

Those samples designated PP (fourth symbol) indicate fabrics in which the parallel-laid web was fed to the hydroentanglement machine with fibres aligned in the direction of processing. The samples designated (VV) indicate fabrics in which the parallel-laid web was turned ninety degrees before feeding to the hydroentanglement machine. i.e.,

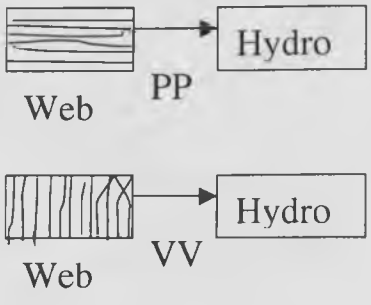

Table 4. 2(b) Experimental plan (viscose fibre)

Sample NO.	Fibre Type	Fibre Fineness (linear density)	Type of Fibre Orientation Distribution	Bonding Method	Porosity Change
VA1PP	Viscose	1.7 dtex	Parallel Laid (Single peak)	Hydroentangled	Original
VA1VV					
VA1N 1				Needlepunched	Original
VA1N 2					Compressed
VA2H			Cross Laid (Bi-modal)	Hydroentangled	Original
VA2N1				Needlepunched	Original
VA2N2					Compressed
VB1PP		3.3 dtex	Parallel Laid (Single peak)	Hydroentangled	Original
VB1VV					
VB1N 1				Needlepunched	Original
VB1N2					Compressed
VB2H			Cross Laid (Bi-modal)	Hydroentangled	Original
VB2N1_1				Needlepunched	Original
VB2N1_2					Compressed
VB2N2					Original
VB2N3					Original

Table 4.2(c) Experimental plan (unbonded webs)

Sample NO.	Fibre Type	Fibre Fineness (linear density)	Fibre Orientation (Type of Fibre Orientation Distribution)
VA1WEB	Viscose	1.7 dtex	Parallel Laid (Single peak)
VA2WEB			Cross Laid (Bi-modal)
VB1WEB		3.3 dtex	Parallel Laid (Single peak)
VB2WEB			Cross Laid (Bi-modal)
PA1WEB	Polypropylene	1.7 dtex	Parallel Laid (Single peak)
PA2WEB			Cross Laid (Bi-modal)
PB1WEB		3.3 dtex	Parallel Laid (Single peak)
PB2WEB			Cross Laid (Bi-modal)

4.2 GENERAL CONSIDERATIONS IN THE DESIGN OF THE FABRIC SAMPLES

The structural parameters of the fabrics investigated in this work were chosen to reflect the construction of commercial nonwoven wound dressing structures.

Mechanically bonded nonwoven fabrics used as absorbent layers in dressings are frequently of low density and around 100 g/m^2. Accordingly, the experimental fabrics produced were $100g/m^2$. To determine the effect of fabric compression on the liquid transport in the fabric, the base fabrics were compressed to achieve a range of fabric thicknesses and thus a range of fabric porosities.

For each type of bonding process, all the bonding parameters were kept identical for all the fabrics.

Fibres may be classified as hydrophilic and hydrophobic, or absorbent and non-absorbent[130]. Commercially, non-absorbent, absorbent and gelling fibres, are used in wound dressings to meet different requirements. In this Chapter, both non-absorbent and absorbent fibres were selected (i.e., Polypropylene and Viscose rayon).

Fibre diameter is believed to influence the permeability of fibrous materials[170]. Typically, the linear density of most staple fibres used in nonwoven wound dressings ranges from 1.0 dtex to 5.0 dtex. Thus, two fibre finenesses (1.7 dtex and 3.3 dtex), were selected for each type of fibre. The fibre lengths were similar so as to clearly determine the effect of the fibre fineness. The fibre diameter was also measured with the use of an optical microscope. The specifications of the two fibres are shown in Table 4.3.

Table 4. 3 The specifications of fibres used in making fabrics

	Polypropylene		Viscose	
Fibre type and Supplier	FM100M (Asota)		Fibro O (Acordis)	
Fibre fineness (dtex)	1.7	3.3	1.7	3.3
Fibre diameter (μm)	15.3	30.6	12.5	25.0
Fibre length (mm)	60		51	
Fibre crimp (Approx. crimps/cm)	6.5	6.5	6.0	6.0
Fibre density (g/cm^3)	0.90		1.38	
PH of fibre surface	7-8		5-7	
Fibre finish	Fatty-acid-glucose-ether		Mixture of sodium oleate and oleic acid	

It should be noted that the polypropylene fibres obtained from the fibre manufacturer were coated with a fibre finish that had a low fibre-water interface tension making the fibre surface hydrophilic. The application level of the finishes was 0.18~0.25% OWF.

4.3 FABRIC MANUFACTURING PROCEDURE

4.3.1 Experimental Approach

The fabric production procedures used to prepare the experimental fabrics are illustrated in Figure 4.1.

Figure 4. 1 Nonwoven fabric production procedure

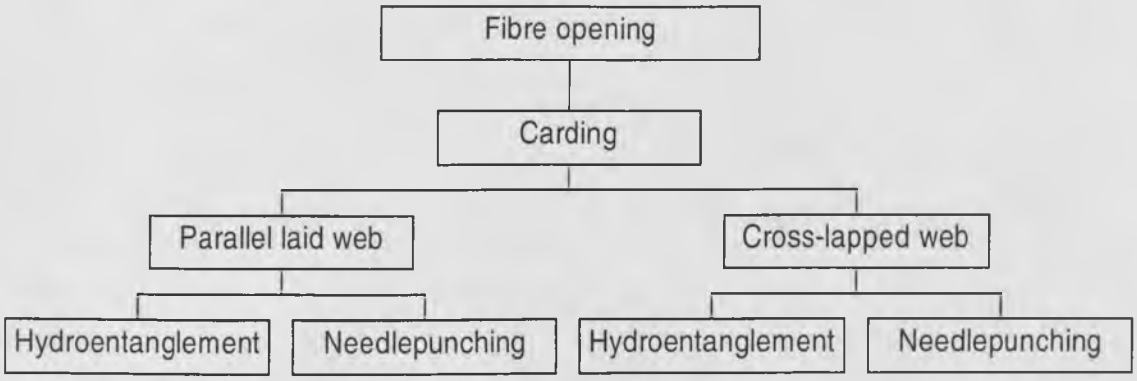

4.3.2 Machine Parameters

In the manufacture of each type of fabric, the operating settings of the processes were identical. The details of the main operating settings of the card, lapper, needlepunching machine and hydroentanglement machine are presented in Tables 4.4 and 4.5.

Table 4. 4 Settings of card, lapper, and needlepunching machine

Parameter	Machine	Setting
Set Weight (g)	Carding Machine	126 (varied)
Feed Roller (rpm)		169
Feed Speed (m/min)		0.6
Card Speed (rpm)		75
Lapper (rpm)	Lapper	0.629
Top Sheet (rpm)		11.3
Bottom Lattice (rpm)		5.3
Loom (rpm)	Needle Loom	56.3
Loom Sheet (rpm)		16.7
Loom rod-up (rpm)		1.7
Penetration (mm)		12
Needle density (p/cm^2)		60

Table 4. 5 Settings of the hydroentanglement machine

Parameter	Machine	Setting
Number of jets (jets/m)	Hydroentanglement	1300
Jet outlet diameter (mm)		0.14
Conveyer velocity (m/min)		8
Water pressure (Bar)		40 (one pass)
Total Specific Energy (MJ/Kg)		0.0957

4.4 MEASUREMENT OF FABRIC STRUCTURAL CHARACTERISTICS

After preparing the experimental samples, it was necessary to characterise the structure of the fabrics before further testing. The most important structural parameters of a nonwoven fabric are the thickness, mass per unit area, porosity (porosity = 1 - packing density) and the fibre orientation distribution, the measurement of these parameters is summarised below. The fabric porosity and fabric absorbency are shown in Table 4.6. The measured characteristics of the experimental fabric structures and corresponding fibre orientation distributions are presented in Figures 4.4~4.8.

4.4.1 Thickness Measurement *(d)*

The thickness of a nonwoven fabric, *d* (mm), can be defined as the distance between the face and back of the material measured as the distance between a reference plate on which the nonwoven rests and a parallel pressure - foot that applies a pressure to the fabric[223]. The thickness of the fabric was measured using the Shirley thickness tester in accordance with the standard INDA-IST120.2 (i.e. ASTM D5736-95)[189]. The results for all the samples are shown in Table 4.6.

4.4.2 Mass Per Unit Area (*W*)

The mass per unit area, *W* (g/m^2), of the samples was measured in accordance with the standard INDA IST130.1 (i.e. ASTM D3776-85) [191]. The mass per unit area of all the samples is shown in Table 4.6. The mass per unit area of most of the samples was around 100 g/m^2, which is in accordance with many commercially available fabrics.

Table 4. 6(a) General specifications of experimental fabrics (needlepunched and hydroentangled fabrics)

Sample No	Fabric weight (g/m^2)	Fabric thickness (mm)	Porosity	Sample No	Fabric weight (g/m^2)	Fabric thickness (mm)	Porosity
VA1PP	133.2	1.5	0.935	**PA1PP1**	74.1	7.0	0.988
VA1VV	128.4	1.5	0.938	**PA1VV3**	125.8	3.5	0.961
VA1N1	95.3	3.0	0.977	**PA1VV4**	84.4	2.0	0.954
VA1N2		2.5	0.972	**PA1N1**	126.6	3.9	0.964
VA2H1	101.9	1.2	0.939	**PA1N2**		3.2	0.957
VA2N1	98.3	3.5	0.980	**PA2H3**	120.5	4.7	0.972
VA2N2		2.9	0.975	**PA2N1**	130.3	4.0	0.964
VB1N1	100.1	3.6	0.980	**PA2N2**		3.0	0.952
VB1N2		3.2	0.977	**PB1VV1**	141.0	5.0	0.969
VB1PP1	128.8	1.4	0.933	**PB1VV1'**	105.9	4.9	0.976
VB1VV1	127.8	1.6	0.942	**PB1PP1**	100.1	4.2	0.974
VB2N1_1	100.9	4.7	0.984	**PB1PP2**	153.9	6.5	0.974
VB2N1_2		3.8	0.981	**PB1N1**	123.2	4.2	0.968
VB2N2	80.0	4.2	0.986	**PB1N2**		3.5	0.961
VB2N3	60.0	3.6	0.988	**PB2H2**	98.6	3.2	0.966
VB2H2	117.9	1.3	0.934	**PB2N1**	99.8	3.9	0.972
N/A	N/A	N/A	N/A	**PB2N2**	99.8	3.0	0.963

Table 4.6(b) General specifications of experimental fabrics (unbonded webs)

Sample No	Fabric Weight ($g/m^2 \pm 5\%$)	Fabric thickness (mm)	Porosity
VA1WEB	100.0	4.2	0.974
VA2WEB	100.0	4.5	0.976
VB1WEB	100.0	5.3	0.979
VB2WEB	100.0	5.4	0.980
PA1WEB	100.0	5.5	0.980
PA2WEB	100.0	6.0	0.982
PB1WEB	100.0	4.2	0.974
PB2WEB	100.0	4.4	0.975

Table 4. 7(a) Liquid absorbency of experimental fabrics (unbonded webs)

Sample No	Absorbency	
	(g/g)	(g/m^2)
VA1WEB	17.5	1746.2
VA2WEB	19.2	1918.5
VB1WEB	19.1	1914.2
VB2WEB	21.1	2108.5
PA1WEB	24.2	2422.4
PA2WEB	24.7	2468.0
PB1WEB	21.6	2156.8
PB2WEB	21.8	2180.4

Table 4. 7(b) Liquid absorbency of experimental fabrics (needlepunched and hydroentangled fabrics)

Sample No	Absorbency		Sample No	Absorbency	
	(g/g)	(g/m^2)		(g/g)	(g/m^2)
VA1PP	8.5	1137.4	**PA1PP1**	22.4	1658.9
VA1VV	9.1	1165.3	**PA1VV3**	20.2	2535.0
VA1N1	18.7	1779.4	**PA1VV4**	17.8	1502.3
VA1N2	N/A		**PA1N1**	21.9	2766.3
VA2H1	8.7	884.2	**PA1N2**	N/A	
VA2N1	19.4	1909.1	**PA2H3**	21.0	2530.0
VA2N2	N/A		**PA2N1**	20.5	2676.6
VB1N1	20.8	2084.8	**PA2N2**	N/A	
VB1N2	N/A		**PB1VV1**	20.1	2835.5
VB1PP1	7.8	1003.8	**PB1VV1'**	22.1	2344.7
VB1VV1	7.8	991.7	**PB1PP1**	22.5	2256.9
VB2N1_1	20.1	2026.0	**PB1PP2**	N/A	
VB2N1_2	N/A		**PB1N1**	21.0	2591.6
VB2N2	22.6	1803.1	**PB1N2**	N/A	
VB2N3	20.4	1223.1	**PB2H2**	21.6	2132.1
VB2H2	7.9	929.9	**PB2N1**	20.8	2078.3

4.4.3 Porosity (P_f)

Porosity P_f is defined as the ratio of void volume to the total volume of the fibrous structure and can be expressed as follows[224]:

$$P_f = \left(1 - \frac{\rho_{fabric}}{\rho_{fibre}}\right) = \left(1 - \frac{W}{d\rho_{fibre}} \frac{1}{1000}\right) \quad (4.1)$$

Where, P_f is the fabric porosity, ρ_{fabric} is the fabric density (kg/m^3), ρ_{fibre} is the fibre density (kg/m^3), W is the fabric mass per unit area (g/m^2), and d is the fabric thickness (m). The measured porosities of the experimental fabrics are shown in Table 4.6. It is apparent that the overall porosity of the fabrics was mainly in the range 0.93 to 0.99.

4.4.4 Measurement of Fabric Absorbency

Two types of liquid were used as test fluids in the experimental work as follows:

1. Distilled water
2. Liquid A (reduced surface tension)

Liquid A was a 0.25% solution of a non-ionic surface detergent *SandoClean PC©* Liquid[225] (Polyglycol ether) in distilled water. This is an excellent wetting and penetrating agent in distilled water and was only used for measurements on the hydroentangled polypropylene fabrics because of the high surface tension of the fibre. The absorbency of the hydroentangled polypropylene fabrics was also measured using Liquid A. All the other nonwoven fabrics were measured using distilled water.

The absorptive capacity (i.e., absorbency) of the fabrics was measured using the standard method INDA-IST10.1 (95)[190]. Each specimen was weighed in the dry state and then lowered into distilled water using a wire container. The total weight of the wet specimen was measured and the weight of the supporting screen and dry specimen

subtracted. The ratio of the dry weight and the weight of water absorbed is defined as the absorptive capacity (g/g). The results are shown in Table 4.7.

4.4.5 Fabric Absorbency and Fabric Porosity

It was found that the overall absorbency was largely dependent on fabric porosity. As liquid is absorbed into the fabric, it replaces the void space in the fabric. A linear regression relationship between the absorbency of all the experimental fabrics and their porosities is shown in Figure 4.2.

Figure 4. 2 Relationship between the absorbency and the fabric porosity for all the experimental fabrics

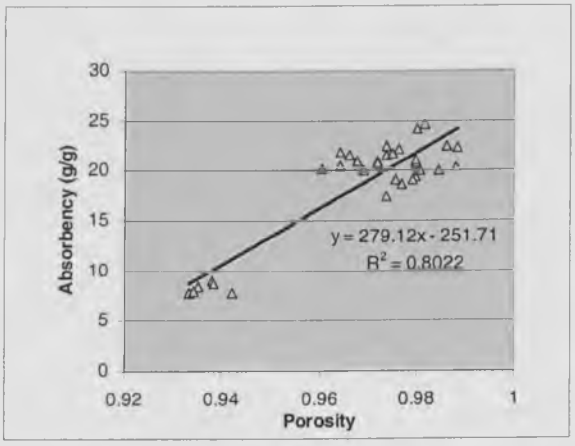

4.4.6 Measurement of the Fibre Orientation Distribution Using Image Analysis

The orientation of a fibre can be described using an orientation angle. The orientation angle can be defined as the angle formed between the fibre axes and a central line (machine direction) of the web as shown in Figure 4.3. The orientation angles of individual fibres can be determined by evaluating fabric photomicrographs or using microscopy and image analysis.

The overall orientation of fibres can be described using a frequency distribution function or a probability density function. Frequency distributions can be obtained by determining the fraction of the total number of fibres falling within a predetermined range of orientation angles. Discrete frequency distributions can be used to estimate continuous probability density functions.

Figure 4. 3 Fibre orientation and the orientation angle

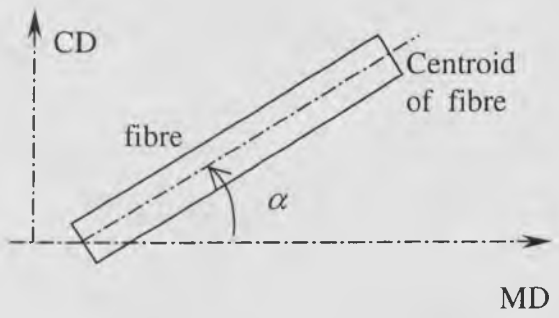

In modelling the properties of nonwoven fabrics, it is important to obtain an accurate measure of the Fibre Orientation Distribution and particularly in any quantitative analysis of the anisotropic properties of nonwoven fabrics.

Image analysis is a computer-based means of converting the visual qualitative features of a particular image into quantitative data. The measurement of the fibre orientation distribution in nonwoven fabrics using image analysis is based on the assumption that in thin materials a two dimensional structure can be assumed, although it is known that the fibres in a nonwoven are generally arranged in three dimensions. However, there is currently no generally accepted way of characterising the fabric structure in terms of three-dimensional geometry. The fabric geometry is reduced to two dimensions by evaluation of the planar projections of the fibres within the fabric. The assumption of a two-dimensional fabric structure is adequate to describe thin fabrics.

4.4.6.1 Review of Techniques for Measuring Fibre Orientation Distribution

A number of techniques for measuring Fibre Orientation Distribution have been reported in the literature. A direct visual experimental method for manually measuring fibre orientation was first described by Petterson[92]. This method produces the most accurate measurements, but it is tedious and time-consuming. After comparing with other methods, Hearle and co-workers[90, 226] found that visual methods are the most reliable way to evaluate the fibre orientation and they used a projection microscope method to measure both fibre orientation and curl. They manually measured fibre segment angles relative to a given direction and determined the lengths of segment curves within a given range. However, the application of this method is still limited by the time-consuming work required in visual examinations.

In order to obtain a faster and still accurate way to measure the fibre orientation distribution, various indirect-measuring techniques have been investigated. Kallmes[227] and others[228] introduced the zero span tensile testing method for predicting the fibre orientation distribution in a fibre web. Short span tensile analysis was also used by Cowan and Cowdrey[229]. Chuleigh[230] developed an optical processing method in which an opaque mask was used in a light microscope to highlight fibre segments that are oriented in a known direction. Stenemur[231] devised a computer system to monitor fibre orientation or running webs based on the light differentiation phenomenon. Other methods include the microwave method[93], ultrasound[232], light diffraction methods[233], light reflection and light refraction[234], electrical measurements[235, 236], and liquid-migration-pattern analysis[237, 238]. Methods that employ X-ray-diffraction analysis[239] and X-ray differentiation patterns of fibre webs have also been tried[240].

More recently, image analysis has been employed to identify fibres and their orientation[241, 242, 243, 244], and computer simulation techniques have come into use for the creation of computer models of various nonwoven fabrics[245, 246, 247, 248]. Huang and Bressee[241] developed a random sampling algorithm and software to analyse fibre orientation in thin webs. In this method, fibres are randomly selected and traced to estimate the orientation angles, and test results showed excellent agreement with results from visual measurements. Xu and Ting[248]also used image techniques to measure structural characteristics of fibre or fibre bundle segments in a thin nonwoven fabric. The structural characteristics measured included length, thickness, curl and the orientation of fibre segments. Recently, Pourdeyhimi et al[249, 250, 251, 252] completed a series of studies on the fibre orientation of nonwovens by using an image analyzer to analyse the fibre orientation in which image processing techniques such as computer simulation, fibre tracking, Fourier transforms and flow field techniques were employed.

In contrast to many two-dimensional imaging techniques used for thin nonwoven fabrics, (based on the orientation distribution function (ODF) of a fibrous structure of the Hilliard-Komori-Makishima theory[253]), Gilmore et al[254] tried to visualise and to quantify the three dimensional structures of thick nonwovens via X-ray tomographic techniques.

4.4.6.2 Introduction of the Quantimet 570 System

In this work, the fibre orientation distribution was measured using a Quantimet 570 image analysis system[255]. The Quantimet 570 is based on a computer system operating with an integrated menu-driven image analysis software package (Quic) in which numerous functions can be performed, such as image capture, grey image edit, binary

image threshold and detect, binary image edit and transforms, and feature measurement functions. A video camera and lighting system are used in the main imaging system but live connection to an SEM and other digital sources is also possible.

Images taken from the camera are stored, processed and then measured. Two lenses were available, which could be fitted to the black and white COHU CCD camera to give magnifications in the range X 1.5-X8 (first lens) and X 25 magnification (second lens). A direct link from a Cambridge 360 Scanning Electron Microscope to the Q570 was also employed for part of the work[255].

4.4.6.3 Operating Principles of the Quantimet 570

The main stages of image analysis using the Q570 have been previously outlined[255]. A series of several sequential operations is required to perform image analysis, and the following general procedures are usually carried out[256]:

1. Production of a grey image of the sample fabric.
2. Processing the grey image.
3. Detection of the grey image and conversion into binary form.
4. Storage and processing of the binary image.
5. Measurement of the fibre orientation and output of results.

4.4.6.4 Measurement of the Fibre Orientation Distribution in the Experimental Nonwoven Fabrics

A test procedure using the Q570 for the measurement of fibre orientation in woollen slubbings has been given by Russell[256]. In the present work, the existing program was modified to allow measurement of the fibre orientation distribution in nonwoven fabrics.

The modified measurement routine was programmed in QBASIC using the Quic system and is shown in Appendix 1.

In the procedure, a sample of fabric was placed on a transparent glass plate and illuminated by transmitted light. The image was then captured using a CCD camera (X 20) and displayed on a VGA monitor. After calibration of the system and the capture of the grey image, editing of the image was undertaken. A binary image was obtained from the grey image using an appropriate threshold level (150). The binary image was then transformed to produce a skeletonised image. The final fibre orientation distribution was obtained in terms of the segment frequency vs. orientation angles.

4.4.6.5 Fibre Orientation Distributions of the Experimental Fabrics

The fibre orientation distributions of the webs, from which the sample fabrics reported in section 4.3 were obtained, are shown in Figures 4.4 to 4.7. In the results, the number of segments measured in each sample was typically 1800-2300.

Figure 4. 4 Fibre orientation distributions for the parallel-laid webs (polypropylene fibre)

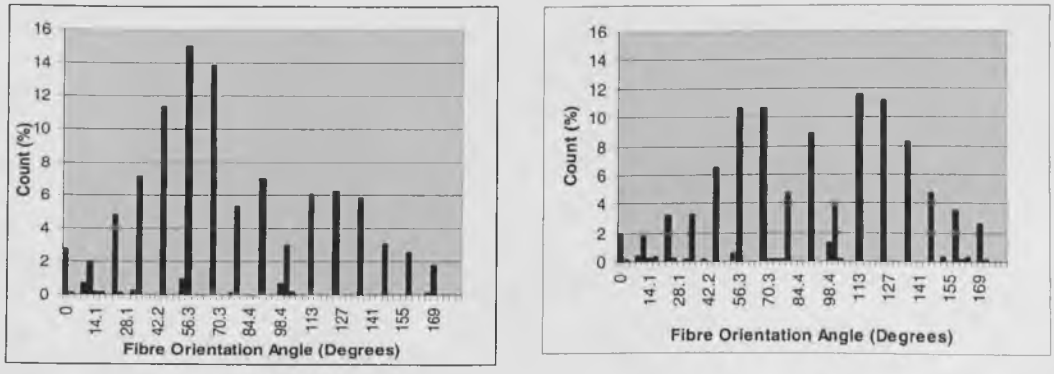

(a) 1.7dtex (b) 3.3 dtex

Note: Count (%) = Frequency (%)

Figure 4. 5 Fibre orientation distributions for the parallel-laid webs (viscose fibre)

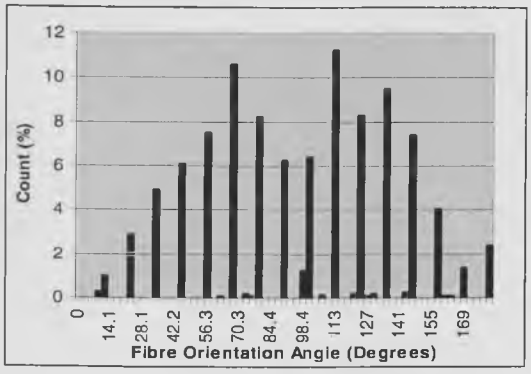

(a) 1.7 dtex

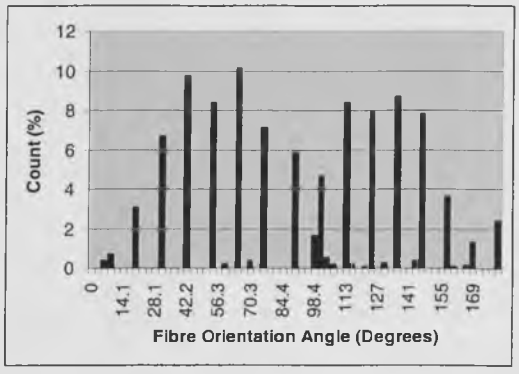

(b) 3.3 dtex

Figure 4. 6 Fibre orientation distribution for cross-laid webs (polypropylene fibre)

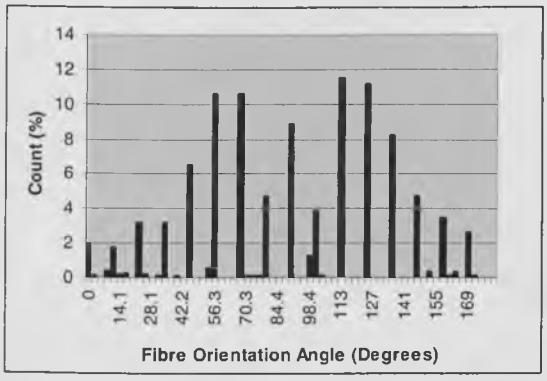

(a) 1.7 dtex

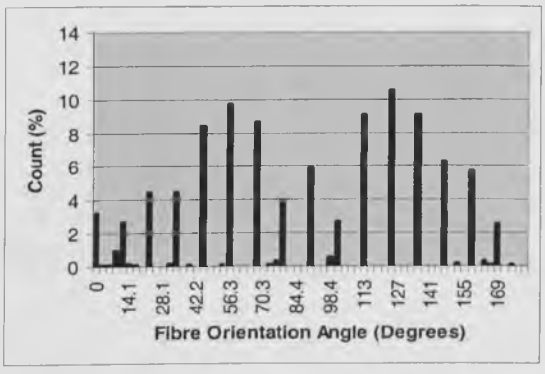

(b) 3.3 dtex

Figure 4. 7 Fibre orientation distribution for cross-laid webs (viscose fibre)

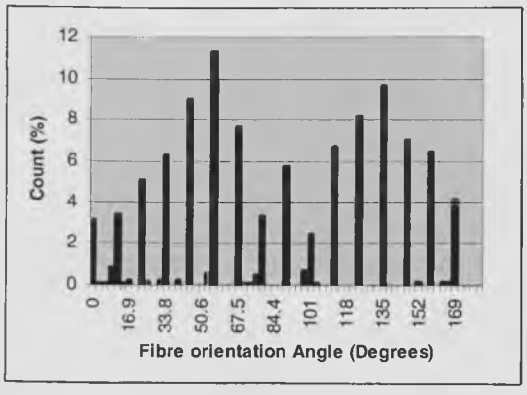

(a) 1.7 dtex

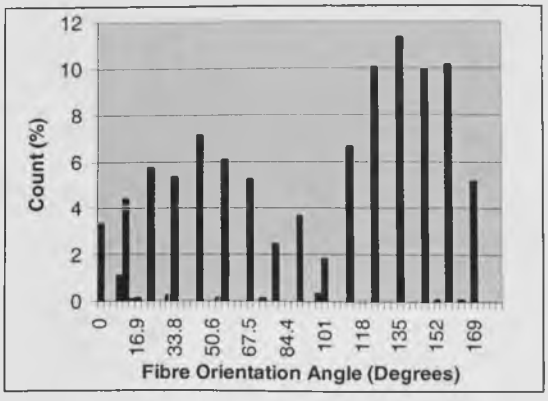

(b) 3.3 dtex

Count (%) = Frequency (%)

In this work, only the fibre orientation distributions for the unbonded webs were measured. The fibre orientation distributions in the needlepunched and hydroentangled fabrics were not measured because the fibre orientation distributions in these fabrics were different in adjacent regions. Additionally, the fibre orientation distributions in the bonded areas (i.e., the jet or needle marked areas) could not be determined because the areas containing these marks (produced by hydroentanglement and needlepunching respectively) were too small to be measured.

Fibre type and the fibre fineness are believed to influence the fibre orientation in carded webs since it is known that the fibre type and fibre fineness influence the occurrence of fibre hooks[257, 258, 259, 260]. Thus, it may be expected that both fibre type and fibre fineness will also affect the anisotropy of liquid transport in the nonwoven fabric.

Statistically, the CV% of the fibre orientation distributions characterises the variation of the data. The CV% of fibre orientation can be used to describe the anisotropy of the nonwoven structure. The overall CV% of fibre orientation obtained for each of the webs is shown in Table 4.8.

Table 4. 8 Standard deviation and CV% of mean angles in the fibre orientation distribution

Parameters	P.P Webs				Viscose Webs			
	Parallel laid		Cross Laid		Parallel laid		Cross Laid	
Fibre Fineness (dtex)	1.7	3.3	1.7	3.3	1.7	3.3	1.7	3.3
Mean Angle (Degrees)	75.5^0	91.1^0	93.7^0	89.1^0	104.4^0	99.3^0	84.7^0	96.0^0
STD. DEV (Degrees)	40.8^0	41.7^0	43.7^0	47.1^0	47.6^0	42.7^0	52.4^0	51.5^0
CV (%)	54.1	45.4	47.7	52.9	45.6	43.0	61.9	54.6

As shown in Table 4.8 and Figures 4.4 to 4.7, it was established that the structural anisotropy of carded webs (and parallel-laid webs) composed of different fibre diameters differed as indicated below:-

polypropylene (1.7dtex)>polypropylene (3.3 dtex);

Viscose (3.3 dtex) >Viscose (1.7 dtex)

The cross-laid webs differed from the parallel-laid webs in the following two aspects:-

1) The anisotropy of fibre orientation in the cross-laid webs was smaller than that of the parallel-laid webs.

2) The maximum fibre orientation in the cross-laid webs was around 45^0~90^0 degrees different from the maximum fibre orientation in the parallel-laid webs.

Examples of the fibre orientation distributions obtained for two commercial nonwoven wound dressings, (Sorbsan and Soffban Natural, reported in Chapter 2), are shown in Figures 4.8(a) and 4.8(b) respectively. Sorbsan is a parallel-laid unbonded web composed of calcium alginate fibre and Soffban Natural is a needled fabric composed of cellulosic fibre.

Figure 4. 8 Fibre orientation distributions for the commercial nonwoven wound dressing fabrics

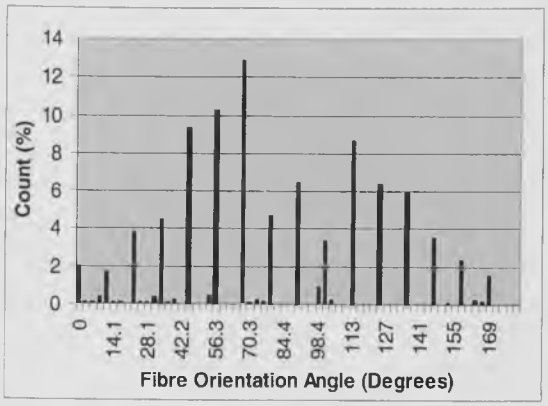

(a) Sorbsan

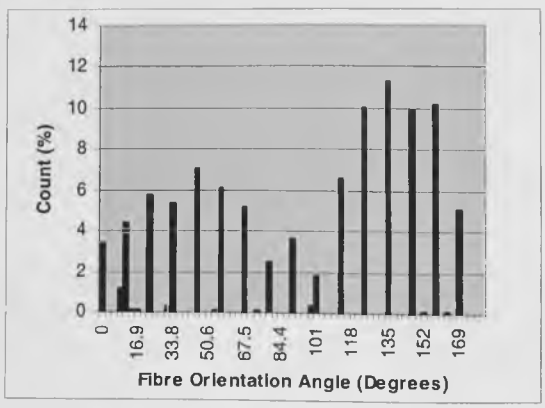

(b) Soffban Natural

It is apparent that the distributions are similar to those obtained for the experimental fabrics.

4.5 STRUCTURAL CHARACTERISTICS OF THE EXPERIMENTAL NONWOVEN FABRICS

Important elements of nonwoven fabric structure are fibre orientation[90], fibre curl[253], and the freedom of movement of fibres between the bond points[94]. Many researchers have reported that the anisotropy of mechanical properties in nonwoven fabrics can be explained by anisotropy in the fabric structure, particularly, the fibre orientation distribution[91].

Anisotropy of the fabric structure arises from the methods of nonwoven fabric manufacture. For nonwoven fabrics made from carded webs such as those produced in the present work, the methods of web formation and subsequent web bonding are particularly important.

4.5.1 Characteristics of the Unbonded Web Structures

In this work, two main classes of carded structure are considered, i.e., cross-laid and parallel-laid. A schematic of the general geometric arrangement of fibres in such webs is shown in Figure 4.9 (a) and (b).

The term parallel-laid is generally used to describe webs with fibres preferentially arranged in one direction (see Figure 4.9(a)).

Cross-laid webs are usually made by folding or cross lapping of carded webs. Cross-laid webs can be balanced, with approximately the same number of fibres in both directions, or unbalanced, with more fibres oriented in one direction than the other. Figure 4.9(b) shows a schematic representation of a cross-laid web.

Figure 4. 9 The typical geometric arrangement of fibres in Cross-laid and Parallel-laid web.

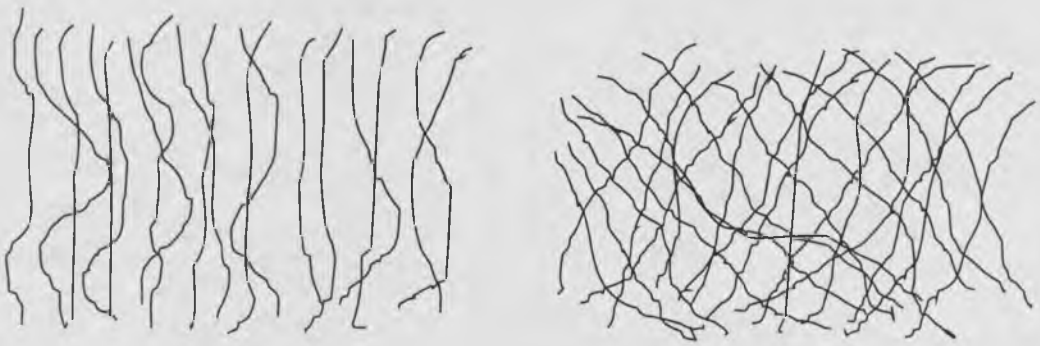

(a) Parallel-laid web (b) Cross-laid web

The frequency distribution and probability density function of a typical cross-laid web is bimodal (showing two local maximum over a 180-degree range of orientation angles). Cartesian plots of these functions have a characteristic 'W' shape for cross-laid webs. In some cases, the two predominant directions may be offset by around 45^0~90^0 as shown in Figures 4.6 and 4.7 and the offset is controlled by the cross-lapping process.

4.5.2 Characteristics of the Needlepunched Nonwoven Structures

Needle-punched nonwoven fabrics have a characteristic structural architecture resulting from their method of manufacture. The reorientation of fibres and the migration of fibres from the surface to the interior of the web[262] are shown in Figure 4.10. Needle

marking may also occur (see Figure 4.10), which is visible as a series of punch holes joined by reoriented fibres in the fabric plane running in the machine direction. The shape and number of the holes depends mainly on the number of needles in the needle board, the size of the needles, the fibre type and the punch density.

Figure 4. 10 Structure of needlepunched fabrics

(a) Pillar structure in the cross section[262]

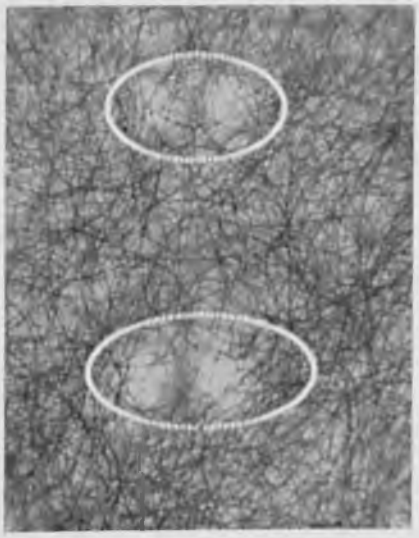

(b) Appearance of needle marks in the fabric surface of experimental fabric

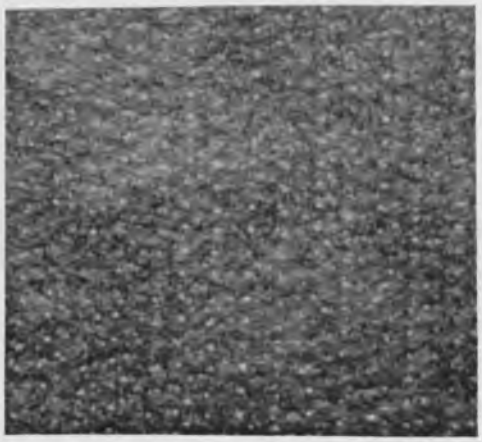

(c) Cross section of a needle mark[262]. (d). Appearance of needle marking in the surface of experimental needled fabric.

The depth of needle penetration, the number of barbs that pass through a web and the distance each barb and its attached fibres travel are important variables in the punching process. Previously, the effects of changes in penetration depth and the number of barbs[94, 261, 262] on the fabric structure have been investigated. These experiments showed that fabric strength is influenced by alterations in barb position within the web. Maximum fabric tenacity from a given web can be obtained by using only three barbs if the depth of penetration is adjusted accordingly. In needlepunched fabrics, many fibres are aligned in the transverse direction[94] and have greater porosity and a larger number of curved inter-connected pore channels than woven fabrics.

Previous studies have also been completed on needle-punched fabrics to study the relationship between the anisotropic structure and the anisotropy of fabric tensile properties. Backer and Petterson[92] developed a fibre network theory for estimating the tensile properties of nonwoven fabrics based on measurements of fibre orientation in needle felts. Hearle and Stevenson[90, 91] also found that the stress-strain properties of nonwoven fabrics were dictated by the orientation distribution of fibre segments. Hearle et al[262] reported the effect of needle penetration on the appearance of needlefelts (see Figure 4.11). He found that the punched loops do not protrude from the bottom surface of the fabric when the needle penetration is small, the resulting fabric appearance and needle marks are illustrated in Figure 4.11(a). He found that a pseudo-knitted appearance resulting from the linked loops of fibre tufts punched by the needle barbs could be detected on the fabric surface[262] when the needle penetration is large, as illustrated in Figure 4.11(b). However, no research on the influence of these structural characteristics on fabric anisotropy has been reported.

Figure 4. 11 Needled fabric structures and the influence of process conditions[262]

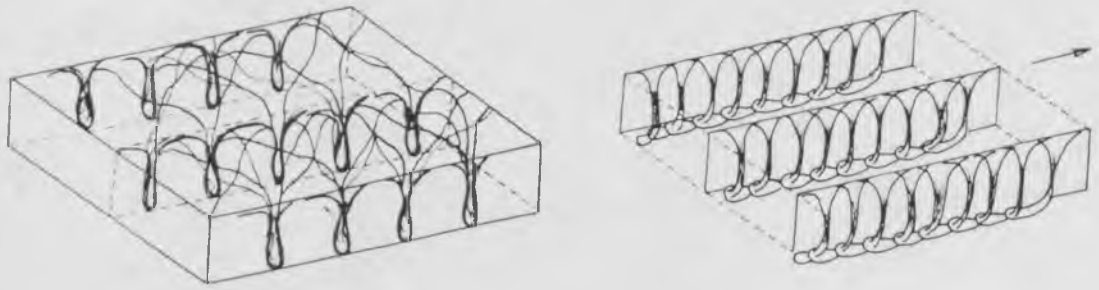

(a) low level of needling density and low needle penetration

(b) high level of needling density and high needle penetration

It is apparent from the present work that the structure of needlepunched fabrics is not homogeneous. Needle marks (see Figure 4.10) were present and the fabrics essentially comprised of two different areas. The first area (between the needle marks), is not disturbed by the needlepunching process and retains the same structure as the original unbonded web. The second needle-marked areas contain fibres oriented approximately perpendicular to the fabric plane. Other fibres are realigned in the machine direction. This reorientation of fibres appears to increase the structural anisotropy as compared with the unbonded webs.

4.5.3 Characteristics of Hydroentangled Fabric Structure

In common with needlepunching, hydroentanglement changes the structure of the unbonded web. Fibres are reoriented both in the machine direction and in the vertical direction (perpendicular to the fabric surface). Since fabrics are consolidated mainly in the areas where the water jets impact, jet marks (see Figure 4.12) are formed on the

fabric surface, which appear as visible 'lines' on the jet-side of the fabric running in the machine direction (see Figure 4.12).

Figure 4. 12 Jet marks in the surface of the experimental hydroentangled fabrics

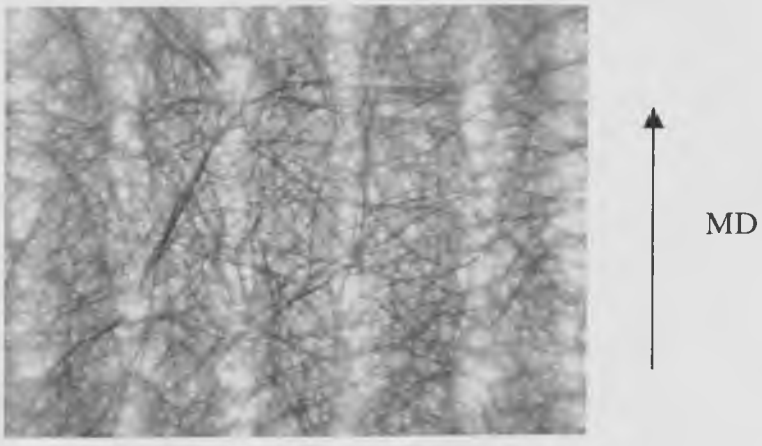

Figure 4. 13 Cross section of an experimental hydroentangled fabric composed of polypropylene fibre

Qiao[263] studied the structural characteristics of hydroentangled fabric using different processing parameters. There is no one type of hydroentangled fabric structure. At lower water jet pressure, only a small portion of fibres in the surface of the web are entangled and reoriented into the vertical direction (see Figure 4.13). At a high water jet pressure,

some fibres may be reoriented to the reverse side of the web and some of these fibres can project on the reverse side.

As in needling, jet marks are formed in the fabric surface which become more pronounced as the specific energy introduced to the web rises. Furthermore, these marks are aligned in the machine direction. Even if the carded web is an isotropic structure, the preferential orientation of the fibres in the machine direction resulting from hydroentanglement produces an anisotropic structure. This structural feature is believed to have markedly influenced the liquid transport characteristics of the experimental fabrics.

It was noted that the structure of the polypropylene hydroentangled fabric was different to the fabric made from viscose rayon fibre (see Fig. 4.13). It is noted that the specific flexural rigidity of polypropylene fibre is much higher than the viscose (see Table 4.9), and it is also known that polypropylene has higher compression recovery, bending recovery and tensile recovery[264], (compared to viscose rayon[95]). It would appear that the fibre rigidity and the bending recovery influence the ability of the jet to produce fibre entanglement during hydroentanglement. For the hydroentangled fabric composed of polypropylene, only the fibres in the surface of the resulting fabric were effectively bonded, and the fibres inside the fabric were poorly entangled. The fabric surface was therefore more compact than the fabric core (see Fig. 4.13).

Table 4. 9 Specific flexural rigidity of polypropylene and viscose fibres

Specific Flexural Rigidity	**Viscose**	**Polypropylene**
($mN.mm/tex^2$)	0.35	0.51

Also, it is interesting to note that the hydroentangled fabrics made from the parallel-laid polypropylene webs had higher packing density when the fabric was produced from webs with fibres aligned across the width of machine (fabric PA1VV1 compared to fabric PA1PP1). That is, fabric PA1VV1 was more compact than fabric PV1PP1 and had a higher degree of fibre entanglement.

The fabrics composed of viscose rayon were visually more compact than the polypropylene fabrics.

CHAPTER 5 THE EFFECT OF FABRIC STRUCTURAL PARAMETERS ON THE ANISOTROPY OF LIQUID TRANSPORT IN NONWOVEN WOUND DRESSING FABRICS

In Chapter 1, it was indicated that wound dressings require particular liquid handling properties depending on the specific application. To construct wound dressings so that they meet the specific requirements of the product application, the structural architecture of the material needs to be engineered so that 'predictable' or 'controlled' fluid handling properties can be obtained. Thus, in addition to the fibre composition, the structural characteristics of the nonwoven fabric are key to understanding and optimising the performance of wound dressing applications and it is necessary to understand how the fabric structure influences liquid transport in such fabrics. The aim of this chapter is to elucidate the influence of nonwoven fabric structure on the anisotropy of liquid transport using the newly constructed measuring system described in Chapter 3 and the fabrics produced in Chapter 4.

5.1 DEFINITION OF TERMS

5.1.1 Anisotropy of Permeability

As indicated before, the directional permeability of a porous fabric obeys Ferrandon's equation[170]. The anisotropy of fabric permeability, ω_k, was defined in section 3.9.4 as the ratio of the two principle permeabilities as follows:

$$\omega_k = \frac{k_2}{k_1} \qquad (5.1.1)$$

Where k_1 and k_2 are the principle permeabilities in the two orthogonal directions ϕ and $(\phi + \frac{\pi}{2})$ in the fabric plane using a Cartesian coordinate system x_1 and x_2 respectively. The angle ϕ is called the characteristic angle. The terms k_1, k_2 and ϕ are defined in Ferrandon's equation (see equation 3.9.4.2).

5.1.2 Anisotropy of Liquid Absorption

The anisotropy of liquid absorption in a fabric is defined as the ratio of the volumetric flow rate in the two principle directions.

The liquid absorption rate can also be described using Darcy's Law[104], where the driven pressure in the direction of liquid absorption θ is the capillary pressure, $p(\theta)$. According to Darcy's law, the ratio of flow rate in liquid absorption, ω_a, can be rewritten as follows:-

$$\omega_a = \frac{k_2 p_2}{k_1 p_1} \qquad (5.1.2)$$

Where p_1 and p_2, are the capillary pressures in the same directions as the principle permeabilities, k_1 and k_2, respectively.

Although the directional capillary pressure $p(\theta)$ is determined by the properties of the liquid and the fabric structure (especially the fibre orientation distribution)[265], the differences in directional capillary pressure in different directions of the fabric are dominated by the anisotropy of the fabric structure. That is, the anisotropy of liquid absorption in a homogeneous structure is dominated by the instrinsic anisotropy of the fabric structure.

5.2 DETERMINATION OF THE ANISOTROPY OF PERMEABILITY AND LIQUID ABSORPTION FROM THE EXPERIMENTAL DATA

According to the definitions of the anisotropy of permeability and liquid absorption given in sections (3.10.4) and (5.1), the stages involved in calculating these parameters from the measured results of the new capacitance system (see Chapter 3) are now described.

5.2.1 Stage 1

The ratio of the mass of liquid in the fabric per unit voltage of the signal is defined in equations (3.10.3.1) and (3.10.3.2), which can be written as follows:-

$$\psi = \frac{M(T)}{\sum_{i=1}^{9} V_i(T)} \quad (g/volt), \quad (i=1, 2, \ldots 9) \qquad (5.3.1)$$

Where $V_i(T)$ is the measured voltage in the i_{th} segment at the moment T, and $M(T)$ is the mass of the liquid that has been retained by the fabric during testing at the moment T.

5.2.2 Stage 2

The volumetric (or mass) rate of liquid transmission per minute of the i_{th} segment, ω_i, in each segment (i.e. in all eight directions in the measuring system) is therefore given by the following equation:-

$$\omega_i = \frac{V_i(T)}{T}\psi \quad (g/s) \qquad (5.3.2)$$

5.2.3 Stage 3

The permeability of the test fabric in the i_{th} segment can be calculated by substituting ω_i, the fabric thickness d, and time T into the equation (3.10.3.12).

5.2.4 Stage 4

The ratio of the permeability of the fabric in the direction of each segment to the permeability of the fabric in the machine direction (i.e., in the direction of the 1_{st} segment (at 0 degrees)) is calculated.

5.2.5 Stage 5

Since directional permeability obeys Ferrandon's equation[170] as shown in equation (5.1.4), all the ratios of permeability in each segment (direction) were substituted into equation (5.1.4) and the Least Square Residual Algorithm[222] was used to obtain the principle specific permeabilities k_1, k_2 and the principle angle ψ .

5.2.6 Stage 6

The ratio, k_2/k_1, is obtained as the anisotropy of permeability from forced flow experiments where the hydraulic pressures from the liquid source point in each direction were identical. In liquid absorption, this calculated ratio is actually the anisotropy of absorption where the capillary pressures in each direction are not the same.

5.3 STUDY OF THE ANISOTROPY OF PERMEABILITY AND LIQUID ABSORPTION IN THE EXPERIMENTAL FABRICS

The new measuring device described in Chapter 3 was used to determine the liquid transport properties of a wide range of nonwoven fabrics designed for use as dressings (described in Chapter 4). The testing procedures are described in section (3.9).

5.3.1 Measurement Conditions

5.3.1.1 Set-up of the Measuring System

The distance between the upper plate and lower plates was decided according to the thickness of the sample. The settings used are shown in Table 5.1.

Table 5. 1 Distance between plates of capacitance transducers

Hydroentangled polypropylene and unbonded webs	9 mm
Needlepunched fabrics and hydroentangled viscose rayon fabrics	5 mm

Two types of liquid were used as test fluid in the experimental work, distilled water and Liquid A (reduced surface tension, see section 4.4.4). Liquid A was only used for measurements on the hydroentangled polypropylene fabrics due to its high liquid-fibre interface tension, and the other nonwoven fabrics were measured using distilled water.

5.3.1.2 Fabrics Used for Evaluation

The specification of the fabrics used for testing were described earlier (see Tables 4.2 and 4.6 in Chapter 4). The test samples may be summarised as follows:

1. Unbonded webs.

2. Needlepunched fabrics made from the unbonded webs.

3. Hydroentangled fabrics made from the unbonded webs.

All three types of structure were used in the measurement of the anisotropy of permeability; but only the needlepunched fabrics and the hydroentangled viscose fabric were used to measure the anisotropy of absorption. This is because the surface tension of the hydroentangled polypropylene fabrics was much lower than that of the distilled water and so the water could not penetrate into the fabric at a small external hydraulic pressure.

5.3.2 Experimental Results

5.3.2.1 Measured Results of Anisotropy of Permeability: Forced Liquid Flow Through the Fabrics at a Constant Flow Rate

Table 5.2 shows the measured results of the volumetric ratio of liquid flow through the fabric in eight directions. Generally R^2 values of around 0.9 were obtained.

Table 5.3 shows the measured results of permeabilities in eight directions at a time (T) in the fabric samples.

Table 5.4 shows the relative ratio of permeabilities in each direction to the permeabilities in the machine direction in each of the fabric samples.

Table 5.5 shows the empirical anisotropy of permeability for each fabric sample and its characteristic angle.

Table 5.6 shows the calculated permeability from the obtained principle permeabilities and its characteristic angles in terms of the hydraulic pressure, $P_0(T)$, in eight directions for each of the fabric samples.

5.3.2.2 Measured Results of the Anisotropy of Liquid Absorption in the Fabrics due to Capillary Pressure

Table 5.7 shows the measured results of the absorption ratio as the liquid spreads in eight directions in the fabric samples. Generally R^2 values of around 0.9 were obtained.

Table 5.8 shows the measured results of the product of permeability and the capillary pressure in eight directions ($k\Delta p$) at a time (T) in the sample fabrics.

Table 5.9 shows the ratio of liquid absorption in each separate direction to the corresponding liquid absorption in the machine direction in all the fabrics (i.e., the relative ratio of the product of permeability and its corresponding capillary pressure in each direction to that in the machine direction for each of the fabric samples).

Table 5.10 shows the empirical anisotropy of liquid absorption in each fabric and its principle angle.

Table 5.11 shows the calculated product of permeability and its corresponding capillary pressure ($k\Delta p$) in all eight directions in the fabrics.

In Tables 5.1~5.11, 0 and 90 degrees represent the machine direction (MD) and the cross direction (CD) respectively. All the symbols used in these tables to denote different fabrics have been reproduced from Tables (4.1) and (4.2) in section 4.1 of Chapter 4.

For the purpose of comparison, test results for three commercial wound dressing fabrics have also been included (Sorbsan, Soffban Natural and Lantor).

Table 5. 2(a) Measured flow rates (g/s) in forced flow through the fabrics in different directions

Angles (Degrees)	0^0 (MD)	45^0	90^0	135^0	180^0	225^0	270^0	315^0	Sum
PA1WEB	0.098	0.064	0.038	0.047	0.063	0.059	0.030	0.065	0.472
PA2WEB	0.036	0.027	0.046	0.027	0.028	0.024	0.052	0.058	0.303
PB1WEB	0.048	0.034	0.029	0.030	0.047	0.028	0.023	0.024	0.268
PB2WEB	0.046	0.038	0.040	0.018	0.013	0.043	0.048	0.046	0.280
VA2WEB	0.056	0.052	0.039	0.047	0.052	0.046	0.031	0.044	0.377
VA1WEB	0.044	0.054	0.059	0.051	0.013	0.048	0.088	0.079	0.447
VB1WEB	0.104	0.077	0.054	0.053	0.047	0.040	0.013	0.063	0.462
VB2WEB	0.053	0.062	0.065	0.060	0.020	0.054	0.090	0.084	0.500
PA2N1	0.031	0.031	0.017	0.030	0.035	0.030	0.029	0.026	0.240
PA2N2	0.029	0.042	0.021	0.022	0.043	0.046	0.032	0.018	0.262
PA1N1	0.024	0.029	0.013	0.015	0.035	0.031	0.017	0.012	0.182
PA1N2	0.017	0.022	0.008	0.015	0.023	0.023	0.007	0.006	0.126
PB1N1	0.043	0.042	0.035	0.044	0.046	0.040	0.035	0.030	0.328
PB1N2	0.043	0.030	0.028	0.030	0.036	0.034	0.025	0.037	0.273
PB2N1	0.053	0.051	0.025	0.037	0.057	0.071	0.065	0.057	0.427
PB2N2	0.044	0.031	0.023	0.031	0.032	0.034	0.029	0.028	0.261
VA1N1	0.021	0.023	0.009	0.025	0.034	0.033	0.028	0.019	0.199
VA1N2	0.040	0.045	0.017	0.031	0.036	0.035	0.036	0.033	0.284
VA2N1	0.028	0.030	0.017	0.028	0.033	0.034	0.034	0.029	0.243
VA2N2	0.037	0.035	0.017	0.036	0.037	0.039	0.037	0.041	0.291
VB1N1	0.025	0.041	0.021	0.035	0.042	0.049	0.030	0.017	0.272
VB1N2	0.045	0.047	0.021	0.042	0.049	0.047	0.042	0.038	0.343
VB2N1_1	0.045	0.038	0.040	0.040	0.034	0.030	0.041	0.040	0.317
VB2N1_2	0.057	0.084	0.029	0.051	0.056	0.067	0.071	0.050	0.485

Table 5. 2(b) Measured flow rates (g/s) in forced flow through the fabrics in different directions

Angles (Degrees)	0^0 (MD)	45^0	90^0	135^0	180^0	225^0	270^0	315^0	Sum
VB2N3	0.070	0.071	0.027	0.057	0.065	0.066	0.061	0.054	0.493
PA1PP1	0.080	0.013	0.054	0.101	0.080	0.042	0.037	0.137	0.559
PA1VV3	0.019	0.014	0.018	0.019	0.023	0.017	0.015	0.014	0.143
PA1VV4	0.029	0.019	0.015	0.023	0.033	0.023	0.025	0.025	0.195
PA2H3	0.035	0.035	0.029	0.022	0.052	0.048	0.030	0.022	0.278
PB1PP2	0.044	0.042	0.031	0.034	0.085	0.080	0.052	0.039	0.418
PB1VV1_1	0.045	0.032	0.029	0.046	0.062	0.048	0.041	0.045	0.355
PB1VV1_2	0.042	0.041	0.044	0.029	0.060	0.041	0.046	0.033	0.342
PB2H2	0.044	0.037	0.034	0.024	0.061	0.019	0.026	0.030	0.282
VA1PP	0.021	0.003	0.004	0.024	0.041	0.006	0.004	0.005	0.113
VA1VV	0.259	0.029	0.022	0.008	0.397	0.102	0.039	0.005	0.889
VA2H1	0.077	0.007	0.009	0.076	0.047	0.019	0.018	0.026	0.293
VB1VV1	0.063	0.004	0.000	0.002	0.002	0.010	0.005	0.009	0.115
VB2H2	0.037	0.017	0.028	0.107	0.134	0.013	0.008	0.007	0.394
SORBSAN	0.027	0.022	0.028	0.028	0.026	0.021	0.018	0.025	0.208
SOFFBAN NATURAL	0.093	0.039	0.032	0.096	0.054	0.073	0.092	0.109	0.591
LANTOR	0.416	0.320	0.252	0.435	0.442	0.111	0.106	0.214	0.654

Table 5. 3(a) Measured permeability of the fabrics in different directions

Angle (Degrees)	0^0 (MD)	45^0	90^0	135^0	180^0	225^0	270^0	315^0
PA1WEB	1.26E-07	7.88E-08	4.46E-08	5.56E-08	7.73E-08	7.17E-08	3.38E-08	8.09E-08
PA2WEB	3.81E-08	2.78E-08	4.98E-08	2.76E-08	2.86E-08	2.42E-08	5.73E-08	6.41E-08
PB1WEB	8.02E-08	5.54E-08	4.62E-08	4.77E-08	7.88E-08	4.53E-08	3.52E-08	3.83E-08
PB2WEB	7.02E-08	5.77E-08	5.98E-08	2.47E-08	1.8E-08	6.58E-08	7.58E-08	6.94E-08
VA2WEB	6.08E-08	7.37E-08	8.40E-08	7.26E-08	4.75E-08	6.97E-08	9.02E-08	8.33E-08
VA1WEB	8.85E-08	7.58E-08	1.67E-08	7.00E-08	1.37E-07	1.21E-07	6.34E-08	7.96E-08
VB1WEB	1.34E-07	9.66E-08	6.51E-08	6.47E-08	5.66E-08	4.77E-08	1.39E-08	7.75E-08
VB2WEB	6.49E-08	7.69E-08	8.04E-08	7.35E-08	2.14E-08	6.51E-08	1.15E-07	1.07E-07
PA2N1	5.45E-08	5.44E-08	2.73E-08	5.17E-08	6.17E-08	5.17E-08	5.06E-08	4.41E-08
PA2N2	6.16E-08	9.49E-08	4.45E-08	4.6E-08	9.75E-08	1.04E-07	6.9E-08	3.62E-08
PA1N1	3.89E-08	4.8E-08	2.09E-08	2.37E-08	5.91E-08	5.33E-08	2.79E-08	1.91E-08
PA1N2	3.43E-08	4.69E-08	1.59E-08	3.13E-08	4.8E-08	4.88E-08	1.32E-08	1.17E-08
PB1N1	7.17E-08	6.92E-08	5.63E-08	7.36E-08	7.6E-08	6.61E-08	5.71E-08	4.76E-08
PB1N2	8.66E-08	5.8E-08	5.54E-08	5.77E-08	7.15E-08	6.83E-08	4.89E-08	7.36E-08
PB2N1	8.6E-08	8.33E-08	3.68E-08	5.74E-08	9.29E-08	1.19E-07	1.08E-07	9.26E-08
PB2N2	1.03E-07	7.02E-08	4.96E-08	6.95E-08	7.34E-08	7.75E-08	6.44E-08	6.23E-08
VA1N1	4.54E-08	4.83E-08	1.68E-08	5.27E-08	7.62E-08	7.43E-08	6.17E-08	3.97E-08
VA1N2	1.12E-07	1.27E-07	4.44E-08	8.38E-08	9.88E-08	9.64E-08	9.86E-08	9.03E-08
VA2N1	5.28E-08	5.6E-08	2.98E-08	5.28E-08	6.15E-08	6.51E-08	6.52E-08	5.36E-08
VA2N2	8.82E-08	8.38E-08	3.86E-08	8.46E-08	8.88E-08	9.39E-08	8.77E-08	9.85E-08
VB1N1	4.29E-08	7.47E-08	3.63E-08	6.36E-08	7.74E-08	9.1E-08	5.39E-08	2.74E-08
VB1N2	9.49E-08	1.01E-07	4.07E-08	8.83E-08	1.06E-07	1.01E-07	8.99E-08	8.01E-08

Table 5.3(b) Measured permeability in the fabrics in different directions

Angle (Degrees)	0^0 (MD)	45^0	90^0	135^0	180^0	225^0	270^0	315^0
VB2N1_1	6.11E-08	5.1E-08	5.4E-08	5.39E-08	4.54E-08	3.89E-08	5.54E-08	5.39E-08
VB2N1_2	9.03E-08	1.37E-07	4.19E-08	7.95E-08	8.8E-08	1.06E-07	1.13E-07	7.72E-08
VB2N3	1.31E-07	1.33E-07	4.62E-08	1.04E-07	1.19E-07	1.22E-07	1.12E-07	9.82E-08
PA1PP1	8.01E-08	1.04E-08	5.21E-08	1.03E-07	7.98E-08	3.92E-08	3.38E-08	1.43E-07
PA1VV3	3.68E-08	2.78E-08	3.61E-08	3.78E-08	4.7E-08	3.34E-08	2.89E-08	2.71E-08
PA1VV4	9.98E-08	6.21E-08	4.95E-08	7.94E-08	1.17E-07	7.95E-08	8.56E-08	8.61E-08
PA2H3	4.82E-08	4.87E-08	3.99E-08	2.99E-08	7.55E-08	6.82E-08	3.07E-08	2.9E-08
PB1PP2	4.27E-08	4.08E-08	2.92E-08	3.25E-08	8.83E-08	8.21E-08	5.16E-08	3.79E-08
PB1VV1_1	5.95E-08	4.12E-08	3.68E-08	6.12E-08	8.5E-08	6.44E-08	5.39E-08	5.94E-08
PB1VV1_2	5.61E-08	5.48E-08	5.83E-08	3.68E-08	8.15E-08	5.37E-08	6.07E-08	4.24E-08
PB2H2	6.43E-08	5.36E-08	4.88E-08	3.29E-08	9.21E-08	2.55E-08	3.58E-08	4.3E-08
VA1PP	1.01E-07	1.22E-08	1.82E-08	1.19E-07	2.06E-07	2.58E-08	1.66E-08	1.99E-08
VA1VV	1.43E-06	1.35E-07	9.61E-08	3.12E-08	2.28E-06	5.23E-07	1.83E-07	2E-08
VA2H1	4.66E-07	3.38E-08	4.64E-08	4.6E-07	2.71E-07	1.03E-07	9.5E-08	1.4E-07
VB1VV1	2.87E-07	1.27E-08	7.95E-10	5.35E-09	3.02E-10	3.83E-08	1.79E-08	3.53E-08
VB2H2	1.83E-07	7.88E-08	1.34E-07	5.85E-07	7.46E-07	5.66E-08	3.27E-08	2.89E-08
SORBSAN	2.49E-07	1.97E-07	2.55E-07	2.61E-07	2.38E-07	1.99E-07	1.59E-07	2.37E-07
SOFFBAN NATURAL	2.82E-07	1.11E-07	8.79E-08	2.92E-07	1.55E-07	2.15E-07	2.79E-07	3.37E-07
LANTOR	1.21E-06	9.14E-07	7.07E-07	1.27E-06	1.29E-06	2.92E-07	2.78E-07	5.91E-07

Table 5. 4(a) Ratio of permeability in the fabrics in different directions

Angle (Degrees)	0^0 (MD)	45^0	90^0	135^0	180^0	225^0	270^0	315^0	360^0
PA1WEB	1	0.632	0.362	0.447	0.629	0.557	0.265	0.616	1
PA2WEB	1	0.689	1.208	0.844	0.794	0.684	1.416	1.595	1
PB1WEB	1	0.67	0.57	0.59	0.956	0.568	0.467	0.532	1
PB2WEB	1	0.791	0.907	0.358	0.344	0.889	1.255	0.654	1
VA2WEB	1	1.213	1.382	1.194	0.782	1.147	1.484	1.371	1
VA1WEB	1	0.857	0.189	0.792	1.548	1.369	0.716	0.9	1
VB1WEB	1	0.721	0.486	0.483	0.423	0.356	0.104	0.578	1
VB2WEB	1	1.185	1.239	1.132	0.329	1.004	1.771	1.646	1
PA2N1	1	0.998	0.5	0.948	1.131	0.948	0.927	0.809	1
PA2N2	1	1.54	0.722	0.747	1.582	1.683	1.121	0.587	1
PA1N1	1	1.233	0.536	0.609	1.519	1.37	0.716	0.492	1
PA1N2	1	1.366	0.463	0.911	1.397	1.42	0.384	0.34	1
PB1N1	1	0.965	0.785	1.026	1.06	0.921	0.796	0.663	1
PB1N2	1	0.669	0.639	0.667	0.825	0.788	0.565	0.85	1
PB2N1	1	0.969	0.428	0.668	1.081	1.385	1.252	1.078	1
PB2N2	1	0.685	0.484	0.677	0.716	0.756	0.628	0.608	1
VA1N1	1	1.065	0.371	1.163	1.679	1.638	1.361	0.876	1
VA1N2	1	1.131	0.396	0.748	0.881	0.86	0.879	0.805	1
VA2N1	1	1.061	0.564	1.001	1.166	1.233	1.236	1.015	1
VA2N2	1	0.949	0.438	0.959	1.006	1.064	0.993	1.116	1
VB1N1	1	1.743	0.845	1.482	1.805	2.122	1.256	0.639	1
VB1N2	1	1.068	0.429	0.93	1.112	1.063	0.947	0.843	1
VB2N1_1	1	0.834	0.883	0.882	0.743	0.636	0.907	0.881	1
VB2N1_2	1	1.514	0.463	0.88	0.974	1.176	1.255	0.855	1

Table 5. 4(b) Ratio of permeability in the fabrics in different directions

Angle (Degrees)	0^0 (MD)	45^0	90^0	135^0	180^0	225^0	270^0	315^0	360^0
VB2N3	1	1.018	0.354	0.798	0.914	0.937	0.857	0.752	1
PA1PP1	1	0.13	0.651	1.291	0.997	0.489	0.422	1.791	1
PA1VV3	1	0.756	0.982	1.028	1.276	0.909	0.786	0.737	1
PA1VV4	1	0.622	0.496	0.795	1.173	0.796	0.858	0.863	1
PA2H3	1	1.01	0.828	0.621	1.567	1.416	0.845	0.602	1
PB1PP2	1	0.954	0.684	0.761	2.066	1.921	1.206	0.887	1
PB1VV1_1	1	0.692	0.618	1.029	1.43	1.083	0.906	0.999	1
PB1VV1_2	1	0.977	1.039	0.657	1.453	0.959	1.083	0.756	1
PB2H2	1	0.833	0.759	0.512	1.433	0.396	0.557	0.669	1
VA1PP	1	0.121	0.18	1.18	2.042	0.256	0.165	0.197	1
VA1VV	1	0.094	0.067	0.022	1.587	0.364	0.128	0.014	1
VA2H1	1	0.072	0.099	0.988	0.581	0.221	0.204	0.301	1
VB1VV1	1	0.044	0.003	0.019	0.001	0.134	0.063	0.123	1
VB2H2	1	0.432	0.732	3.199	4.083	0.31	0.179	0.158	1
SORBSAN	1	0.791	1.023	1.048	0.952	0.796	0.637	0.950	1
SOFFBAN NATURAL	1	0.393	0.312	1.034	0.551	0.762	0.991	1.196	1
LANTOR	1	0.756	0.585	1.048	1.067	0.242	0.230	0.489	1

Table 5. 5(a) Anisotropy of permeability in the fabrics

	K_1	K_2	ϕ	*RSM*	k_1/k_2	k_2/k_1
PA1WEB	0.374	0.897	-4.192^0	0.173	0.419	2.425
PA2WEB	1.437	0.768	-25.713^0	0.483	1.875	0.539
PB1WEB	0.453	0.991	-2.7490	0.052	0.459	2.213
PB2WEB	1.058	0.633	20.853^0	0.788	1.670	0.606
VA2WEB	1.478	0.974	-14.181^0	0.077	1.517	0.659
VA1WEB	0.607	1.332	-6.627^0	0.601	0.456	2.194
VB1WEB	0.361	0.816	-0.651^0	0.380	0.442	2.263
VB2WEB	1.642	0.850	-14.392^0	0.663	1.931	0.518
PA2N1	0.756	1.073	-9.736^0	0.124	0.704	1.420
PA2N2	0.715	1.698	-34.523^0	0.341	0.421	2.375
PA1N1	0.530	1.604	-25.379^0	0.214	0.331	3.025
PA1N2	0.458	1.800	-26.097^0	0.332	0.254	3.932
PB1N1	0.783	1.034	-11.789^0	0.069	0.757	1.321
PB1N2	0.607	0.944	2.652^0	0.047	0.643	1.555
PB2N1	0.808	1.180	-31.538^0	0.526	0.685	1.461
PB2N2	0.547	0.911	-6.502^0	0.069	0.600	1.667
VA1N1	0.890	1.388	-25.314^0	1.042	0.641	1.560
VA1N2	0.670	1.053	-20.787^0	0.185	0.636	1.571
VA2N1	0.928	1.129	-25.362^0	0.280	0.822	1.217
VA2N2	0.830	1.053	5.065^0	0.242	0.789	1.268
VB1N1	0.901	1.917	-39.477^0	1.020	0.470	2.127
VB1N2	0.751	1.117	-17.908^0	0.183	0.673	1.487
VB2N1_1	0.795	0.932	36.003^0	0.086	0.853	1.172
VB2N1_2	0.770	1.321	-39.280^0	0.403	0.583	1.715

Table 5.5(b) Anisotropy of permeability in the fabrics

	k_1	K_2	ϕ	*RSM*	k_1/k_2	k_2/k_1
VB2N3	0.653	1.055	-18.369^0	0.160	0.620	1.614
PA1PP1	0.377	2.039	29.417^0	0.242	0.185	5.402
PA1VV3	0.805	1.065	5.019^0	0.153	0.756	1.323
PA1VV4	0.631	1.062	8.057^0	0.110	0.594	1.683
PA2H3	0.672	1.396	-25.477^0	0.339	0.481	2.078
PB1PP2	0.822	1.592	-26.320^0	1.377	0.516	1.937
PB1VV1_1	0.775	1.167	10.050^0	0.244	0.664	1.507
PB1VV1_2	0.853	1.129	-23.876^0	0.309	0.756	1.323
PB2H2	0.495	1.124	-1.044^0	0.337	0.440	2.271
VA1PP	0.154	7.094	17.999^0	1.216	0.022	46.025
VA1VV	0.064	14.821	-12.866^0	0.280	0.004	232.593
VA2H1	0.128	4.186	20.424^0	0.369	0.031	32.757
VB1VV1	0.040	0.736	-3.638^0	0.677	0.054	18.515
VB2H2	0.354	6.632	20.968^0	11.134	0.053	18.748
SORBSAN	0.782	1.041	25.814^0	0.081	0.751	1.332
SOFFBAN NATURAL	0.552	1.151	34.450^0	0.447	0.480	2.085
LANTOR	0.405	1.130	13.893^0	0.355	0.359	2.789

Table 5. 6(a) Calculated ratio of permeability from k_1, k_2 and ϕ in different directions

Angle (Degrees)	0^0 (MD)	45^0	90^0	135^0	180^0	225^0	270^0	315^0	360^0
PA1WEB	0.885	0.563	0.376	0.496	0.885	0.563	0.376	0.496	0.885
PA2WEB	0.841	0.821	1.255	1.276	0.841	0.821	1.255	1.276	0.841
PB1WEB	0.976	0.650	0.455	0.598	0.976	0.650	0.455	0.598	0.976
PB2WEB	0.665	0.936	0.983	0.683	0.665	0.936	0.983	0.683	0.665
VA2WEB	0.979	1.121	1.468	1.234	0.979	1.121	1.468	1.234	0.979
VA1WEB	1.216	1.046	0.635	0.693	1.216	1.046	0.635	0.693	1.216
VB1WEB	0.816	0.505	0.361	0.496	0.816	0.505	0.361	0.496	0.816
VB2WEB	0.877	0.972	1.553	1.323	0.877	0.972	1.553	1.323	0.877
PA2N1	1.060	0.941	0.762	0.838	1.060	0.941	0.762	0.838	1.060
PA2N2	1.178	1.624	0.878	0.729	1.178	1.624	0.878	0.729	1.178
PA1N1	1.169	1.306	0.605	0.574	1.169	1.306	0.605	0.574	1.169
PA1N2	1.148	1.376	0.535	0.497	1.148	1.376	0.535	0.497	1.148
PB1N1	1.020	0.943	0.791	0.844	1.020	0.943	0.791	0.844	1.020
PB1N2	0.943	0.725	0.608	0.754	0.943	0.725	0.608	0.754	0.943
PB2N1	1.048	1.151	0.884	0.822	1.048	1.151	0.884	0.822	1.048
PB2N2	0.904	0.724	0.550	0.647	0.904	0.724	0.550	0.647	0.904
VA1N1	1.259	1.305	0.953	0.928	1.259	1.305	0.953	0.928	1.259
VA1N2	0.982	0.961	0.702	0.714	0.982	0.961	0.702	0.714	0.982
VA2N1	1.086	1.102	0.959	0.947	1.086	1.102	0.959	0.947	1.086
VA2N2	1.051	0.909	0.832	0.948	1.051	0.909	0.832	0.948	1.051
VB1N1	1.317	1.897	1.147	0.906	1.317	1.897	1.147	0.906	1.317
VB1N2	1.068	1.015	0.775	0.806	1.068	1.015	0.775	0.806	1.068
VB2N1_1	0.880	0.798	0.838	0.928	0.880	0.798	0.838	0.928	0.880
VB2N1_2	1.027	1.312	0.925	0.773	1.027	1.312	0.925	0.773	1.027

Table 5.6(b) Calculated ratio of permeability from k_1, k_2 and ϕ in different directions

Angle (Degrees)	0^0 (MD)	45^0	90^0	135^0	180^0	225^0	270^0	315^0	360^0
VB2N3	0.994	0.939	0.679	0.707	0.994	0.939	0.679	0.707	0.994
PA1PP1	0.989	0.401	0.470	1.547	0.989	0.401	0.470	1.547	0.989
PA1VV3	1.062	0.895	0.806	0.940	1.062	0.895	0.806	0.940	1.062
PA1VV4	1.048	0.739	0.636	0.852	1.048	0.739	0.636	0.852	1.048
PA2H3	1.164	1.246	0.743	0.713	1.164	1.246	0.743	0.713	1.164
PB1PP2	1.344	1.452	0.908	0.865	1.344	1.452	0.908	0.865	1.344
PB1VV1_1	1.150	0.871	0.783	1.001	1.150	0.871	0.783	1.001	1.150
PB1VV1_2	1.072	1.084	0.889	0.881	1.072	1.084	0.889	0.881	1.072
PB2H2	1.123	0.697	0.495	0.678	1.123	0.697	0.495	0.678	1.123
VA1PP	1.346	0.193	0.170	0.687	1.346	0.193	0.170	0.687	1.346
VA1VV	1.193	0.222	0.067	0.089	1.193	0.222	0.067	0.089	1.193
VA2H1	0.860	0.154	0.145	0.644	0.860	0.154	0.145	0.644	0.860
VB1VV1	0.667	0.087	0.040	0.066	0.667	0.087	0.040	0.066	0.667
VB2H2	2.026	0.420	0.403	1.682	2.026	0.420	0.403	1.682	2.026
SORBSAN	0.980	0.803	0.821	1.005	0.980	0.803	0.821	1.005	0.980
SOFFBAN NATURAL	0.855	0.562	0.663	1.111	0.855	0.562	0.663	1.111	0.855
LANTOR	0.488	0.421	0.764	1.024	0.488	0.421	0.764	1.024	0.488

Table 5. 7 Measured liquid absorption rates (*g/min*) through the fabrics in different directions

Angle (Degrees)	0^0 (MD)	45^0	90^0	135^0	180^0	225^0	270^0	315^0	Sum (g/min)
PA2N1	3.93E-03	3.29E-03	5.15E-03	6.20E-03	4.14E-03	3.19E-03	2.19E-03	5.23E-03	3.46E-02
PA2N2	6.03E-03	5.52E-03	3.67E-03	5.83E-03	7.94E-03	7.07E-03	5.18E-03	6.08E-03	4.31E-02
PA1N1	5.01E-03	5.54E-04	2.31E-04	4.48E-03	1.20E-02	6.59E-03	1.78E-03	5.66E-03	3.75E-02
PA1N2	1.68E-02	2.23E-02	8.36E-03	1.55E-02	2.28E-02	2.31E-02	7.07E-03	6.34E-03	1.26E-01
PB1N1	9.01E-03	4.74E-03	6.99E-03	8.20E-03	4.55E-03	2.91E-03	3.42E-03	1.89E-02	6.14E-02
PB1N2	1.63E-02	1.29E-02	8.32E-03	5.85E-03	5.85E-03	1.24E-02	1.06E-02	1.37E-02	8.92E-02
PB2N1	1.65E-02	1.82E-02	1.18E-02	1.80E-02	1.98E-02	1.62E-02	1.81E-02	1.45E-02	1.39E-01
VA1N1	5.05E-03	7.27E-03	3.14E-03	4.56E-03	6.21E-03	7.09E-03	4.62E-03	3.91E-03	4.35E-02
VA1N2	1.22E-02	9.17E-03	9.41E-03	9.72E-03	4.65E-03	6.52E-03	9.04E-03	1.33E-02	7.70E-02
VA2N1	1.32E-02	7.98E-03	1.04E-02	1.17E-02	4.01E-03	9.22E-03	8.04E-03	1.28E-02	8.02E-02
VA2N2	1.22E-02	1.42E-02	6.03E-03	1.26E-02	1.41E-02	1.20E-02	1.33E-02	1.25E-02	1.00E-01
VB1N1	1.52E-02	1.63E-02	4.30E-03	4.42E-03	4.62E-03	9.02E-03	7.76E-03	6.47E-03	7.05E-02
VB1N2	9.12E-03	4.52E-03	1.05E-03	2.50E-03	3.31E-03	6.17E-03	5.37E-03	6.00E-03	3.95E-02
VB2N1_	1.83E-02	9.17E-03	1.87E-02	1.73E-02	1.30E-02	1.41E-02	1.32E-02	1.33E-02	1.22E-01
VB2N1_	3.38E-03	2.65E-03	2.38E-03	3.41E-03	4.98E-03	3.87E-03	3.19E-03	3.06E-03	2.80E-02
VB2N2	2.22E-02	8.93E-03	6.48E-03	1.09E-02	2.83E-02	1.67E-02	1.09E-02	1.77E-02	1.26E-01
VB2N3	1.29E-02	1.69E-02	5.45E-03	9.58E-03	9.61E-03	7.37E-03	1.16E-02	1.06E-02	8.78E-02
VA1VV	1.40E-02	2.37E-03	9.50E-04	2.76E-03	1.30E-02	4.36E-03	3.06E-04	9.17E-04	4.72E-02
VA2H1	5.18E-02	1.07E-02	9.60E-03	3.32E-02	5.32E-02	1.76E-02	1.39E-02	1.75E-02	2.21E-01
VB1VV1	2.05E-02	2.01E-03	1.12E-03	4.85E-03	2.21E-02	4.53E-03	2.66E-03	3.91E-03	6.54E-02
VB2H2	5.74E-03	2.71E-03	1.32E-03	5.09E-03	1.88E-02	3.36E-03	7.07E-04	9.14E-04	4.17E-02
SORBSAN	8.66E-03	1.10E-02	6.71E-03	7.52E-03	1.68E-02	1.70E-03	1.08E-02	8.57E-03	8.96E-02
SOFFBAN NATURAL	9.93E-02	2.37E-02	7.67E-02	5.38E-02	7.19E-02	1.90E-02	1.42E-02	4.57E-02	4.11E-01

Table 5. 8 Measured liquid absorption (m^2*$P(T)$) in the fabrics in different directions

Angle (Degrees)	0^0 (MD)	45^0	90^0	135^0	180^0	225^0	270^0	315^0
PA2N1	6.05E-09	4.96E-09	8.14E-09	9.99E-09	6.41E-09	4.80E-09	3.16E-09	8.28E-09
PA2N2	1.27E-08	1.16E-08	7.35E-09	1.23E-08	1.72E-08	1.52E-08	1.08E-08	1.29E-08
PA1N1	9.01E-09	7.49E-10	2.72E-10	7.96E-09	2.37E-08	1.22E-08	2.84E-09	1.03E-08
PA1N2	3.43E-08	4.69E-08	1.59E-08	3.13E-08	4.80E-08	4.88E-08	1.32E-08	1.17E-08
PB1N1	1.41E-08	6.95E-09	1.07E-08	1.27E-08	6.64E-09	4.04E-09	4.84E-09	3.17E-08
PB1N2	2.95E-08	2.28E-08	1.41E-08	9.59E-09	9.60E-09	2.19E-08	1.84E-08	2.44E-08
PB2N1	3.83E-08	4.29E-08	2.66E-08	4.22E-08	4.68E-08	3.78E-08	4.26E-08	3.33E-08
VA1N1	1.06E-08	1.59E-08	6.27E-09	9.50E-09	1.33E-08	1.54E-08	9.63E-09	8.02E-09
VA1N2	3.27E-08	2.40E-08	2.47E-08	2.56E-08	1.14E-08	1.65E-08	2.36E-08	3.60E-08
VA2N1	2.47E-08	1.42E-08	1.91E-08	2.16E-08	6.65E-09	1.67E-08	1.44E-08	2.39E-08
VA2N2	2.66E-08	3.15E-08	1.22E-08	2.75E-08	3.11E-08	2.61E-08	2.91E-08	2.72E-08
VB1N1	2.81E-08	3.02E-08	6.96E-09	7.17E-09	7.52E-09	1.58E-08	1.34E-08	1.09E-08
VB1N2	1.91E-08	8.83E-09	1.74E-09	4.60E-09	6.27E-09	1.24E-08	1.07E-08	1.21E-08
VB2N1_1	2.47E-08	1.14E-08	2.51E-08	2.31E-08	1.68E-08	1.85E-08	1.72E-08	1.73E-08
VB2N1_2	5.42E-09	4.14E-09	3.67E-09	5.47E-09	8.30E-09	6.30E-09	5.08E-09	4.85E-09
VB2N2	3.28E-08	1.20E-08	8.35E-09	1.49E-08	4.29E-08	2.39E-08	1.49E-08	2.55E-08
VB2N3	2.29E-08	3.07E-08	8.80E-09	1.64E-08	1.65E-08	1.23E-08	2.03E-08	1.83E-08
VA1VV	6.44E-08	9.08E-09	3.27E-09	1.07E-08	5.92E-08	1.79E-08	9.05E-10	3.14E-09
VA2H1	3.13E-07	5.58E-08	4.92E-08	1.93E-07	3.22E-07	9.59E-08	7.39E-08	9.54E-08
VB1VV1	9.02E-08	6.96E-09	3.62E-09	1.85E-08	9.79E-08	1.72E-08	9.54E-09	1.46E-08
VB2H2	2.95E-08	1.29E-08	5.79E-09	2.58E-08	1.08E-07	1.63E-08	2.89E-09	3.85E-09
SORBSAN	7.55E-08	9.85E-08	5.70E-08	6.47E-08	1.55E-07	1.58E-07	9.68E-08	7.46E-08
SOFFBAN NATURAL	3.34E-07	7.09E-08	2.53E-07	1.73E-07	2.36E-07	5.60E-08	4.08E-08	1.45E-07

Table 5. 9 Ratio of liquid absorption in the fabrics in different directions

Angle (Degrees)	0^0 (MD)	45^0	90^0	135^0	180^0	225^0	270^0	315^0
PA2N1	1	0.821	1.347	1.652	1.060	0.794	0.523	1.369
PA2N2	1	0.907	0.577	0.963	1.353	1.192	0.846	1.010
PA1N1	1	0.083	0.030	0.884	2.633	1.357	0.315	1.145
PA1N2	1	1.366	0.463	0.911	1.397	1.420	0.384	0.340
PB1N1	1	0.493	0.757	0.902	0.471	0.287	0.343	2.248
PB1N2	1	0.774	0.479	0.325	0.326	0.744	0.626	0.827
PB2N1	1	1.118	0.694	1.100	1.220	0.985	1.111	0.867
VA1N1	1	1.493	0.590	0.894	1.256	1.451	0.906	0.754
VA1N2	1	0.734	0.755	0.783	0.347	0.504	0.723	1.100
VA2N1	1	0.575	0.771	0.873	0.269	0.674	0.580	0.967
VA2N2	1	1.186	0.459	1.037	1.172	0.981	1.096	1.026
VB1N1	1	1.075	0.248	0.255	0.268	0.562	0.477	0.390
VB1N2	1	0.462	0.091	0.240	0.328	0.651	0.559	0.632
VB2N1_1	1	0.464	1.019	0.936	0.681	0.750	0.697	0.700
VB2N1_2	1	0.764	0.678	1.010	1.531	1.162	0.937	0.895
VB2N2	1	0.365	0.255	0.454	1.311	0.731	0.456	0.780
VB2N3	1	1.339	0.384	0.717	0.720	0.536	0.885	0.798
VA1VV	1	0.141	0.051	0.167	0.919	0.277	0.014	0.049
VA2H1	1	0.178	0.157	0.616	1.029	0.306	0.236	0.304
VB1VV1	1	0.077	0.040	0.206	1.086	0.191	0.106	0.162
VB2H2	1	0.437	0.196	0.875	3.656	0.555	0.098	0.131
SORBSAN	1	1.305	0.756	0.858	2.060	2.088	1.283	0.989
SOFFBAN NATURAL	1	0.212	0.756	0.516	0.706	0.167	0.122	0.432

Table 5. 10 Anisotropy of liquid absorption in the fabrics

	k_1p_1	k_2p_2	ϕ	*RSM*	k_1p_1/k_2p_2	k_2p_2/k_1p_1
PA2N1	0.752	1.501	41.923^0	0.392	0.501	1.996
PA2N2	0.804	1.155	-6.287^0	0.201	0.696	1.437
PA1N1	0.424	1.834	13.327^0	2.884	0.231	4.325
PA1N2	0.458	1.800	-26.097^0	0.332	0.254	3.932
PB1N1	0.401	1.725	35.283^0	1.200	0.232	4.304
PB1N2	0.535	0.828	-20.211^0	0.440	0.646	1.548
PB2N1	0.918	1.093	-11.985^0	0.158	0.840	1.191
VA1N1	0.695	1.514	-33.376^0	0.148	0.459	2.178
VA1N2	0.948	0.627	40.689^0	0.362	1.512	0.661
VA2N1	0.601	0.918	38.000^0	0.386	0.654	1.528
VA2N2	0.873	1.105	-8.005^0	0.295	0.790	1.265
VB1N1	0.307	1.077	-24.383^0	0.525	0.285	3.511
VB1N2	0.340	0.806	-9.245^0	0.507	0.421	2.374
VB2N1_1	0.712	0.903	32.215^0	0.254	0.788	1.269
VB2N1_2	0.807	1.177	-0.853^0	0.307	0.686	1.458
VB2N2	0.381	1.115	3.695^0	0.207	0.342	2.925
VB2N3	0.664	0.980	-20.282^0	0.519	0.677	1.477
VA1VV	0.068	1.976	-11.385^0	0.025	0.034	29.164
VA2H1	0.183	1.269	12.035^0	0.060	0.145	6.920
VB1VV1	0.081	1.151	5.473^0	0.015	0.071	14.142
VB2H2	0.263	1.887	0.344^0	5.024	0.139	7.174
SORBSAN	0.882	1.763	-33.021^0	1.205	0.500	1.998
SOFFBAN NATURAL	0.241	1.015	11.926^0	0.370	0.237	4.219

Table 5. 11 Calculated ratio of liquid absorption from k_1p_1, k_2p_2 and ϕ in different directions

Angle (Degrees)	0^0 (MD)	45^0	90^0	135^0	180^0	225^0	270^0	315^0
PA2N1	1.039	0.753	0.968	1.497	1.039	0.753	0.968	1.497
PA2N2	1.149	0.986	0.807	0.912	1.149	0.986	0.807	0.912
PA1N1	1.559	0.538	0.442	0.957	1.559	0.538	0.442	0.957
PA1N2	1.148	1.376	0.535	0.497	1.148	1.376	0.535	0.497
PB1N1	0.820	0.410	0.539	1.576	0.820	0.410	0.539	1.576
PB1N2	0.777	0.755	0.559	0.570	0.777	0.755	0.559	0.570
PB2N1	1.084	1.034	0.924	0.964	1.084	1.034	0.924	0.964
VA1N1	1.116	1.445	0.831	0.711	1.116	1.445	0.831	0.711
VA1N2	0.778	0.628	0.732	0.945	0.778	0.628	0.732	0.945
VA2N1	0.765	0.604	0.691	0.911	0.765	0.604	0.691	0.911
VA2N2	1.100	1.008	0.877	0.945	1.100	1.008	0.877	0.945
VB1N1	0.754	0.821	0.349	0.337	0.754	0.821	0.349	0.337
VB1N2	0.778	0.549	0.345	0.423	0.778	0.549	0.345	0.423
VB2N1_1	0.839	0.719	0.757	0.891	0.839	0.719	0.757	0.891
VB2N1_2	1.177	0.963	0.807	0.952	1.177	0.963	0.807	0.952
VB2N2	1.106	0.534	0.382	0.606	1.106	0.534	0.382	0.606
VB2N3	0.927	0.905	0.691	0.704	0.927	0.905	0.691	0.704
VA1VV	0.971	0.202	0.070	0.097	0.971	0.202	0.070	0.097
VA2H1	1.010	0.246	0.191	0.461	1.010	0.246	0.191	0.461
VB1VV1	1.029	0.131	0.082	0.182	1.029	0.131	0.082	0.182
VB2H2	1.887	0.458	0.263	0.466	1.887	0.458	0.263	0.466
SORBSAN	1.360	1.690	1.036	0.902	1.360	1.690	1.036	0.902
SOFFBAN NATURAL	0.892	0.311	0.249	0.518	0.892	0.311	0.249	0.518

5.4 OBSERVATIONS ON THE INFLUENCE OF FABRIC STRUCTURAL PARAMETERS ON THE ANISOTROPY OF LIQUID TRANSPORT

The anisotropy of liquid transport here refers to the anisotropy of permeability and the anisotropy of liquid absorption. The fabric structural parameters discussed are the fibre orientation distribution, fibre diameter and the fabric porosity.

5.4.1 The Influence of Nonwoven Fabric Structure on the Anisotropy of Permeability

5.4.1.1 Effect of the Fibre Orientation Distribution

The fibre orientation distribution will influence the anisotropy of the nonwoven fabric structure[90], and thus it may be expected to influence the anisotropy of permeability. It was shown in Chapter 4 that parallel-laid and cross-laid webs have different fibre orientation distributions, and parallel-laid webs have a predominant fibre orientation in the machine direction. From Figures 4.4 to 4.7, it is apparent that the structural anisotropy of the fabrics made from parallel-laid webs was higher than the fabrics made from cross-laid webs.

Additionally, it is apparent from Figure 5.1 that the anisotropy of permeability in structures (unbonded webs, needlepunched and hydroentangled structures) made from such parallel-laid webs is generally higher than in fabrics made from cross-laid webs.

It is also evident in Table 5.2 that the direction of the maximum liquid flow rate in a cross-laid webs differs by around 90 degrees from that in a parallel-laid web. This may be expected because of the respective fibre orientation distributions (see Figures 4.4~4.7).

Figure 5. 1 Influence of fibre fineness on the anisotropy of permeability

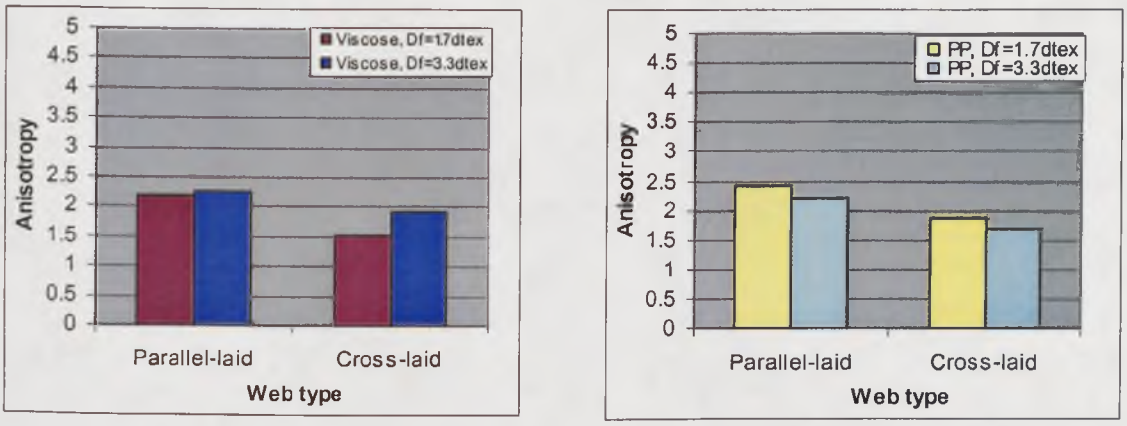

(a) Unbonded webs

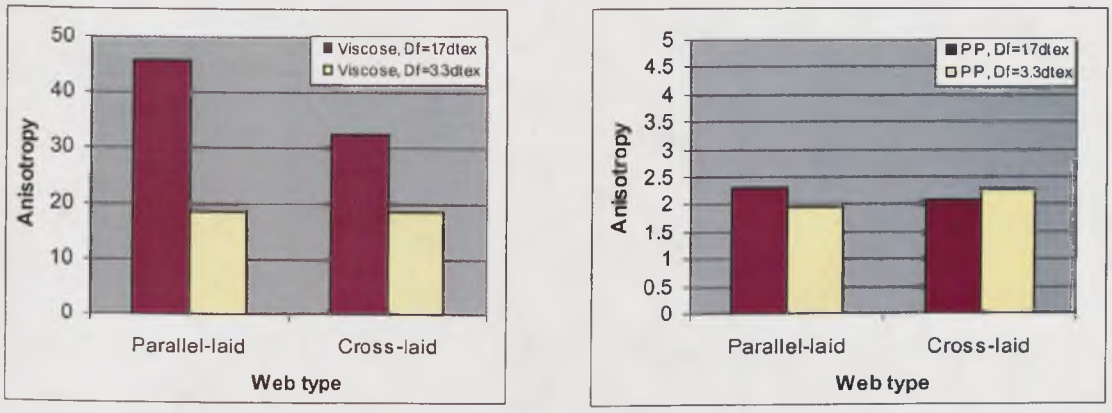

(b) Hydroentangled fabrics

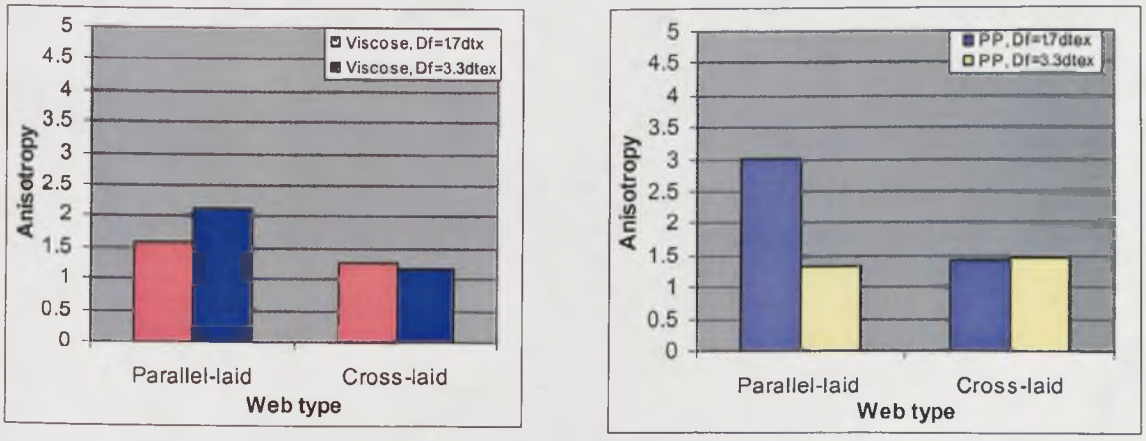

(c) Needlepunched fabrics

5.4.1.2 Effect of Bonding Method

The bonding method influences the local variations in the fabric structure, and for this reason it is considered in this section.

5.4.1.2.1 Unbonded Webs

For the unbonded webs, it is evident from Figure 5.1(a) that the anisotropy of permeability of the parallel-laid webs was greater than the anisotropy of permeability in the cross-laid webs. It was also noted that the direction of the maximum permeability in the parallel-laid webs differed by about 45~90 degrees from the direction of maximum permeability in the cross-laid structures.

5.4.1.2.2 Needlepunched Nonwovens

All the needlepunched fabrics were made from the webs referred to section (4.3). From Figure 5.1, it is apparent that the anisotropy of permeability in the needlepunched fabrics was greater than the anisotropy of permeability of their original webs.

It is interesting to note that the maximum permeability in all the needlepunched fabrics was in the machine direction, irrespective of the original method of web formation (cross-laid or parallel-laid).

This is thought to be due to the presence of the needle marks in the machine direction of the fabric which appear to act as conduits for liquid transport. Further, it is known that many fibres in the pillars are aligned perpendicular to the fabric plane, and that fibres aligned in the cross direction are also reoriented in the machine direction during the process. Thus, needle marks may interrupt liquid flow in the cross direction when liquid is transporting through the fabric.

5.4.1.2.3 Hydroentangled Nonwovens

Similar to the needlepunched fabrics, it is apparent from Figure 5.1 that the anisotropy of permeability in the hydroentangled fabrics was up to ten times greater than the anisotropy of permeability in the original webs. In this study, the highest anisotropy of permeability was found in the hydroentangled fabrics.

It is also noteworthy that the maximum permeability in the hydroentangled fabrics, (similar to needlepunched nonwovens), was always in the machine direction, even for fabrics made from cross-laid webs. This is believed to be due to changes in local fabric structure induced by the process, particularly the formation of jet marks, which are believed to conduits for liquid to travel.

It is apparent that the anisotropy of permeability in the hydroentangled fabrics made from polypropylene fibre were not as high as the corresponding needlepunched fabrics. It will be recalled from section 4.5.3 in Chapter 4 that the fibres inside the polypropylene hydroentangled fabric were poorly entangled and only fibres in the surface of the fabric were effectively bonded (see Figure 4.13). Therefore, the magnitude of the anisotropy of permeability in the hydroentangled polypropylene fabric is similar to that of its original web.

Also, for hydroentangled fabrics made from identical parallel-laid webs of polypropylene fibres but bonded with fibres oriented predominantly in the machine direction (MD) and cross direction (CD) respectively, it is interesting to note that the anisotropy of permeability in the fabric bonded in the direction perpendicular to the fibre orientation (fabric PA1PP1) is much greater than that in the fabric bonded in the

direction parallel to the fibre orientation (fabric PA1VV1). This corresponds to their structural characteristics (see section 4.5.3).

For hydroentangled fabrics of viscose fibres, it is evident that the maximum permeability was in the machine direction and that the anisotropy of permeability of this group of fabrics was up to ten times greater than that of the original webs.

5.4.1.3 Effect of Fibre Type and Fibre Fineness on the Anisotropy of Permeability

The effect of fibre fineness together with the fibre type (polypropylene and viscose fibre) on the anisotropy of permeability is shown in Figures 5.2~5.3.

It is known that permeability is not directly related to the fibre type and fibre surface properties[170], and that theoretically, fibre diameter can only determine the permeability and not affect the anisotropy of permeability[266]. However, it is evident that there is a difference in the fibre orientation distribution (FOD) of the fabrics made from different fibre types and different fibre finenesses (see section 4.4.6.5). The reason for this is unclear, but fibre surface properties and physical properties (such as fibre diameter) may be expected to markedly influence web formation and bonding in the process of nonwoven manufacture[258]. This may influence fabric structure. (e.g., the effect of polypropylene in hydroentangled fabrics, see section 4.5.3). In particular, fibre type and fibre fineness will influence the ratio of hooked fibres and the fibre orientation distribution in a carded web[258] (see section 4.5), subsequently this will influence the fibre orientation distribution in the unbonded webs and thus influence the anisotropy of liquid transmission in the corresponding nonwoven fabrics.

Figure 5. 2 Influence of fibre linear density on the anisotropy of permeability (unbonded webs)

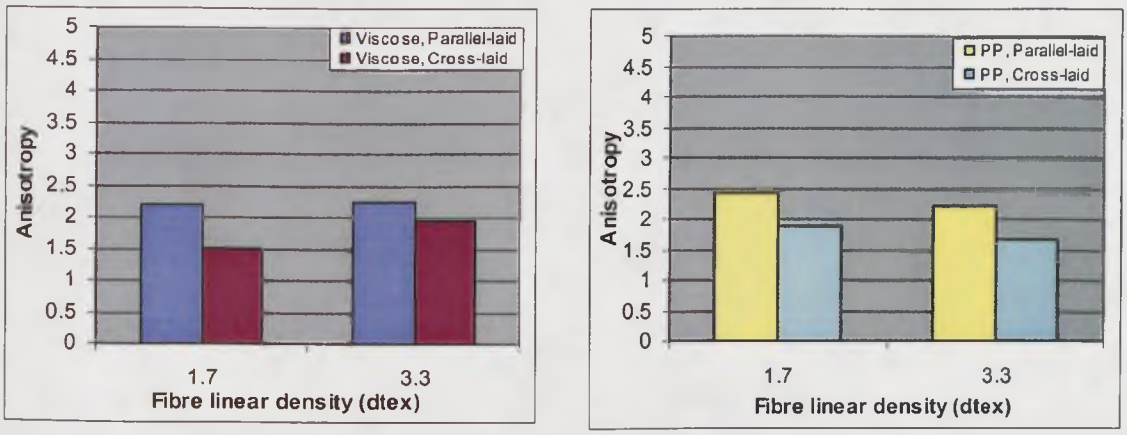

(a) Viscose web (b) polypropylene web

Figure 5. 3 Influence of web structure on the anisotropy of permeability (needlepunched fabrics)

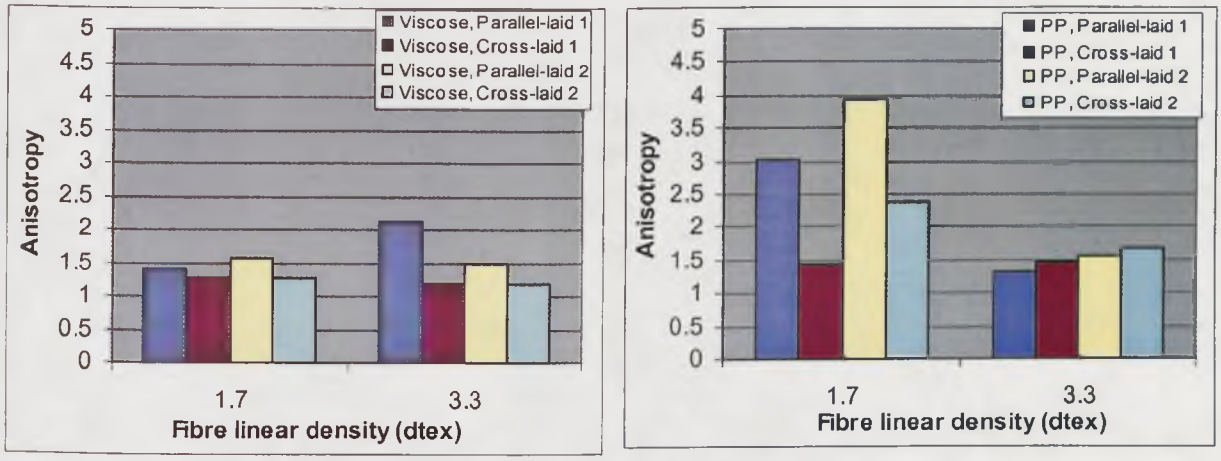

(a) Needlepunched viscose fabrics (b) Needlepunched polypropylene fabrics

5.4.1.3.1 Unbonded Webs and Needlepunched Nonwovens

It is evident from Figures 5.2 and 5.3 that the anisotropy of permeability of these fabrics has the following order:

polypropylene (1.7dtex)>polypropylene (3.3 dtex);

Viscose (3.3 dtex) >Viscose (1.7 dtex)

It should be noted that the direction of the maximum permeability in both the parallel-laid and cross-laid unbonded webs corresponds to the maximum fibre orientation in the webs respectively. However, due to needle marking in the machine direction, the maximum permeability in needlepunched fabrics, (unlike that of their original webs), are all in the machine direction, even for fabrics made from cross-laid webs.

5.4.1.3.2 Hydroentangled Nonwovens

The anisotropy of permeabilities of the hydroentangled nonwovens composed of either polypropylene or viscose fibre followed the same order as for the needlepunched fabrics irrespective of the method of web formation (see Figure 5.4):-

polypropylene (1.7dtex)>polypropylene (3.3 dtex);

Viscose (3.3 dtex) >Viscose (1.7 dtex)

Figure 5. 4 Influence of web structure on the anisotropy of permeability (hydroentangled fabrics)

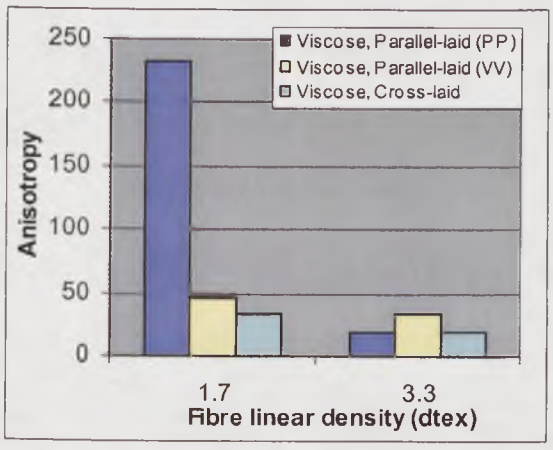

(a) Hydroentangled viscose fabrics

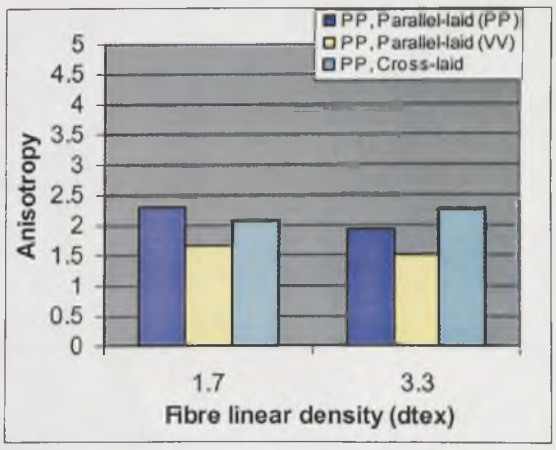

(b) Hydroentangled polypropylene fabrics

Also, the maximum permeability in the hydroentangled fabrics was in the machine direction. This is believed to be due to jet marking on the surface of the fabric running in the machine direction.

5.4.1.4 Effect of Fabric Porosity on the Anisotropy of Permeability

It is acknowledged by many researchers[106, 111] that the fabric porosity influences the permeability of porous media. Although it has been shown that the porosity of unidirectional fibrous structures influences the permeability in the direction of fibre orientation and the permeability perpendicular to the fibre orientation in two different ways, there are no existing studies on how porosity influences the anisotropy of permeability in nonwoven structures.

Figure 5.5 shows that the anisotropy of permeability in most nonwoven structures increases with increases in the fabric porosity. There are two possible reasons for this. Firstly, we know that the overall permeability of the fabric decreases with a decrease in the fabric porosity. With a decrease in fabric porosity, the decrease in one principle permeability may be larger than the decrease of the other principle permeability. Secondly, since in this study the decrease in the fabric porosity was achieved by compression of the fabric, some realignment of fibres in the fabric can not be ruled out. Since the porosity of all the fabrics used in this study was over 96%, it is not clear whether this conclusion will hold for lower fabric porosities.

Figure 5. 5 Influence of fabric compression on the anisotropy of permeability

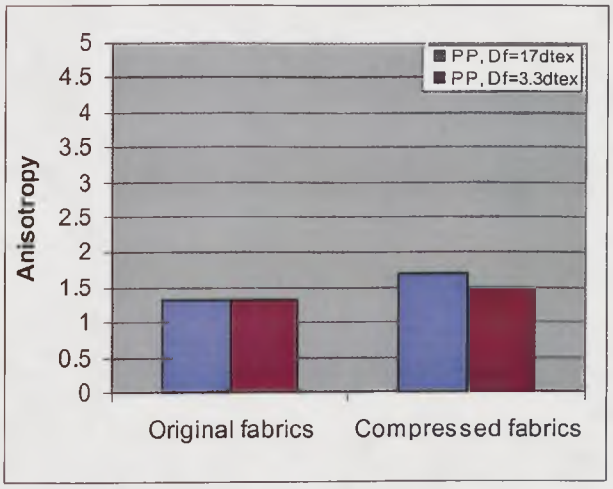

(a) Hydroentangled polypropylene fabrics

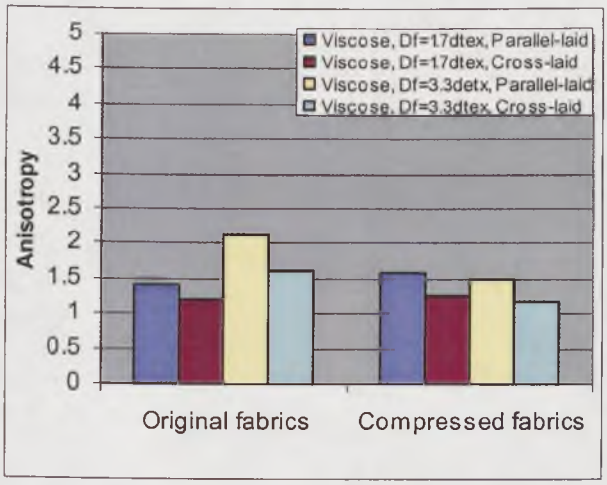

(b) Needlepunched viscose fabrics

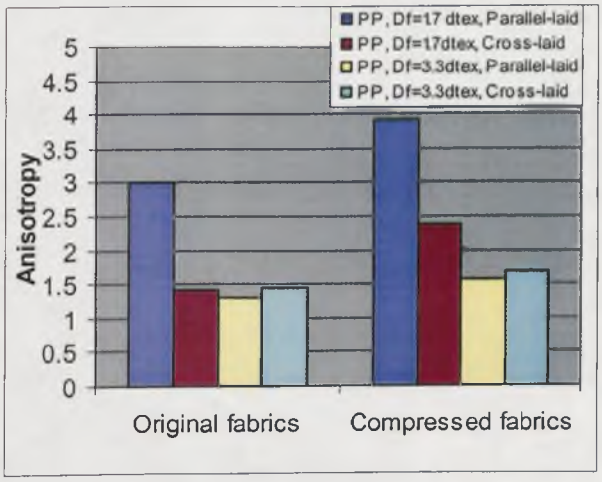

(c) Needlepunched polypropylene fabrics

5.4.2 The Influence of Fabric Structural Parameters on the Anisotropy of Liquid Absorption

The results for the anisotropy of liquid absorption are shown in Tables 5.6 to 5.10. From the definition of the anisotropy of liquid absorption, it is apparent that it has two components, that is, the anisotropy of permeability and the anisotropy of capillary

pressure. Therefore, the factors influencing the anisotropy of permeability in a fabric will at the same time influence the anisotropy of liquid absorption.

From the experimental results shown in Figures 5.6 to 5.9, it is clear that there are differences in the anisotropy of liquid absorption between fabrics with different structural parameters (such as fibre fineness and fabric porosity). Theoretically, the effect of changing the bonding method and the fibre fineness on the anisotropy of absorption and the anisotropy of the permeability is similar.

However, there are differences between the anisotropy of permeability and the anisotropy of absorption.

5.4.2.1 The Anisotropy of Liquid Absorption and the Anisotropy of Permeability

Comparisons of the anisotropy of liquid absorption and the anisotropy of permeability are shown in Figure 5.6.

It is apparent in Figure 5.6 that the anisotropy of liquid absorption is always greater than the anisotropy of permeability for all the fabric samples. This is because the anisotropy of liquid absorption is the product of the anisotropy of permeability and the anisotropy of capillary pressure (see equation 5.1.2), and the anisotropy of capillary pressure is also determined by the fibre orientation and other fabric structural parameters[265].

Figure 5. 6 Comparison of the anisotropy of liquid absorption (capillary flow) and the anisotropy of permeability (forced flow)

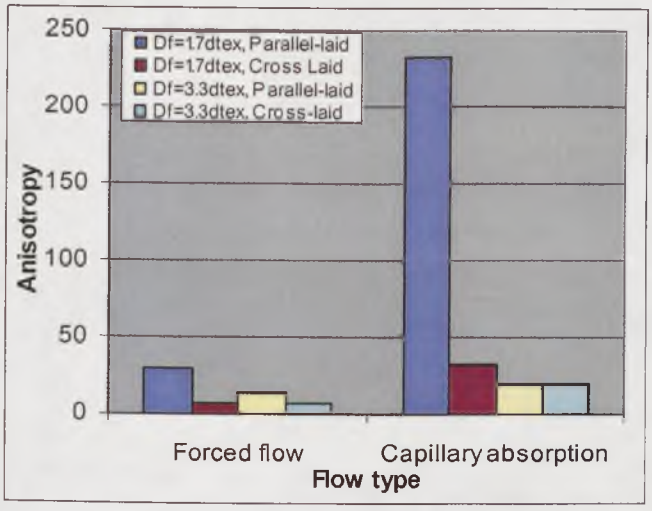

(a) Hydroentangled viscose fabrics

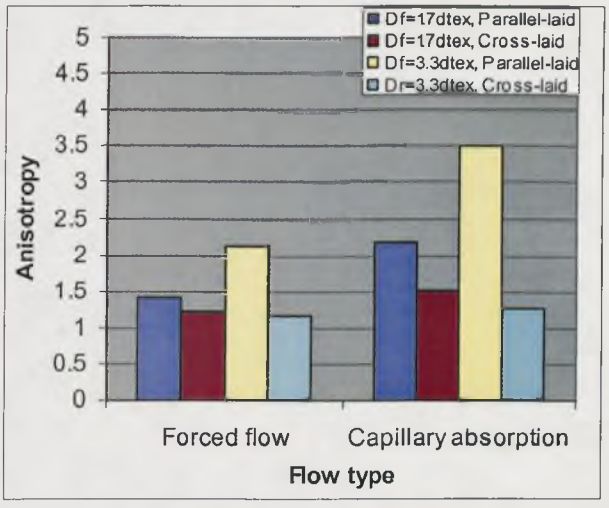

(b) Needlepunched viscose fabrics

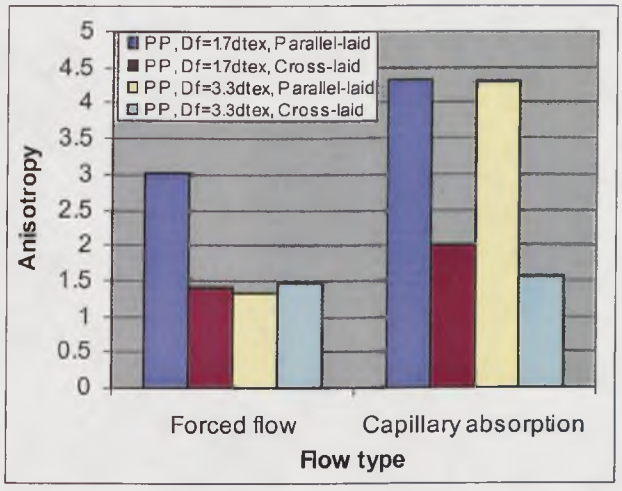

(c) Needlepunched polypropylene fabrics

5.4.2.2 The Effect of Fibre Type and Fibre Fineness on the Anisotropy of Liquid Absorption

As the effect of fibre type and fibre fineness on the anisotropy of permeability (shown in section 5.3.1.3), it is evident in Figures 5.7~5.8 that the anisotropy of liquid absorption also varies with fibre type and fibre fineness.

Figure 5. 7 Influence of fibre fineness on the anisotropy of liquid absorption

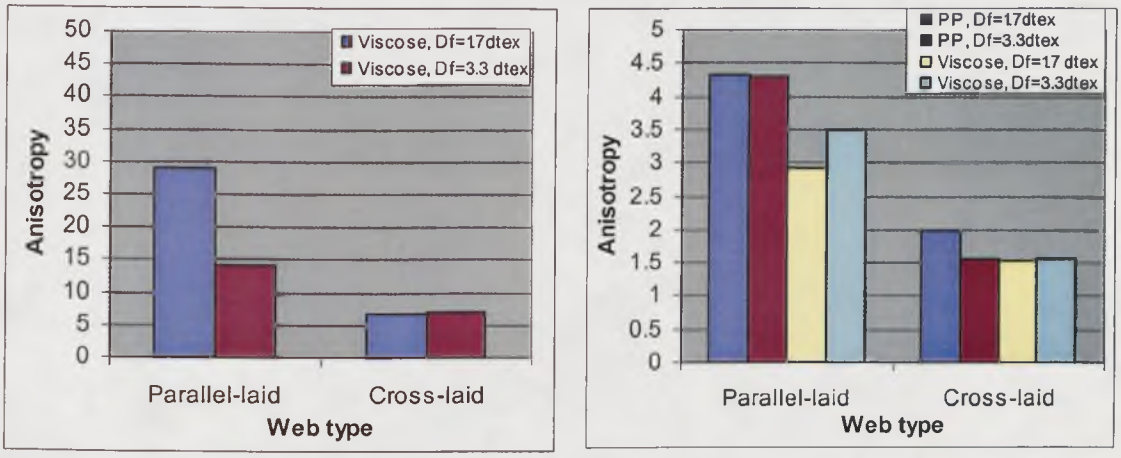

(a) Hydroentangled viscose fabrics (b) Needlepunched fabrics

Figure 5. 8 Influence of web structure on the anisotropy of liquid absorption

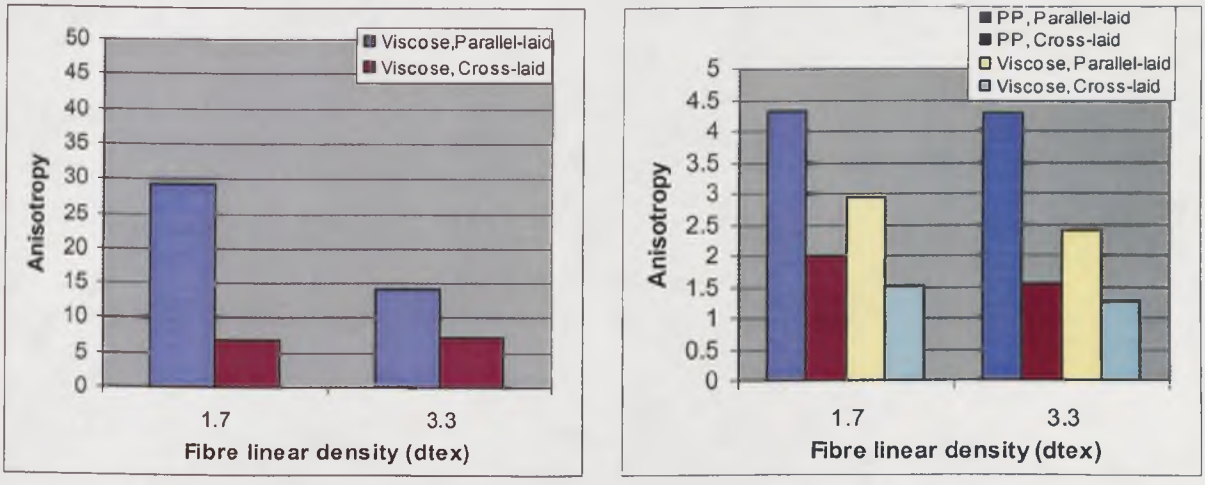

(a) Hydroentangled viscose fabrics (b). Needlepunched fabrics

The liquid absorption is known to be dominated by capillary pressure in porous materials, and according to the Laplace equations[129]. The capillary pressure is determined by the capillary tube diameter, the surface tension of the liquid and the

contact angle between the interfaces. Therefore, the fibre type and fibre finish will influence the absorption rate of the fabric. However, the anisotropy of liquid absorption in the fabric plane should not be influenced by the fibre finish on the fibre surface and the fibre fineness as long as the fabric is homogeneous and the surface finish on all the fibres in the fabric is the same.

5.4.2.3 The Effect of Porosity on the Anisotropy of Liquid Absorption

In contrast to the effect of porosity on the anisotropy of permeability, it is evident from Figure 5.9 that the lower the porosity, the higher the anisotropy of liquid absorption. The reason for this finding is not clear, but it seems that the anisotropy of the capillary pressure in nonwoven fabrics increases with a decrease in the fabric porosity[265].

Figure 5. 9 Influence of fabric compression on the anisotropy of liquid absorption

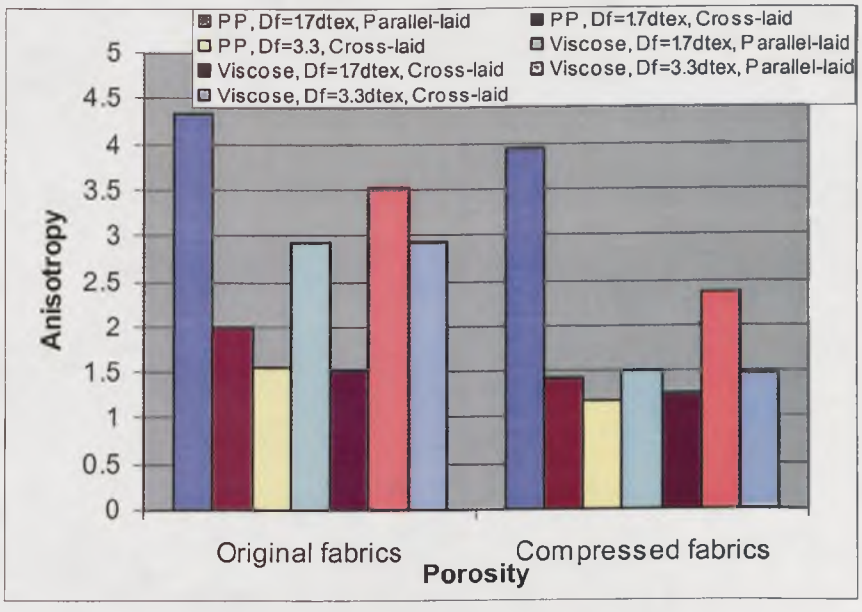

5.4.3 Comparison of the Anisotropy of Liquid Transport in the Experimental and Commercial Fabrics

Results for the anisotropy of permeability and the anisotropy of liquid absorption in the experimental and commercial wound dressing fabrics are shown in Figures 5.10 and 5.11 respectively. Of the commercial wound dressing fabrics, Sorbsan is a compressed but unbonded fibrous structure composed of a calcium alginate fibre, whereas Soffban Natural is composed of cellulosic fibre and the Lantor dressing is composed of polyester fibre. Both are believed to be needlepunched fabrics.

From Figures 5.10 and 5.11, it is apparent that either the anisotropy of permeability or the anisotropy of liquid absorption in the experimental and commercial fabrics are in a similar range.

Figure 5. 10 Comparison of the anisotropy of permeability in the experimental fabrics and typical commercial nonwoven wound dressing fabrics

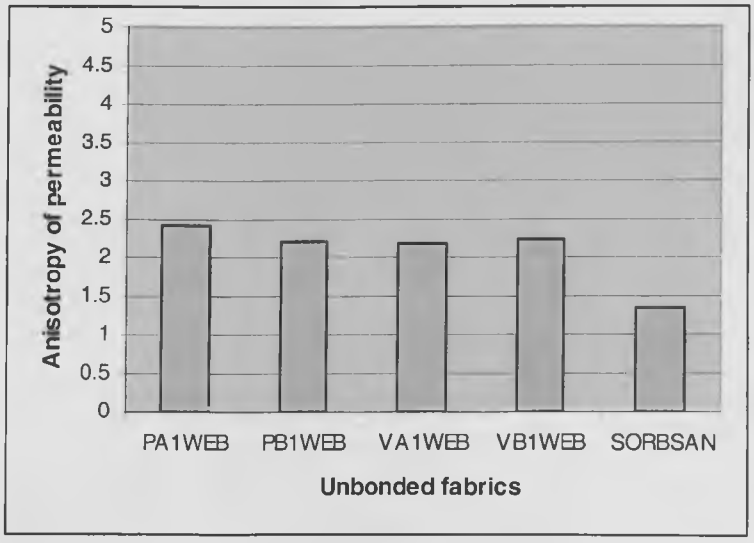

(a) Unbonded fabrics

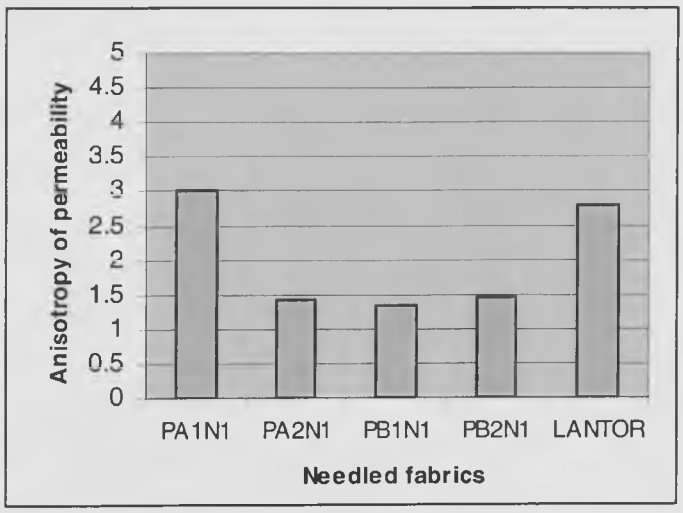

(b) Needlepunched fabrics composed of synthetic fibres

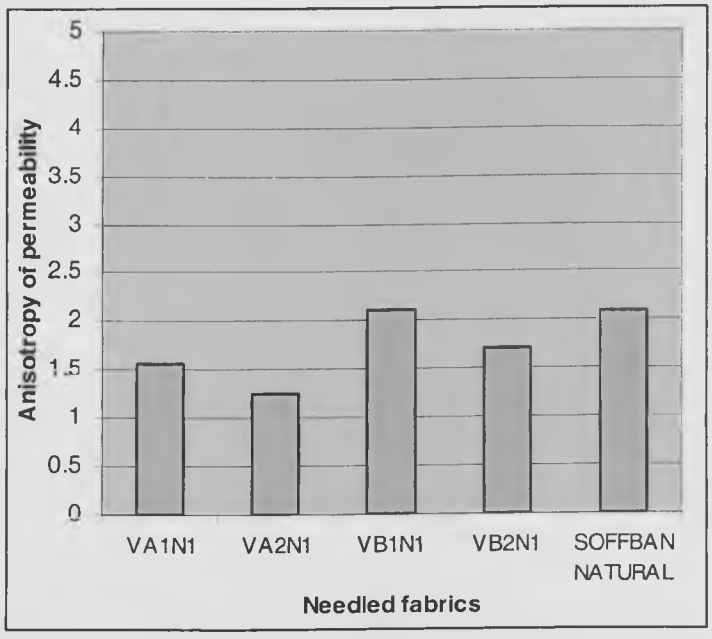

(c) Needlepunched fabrics composed of viscose fibres

Figure 5.11 Comparison of the anisotropy of liquid absorption in the experimental fabrics and typical commercial nonwoven wound dressing fabrics

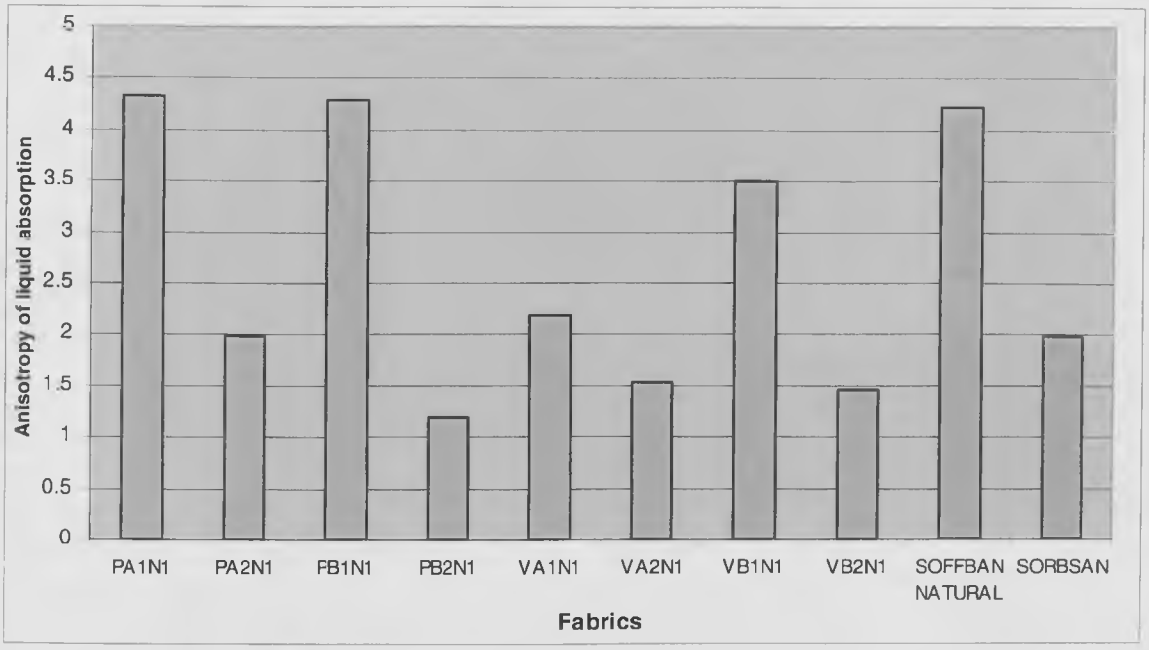

The anisotropy of permeability and the anisotropy of liquid absorption in the unbonded web and needlepunched commercial fabrics are shown in Figure 5.12. It is clear that the needlepunched fabrics (i.e., Soffban Natural and Lantor) have a higher anisotropy of both permeability and liquid absorption compaered to the unbonded dressing (i.e. Sorbsan). This finding is in agreement with the conclusions obtained for the experimental fabrics.

Figure 5. 12 Anisotropy of permeability and the anisotropy of liquid absorption in unbonded and needlepunched fabrics in typical commercial nonwoven wound dressing fabrics

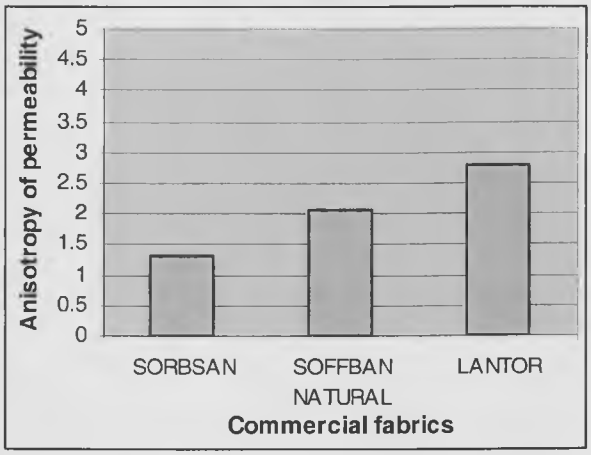

(a) Anisotropy of permeability

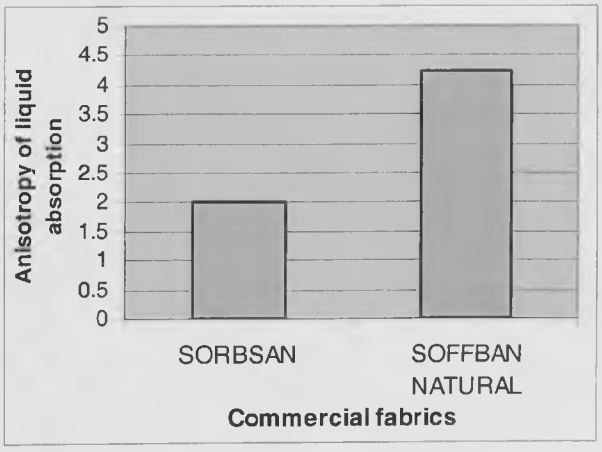

(b) Anisotropy of liquid absorption

CHAPTER 6 THEORETICAL ANALYSIS OF THE DIRECTIONAL PERMEABILITY IN HOMOGENEOUS NONWOVEN STRUCTURES

In order to understand the effect of fabric structural parameters on the anisotropy of liquid transport in the fabric, it is now possible to establish a theoretical model of the anisotropic permeability in nonwoven fabric structures based on the findings in Chapter 5.

This chapter aims to establish the relationship between fibre orientation and the directional permeability of homogeneous nonwoven fabrics using a modified drag force theory. In this approach, fabric structural parameters, such as fibre diameter, the fibre orientation distribution and porosity are all considered and new models of permeability for two- and three-dimensional structures are presented. A basic model of permeability in fibrous structures is presented based on drag force theory. and the application of this model to structures having different fibre arrangements is also investigated.

6.1 RELATIONSHIP BETWEEN DIRECTIONAL PERMEABILITY AND FIBRE ORIENTATION

It has been shown that the permeability of isotropic, homogeneous, porous fibrous structures is dependent on fabric structural parameters, such as fibre diameter and fabric porosity[106, 111]. It has also been pointed out that unidirectional fibrous materials have different permeabilities in two principle directions and this is influenced by fabric structure[107, 109, 111, 114]. The directional permeability of porous materials is dependent on the anisotropy of the intrinsic structure[170], which is influenced by the fibre orientation

distribution[266]. However, no analysis has been previously presented that shows the relationship between the directional permeability of nonwoven fabrics and the structure of such fabrics.

In this chapter, a new general model of the directional permeability in homogenous, anisotropic nonwoven structures is presented based on drag force theory and Darcy's Law[266, 267]. Structural parameters in the fabric are considered, including fibre diameter, porosity and the fibre orientation distribution. The governing equations of the local permeability in two- and three-dimensional structures are derived, which allow the permeability in any direction in the fabric to be calculated.

In this chapter, the permeability in idealised structures is also discussed and the application of a newly derived model of directional permeability is described for a range of specific fibre orientation profiles.

6.2 BACKGROUND CONSIDERATIONS

Directional permeability in fabrics is believed to be important in determining the performance of many nonwoven structures used in medicine and hygiene. The established theory of laminar fluid flow through homogeneous porous materials such as nonwovens is based on Darcy's Law[104], which can be written as follows:

$$Q = -\frac{k}{\eta}\frac{\Delta p}{L} \qquad (6.2.1)$$

Where Q is the volumetric flow rate of the fluid flow, η is the viscosity of the fluid, Δp is the pressure drop along the conduit length of the fluid flow L, and k is the specific permeability of the porous material.

In Darcy's Law, the permeability is governed by the effects of certain structural features on the liquid flow. For isotropic materials, the permeability will be the same throughout the entire structure but in an anisotropic one, it will vary from region to region. The permeability in fibrous structures is believed to be closely related to fibre orientation [268] which is believed to influence the structural anisotropy of nonwoven fabrics.

6.3 THEORETICAL BACKGROUND

Many theoretical and empirical models of the permeability in fibrous materials have been published. The existing theoretical models of permeability can be grouped into two main categories based on:

(i) Capillary channel theory, e.g., Kozeny[105], Carman[106], Davies[112], Piekaar and Clarenburg[269], Dent[270] and Shen[118] and

(ii) Drag force theory, e.g., Emersleben[107], Brinkman[108], Iberall[110], Happel[111], Kuwabara[113], Cox[271], and Sangani and Acrivos[272].

Most of the permeability models established for textile fabrics are based on capillary theory. However, it has been argued that models based on capillary theory are unsuitable for highly porous media where the porosity is greater than 0.8 (see for example, Carman[106]).

Thus, drag force theory is believed to be more applicable to highly porous materials containing fibres, such as nonwoven fabrics, where the single fibres can be regarded as elements within the fluid that can not be displaced (see Scheidegger[170]).

In drag force theory, the walls of the pores in the structure are treated as obstacles to an otherwise straight flow of the fluid. The drag of the fluid acting on each portion of the wall is estimated from the Navier-Stokes equations, and the sum of all the 'drags' is assumed to be equal to the total resistance to flow in the porous material, (i.e. equal to η / k, according to Darcy's law in equation 6.2.1). However, none of the existing theories has been developed specifically to model directional permeability in nonwoven fabrics.

6.3.1 Drag Force Theory in Isotropic Fibrous Materials

Iberall[110] adopted the drag force models obtained by Emersleben[107] and Lamb[114] and established a model of permeability for a material having a random distribution of cylindrical fibres of circular cross section and identical fibre diameter. The model accounted for the permeability on the basis of the drag forces acting on individual elements in the structure. It was assumed that the flow resistivity of all random distributions of fibres per unit volume does not differ. The resistivity was obtained by assuming the fabric has an isotropic structure in which the number of fibres in each axis is equal and one of the axes is along the direction of macroscopic flow.

6.3.2 Drag Force Theory in Unidirectional Fibrous Materials

Happel[111], Kuwabara[113], Sparrow and Loeffler[273] and Drummond and Tahir[274] have given detailed analyses of the permeability in unidirectional fibrous materials. They obtained the permeability using a so-called 'unit cell' theory, or 'free surface' theory, in which the

fibres are assumed to be arranged in a periodic pattern such as a square or triangular array. For each array it is possible to define a 'unit cell', i.e. a polygon with a rod at the centre, such that the flow in the cell is the same as in the array. The permeability of unidirectional fibrous materials can then be solved using the Navier-Stokes equation in the unit cell with appropriate boundary conditions. Happel[111] also compared his theoretical results with some experimental data produced by other researchers and showed their agreement was good when the fabric porosity is greater than 0.5. Sullivan[275] and Davies[112] have also completed a considerable body of experimental work in this area.

Unlike capillary flow theory, drag force theory and unit cell theory demonstrate the relationship between permeability and the internal structural architecture of the material. However, previous approaches can not be applied to normal anisotropic materials, such as nonwoven fabrics, because the existing models of drag force theory are based on the assumption that fibres are oriented either in homogenous-isotropic or in specific unidirectional alignments. In contrast, the approach presented here is designed to demonstrate a more generally applicable relationship between directional permeability and the structure of the fabric.

6.4 DIRECTIONAL PERMEABILITY IN HOMOGENEOUS ANISOTROPIC FIBROUS MATERIALS

6.4.1 Assumptions

The approach described here is specifically focused on the permeability of nonwovens which usually have high porosity and anisotropic properties. Initially, in order to simplify the problem, the fibres in the Z-direction are not considered in the model. Of course, in

practice many nonwoven fabrics have fibres aligned in the Z-direction and later in this chapter a directional permeability model for three-dimensional nonwoven fabric structures is obtained by expansion of the two-dimensional model. In the new theory, the following assumptions are made:

(i) The fibres constituting the fabric are of the same diameter and are distributed horizontally in-plane and in two-dimensions. No fibres are aligned in the Z-direction.

(ii) The flow resistivity of the fibres per unit volume in the entire structure of the fabric is equal, i.e. the fabric is homogeneous.

(iii) The number of fibres oriented in each direction is not the same, but obeys the function of the fibre orientation distribution, $\Omega(\alpha)$, where α is the fibre orientation angle. The drag forces acting in two orthogonal directions (one of which is along the direction of macroscopic flow) are not the same.

(iv) The distance between fibres and the length of individual fibres is much larger than the fibre diameter, i.e. the structure has high porosity. The disturbance of the flow due to adjacent fibres is assumed to be negligible.

(v) The inertial forces of the fluid are negligible, i.e. the fluid has a low local Reynolds number *Re,* and the pressure drop between planes perpendicular to the direction of the macroscopic flow is equal to the drag force on all elements between the planes.

(vi) The pressure drop necessary to overcome the viscous drag is linearly additive for the various fibres, whether they are arranged parallel, perpendicular or in any other direction relative to the flow.

6.4.2 Development of the Alternative Theory

In the new theory, the drag forces in each flow direction are obtained using Happel's equations for unidirectional fibre bundles (see Happel[111]). Happel's first equation is the permeability in the flow direction parallel to the fibre length and the second is the permeability in the flow direction perpendicular to the fibre length. From these two equations, the drag force per unit length acting on a single fibre surrounded by similar fibres and all oriented along the direction of flow, f_p, can be deduced:

$$f_p = \frac{8\pi\eta Q}{S} \qquad (6.4.1)$$

where $S = [2\ln\varepsilon - 4\varepsilon + 3 + \varepsilon^2]$ and ε is the volume fraction of the solid material.

The drag force per unit length acting on a single fibre oriented perpendicular to the fluid flow, f_v, can be deduced from Happel's equations as follows (Happel[111]):

$$f_v = \frac{8\pi\eta Q}{T} \qquad (6.4.2)$$

where $T = [\ln\varepsilon + \frac{1-\varepsilon^2}{1+\varepsilon^2}]$

f_p or f_v are the pressure differences per unit length for the flow parallel to and perpendicular to the fibre length respectively. The subscripts *p* and *v* represents the flow parallel and perpendicular to the fibres respectively; η is the internal viscosity of the fluid, and Q is the superficial flow velocity of the fluid stream in the porous material. Further, if P_f is the porosity, then the volume fraction of the solid material ε is given by $\varepsilon = 1 - P_f$.

It is then assumed that there are n fibres of a unit length in a unit volume of the fabric and that the dimensionless distribution probability function of the fibre orientation $\Omega(\alpha)$ has the following form (see Mandel[276] and Krcma[94]):

$$\int_0^{\pi} n\Omega(\alpha)d\alpha = n \qquad (6.4.3)$$

where n is a constant for homogenous materials.

Figure 6. 1 Representation of drag theory for fibrous materials in a polar co-ordinate system

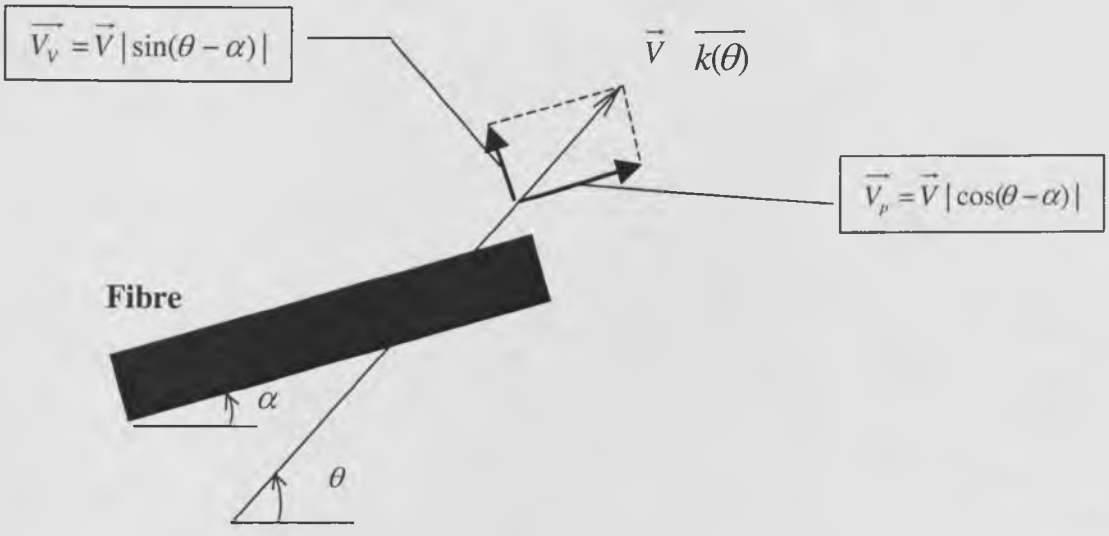

The drag force arising from the fluid flow acting on a single fibre aligned in any orientation in the fabric can be obtained by consideration of Figure 6.1. A fibre of a particular unit length is aligned in the direction α and the fluid flow over the fibre is in the direction θ. Thus, the drag force of the fluid flow acting on the fibre can be deduced according to equation (6.4.1) and equation (6.4.2). The drag force acting on the fibre in the direction θ which is the direction of the flow, $f(\theta)$, can be derived as given in equation (6.4.4) as follows (also see Appendix II):

$$f(\theta) = \frac{8\pi\eta Q\cos^2(\theta-\alpha)}{S} + \frac{8\pi\eta Q\sin^2(\theta-\alpha)}{T} \qquad (6.4.4)$$

It is also suggested that when the ratio of fibre length to fibre diameter is sufficiently large, the total drag force (of a directional flow) on the material (composed of *n* fibres) is equal to the sum of the individual drag forces acting on each fibre (see Happel[111]). Therefore, for a flow in a particular direction θ, the drag force acting on all the fibres (due to a unit volume of the fabric consisting of *n* fibres), $f'(\theta)$ will be:

$$f'(\theta) = n\int_0^{\pi} \Omega(\alpha) f(\theta) d\alpha \qquad (6.4.5)$$

The pressure gradient in the flow direction due to the drag force in a unit volume of the fabric, $\frac{\Delta p}{L}$, is equal to the pressure drop per unit length of flow resulting from the drag force in this direction. Therefore:

$$\begin{aligned}\frac{\Delta p}{L} &= f'(\theta) = n\int_0^{\pi} \Omega(\alpha) f(\theta) d\alpha \\ &= 8\pi\eta Q n\int_0^{\pi} \Omega(\alpha)\left\{\frac{\cos^2(\theta-\alpha)}{S} + \frac{\sin^2(\theta-\alpha)}{T}\right\} d\alpha\end{aligned} \qquad (6.4.6)$$

The number of fibres per unit volume, *n*, is equal to the total fibre length per unit volume, and therefore may be substituted by $n = \frac{4}{\pi\delta^2}\varepsilon$ in equation (6.4.6), where δ is the fibre diameter and ε is the volume fraction of the solid material (defined as $\varepsilon = \frac{\rho_p}{\rho_f}$, where ρ_p is the density of a fibrous pack in a vacuum and ρ_f is the fibre density). Thus, by

substituting equation (6.4.6) into Darcy's law in equation (6.2.1), the directional permeability $k(\theta)$ can be obtained as follows:

$$k(\theta) = -\frac{1}{32}\frac{\delta^2}{\varepsilon}\left\{\frac{ST}{\int_0^{\pi}\Omega(\alpha)\left[T\cos^2(\theta-\alpha)+S\sin^2(\theta-\alpha)\right]d\alpha}\right\} \qquad (6.4.7)$$

Further, if $\Omega(\alpha)$ can be expressed as a finite series, equation (6.4.7) can be rewritten as follows:

$$k(\theta) = -\frac{1}{32}\frac{\delta^2}{\varepsilon}\left\{\frac{ST}{\sum_{\alpha=0}^{\pi}\Omega(\alpha)\left[T\cos^2(\theta-\alpha)+S\sin^2(\theta-\alpha)\right]\Delta\alpha}\right\} \qquad (6.4.8)$$

Furthermore, equation 6.3.7 can be rewritten as follows:

$$\frac{1}{k(\theta)} = \frac{1}{k_{0X}} + \frac{1}{k_{0Y}} \qquad (6.4.9)$$

where the two components k_{0X} and k_{0Y} can be obtained from equation (6.4.7) as follows:

$$k_{0X} = \frac{1}{32}\frac{\delta^2}{\varepsilon}\frac{S}{\int_0^{\pi}\Omega(\alpha)\cos^2(\theta-\alpha)d\alpha}, \quad k_{0Y} = \frac{1}{32}\frac{\delta^2}{\varepsilon}\frac{T}{\int_0^{\pi}\Omega(\alpha)\sin^2(\theta-\alpha)d\alpha} \qquad (6.4.10)$$

Therefore, a new relationship between directional permeability and the fibre orientation distribution is now established in equation (6.4.7) and (6.4.8). Both equations may be considered as special versions of Ferrandon's equation relating specifically to fibrous

structures. One possible limitation of these equations should be noted. Both equations (6.4.7) and (6.4.8) are based on equations (6.4.1) and (6.4.2) which are derived from Happel's equations (see Happel[111]). It is important to note that Happel's equations are based on the assumption that fibres in unidirectional fibre bundles are aligned in square arrays (see Figure 6.2(b)), and of course this may not always be representative of the true structure of a nonwoven fabric. Consequently, the directional permeability equations may in practice, be of limited application when the fibre alignment differs from a square array and for this reason, the present model requires further modification. These refinements to the model are now discussed.

Figure 6. 2 Various cross-sectional arrays of fibre arrangement[272, 274]

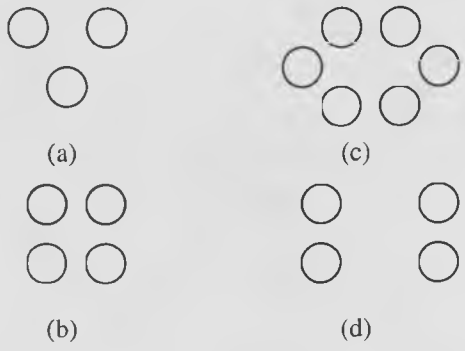

(a) Triangular (b) Square (c) hexagonal and (d) a two-by-one rectangular array

6.4.3 Directional Permeability in Structures with Variable Fibre Alignment

Kuwabara[109], Sparrow and Loeffler[273], Sangani and Acrivos[272] and Drummond and Tahir[274] studied the permeability of fibrous materials having different fibre arrays allowing more widely applicable permeability equations to be obtained for unidirectional

fibre bundles. From their work, more general equations of drag force for flow parallel to the fibre length of a single fibre, f_p, can be derived as follows:

$$f_p = -\frac{8\pi\eta Q}{[4\varepsilon - \varepsilon^2 - 2A - 2\ln\varepsilon]} \qquad (6.4.11)$$

Additionally, a more general equation of the drag force for flow perpendicular to the fibre length of the fibre, f_v, can be obtained as follows:

$$f_v = -\frac{8\pi\eta Q}{[2\varepsilon - C\varepsilon^2 - B - \ln\varepsilon]} \qquad (6.4.12)$$

Where *A*, B and C are constants which depend on the particular geometry of the fibre array. Some values of *A* have been given by Drummond and Tahir[274] for various polygons where: A=1.498 (for a triangular array), 1.478 (for a square array), 1.354 (for a hexagonal array) and 1.130 (for a two-by-one rectangular array) respectively (see Figure 6.2). Elsewhere, Sangani and Acrivos[272] and Drummond and Tahir[274] have suggested other values where B =1.490 (for a triangular array), 1.476 (for a square array), *C*=1.000 (for a triangular array) and 1.774 (for a square array).

Using the same assumptions listed in section 6.4.1, and substituting equations (6.4.11) and (6.4.12) into equations (6.4.3) to (6.4.5), a more general model of the directional permeability in an anisotropic fibre distribution can be obtained as follows:

$$k(\theta) = -\frac{1}{32}\frac{\delta^2}{\varepsilon}\left\{\frac{[2\ln\varepsilon - 4\varepsilon + 2A + \varepsilon^2][\ln\varepsilon - 2\varepsilon + B + C\varepsilon^2]}{\int_0^{\pi}\Omega(\alpha)\left[[\ln\varepsilon - 2\varepsilon + B + C\varepsilon^2]\cos^2(\theta - \alpha\theta) + [2\ln\varepsilon - 4\varepsilon + 2A + \varepsilon^2]\sin^2(\theta - \alpha)\right]d\alpha}\right\} \qquad (6.4.13)$$

Where *A*, *B* and *C* are constants relating to particular fibre arrangements in the structure.

When the material has a high porosity, the term ε^2 can be neglected. Assuming that the permeability perpendicular to the fibre length is half the permeability parallel to the fibre length (Jackson and James[277]), the new equation (6.4.13) can be simplified as follows:

$$k(\theta) = -\frac{1}{32}\frac{\delta^2}{\varepsilon}\left[\frac{[2\ln\varepsilon - 4\varepsilon + 2A + \varepsilon^2]}{\int_0^{\pi}\Omega(\alpha)\left[\cos^2(\theta-\alpha) + 2\sin^2(\theta-\alpha)\right]d\alpha}\right] \qquad (6.4.14)$$

6.4.4 Directional Permeability in Three-dimensional Structures

Equation (6.4.11) and (6.4.12) can be expanded to model permeability in three-dimensional fabrics. Here, ε is the volume fraction of the solid material in the fabric, $\Omega(\vec{f}_i)$ is the fibre orientation distribution in the $\vec{f}_i$ direction, $\vec{\tau}$ is the vector of fluid flow in any direction in the fabric, and $\vec{\theta}_i$ is the angle between the fluid flow in direction $\vec{\tau}$ and the fibre orientation $\vec{f}_i$. Thus, the directional permeability of the fabric in direction $\vec{\tau}$, $k(\vec{\tau})$, can be expanded from equation (6.4.13) to yield equation (6.4.15).

$$k(\vec{\tau}) = -\frac{\delta^2}{32\varepsilon}\left[\frac{[\ln\varepsilon - 2\varepsilon + B + C\varepsilon^2][2\ln\varepsilon - 4\varepsilon + A + \varepsilon^2]}{\sum_{\theta_i=0}^{\pi}\Omega(\vec{f}_i)\left[[\ln\varepsilon - 2\varepsilon + B + C\varepsilon^2]\cos^2\theta_i + [2\ln\varepsilon - 4\varepsilon + A + \varepsilon^2]\sin^2\theta_i\right]}\right] \qquad (6.4.15)$$

6.5 CONSIDERATION OF STRUCTURES WITH SPECIFIC FIBRE ORIENTATION PROFILES

Equations (6.4.7) and (6.4.8) establish the theoretical relationship between the fibre orientation distribution function and the directional permeability in fibrous media such as nonwovens. In order to demonstrate the practical importance of the equations, the permeabilities of some typical anisotropic materials are predicted (see Table 6.1). In all the figures presented in this chapter, the fibre diameter in the fabric is taken arbitrarily as $10\mu m$, and the fluid is assumed to be water where η is taken to be 1.

6.5.1 Homogenous Isotropic Fibrous Structures

Homogenous isotropic materials may be viewed as a 'special' class of anisotropic media. When liquid flows through a two-dimensional, homogenous isotropic fabric, the directional permeability in each direction will be the same, (i.e., for isotropic materials, $k(\theta)$ and $\Omega(\alpha)$ are independent of the fibre orientation). If there are n fibres aligned isotropically, the fibre orientation distribution function will be constant and will be the same in each direction, the orientation distribution function, $\Omega(\alpha)$, can therefore be represented as: $\Omega(\alpha) = 1/\pi$. Thus, the permeability of the homogenous fibrous medium k, is written as (see Table 6.1):

$$k = -\frac{1}{16}\frac{\delta^2}{\varepsilon}\left\{\frac{ST}{S+T}\right\} \qquad (6.5.1)$$

Table 6. 1 Principle permeabilities in various two-dimensional nonwoven structures

Fibrous Structures	Fibre Orientation Distribution Function	Directional Permeability $k(\theta)$	
1. Generalised Equation	$\Omega(\alpha)$	$\frac{1}{k(\theta)}=\frac{1}{k_{0X}}+\frac{1}{k_{0Y}}$	$k_{0X}=-\frac{1}{32}\frac{\delta^2}{\varepsilon}\frac{S}{\frac{\pi}{\int_0}\Omega(\alpha)\cos^2(\theta-\alpha)d\alpha}$ $k_{0Y}=-\frac{1}{32}\frac{\delta^2}{\varepsilon}\frac{T}{\frac{\pi}{\int_0}\Omega(\alpha)\sin^2(\theta-\alpha)d\alpha}$
2. Isotropic Nonwovens (M_R_ISO)	*Constant*		$k_{0X}=-\frac{1}{16}\frac{\delta^2}{\varepsilon}S$, $k_{0Y}=-\frac{1}{16}\frac{\delta^2}{\varepsilon}T$
3. Structure with Unidirectional Fibre Arrangement	$\Omega(\alpha)=\begin{cases}1; & when\ \alpha=\frac{\pi}{2}\\ 0; & when\ \alpha\neq\frac{\pi}{2}\end{cases}$		$k_{0X}=-\frac{1}{32}\frac{\delta^2}{\varepsilon}\frac{S}{\sin^2\theta}$, $k_{0Y}=-\frac{1}{32}\frac{\delta^2}{\varepsilon}\frac{T}{\cos^2\theta}$
3. Structure with Fibres Aligned in Two Orthogonal Directions	$\Omega(\alpha)=\begin{cases}X; & when\ \alpha=0\\ 1-X; & when\ \alpha=\frac{\pi}{2}\end{cases}$		$k_{0X}=-\frac{1}{32}\frac{\delta^2}{\varepsilon}\left[\frac{S}{X\cos^2\theta+(1-X)\sin^2\theta}\right]$ $k_{0Y}=-\frac{1}{32}\frac{\delta^2}{\varepsilon}\left[\frac{T}{X\sin^2\theta+(1-X)\cos^2\theta}\right]$
5. Needle-Punched and Hydro-entangled Nonwovens	$\Omega(\alpha)$		$k_{0X}=-\frac{1}{32}\frac{\delta^2}{\varepsilon}\frac{S}{(1-z)\frac{\pi}{\int_0}\Omega(\alpha)\cos^2(\theta-\alpha)d\alpha}$ $k_{0Y}=-\frac{1}{32}\frac{\delta^2}{\varepsilon}\frac{T}{z+(1-z)\frac{\pi}{\int_0}\Omega(\alpha)\sin^2(\theta-\alpha)d\alpha}$
	$k\mid_Z=-\frac{1}{32}\frac{\delta^2}{\varepsilon}\left\{\frac{ST}{(1-z)S+zT}\right\}$		

Where (1). $S=[2\ln\varepsilon-4\varepsilon+3+\varepsilon^2]$ and $T=[\ln\varepsilon+\frac{1-\varepsilon^2}{1+\varepsilon^2}]$.

(2) z is the fraction of fibres aligned in the Z direction which is perpendicular to the fabric plane, and $k\mid_Z$ is the permeability in the Z direction.

(3). k_{0X} and k_{0Y} are the two components in the equation $\frac{1}{k(\theta)}=\frac{1}{k_{0X}}+\frac{1}{k_{0Y}}$ respectively.

6.5.2. Structures with Unidirectional Fibre Alignment

In a unidirectional structure, the fibres are aligned in only one direction. This is roughly analogous to a parallel-laid web. The fibres in an idealised structure of this kind may be assumed to be composed of straight cylindrical rods aligned parallel to each other. The fibre orientation distribution function of such a structure and the corresponding directional permeability are shown in Table 6.1 along with a range of expressions given by previous workers. Figure 6.3 shows a plot of the predicted directional permeability in unidirectional fibre bundles obtained from the new equation. It would appear that the permeability varies significantly in the direction of flow, although the magnitude of the permeability in the structure is mainly determined by the porosity.

Figure 6. 3 Theoretical permeability in structures having unidirectional fibre orientation

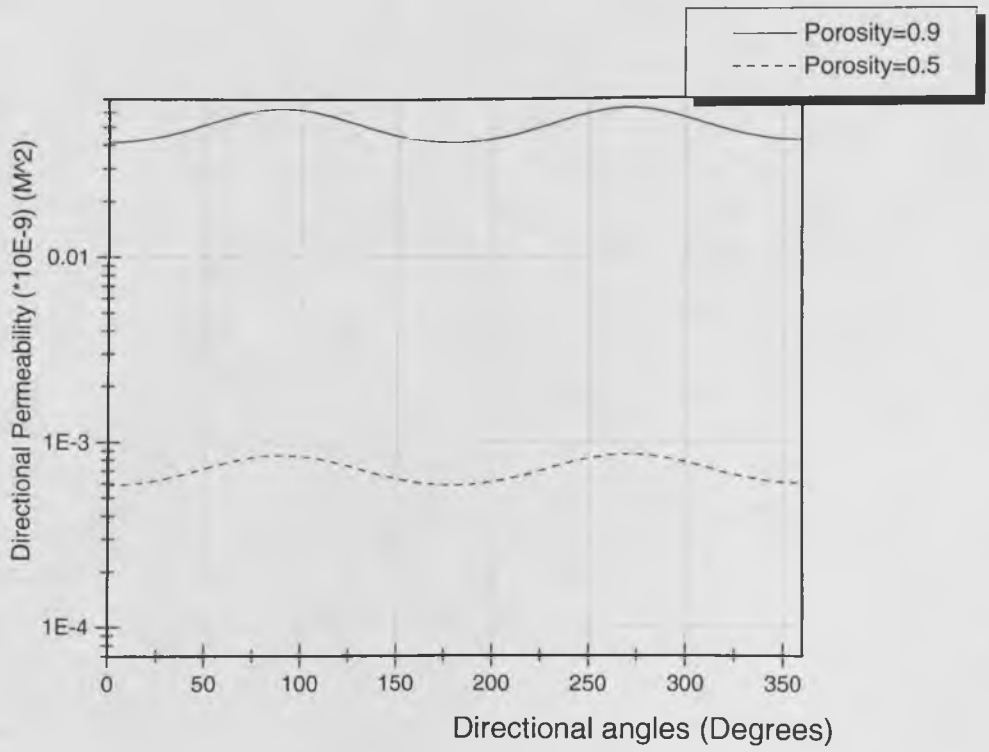

Typical governing equations for the directional permeabilities in such structures in the directions parallel to and perpendicular to the fibre orientation (respectively) may be given as follows (see Table 6.1):

$$\text{When } \theta = \frac{\pi}{2}, \quad k|_{MAX} = -\frac{1}{32}\frac{\delta^2}{\varepsilon}S \tag{6.5.2}$$

$$\theta = 0, \quad k|_{MIN} = -\frac{1}{32}\frac{\delta^2}{\varepsilon}T \tag{6.5.3}$$

From equation (6.5.2) and (6.5.3) for unidirectionally oriented materials, it is clear that the maximum permeability will be in the same direction as the fibres are oriented and the minimum permeability is perpendicular to the direction of fibre orientation. This would also be predicted by capillary channel theory.

It may be noted that equations (6.5.2) and (6.5.3) are essentially the same as those given by Happel[111] and Happel and Brenner[278]. Moreover, if the direction of fluid flow through the fabric is in the Z-direction, which is perpendicular to the fabric plane, the permeability in this direction may be the same as the flow perpendicular to the longitudinal axis of the fibre, and therefore the permeability will be effectively the same as in equation (6.5.3).

6.5.3 Structures with Fibre Alignment in Two Orthogonal Directions

Structures in which fibres are aligned in two orthogonal directions include certain nonwoven composites and some woven fabrics. Here, fibres are assumed to be aligned in two orthogonal directions in the horizontal plane, where *X* percentage of the fibres are aligned in the direction $\alpha = 0$ and *(1-X)* are aligned in the direction $\alpha = \frac{\pi}{2}$. The

Figure 6. 4 Curves showing permeability of structures with fibres aligned in two orthogonal directions

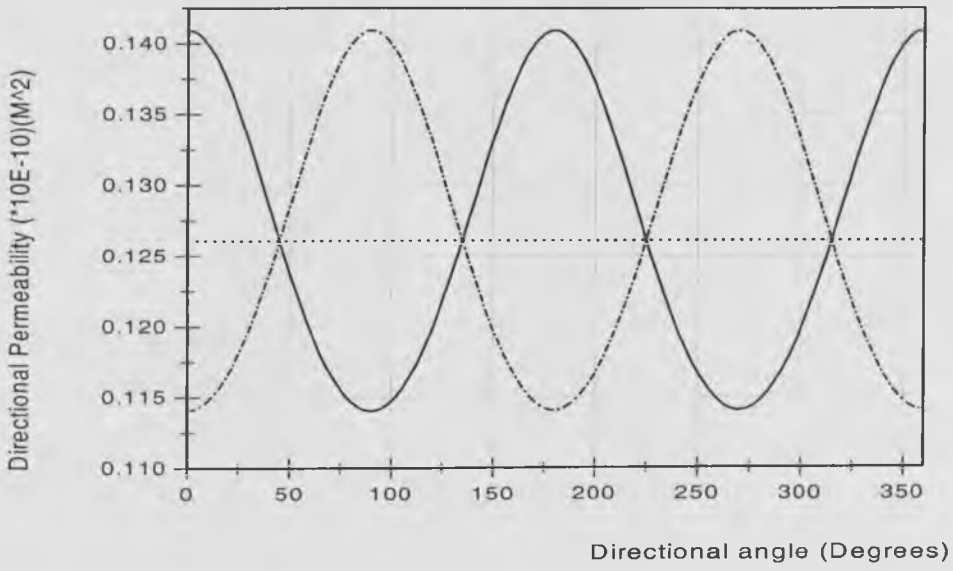

(a) Cartesian directional permeability diagram

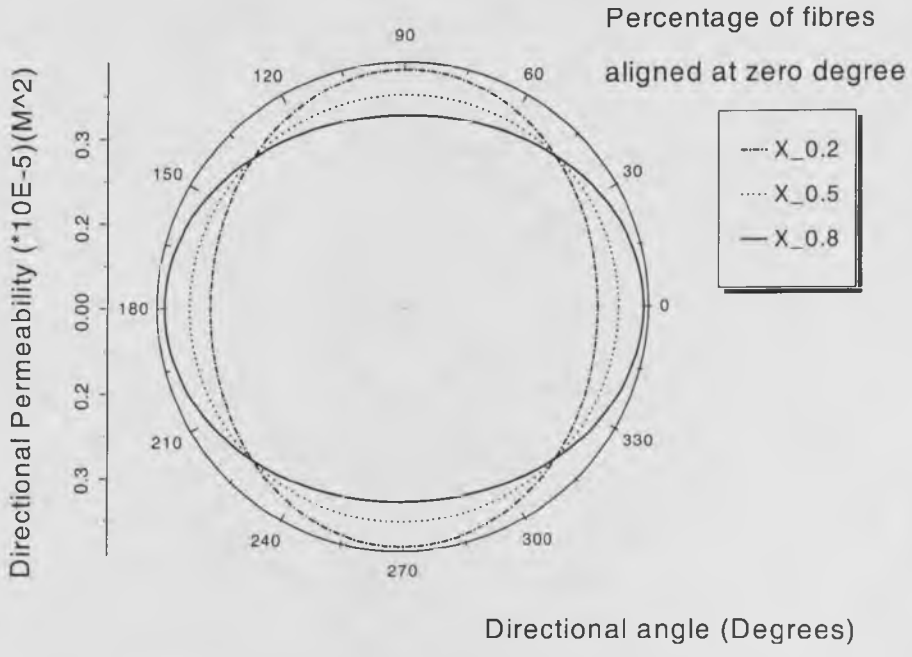

(b) Square root of directional permeability in Polar system

Note: The porosity is taken as 0.8

function of the fibre orientation distribution and the resulting directional permeability for such structures are shown in Table 6.1. The predicted permeabilities using the alternative model are plotted in Figure 6.4 where X=0.2, 0.5 and 0.8 respectively.

It is interesting to note that the maximum permeability occurs in the direction along which most of the fibres are oriented, and the minimum permeability occurs in the orthogonal direction. The direction in which the maximum and minimum permeabilities are obtained and the magnitude of the maximum and minimum permeabilities varies with the ratio of X, fibre diameter and the porosity of the fabric.

Additionally, in Figure 6.4, it is interesting to note that plotting the square root of the permeability in a Polar co-ordinate system does yield an ellipsoid. This clearly corresponds with the results of Ferrandon's equations and the work of others, notably see the book by Scheidegger[170].

Assuming an idealised structure in which fibres are aligned only in two orthogonal directions with an equal number of fibres in both directions, $X=1/2$, we have:

$$k(\theta) = -\frac{1}{16}\frac{\delta^2}{\varepsilon}\left\{\frac{ST}{[T+S]}\right\} \qquad (6.5.4)$$

Since the permeability obtained in each direction of this structure is the same (according to equation (6.5.4)), an important finding of this work is that this model supports the assumption that such structures are isotropic (see Adams and Rebenfeld[124]).

6.5.4 Structures with Fibres Aligned in a Complex Statistical Distribution

If the alignment of fibres in the Z-direction is negligible, the fabric may be viewed as a two-dimensional structure. In many nonwoven fabrics, the fibre orientation distribution in the fabric plane has a complex statistical distribution function (such as skewed, bimodal and multiple-modal distributions) and this has been demonstrated by image analysis[244, 279, 280]. Parallel-laid structures may exhibit a single peak in a distribution histogram of fibre alignment (see Figure 4.4(a)). A compound distribution function is obtained when two or more distribution functions are combined so that the resulting distribution has two or more principle peaks (see Figure 4.4(b)). In practice, fibres in carded and cross-laid structures may be considered to have a compound distribution function.

The statistical distribution functions and their compound distribution function have significant practical importance because the fibre orientation distribution can be obtained experimentally using image analysis or related techniques as shown in section 4.4.4 in Chapter 4.

The general equations of directional permeability (see Table 6.1) can be readily used to predict the permeability if the actual fibre orientation distribution function is obtained. Some examples of the predicted permeability in unbonded nonwoven webs are presented in section 6.7 (see Figures 6.7 and 6.8). These predictions are based on the measured fibre orientation distributions of the webs.

6.5.5 Directional Permeability in Needlepunched and Hydroentangled Nonwoven Fabrics

Although this analysis has focused on the permeability of two-dimensional structures, in reality, fibres in many nonwoven fabrics are aligned in three-dimensional form. For example, in needlepunched and hydroentangled nonwovens, many fibres are aligned perpendicular to the fabric plane and the fibre distribution in the Z-direction can not be neglected.

In order to simplify the calculation of permeability, fibres aligned in the Z-direction in such structures can be simplified and assumed to be aligned in the direction of the fabric thickness and perpendicular to the fabric plane. It is assumed that the fibre distribution in the Z-axis is homogeneous and uniform, and that the number of fibres perpendicular to the fabric plane represents a fraction z of the total number of fibres. Assuming the fluid flow is laminar and in-plane (i.e., the flow along the Z-axis is ignored), the radial directional permeability in the fabric plane $k_r(\theta)$, which is a function of the flow direction θ, can be derived from equation (6.4.8) as follows:

$$k_r(\theta) = -\frac{1}{32}\frac{\delta^2}{\varepsilon}\left\{\frac{ST}{zS + (1-z)\sum_{\alpha=0}^{\pi}\Omega(\alpha)\left[T\cos^2(\theta-\alpha) + S\sin^2(\theta-\alpha)\right]\Delta\alpha}\right\} \qquad (6.5.5)$$

where z is the fraction of fibres aligned perpendicular to the fabric plane.

If the flow is only in the Z-direction, the permeability perpendicular to the fabric plane, $k|_Z$, can be written as:

Table 6. 2 Existing permeability models for isotropic and unidirectional fibrous structures

NAME OF THEORIES		PERMEABILITY (m^2)		NOTES	
Directional Permeability of Unidirectional Fabrics in the Theory $k(\theta)$ (M_R_UNI) (New)		$k(\theta)=-\frac{1}{32}\frac{\delta^2}{\varepsilon}\left\{\frac{ST}{T\sin^2\theta+S\cos^2\theta}\right\}$		Directional Permeability of Unidirectional Fibrous Bundles	Theoretical Models
Ferrandon's theory k_n (Scheidegger (1974))		$\frac{1}{k_n}=\frac{1}{k_1}\cos^2\theta+\frac{1}{k_2}\sin^2\theta$			
Emersleben's Equation (Emersleben (1925))		$k=\frac{1}{C}\frac{\delta^2}{\varepsilon}$	$C=16$		
Happel's Model (Happel (1959))			$C_{//}=\frac{32}{S}$ $C_{\perp}=-\frac{32}{T}$		
Kuwabara's Model (Kuwabara (1959))			$C_{\perp}=\frac{64}{S}$		
Permeability of Isotropic Fabrics in the new theory k (M_R_ISO)(New)			$C=-16\left\{\frac{S+T}{ST}\right\}$	Permeability of Isotropic Structures	
Iberall's Model (Iberall (1950))			$C=\frac{16(4-\ln Re)}{3(2-\ln Re)}\frac{1}{(1-\varepsilon)}$		
Kozeny-Carman's theory	Rushton's Equation for woven fabrics (Rushton (1968))	$k=\frac{1}{C}\frac{(1-\phi)^3}{\varepsilon^2}\delta^2$	$C=16\tau k_0$		
	Sullivan's Equation k (Sullivan & Hertel (1940))		$C=\frac{32}{\xi}$	Permeability of Anisotropic Structures	
	Shen's model (Shen (1996))		$C=128$	Permeability of Isotropic Structures	Empirical Models
	Davies' Model (Davies (1952))	$k=\frac{1}{64\varepsilon^{\frac{3}{2}}\left[1+56\varepsilon^3\right]}\delta^2$			

Where (1). τ --Roughness factor, k_0--the Kozeny constant, ξ the orientation factor.

(2). k_1 and k_2 are two principle permeabilities respectively.

(3). $S=[2\ln\phi-4\phi+3+\phi^2]$ and $T=[\ln\phi+\frac{1-\phi^2}{1+\phi^2}]$

(4). $C_{//}$ and $C_{\perp}$ are the coefficient for permeability in the direction parallel and perpendicular to the fibre orientation respectively in Happel's equation.

Table 6. 2 Existing permeability models for isotropic and unidirectional fibrous structures

NAME OF THEORIES		PERMEABILITY (m^2)		NOTES	
Directional Permeability of Unidirectional Fabrics in the Theory $k(\theta)$ (M_R_UNI) (New)		$k(\theta)=\frac{1}{32}\frac{\delta^2}{\varepsilon}\left\{\frac{ST}{T\sin^2\theta+S\cos^2\theta}\right\}$		Directional Permeability of Unidirectional Fibrous Bundles	Theoretical Models
Ferrandon's theory k_n (Scheidegger (1974))		$\frac{1}{k_n}=\frac{1}{k_1}\cos^2\theta+\frac{1}{k_2}\sin^2\theta$			
Emersleben's Equation (Emersleben (1925))		$k=\frac{1}{C}\frac{\delta^2}{\varepsilon}$	$C=16$		
Happel's Model (Happel (1959))			$C_{//}=\frac{32}{S}$ $C_{\perp}=-\frac{32}{T}$		
Kuwabara's Model (Kuwabara (1959))			$C_{\perp}=\frac{64}{S}$		
Permeability of Isotropic Fabrics in the new theory k (M_R_ISO)(New)			$C=-16\left\{\frac{S+T}{ST}\right\}$	Permeability of Isotropic Structures	
Iberall's Model (Iberall (1950))			$C=\frac{16(4-\ln Re)}{3(2-\ln Re)}\frac{1}{(1-\varepsilon)}$		
Kozeny-Carman's theory	Rushton's Equation for woven fabrics (Rushton (1968))	$k=\frac{1}{C}\frac{(1-\phi)^3}{\varepsilon^2}\delta^2$	$C=16\tau k_0$		
	Sullivan's Equation k (Sullivan & Hertel (1940))		$C=\frac{32}{\xi}$	Permeability of Anisotropic Structures	
	Shen's model (Shen (1996))		$C=128$	Permeability of Isotropic Structures	Empirical Models
	Davies' Model (Davies (1952))	$k=\frac{1}{64\varepsilon^{\frac{3}{2}}\left[1+56\varepsilon^3\right]}\delta^2$			

Where (1). τ --Roughness factor, k_0--the Kozeny constant, ξ the orientation factor.

(2). k_1 and k_2 are two principle permeabilities respectively.

(3). $S=[2\ln\phi-4\phi+3+\phi^2]$ and $T=[\ln\phi+\frac{1-\phi^2}{1+\phi^2}]$

(4). $C_{//}$ and $C_{\perp}$ are the coefficient for permeability in the direction parallel and perpendicular to the fibre orientation respectively in Happel's equation.

$$k|_z = -\frac{1}{32}\frac{\delta^2}{\varepsilon}\left\{\frac{ST}{(1-z)S+zT}\right\} \qquad (6.5.6)$$

6.6 COMPARISON OF EXISTING MODELS OF PERMEABILITY WITH THE NEW MODEL

For two-dimensional materials, a considerable amount of theoretical and experimental work has been presented by other workers for both isotropic and unidirectional fibrous materials[202, 278]. The following discussion is based on consideration of the calculated permeabilities predicted by these models. The existing models (for both isotropic and unidirectional fibrous structures) are listed in Table 6.2 together with the newly proposed models (denoted as M_R_ISO(New) and M_R_UNI(New)). The new models of permeability for various idealised fibrous structures are also shown in Table 6.1.

6.6.1 Specific Permeability and the Permeability Coefficient

In practical applications of Darcy's law[104], there are two types of permeability coefficient that require definition. The specific permeability k, (which is also called specific permeability or absolute permeability and is used in theoretical models), depends on the pore structure of the porous medium itself and represents the void capacity through which a fluid can flow. The specific permeability k is defined in Darcy's Equation[170] as: $v = -\frac{k}{\eta}\frac{dp}{dx}$, where v is the superficial flow rate of the fluid (m/s); η is the liquid viscosity ($Pa.s$); dp is the difference in hydraulic pressure (Pa); dx is the conduit distance (m) and k is the specific permeability (m^2). In most engineering applications the preference is to use the permeability coefficient K, which is also referred to as conductivity or Darcy's coefficient. This characterises a fluid flowing through the porous medium in a unit of the

superficial flow rate. The permeability coefficient K is defined in the following expression of Darcy's law: $v = K * i$. Where v is the superficial flow rate of the fluid (m/s); i is the hydraulic gradient, (i.e., the differential hydraulic head per conduit distance (m/m)); and K is the permeability coefficient (m/s).

The relationship between k and K is given as: $k = K\eta/\rho g\ (m^2)$, where ρ is the liquid density (kg/m^3) and g is the gravity accelerator constant (m/s^2). When the liquid is water at a temperature of 20^0C, the constant becomes, $k(m^2) = 1.042 \times 10^{-7} K(m/s)$.

The following comparison of the existing models of permeability is concerned with the specific permeability k. All the comparative results are summarised in Figure 6.5 and 6.6 and Table 6.2.

6.6.2 Permeability in Isotropic Fibrous Media

Many theoretical models of permeability[110, 281] and empirical equations[112, 113, 118] in fibrous structures are based on the assumption that the structure in question is homogenous and isotropic. The new theory can also give an equation for isotropic fibrous structures (see equation (6.5.1)).

As mentioned in section 6.3, the Kozeny equation[105] and its derivations[281, 112, 118] is based on capillary channel theory and agrees with experimental data very well so long as the porosity is low (<0.8), (see Figure 6.5(a)). However, it is shown in Figure 6.5(b) that this type of equation is not applicable for fluid flow in high porosity media (where porosity >0.8). In Figure 6.5(a) and 6.5(b), Rushton's equation is based on a consideration of

Figure 6. 5 Comparison of the existing permeability models for homogenous isotropic materials and the new model (M_R_ISO)

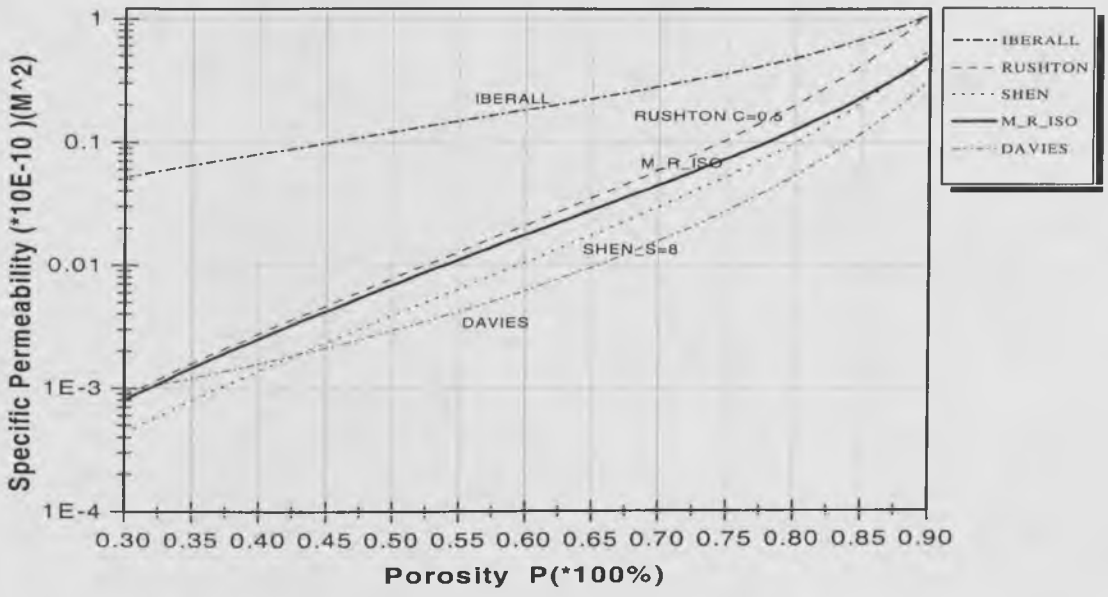

(a) (P=0.30-0.90)

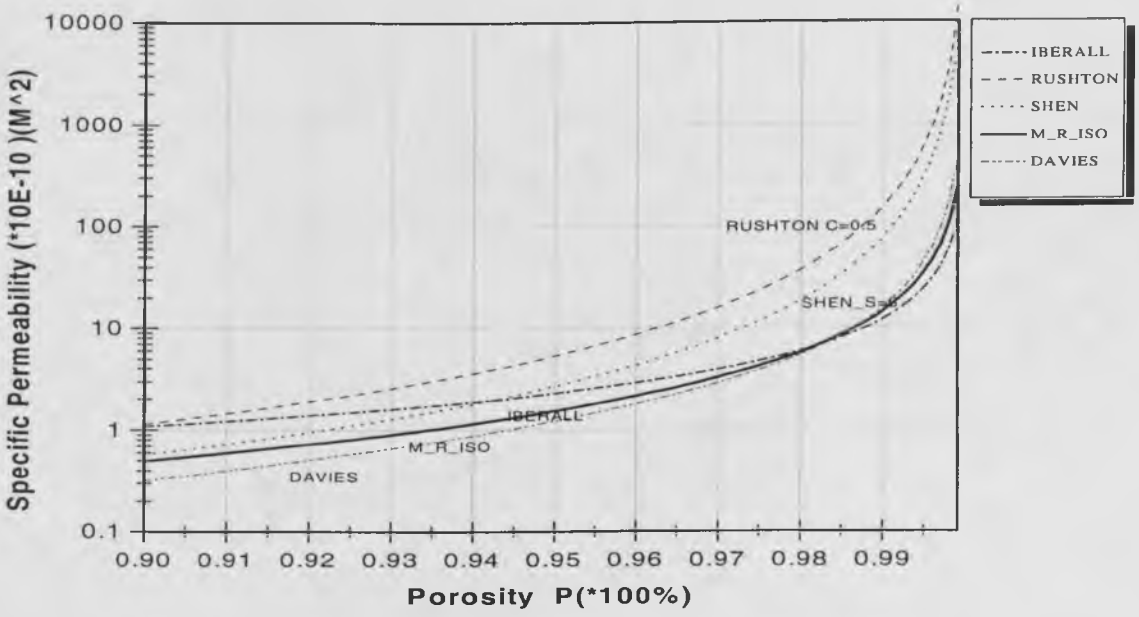

(b) (*P*=0.90-1.0)

Note: In Rushton's equation, the product of the roughness factor and Kozeny constant φk_0 is taken as 0.5

woven structures and is an example of Kozeny's theory applied to fabrics[281]. It is clear from Figure 6.5 that there is a large difference between the results of Rushton's equation[281] and empirical equations at high fabric porosities, but this difference is relatively small at low fabric porosities.

Iberall's equation[110] for isotropic fibrous material is based on drag force theory and aims to avoid the problems that exist with permeability models based on capillary channel theory. However, from Figure 6.5(a) it is apparent that in low porosity fabrics (where P<0.8), Iberall's equation gives predicted permeability results that are much higher than those obtained from empirical models but agrees with the current theory when $P \rightarrow 1$ as shown in Figure 6.5(b).

Several empirical models are also shown in Figure 6.5. Shen's experimental results[118] are based on both the cross-plane permeability and the in-plane permeability of needlepunched nonwoven fabrics. His empirical equation is claimed to be valid for porosities ranging from 0.3 to 0.8. Davies' equation[112] is obtained from experimental results of air permeability in glass fabrics having a porosity of 0.70~0.99. Shen's equation agrees with Rushton's equation for relatively low porosities of between 0.3~0.8. Davies' equation appears to provide reasonable predictions for structures having higher porosities of 0.70~0.99.

The permeability of homogenous fibrous structures deduced from the new theory, equation (6.5.1), is denoted as M_R_ISO in Figure 6.5, and is in good agreement with capillary theory at low porosity and is also in reasonable agreement with the results of empirical models (see Figure 6.5). Predicted results from the new model are in close

Figure 6. 6 Comparison of the existing permeability models and the new models (M_R_30, M_R_45 and M_R_60) for unidirectional fibrous materials

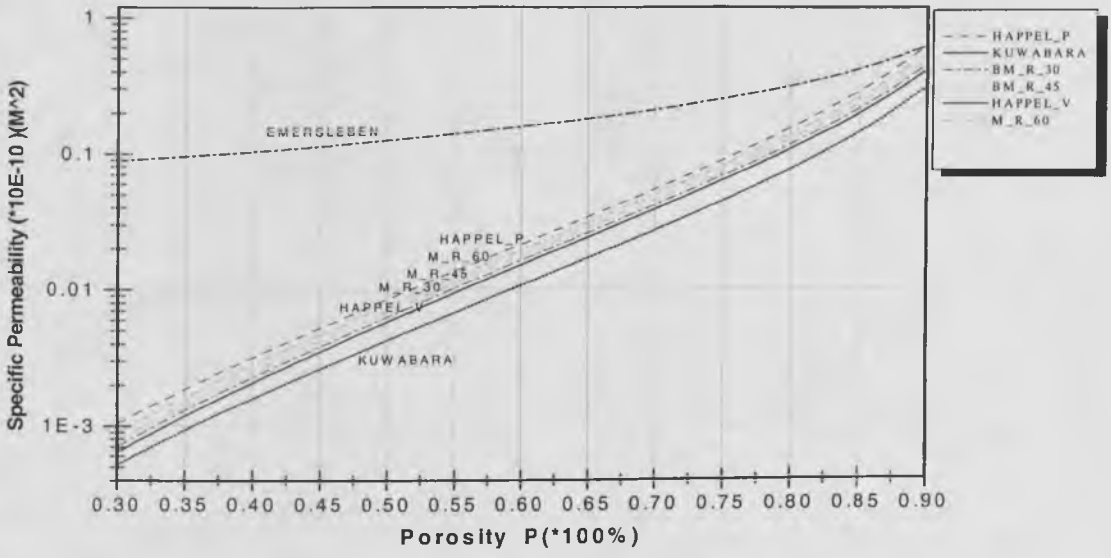

(a) (P=0.30-0.9)

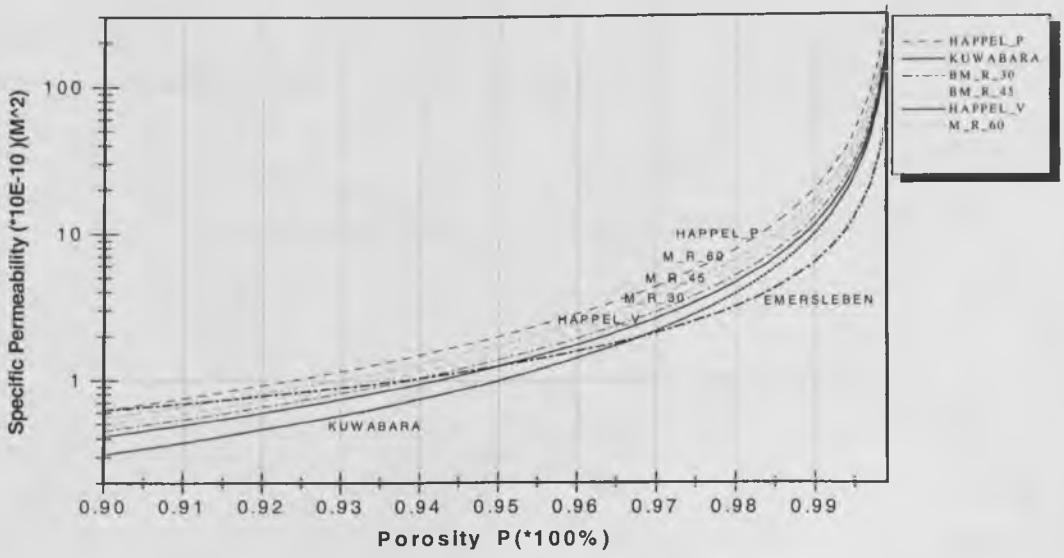

(b) (P=0.90-1.00)

Note: M_R_30, M_R_45 and M_R_60 are referred to as the directional permeabilities of unidirectional fabrics $k(\theta) = -\frac{1}{32}\frac{\delta^2}{\phi}\left\{\frac{ST}{T\sin^2\theta + S\cos^2\theta}\right\}$ when $\theta = \frac{\pi}{6}, \frac{\pi}{4}$ and $\theta = \frac{\pi}{3}$ respectively.

agreement with the empirical data from both Shen's equation at low porosity (P=0.3~0.8) and with Davies' equation at higher porosity (P=0.85~0.99). It would appear that the new model is applicable for both low and high porosity fibrous structures.

6.6.3 Permeability in Unidirectional Structures

In addition to isotropic structures, a number of theoretical studies have been presented for unidirectional fibrous structures[107, 111, 109, 272, 273, 282]. Several theoretical models for unidirectional fibrous structures are illustrated in Figure 6.6. For a wide range of porosities, many researchers (Happel and Brenner[278], Sangani and Acrivos[272], Drummond and Tahir[274]) have found that Happel's equation for unidirectional permeability (which is also included in the new model) is in close agreement with experimental data.

Three other newly derived equations are also included in Figure 6.6 where the direction of flow, with respect to the direction of fibre orientation, is taken to be 30^0, 45^0 and 60^0. It is interesting to note that the new equations do not predict the minimum permeability at a flow direction perpendicular to the predominant direction of fibre orientation. It is also notable that the differences between the predicted permeabilities at 30^0, 45^0 and 60^0 are very small especially when the porosity is quite high.

6.7 PREDICTED AND MEASURED ANISOTROPY OF PERMEABILITY IN EXPERIMENTAL NONWOVEN STRUCTURES

In Chapter 5, the structural parameters of eight webs and the corresponding nonwoven fabric structures made from them were presented. According to the new model, the permeabilities and the anisotropy of the permeabilities of these fabrics can be predicted using equation 6.4.7.

The measured anisotropy of permeability of the fabrics was also given in Table 5.5 in Chapter 5. Therefore, comparisons of the predicted and measured anisotropies of permeability are now considered.

6.7.1 Predicted and Measured Anisotropy of Permeability in Unbonded Webs

The predicted permeabilities of the unbonded webs reported in Chapter 5 are shown in Figures 6.7 and 6.8. A comparison between the predicted and measured anisotropies of permeability of these fabrics is summarised in Table 6.3 and Figure 6.9.

It is evident in Figure 6.9 that the predicted and the measured anisotropies of permeability are linearly related. Thus, the newly constructed model of permeability may be a very useful tool in predicting the actual permeability of fibrous webs. However, there are differences between the predicted and the measured characteristic angles of permeability (see Table 6.3).

Figure 6. 7 Predicted permeability of different web samples (polypropylene fibre)

(90^0 is the Machine Direction)

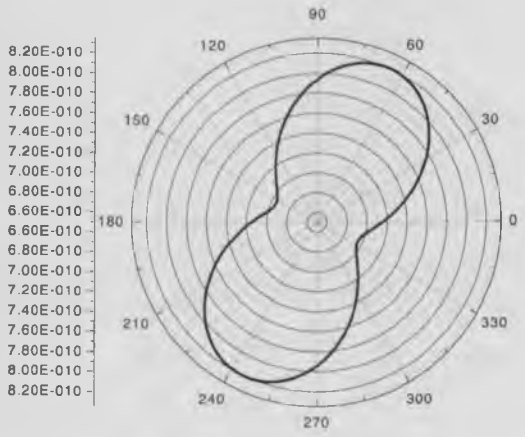

(a) Sample PA1

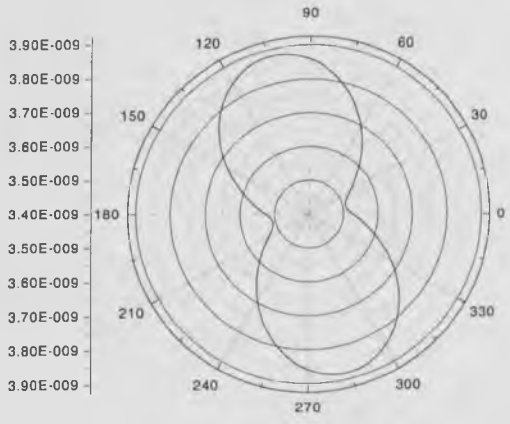

(b) Sample PB1

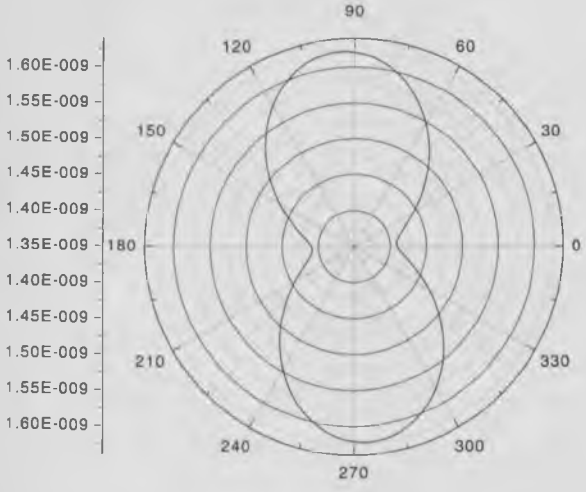

(c) Sample PA2

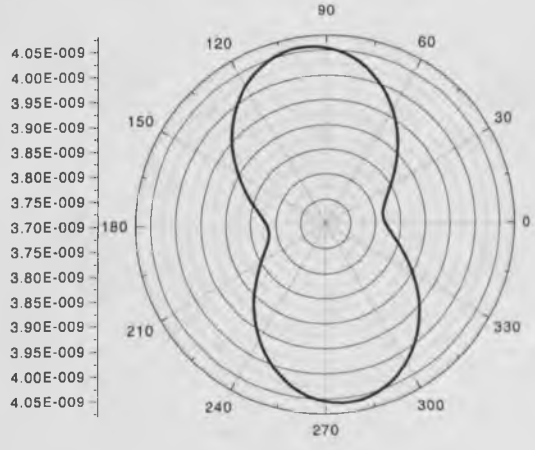

(d) Sample PB2

Figure 6. 8 Predicted permeability of different web samples (viscose fibre)

(90^0 is the Machine Direction)

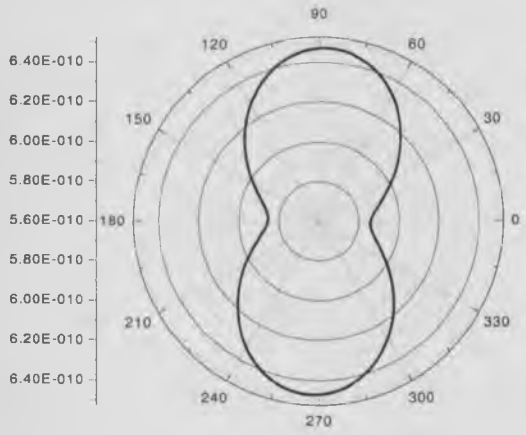

(a) Sample VA1

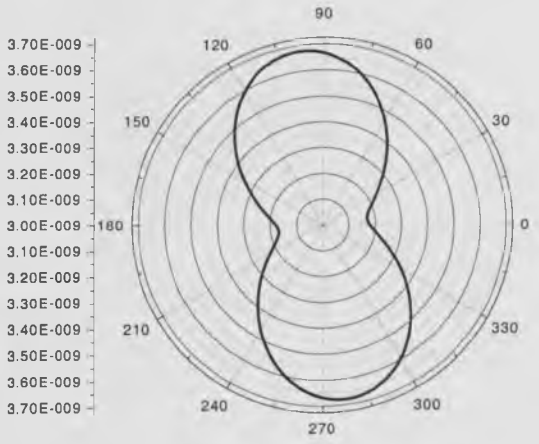

(b) Sample VB1

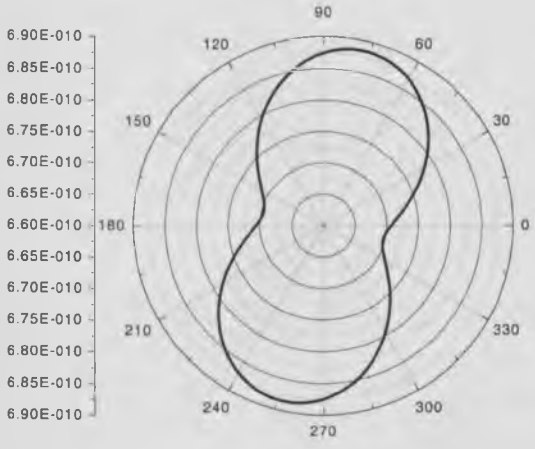

(c) Sample VA2

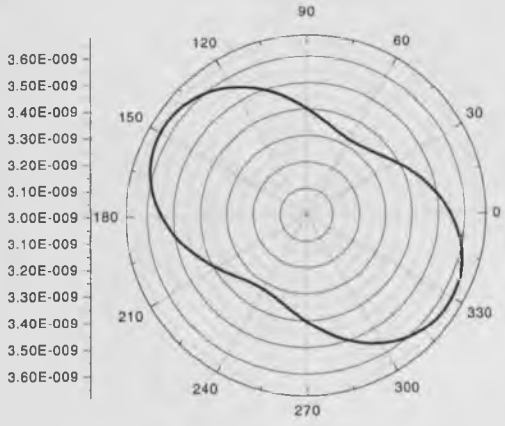

(d) Sample VB2

Table 6. 3 Predicted and measured anisotropy of permeability of the experimental unbonded webs

	Anisotropy of Permeability		Minimum Principle Angle of Permeability	
	Measured	Predicted	Measured	Predicted
PA1	2.425	1.181	-3.19^0	25.31^0
PB1	2.213	1.106	-2.75^0	13.06^0
PA2	1.875	1.151	-25.71^0	5.63^0
PB2	1.670	1.064	20.85^0	8.44^0
VA1	2.194	1.105	-6.63^0	2.81^0
VB1	2.226	1.161	-0.65^0	8.44^0
VA2	1.517	1.028	-13.18^0	13.06^0
VB2	1.931	1.094	-13.39^0	59.06^0

Figure 6. 9 Predicted and measured anisotropy of permeability of the experimental unbonded webs

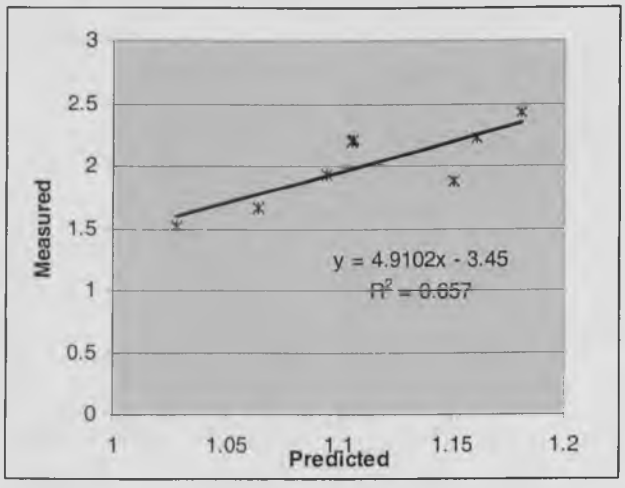

6.7.2. Anisotropy of Permeability in Non-homogeneous Nonwoven Structures

The measured anisotropies of permeability of the experimental needlepunched and hydroentangled nonwoven fabrics produced in Chapter 4 are shown in Table 5.5 (see Chapter 5). The predicted anisotropies of permeability in these fabrics are very similar to those in Figures 6.7 and 6.8.

In Chapter 4, it was reported that needlepunched and hydroentangled nonwoven fabrics were not homogeneous. Therefore, the permeabilities of needled and hydroentangled fabrics cannot be accurately predicted using the new models because they are valid only for homogeneous nonwoven structures (such as the experimental unbonded webs and commercial fabrics such as Sorbsan). This heterogeneity also explains why the measured anisotropy of permeability in the bonded fabrics was greater than the predicted anisotropy of permeability.

It is apparent that there are large differences in the anisotropy of permeability between homogeneous and non-homogeneous nonwoven fabrics. For homogeneous fabrics, there are two features of the anisotropy of permeability. First, the largest anisotropy of permeability in homogeneous nonwoven fabric will be theoretically obtained in unidirectional structures, and the anisotropy of permeability in such structures is identical to the ratio of the principle permeabilitites determined by the two Happel's equations[111]. The ratio varies with the fabric porosity as shown in Figure 6.10.

According to Figure 6.10 and other researchers[277], it is apparent that the maximum anisotropy of permeability for a homogeneous nonwoven structure should not be greater than 2. As the porosities of the experimental fabrics ranged from 0.93 to 0.99, the

maximum anisotropy of permeability in homogeneous unidirectional nonwoven structures should range from 1.55-1.73 (according to Happel's equations).

Figure 6. 10 Predicted anisotropy of permeability of unidirectional nonwoven structures

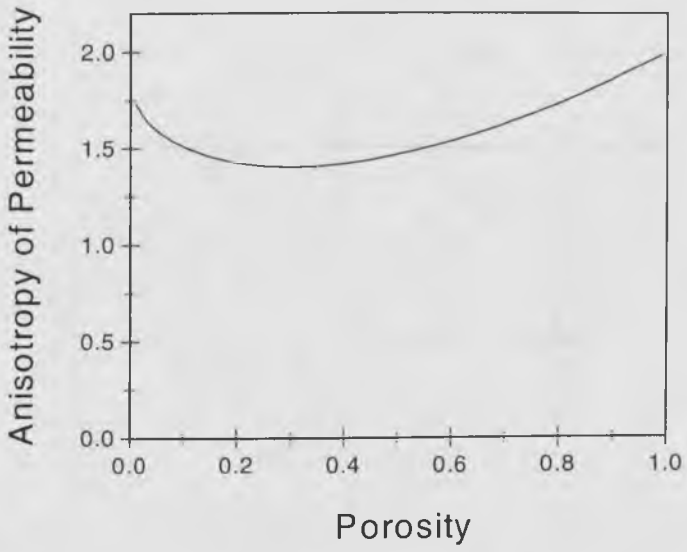

Secondly, the direction of the predicted principle permeability in homogeneous nonwoven structures varies markedly with the fibre orientation distribution.

In contrast to homogeneous nonwoven structures, the following two features of the anisotropy of permeability for needlepunched and hydroentangled fabrics (as shown in Table 5.5) should be noted:

(1). Most of the measured anisotropies of permeability are near to or higher than the maximum predicted anisotropy of permeability (1.55-1.73) for a homogeneous structure in the corresponding porosity range (0.93-0.99). In thirty-eight separate results, the maximum measured anisotropy of permeability was 232. The measured anisotropies of permeability can be grouped as follows:-

$\leq 1.55 = 10$;

≥ 1.55 and $\leq 2 = 11$

$\geq 2 = 16$

(2). The directions of the principle permeability in these fabrics rarely varied with the fibre orientation distribution of the web but was always in the machine direction (or within a narrow range of $\pm 30^0$ around the machine direction).

The measured and predicted anisotropies of permeability in commercial nonwoven wound dressings reported in Chapter 2 (Sorbsan and Soffban Natural) are also shown in Table 6.4 and Figure 6.11. It is apparent that the measured anisotropy of permeability in needlepunched fabric (Soffban Natural) is greater than that in the unbonded fabric (Sorbsan), although the predicted anisotropy of permeability of these two fabrics is similar. Since it is known from section 4.4 that the Sorbsan fabric (the fibre orientation distribution shown in Figure 4.8(a) is a single peak) is more anisotropic than Soffban Natural (the fibre orientation distribution shown in Figure 4.8(b) is bimodal), it is believed that the increased anisotropy of permeability was introduced by the needlepunching process.

Therefore, it is clear that the anisotropy of permeability in bonded fabrics is determined by their structural characteristics. The mechanical bonding process appears to introduce marked heterogeneity in the fabric structure by reorienting fibres which increases local variations in the fabric porosity and fibre orientation.

Table 6. 4 Predicted and measured anisotropy of permeability in commercial nonwoven wound dressing fabrics

	Anisotropy of Permeability		Minimum Principle Angle of Permeability	
	Measured	Predicted	Measured	Predicted
SORBSAN	1.332	1.123	25.81^0	-16.88^0
SOFFBAN NATURAL	2.085	1.126	34.45^0	-50.63^0

Figure 6. 11 Predicted and measured anisotropy of permeability in commercial nonwoven wound dressing fabrics

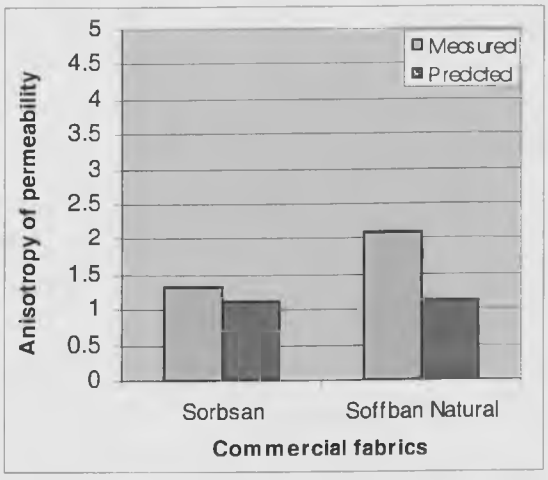

6.8 SUMMARY OF THE NEW MODELS

Equations have been derived to model the directional permeability in two- and three-dimensional fibrous materials from previous drag force equations. Equations (6.4.7) and (6.4.8) highlight a very important aspect of the unit cell theory of permeability because in this work it has been demonstrated for the first time that the permeability of a fibrous structure is not a constant but varies with the fibre orientation (see equation (6.4.7)).

Happel's equations[111] are constrained to materials having unidirectional fibre orientation, and this limits their practical application. In contrast, the alternative model presented in

equations (6.4.7) and (6.4.8) allows the permeability in all directions to be calculated. When equation (6.4.7) or (6.4.8) is applied to unidirectional materials and $\theta = 0 \ \ or \ (\frac{\pi}{2})$, the two equations can be reduced to a form that is essentially the same as Happel's equations.

The new equations for directional permeability appear to be generally applicable and in close agreement with existing empirical models for both low and high porosity homogeneous structures. The main conclusions of the theoretical approach may be summarised as follows:

1. The planar directional permeability in fibrous materials such as nonwovens can be deduced by drag theory, and for two-dimensional structures can be expressed as in equation (6.4.7), or more generally as in equation (6.4.13).

2. The directional permeability equations (6.4.7) and (6.4.13) can be expanded for application to three-dimensional fibrous structures, but at present this may be of limited practical application because of the practical difficulties that exist in measuring fibre orientation in three dimensions. In the future, it is likely that techniques will be developed to allow such measurements to be made.

3. In contrast to existing permeability models which are either applicable to isotropic materials or to unidirectional fibre bundles, the new equations (6.4.7) and (6.4.8) presented in this work allow calculation of the anisotropy of permeability in a range of structures, including isotropic fibrous materials, unidirectional fibre bundles and structures with two orthogonal fibre alignments.

4. Existing empirical and theoretical models for isotropic fibrous structures (such as nonwovens) tend to be valid only for a narrow range of porosities. The results from the new equation for isotropic fibrous structures (equation (6.5.1)) are in close agreement with previously obtained empirical data for both low and high porosity structures.

5. The new equations of permeability for unidirectional fibre bundles expand the application of Happel's equations which have been shown to be in agreement with experimental results over a wide range of porosities.

6. The planar directional permeability and permeability in the Z-direction of idealised nonwoven structures can be expressed as in equations (6.5.5) and (6.5.6) respectively. These equations are expected to be of practical use for many nonwoven fabrics.

7. The bonding process appears to introduce heterogeneity in the fabric structure. Two features of the anisotropy in heterogeneous nonwoven structures (such as needlepunched and hydroentangled fabrics) were found. The first is that the anisotropy of permeability in such fabrics is usually near to or higher than the predicted anisotropy of permeability (1.55-1.73) in a homogeneous structure for a corresponding porosity range (0.93-0.99). The other is that the directions of the principle permeability in these bonded fabrics rarely varied with the fibre orientation distribution. The principle permeability was always in the machine direction or within a narrow range ($\pm 30^0$) of the machine direction.

CHAPTER 7 CONCLUSIONS AND SUGGESTIONS FOR FURTHER WORK

It has been demonstrated that the liquid transport properties of nonwoven fabrics used in wound care depends both on the properties of the constituent fibres and on the spatial arrangement of the fibres in the assembly. Additionally, this research has highlighted the influence of the geometrical structure on the anisotropy of liquid transport in nonwoven structures of the type used in wound dressing applications.

7.1 CONCLUSIONS

The primary focus of this work was to investigate the influences of the structural characteristics of nonwoven fabrics on the liquid transport characteristics of nonwoven fabrics.

By performing preliminary strip tests on commercial nonwoven wound dressings, it was established that there is significant anisotropy of liquid absorption in such fabrics no matter what the fibre composition of the fabric. It was evident that the anisotropy in liquid absorption is influenced by anisotropy in the fabric structure, which may be influenced by the fibre orientation distribution. It was also apparent that there were no previous studies of the relationship between the fibre orientation distribution and the anisotropy of liquid transport in nonwoven fabrics.

After comparison of various measurement methods, a novel computer integrated capacitance system for measuring multiple-directional liquid transport in nonwoven wound dressing structures was constructed to simulate practical liquid absorption

conditions. Using this dynamic measuring instrument, tests of liquid absorption and liquid transport in up to eight directions in the fabric plane were undertaken for both commercial nonwoven wound dressings and numerous experimental nonwoven sample fabrics.

A method was introduced to obtain the anisotropy of permeability and the anisotropy of liquid absorption in fabrics using the new measurement system.

It was concluded that unbonded nonwoven webs can be modelled as homogeneous anisotropic structures, but such webs are not homogeneous after needlepunching or hydroentanglement. Thus, such bonding processes appear to make nonwoven structures more anisotropic and heterogeneous.

Experimental studies established that the fibre orientation distribution and the fabric porosity in homogeneous anisotropic nonwovens dominated the anisotropy of the liquid flow in such structures. However, the liquid flow through needled and hydroentangled fabrics was more complex and is influenced by a combination of local differences in the fibre orientation distribution and fabric porosity.

It would appear that modifying the fibre orientation distribution of nonwoven fabric is a very effective method for obtaining desirable anisotropic or isotropic fabric structures. The marked increases in anisotropy resulting from different types of mechanical bonding are also noteworthy when considering the design of fabrics with particular liquid handling characteristics.

A unique model for predicting the directional permeability of homogeneous anisotropic nonwoven fabrics has been developed based on Happel's equations.

In contrast to existing permeability models which are either applicable to isotropic materials or to unidirectional fibre bundles, the directional permeabilities of several idealised nonwoven structures (isotropic fibrous materials, unidirectional fibre bundles, structures with two orthogonal fibre alignments and structures with certain fibre orientation distributions) were studied based on the new model, and it was established that the specific permeability in nonwoven fabrics depends on the fibre diameter, fabric porosity and the fibre orientation distribution. All these parameters can be readily measured.

Existing empirical and theoretical models for isotropic nonwoven structures tend to be valid only for a narrow range of porosities. The results from the new model for isotropic fibrous structures (equation 6.5.1) are in close agreement with previously obtained empirical data for both low and high porosity structures.

The new models for predicting the anisotropy of specific permeability in nonwovens were examined by comparing them with experimental results, and it was found that the models are suitable for use with homogeneous nonwoven structures (e.g. unbonded webs) but not suitable for heterogeneous nonwoven structures such as needlepunched and hydroentangled nonwoven fabrics.

Other main findings from this work may be summarised as follows:

- The liquid absorbency of nonwoven fabrics is related to fabric porosity.

- Fibre type and fibre linear density appear to affect fibre alignment in web formation and thus influence the fibre orientation distribution in nonwoven fabrics.

- The fibre entanglement during hydroentanglement and the structure of hydroentangled fabric may also be affected by the specific flexural rigidity, compression recovery, and bending recovery of the fibre.

- The bonding process appears to introduce heterogeneity in the fabric structure. Both needlepunched and hydroentangled fabrics have been found to be a non-homogeneous fibrous structures due to needling marks and jet marks respectively.

7.2 SUGGESTIONS FOR FURTHER WORK

It is possible to modify the new measurement system to enhance the transducer sensitivity and to measure liquid flow in up to 16 or more directions in the fabric plane.

Although the liquid transport in homogeneous nonwoven structures has been studied and a new model has been proposed, the mechanism of liquid transport in non-homogeneous structures requires further investigation. There are structural heterogeneities in nonwoven fabrics, such as spatial variations in the arrangement of fibres. This variation is evident in areal density, fibre orientation, fibre crimp, and in the degree of fibre entanglement. Such structural heterogeneities result in local variations in permeability that will produce deviations from the smooth-ellipse-like flow fronts

when liquid is absorbed by fabrics. Since the variations are local, the shapes of the flow fronts for heterogeneous structures are not reproducible[202].

The transport of non-Newtonian fluids such as blood and body fluid was beyond the scope of the research, but future work is still required to determine the effect of body fluid transport in anisotropic nonwoven structures. This assumes substitute fluids can be made that behave in the same way as real body fluids.

Further work is also required to establish the effect of liquid transport using different pressures.

The research presented in this thesis has revealed the mechanisms of liquid transport and liquid absorption, and has demonstrated the effect of important fabric structural parameters on these liquid handling characteristics. In future studies, the effect of other structural parameters such as fibre length and fibre cross sections on the liquid transport need to be elucidated. Also, the simultaneous liquid transport in all three-dimensions of the fabric structures is an important area for further research.

APPENDIX I Modified Routine for Measuring Fibre Orientation Distributions in Image Analyser.

```
10 rem  FIBRE ORIENTATION CHARACTERISATION OF NONWOVENS
20 dim a(5000),b(5000), c(5000)
30 rem  machine direction vertical (black fibres)
40 rem black source(15.6/17 mag-25*latter)
50 clearimages
55 display 0 1 2 1
60 pausetext 1,"MACHINE DIRECTION VERTICAL"
70 qmenu "image_setup"
80 pausetext 1,"  "
90 qmenu "calibrate"
100 riasettings "cal_value",cal
110 pausetext 1,"ACQUIRE IN 0"
120 qmenu "acquire"
130 average 0 5 1 0 7 0
140 greysub 0 1 2
150 greyset 140 3
160 greyadd 2 3 4
170 btoph 4 8 255 2:sub8 4 8 5
180 wtoph 4 8 255 2:add8 5 8 8
190 setgamma 161,-27
200 anamorph 8 9 6 10
210 greymove 9 0
220 rem Black sharpen Source Prelim contrast increase
230 anamorph 0 1 6 8
240  btoph 1 0 256 1 : sub8 1 0 0
250 greyinvert 0 1
260 greyfill 1 23 1 1
270 greymove 23 1
```

```
370 mframe 0 0 512 480
380 pausetext 1,"ADJUST FRAMES INTO BODY OF FABRIC"
390 qmenu "frames"
400 riasettings "mframex",x1
410 riasettings "mframey",y1
420 riasettings "mframew",w1
430 riasettings "mframeh",h1
440 wgline 1 x1 0 x1 511 0
450 wgline 1 0 y1 511 y1 0
460 wgline 1 x1+w1 0 x1+w1 511 0
470 wgline 1 0 y1+h1 511 y1+h1 0
480 pausetext 1,"DETECT WHITE IN 1"
490 qmenu "detect"
500 pausetext 1,"EDIT 1 TO 8"
510 qmenu "bin_edit"
520 binmove 8 1
530 binwskel 1 2
540 chrpoint 2 3 1
550 bindilate 3 4 256 1.5
560 binx 1 4 5 1 0 1
570 edgefeat 5 11
580 binmove 11 5
590 display 0 1 3 32
600 cls
610 setftrpar "8,35,32,11,1,2,3,63"
620 ftrgrey 0 : measfeat 5 1 10 3000000 : clraccept
630  acceptfeat 1 12 812813
640 acceptxfer 5 6
650 histoclear 1
652 pausetext 1, "Dist Number should be 1, Orientation range should be 0-180"
653 pausetext 2, "To get histogram, click CLEAR, then click HISTOGRAM"
```

```
 654 pausetext 3, "To save data to disk, click PRINT"
 655 qmenu "histogram"
680 rhistostats 1 stats(1) 0
 690 mm=stats(2)
720 rhistostats 1 stats(1) 0
 730 nn=stats(1)
 740 histoclear 1
770  RFEATNUM NUM(1)
 780  FOR I= 1 TO NUM(2)
 790   RFEATRES I-1 32 FEATS(2)
 795 c(i)=FEATS(2)
 800 test FEATS(2)>90 then 810 else 825
 810 a(I)=180-FEATS(2)
 820 goto 828
 825 a(I)=FEATS(2)
 828 next I
864 sum=0
 866  for x=1 to NUM(2)
 870 b(x)=sin(a(x)*3.1416/180)
890  sum=sum+b(x)
 900  next x
930  qmenu "bin_edit"
 940 measfield 10
 950 rfieldres field(1)
 960 measfield 1
 970 rfieldres fieldarray(1)
 980 print " "
 990 print "DO YOU WISH TO PRINT DATA Y/N ?"
1000 input m$
1010 test m$="y" then 1020 else 1160
1020 open #1 "prn"
```

```
1030 print #1:" "
1040 print #1:"PERFECT ALIGNMENT FACTOR (w.r.t.vertical axis)=100"
1050 print #1:"PERFECT ALIGNMENT FACTOR (w.r.t.horizontal axis)=0"
1060 print #1:"ACTUAL ALIGNMENT FACTOR =100*sum/NUM(2)
     ="100*sum/NUM(2)
1070 print #1:"STANDARD DEVIATION OF ORIENTATION =",mm,"degrees"
1080 print #1:"ANISOTROPY (h/v.intercepts) = ",fieldarray(3)/fieldarray(4)
1090 print #1:"AREA EXAMINED =",w1*h1*cal*cal,"sq.mm"
1100 print #1:"AREA FRACTION = ",fieldarray(1)/(w1*h1)
1110 print #1:"NUMBER OF FIBRE SEGMENTS =",NUM(2)
1120 print #1:"FIBRE SEGMENT DENSITY =",NUM(2)/(w1*h1*cal*cal),"per
     sq.mm"
1130 print #1:"AVERAGE SEGMENT LENGTH =",nn,"mm"
1140 print #1:"NUMBER OF CROSSOVERS =",field(5)
1150 close #1
1160 binput 6 1
1170 display 0 3 2 2
1180 END
```

Appendix II Electronic Circuits

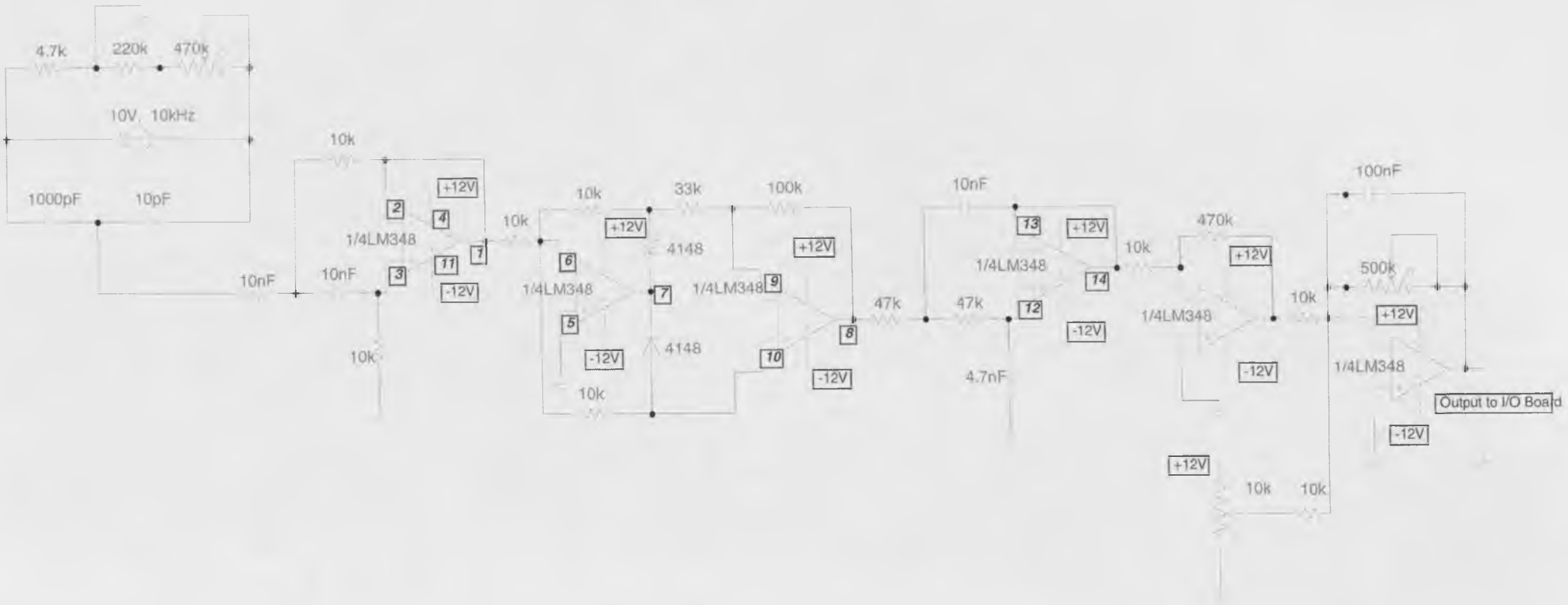

APPENDIX III Drag Force on A Single Fibre

When a fluid flows in the direction θ over a fibre which is aligned in the direction α (as shown in Figure 6.1), the velocity vector of the fluid flow, $\vec{V}$, can be separated into two orthogonal components, $\overrightarrow{V_p}$ and $\overrightarrow{V_v}$,

$$\overrightarrow{V_p} = \vec{V} \,|\cos(\theta - \alpha)|$$

$$\overrightarrow{V_v} = \vec{V} \,|\sin(\theta - \alpha)|$$

Where $\overrightarrow{V_p}$ is the velocity vector parallel to the fibre length and $\overrightarrow{V_v}$ is the velocity vector perpendicular to the fibre length. Thus, according to equations (6.4.1) and (6.4.2), the drag force acting on the fibre, f_p and f_v, will be as follows,

$$\overrightarrow{f_p} = -\frac{8\pi\eta q \,|\cos(\theta - \alpha)|}{[4\phi - \phi^2 - 3 - 2\ln\phi]} = \frac{8\pi\eta q \,|\cos(\theta - \alpha)|}{S}$$

$$\overrightarrow{f_v} = \frac{8\pi\eta\, q \,|\sin(\theta - \alpha)|}{[\ln\phi + \frac{1-\phi^2}{1+\phi^2}]} = \frac{8\pi\eta\, q \,|\sin(\theta - \alpha)|}{T}$$

Consequently, the total drag force in the direction θ, which is the direction of fluid flow, will be $f(\theta)$ (see Ferrandon' equation in Scheidegger's book[170]),

$$\overrightarrow{f(\theta)} = \overrightarrow{f_p} \,|\cos(\theta - \alpha)| + \overrightarrow{f_v} \,|\sin(\theta - \alpha)|$$

$$= \frac{8\pi\eta q \cos^2(\theta - \alpha)}{S} + \frac{8\pi\eta q \sin^2(\theta - \alpha)}{T}$$

REFERENCES

[1]. Turner TD, Which Dressing and Why? in *Wound Care (Eds.)* Westaby S., Heinemann Medical Books, p59--67, London, 1985

[2]. Cusick GE. and Hopkins, T., Absorbent incontinence products, *Textile Progress*, 20(3), p21, 1990.

[3]. Lindsay JD, The anisotropic permeability of paper, TAPPI, May, p223, 1990.

[4]. Odland G., The fine structure of the interrelationship of cells in the human epidermis, *J. Biophys. Biochem. Cytol.*, 4, p529--535, 1958.

[5]. Winter GD, Formation of scab and the rate of epihteliazation of superficial wounds in the skin of the young domestic pig, *Nature*, 193, p293--294, 1962.

[6]. Hinman CD and Maibach H, Effect of air exposure and occlusion on experimental human skin wounds, *Nature*, 200, p377--378, 1963.

[7]. Winter GD, Epidermal regeneration studies in the domestic pig, in Maibach HL and Rovee DT, (Eds), *Epidermal Wound Healing*, Chicago, Year Book Medical Publishers Inc., p159--181,1972.

[8]. Whitby DJ, The biology of wound healing, *Surgery*, 1, p25-26, 1995.

[9]. Steenfos HH, Growth factors and wound healing, *Scand. Plast. Reconstr. Hand. Surg.*, 28, pp95--105, 1993.

[10]. Eaglstein WH and Mertz PM, New Method for assessing epidermal wound healing: The effects of tramcinolone acetonide and polyethylene film occlusion. *J. Invest. Dermatol.*, 71, p382--384, 1978.

[11]. Rovee DT, Effect of local wound environment on epidermal healing, in Maibach HL, Rovee DT., (Eds), *Epidermal Wound Healing*, Chicago, Year Book Medical Publishers Inc., p159--181,1972.

[12]. Barett A., et al, Comparison of synthetic adhesive moisture vapour permeable and fine mesh gauze dressings for split--thickness skin graft donor sites, *Am. J. Surge.*, 145, p379--381, 1983.

[13]. Mandy SH., A new primary wound dressing made of polyethylene oxide gel, *J. Dermal Surge.* 9, 153--155, 1983.

[14]. Grotendorst GR, Chemo attractants and growth factors, In Cohen IK, et al, (Eds.) *Wound Healing*. Philadelphia, WB Saunders, p237--246, 1992.

[15]. Robson MC and Heggers JP., Eicosinoid, cytokines, and free radicals, In Cohen IK, et al, (Eds.) *Wound Healing,* Philadelphia: WB Saunders, p292--304, 1992.

[16]. McGrath MH, Peptide growth factors and wound healing, *Clin. Plast. Surg*., 17, p421--432, 1990.

[17]. Mckay IA and Leigh IM, Epidermal cytokines and their roles in cutaneous wound healing, *Br. J. Dermaltol*., 124, p513--518, 1991.

[18]. Breuing K, et al, EGF-like growth factor present in porcine wound fluid, *Surg. Frum*, 42, p623--625,1991.

[19]. Grotendorst GR., et al, Production of growth factors (PDGF & TGF-beta) at the site of tissue repair, In Hunt TK, et al, (Eds.) *Biological and Clinical Aspects of Tissue Repair*, Alen R Liss, New York, p47--54, 1988.

[20]. Katz MH., et al, Human wound fluid from acute wounds stimulates fibroblast and endothelial cell growth, *J. Am. Acad. Dermatol.* , 25, pp1054--1058, 1991.

[21]. Buchan IA., et al, Laboratory investigation of the composition and properties of pigskin wound exudate under Op-Site, *Burns*, 8, p39--46, 1981.

[22]. Ichiro Ono, et al, Evaluation of cytokines in donor site wound, *Scand. Plast. Reconstr. Hand. Surg.* , 28, p269-273, 1993.

[23]. Nemeth AJ., et al, Stimulatory effect of human wound fluid on epidermal out growth from porcine skin explant cultures, abstracted. *J. Invest. Dermatol*., 86, pp497, 1986.

[24]. Alper JC, et al, The in vitro response of fibroblasts to the fluid that accumulates under a vapour- permeable membrane, *J. Invest. Dermatol*., 84, p513--515,1985.

[25]. Falanga V., Occlusive wound dressings, *Arch. Drematol*., 124(6), pp872-877,1988.

[26]. Mertz PM and Eaglstein WH, The effect of a semi-occlusive dressing on the microbial population in superficial wounds, *Arch. Surge*., 119, pp287--289,1983.

[27]. Stuart Kartz, et al, Semipermeable occlusive dressings: Effects on growth of pathogenic bacteria and reepithelialization of superficial wounds, *Arch. Dermatol*., 122(1), p58--62,1986.

[28]. Alvarez OM, et al, The effect of occlusive dressings on collagen synthesis and re-epithelislization in superficial wounds, *J. Surg. Res.* 35, p142--148, 1983.

[29] . Eaglstein WH., Experiences with biosynthetic dressings, *J. Am. Acad. Dermatol.*, 12, p434-440, 1985.

[30]. May SR, Physiology, immunology, and clinical efficacy of an adherent polyurethane wound dressing: Op-Site, in Wise DL (Eds): *Burn Wound Coverings*, Boca Raton, Fla, CRC Press, p53--78,1983.

[31]. Eatton AC, A controlled trial to evaluate and compare a sutureless skin closure technique (Op-Site skin closure) with conventional skin suturing and clipping in abdominal surgery, *Br. J. Surg.* 67, p857--860, 1980.

[32]. Friedman SJ and Su WPD, Management of leg ulcers with hydrocolloid occlusive dressing, *Arch., Dermatol.*,120, p1329, 1983.

[33] . Alper JC, et al, Moist wound healing under a vapour permeable membrane, *J. Am. Acad. Dermatol.*, 8, p347--353,1983.

[34]. Gores GJ and Messner RL, Improved pressure sore healing with hydrocolloid dressings, *Arch. Dermattol.*, 123, p766--771, 1987

[35]. Holland KTT, et al, A comparison of the in vitro antibacterial and complement activating effect of Op-- Site and TeGaderm dressing, *J. Hosp. Infect.*, 5, p323--328, 1983.

[36]. Thomas S., *Wound Management and Dressings*, The pharmaceutical press, London, 1990

[37] . Merttz PM, et al, Occlusive wound dressings to prevent bacterial invasion and infection, *J. Am. Acad. Dermatol.*, 12, p662-668, 1985.

[38]. Eaglstein WH, et al, Occlusive dressings, *Am. Fam. Physician.* 35, pp211--216, 1987.

[39]. Phillips TJ, Kapoor V., Provan A. and Ellerin T., A randomised prospective study of a hydro-active dressing vs. conventional treatment after shave biopsy excision, *Arch. Dermatol.* 129, p859--860, 1993.

[40]. Jaffe LF and Vanable JW, Electric fields and wound healing, in Eaglstein WH (Eds.): *Clinics in Dermatology: Wound Healing*, Philadelphia, JB Lippincott, p34--44, 1983.

[41]. Falanga V., et al, Electrical stimulation increases the expression of fibroblast receptors for transforming growth factor-beta, abstracted, *J. Invest Dermatol.* 8, p488,1987.

[42]. Eaglstein WH., et al , Optimal use of an occlusive dressing to enhance healing: Effect of delayed application and early removal on wound healing, *Arch. Dermatol.* 124, p392-395, 1988.

[43]. Fisher LB and Maibbach HI, The effect of occlusive and semipermeable dressings on the cell kinetics of normal and wounded human epidermis, in Maibach HI, Rovee DT (Eds.): *Epidermal Wound Healing*. Chicago, Year Book Medical Publishers Inc, pp113--122. 1972.

[44]. Winter GD, Oxygen and epidermal wound healing: (3) Oxygen transport to tissues , in Silver IA, et al (Eds.),: *Advance in experimental Medicine and Biology*. New York, Plenum Publishing Co., p673--678, 1972.

[45]. Silver IA, Oxygen lesions and epithelialization, in Maibach HI, Rovee DT (Eds.): *Epidermal Wound Healing*. Chicago, Year Book Medical Publishers Inc, p291--305, 1972.

[46]. Osment LS, The skin in wound healing, in Menaker L.(Eds.), *Biologic Basis of Wound Healing*, p274--290, 1980.

[47]. Buchan IA, et al, The effect of local infections upon wound healing: An experimental study, *Br. J. Surg.*, 67, p851--855, 1980.

[48]. Balin AK, et al, Oxygen modulates the growth of human cells at physiologic partial pressures, *J. Exp. Med.* 160, p152--166, 1983.

[49]. Banda MJ, et al, Isolation of a nonmutagenic angiogenesis factor from wound fluid, *Proc. Natl. Acad. Sci.* USA, 79, p7773--7777,1982.

[50]. Knighton DR, et al, Oxygen regulates the angiogenesis factors by macrophages, *Science*, 221, p1283--1285, 1983.

[51]. Knighton DR, et al, Regulation of wound healing angiogenesis: Effect of oxygen gradients and inspired oxygen concentrations, *Surgery*, 90, p262--270,1981.

[52]. Horikoshi T., et al, Modulation of proliferation in human epidermal keratinocyte and melanocyte cultures by dissolved oxygen, abstracted, *J. Invest. Dermatol.*, 82, p411, 1984

[53]. Varghese MV, et al, Local environment of chronic wounds under synthetic dressings, *Arch. Dermatol.*, 122, Jan, p52--57, 1986.

[54]. Park GB, Courtney JM, McNair A. and Gaylor JDS, The design and evaluation of a burn wound covering, *Engineering of Medicine*, 7, p11--15, 1978.

[55]. Rahmn MM, In vitro assessment of polymeric burn wound coverings, *M.Sc. Thesis*, University of Strathclyde, Glasgow, 1982.

[56]. Wong P., Physical evaluation of a hydrogel as a burn wound dressing, *M. Sc. Thesis*, University of Strathclyde, Glasgow, 1980.

[57]. Lamke LO, Nilsson GE and Reithner HL, The evaporative water loss from burns and the water vapour permeability of grafts and artificial membranes used in the treatment of burns, *Burns,* 3, p159--165, 1977

[58]. Queen D, Galor JDS, Evans JH, Gaylor JDS, Courtney JM and Reid WH, The in vitro gaseous transmission of wound dressings, *Scan. J. Reconstr. Surg.* 21, p287--289, 1987.

[59]. Standard methods of test for water vapour transmission of materials in sheet form, *ASTM Method E96-66*, 1990.

[60]. British Standard method of measuring the gas permeability of package materials, *B.S. Method 2782*, 1990.

[61]. Queen D, Evans JH, Gaylor JDS, Courtney JM and Reid WH, Preclinical assessment of burn wound dressings, *Burns*, 12, p161--166, 1986.

[62]. Shultis KL, Determinaton of the oxygen permeability of artificial membranes by gas to liquid transfer methods, *M.Sc. Thesis*, University of Minnesota, USA, 1980.

[63]. Wong P., Carbon dioxide transfer in membrane oxygenators and associated membrane, *Ph.D. Thesis*, University of Strathclyde, Glasgow, 1983.

[64]. Eagle ME, Community nurses prospective of wound management products in problematic wounds, *Procs. of Med. Text. Int. Conf. 96*, Bolton, UK, 1996.

[65]. Alper JC, WelshE A. and Magire P., Use of the vapour permeable membrane for cutaneous ulcers: Details of application and side effects, *J. Am. Acad. Dermatol.* 11, p858--866, 1983.

[66]. Zitell JA, Delayed wound healing with adhesive wound dressing, *J. Dermatol. Surg. Oncol.,* 10, p709--710, 1983.

[67]. Varley SJ, Barnett SE and Scales JT, Wound healing and the effects of dressing, *Conference on Medical Applications of Textiles*, University of Leeds, 1981.

[68]. Winter TD, A note on wound healing under dressing with special reference to perforated-film dressings, *J. Invest. Derm.*, 45(4), p299, 1965.

[69]. Thomas S, Foam Dressings: A guide to the properties and uses of the main foam dressings available in the UK., *J.Wound Care*, 2(3), p153, 1993

[70]. Winter TD, Epidermal wound healing under a new polyurethane foam dressing (Lyofoam). *Plast. Recon. Surg.*, 56 (5), p531, 1975

[71]. Bishop WI, *The early history of surgery*, Robert Hale, London, p163, 1980

[72]. Turner TD, *Pharm. J.*, 22, p421, 1979

[73]. Turner TD, The functional development of wound management products, *Conference on Medical Applications of Textiles*, University of Leeds, 1981.

[74]. Burrow TR and March BS, The development of fibres for use in wound dressings, textiles in health care, *The 2nd Leeds Medical Applications of Textiles Conference*, University of Leeds, Sept., 1985.

[75]. Anon. *Medical Textile*, Nov.,pp7, 1996.

[76]. Anon. *Medical Textile*, Mar., pp8, 1996.

[77]. Anon. *Medical Textile*, Jan., pp4, 1996

[78]. Anon. *Medical Textile*, Sept.,pp6, 1996

[79]. *US patent 5,531,670*, 1996

[80]. Anon. *Nonwoven Ind.* 22(3), p80-81, 1991.

[81]. Anon. *http://www.smtl.co.uk/WMPRC/DataCards/*

[82]. Anon. *http://www.smith-nephew.com/UK/*

[83]. Anon. *Int. nonwovens Bull.* , 2(3), p56, 1991.

[84]. Anon. *Int. nonwovens Bull.* , 2(3), p56, 1991.

[85]. Anon. *Medical Textile*, Jan., p12, 1996

[86]. *US patent 5,470,576, 1995*

[87]. *US patent 5,520,925*, 1996

[88]. *US patent 5,465,735*, 1995

[89]. *US patent 5,529,783*, 1996

[90]. Hearle JWS and Stevenson PJ, Nonwoven fabric studies, part 3: The anisotropy of nonwoven fabrics, *T.R.J.*, 33, pp877-888, 1963

[91]. Hearle JWS and Stevenson PJ, Nonwoven fabric studies, part 4: Prediction of tensile properties, *T. R. J.*, 34, pp181--191, 1963.

[92]. Backer S. and Petterson DR, Some principles of nonwoven fabrics, *T. R. J.*, 30, pp704-711, 1960.

[93]. Osaki S., Dielectric anisotropy of nonwoven fabrics by using the microwave method, *TAPPI*, 72, p171, 1989.

[94]. Krcma R., *Manual of Nonwoven Textiles*, Textile Trade Press, Manchester, 1972.

[95]. Morton WE and Hearle JWS, *Physical Properties of Textile Fibres*, The Textile Institute, London, 1993.

[96]. Hearle JWS and Ozsanlav V., Nonwoven fabric studies, part 1: A theoretical model of tensile response incorporating binder deformation, *J. T. I.*, 70, pp19--28, 1979.

[97]. Wrotnowski AC, Felt filter media, *Filtration and Separation*, Sept./Oct., p426-431, 1968.

[98]. Lambard G., et al, Theoretical and Experimental opening size of heat-bonded geotextiles, *T.R.J.*, April, p208-217, 1988.

[99]. Faur Y., et al., Theoretical and Experimental determination of the filtration opening size of geotextiles, *3rd International Conference on Geotextiles,* Vienna, Austria, p1275-1280, 1989.

[100]. Hsieh YL and Yu B., Wetting and retention properties of fibrous materials, part 1: Water wetting properties of woven fabrics and their constituent single fibres, *T. R. J.*, 62, p677--685, 1992.

[101]. Hsieh YL and Wu M., Wetting characteristics of poly(p-phenylene-terephhtalamide) single fibres and their adhesion to epoxy, *J. Colloid. Interf. Sci.,* 144(1), p127--144, 1991.

[102]. Hsieh YL, Wetting contact angle derivations of cotton assemblies with varying perimeters, *T. R. J.*, 64, pp553--554, 1993.

[103]. Hsieh YL, Miller A. and Thompson J., Wetting pore structure, and liquid retention of hydrolyzed polyester fabrics, *T. R. J.*, 66(1), p1-10, 1996

[104]. Darcy H., *Les fontaines publiques de la ville de Dijon*, Dalmont, Paris, 1856.

[105] . Kozeny J., *Royal Academy of Science*, Vienna, Proc. Class 1, 136, p271, 1927.

[106] . Carman PC, *Flow of Gases through Porous Media*, Academic Press, New York, 1956.

[107] Emersleben VO, Das darcysche filtergesetz, *Phsikalische Zeitschrift*, 26, p601, 1925.

[108] . Brinkman HC, On the permeability of media consisting of closely packed porous particles, *Applied Scientific Research*, A1, p81, 1948.

[109] . Kuwabara SJ, 1959. The forces experienced by randomly distributed parallel circular cylinder or spheres in a viscous flow at small Reynolds numbers, *J. Phys. Soc. Japan*, 14, p527.

[110] Iberall AS, 1950. Permeability of glass wool and other highly porous media, *J. Res. Nat. Bur Stand.*, 45, p398.

111. Happel J., 1959. Viscous flow relative to arrays of cylinders, *J. Amer. Inst. Chem. Eng.,* 5, p173.

[112] . Davies CN, 1952, "The separation of airborne dust and particles", *Proc. Inst. Mech. Eng.*, London, B1, p185-213.

[113]. Subramaniam V., Madhnsoothanan M. and Debnath LR, 1988, Air permeability of blended nonwoven fabrics, 58, *T. R. J.*, p677.

[114]. Lamb H., 1932. *Hydrodynamics. (*6th ed.), Cambridge University Press, London.

[115]. Nguyen HV and Durso DF, Absorption of water by fibre webs: An illustration of the diffusion-type transport, *TAPPI, Proceedings of the International Dissolving and Speciality Pulps Conference*, Boston, pp137--141, 1983

[116]. Gillespie T., The capillary rise of a liquid in a vertical strip of filter paper, *J. Colloid. Sci.*, 14, p123--130, 1959.

[117]. Ghali K., et al, Experimental techniques for measuring parameters describing wetting and wicking in fabrics, *T.R.J.*, 64, p106--111, 1993.

[118]. Shen X., An application of needle punched nonwovens in the wet press casting of concrete, *Ph.D. Thesis*, University of Leeds, Leeds, UK, 1996

[119]. Ito H. and Yoichiro M., Water transport along textile fibres as measured by an electrical capacitance technique, T.R.J., July, pp414--420, 1993.

[120]. Stay A., Die platte-kondensator methode zur measung der enlanfgeshwindigbeit, *Melliand Textilber*, 46, p1427--1431, 1968.

[121]. Tagaya H., et al, Measurement of capillary rise in fabrics by electric capacitance method, *Sen-i. Gakkaishhi*, 47, p422--430, 1987

[122]. Zantam RV, *Geotextile and geomembrance in civil engineering*, John Wiley, New York, p181--192, 1986.

[123]. Adams KL, et al, Radial penetration of a viscous liquid into a planar anisotropic porous medium, *Int. J. of Multiphase Flow*, 14(2), p203--215, 1988

[124]. Adams KL, et al, In plane flow of fluids in fabrics structure, Flow Characterization, *T. R. J.*, 57, p647--654, 1987

[125]. Montagomery SM., Directional in-plane permeabilities of geotextile, *Geotextile and Geomembrance*, 7, p275--292, 1988.

[126]. L.Van der Sluys and Diericky W., The applicability of Darcy's Law in determining the water permeability of geotextiles, *Geotextiles and Geomembranes*, 5, p283--299, 1987.

[127]. Ogink HJM, Investigations on the hydraulic characteristics of synthetic fabrics, *Publications No.146, Delfts Hydraulic Laboratory*, 1975

[128]. Harnett PR. and Mehta PN, A survey and comparison of laboratory test methods for measuring wicking, *T. R. J.*, 54, p471--478, 1984.

[129]. Kissa E., Wetting and Wicking, *T.R.J.* 66, p660, 1996.

[130]. Chatterjee, PK, *Absorbency,* Elsevier, NY, 1985.

[131]. Johnson RE and Dettre RH, in Contact Angle, Wettability and Adhesion, *Advances in Chemistry Series*, Gould RF (*Eds.*), 43, American Chemistry Society, Washington, DC, 1964, p112.

[132]. Miller B. and Tymokin I., Spontaneous Transplanar uptake of liquids by fabrics, *T.R.J*, 54, p706-p712,1983.

[133]. Miller B., Surface Characterization of Fibres and Textiles, Part II, *Eds. by Schick*, MJ, Marcel Dekker, NY, 1977, p47.

[134]. Tagawa M., Gotoh K., Yasukawa A. and Ikuta M., Estimation of surface free from energies & Hawaker constants for fibrous solids by wetting force measurements, *Colloid Polymer Science*, 268, p689, 1990.

[135]. Bateup BO, Cook JR, Feldman HD and Fleischfresser BE, Wettability of wool fibres, *T. R. J.*, 46, 720, 1976.

[136]. Dyba RV and Miller B., Dynamic measurements of the wetting of single filaments, *T.R.J.*, 40, p884, 1970.

[137]. Dyba RV and Miller B., Dynamic wetting of filaments in solutions, *T.R.J.*, 41, p978, 1971

[138]. Kamath YK, Dansizer CJ., Hornby S. and Weigmann HD, Surface wettability scanning of long filaments by a liquid emmbrane method, *T.R.J.*, 57, p205, 1987.

[139]. Kissa E., Detergency, Theory and Technology, *Surfactant Science Ser.*, 20, Cutler and Kissa E, (*Eds.*), Marcel Dekker, NY, 1987, p193.

[140]. Newman AW and Good RJ, Techniques of measuring contact angles, *Surface and Colloid Science*, 11, Good RJ and Stromberg PR (Eds.) Plenum Press, New York, pp31, 1977

[141]. Bruil HG and Van Aartsen JJ, The determination of contact angles of aqueous surfacant solutions on powders, *J. Colloid and Polymer Sci.*, p32, 252, 1979.

[142]. Washburn EW, *Phys. Rev.*, 17, p273, 1921.

[143]. Sarraf AH, The wetttability and wetting of textile fibres, *M.Sc. Dissertation*, University of Leeds, Leeds, UK., 1985.

[144]. Hollies NRS, Kaessinger MM, Watson S. and Bogaty H., Water transport mechanisms in textile materials, Part 1: the role of yarn roughness in capillary-type penetration, *T. R. J.*, 26, p829, 1956

[145]. McLaughlin JR, Trounson ME, Stewart RG and Mckinnon AJ, Surfactant solution transport in wool yarn. III. Immersion absorption, *T. R. J.*, 58, p501, 1988.

[146]. Poiseuille JL, *C.R. Acad. Sci.*, Paris, 11, p961, p1041, 1840; 12, p112, 1841.

[147]. Lucas R., *Kolloid Z.*, 23, p15, 1918.

[148]. Hollies NRS, Kaessinger MM, Watson S. and Bogaty H., Water transport mechanisms in textile materials, Part 2: capillary type penetration in yarns and fabrics. *T. R. J.*, 27, pp8--13, 1957.

[149]. Minor FW, Schwartz AM, Buckles LC and Wulkow EA, The migration of liquids in textile assemblies, *T. R. J.*, 29, p931, 1959.

[150]. Minor FW, Schwartz AM, Buckles LC and Wulkow EA, *Amer. Dyestuff. Rep.*, 49, p419, 1960

[151]. Peek RL and McLean DA, *Ind. Eng. Chem. Anal., Ed. 6*, p85,1934

[152]. Bayer LD, *Soil Physics*, Wiley and Sons, New York, p222, 1948.

[153]. Robinson C., Topp NE and Breakbane ME, *Discussions Faraday Soc.*, P273, 1948.

[154]. Lord PR, A comparison of the performance of open-end and ring spun yarns in Terry towelling, *T. R. J.*, 44, pp516, 1973.

[155]. Fisher LR and Lark PD, An experimental study of the Washburn equation for liquid flow in a very fine capillary, *J. Colloid Interface Sci.*, 69, p486, 1979.

[156]. Joos P., Van Remoortere P. and Bracke M, *J. Colloid Interface Sci.*, 136, p189, 1990.

[157]. Jeje AA, Rates of spontaneous movement of water in capillary tubes, *J. Colloid Interface Sci.*, 69, p420,1979.

[158]. Hodgson KT and Berg JC, The effect of surfactants on wicking flow in fibre networks, *J. Colloid Interface Sci.*, 121, p22, 1988.

[159]. De Boer JJ, The wettability of scoured and dried cotton fabrics, *T.R.J.*, 50, p624, 1980.

[160]. Rowland SP, Stanonis DJ and King WD, Penetration-sorption of cotton fibres measured by immersed weight, *J. Appl. Polym Sci*, 25, p2229, 1980.

[161]. Rowland SP and Bertoniere NR, Some interactions of water-soluble solutes with cellulose and Sephadex, *T. R. J.*, 46, p770, 1976.

[162]. Stanonis DJ and Rowland SP, Interactions of Carbamates and their N-Methylol derivatives with cotton and Sephadex, measured by gel filtration, *T. R. J.*, 49, p72, 1979.

[163]. Yatagai M. and Komaki M., Changes of water absorbency of fabrics due to soiling with oil, *Japan Research Association of Textile End-uses*, 33, pp684--688, 1992.

[164]. Yatagai M., The influence of soiling on the water transfer characteristics of clothing materials, *Descente Sports Science*, 14, pp209--216, 1993

[165]. Yatagai M., Correlation between wettability and water absorbency of soiled fabric, *T. R. J.*, 64, pp461--465, 1993.

[166]. Choi H., et al, Cotton nonwovens as oil spill clean-up sorbets, *T. R. J.*, 63, pp211-218, 1993

[167]. Choksi PV, Spaeth EE and Shiff JA, *INDA Technical Symposium*, p29, 1977.

[168]. Rudd DF, *J. Phys. Chem.*, 64, p1254, 1960

[169]. Bird RB, Stewart WE, and Lightfoot EN, *Transport Phenomena*, J. Wiley, NY, 1960

[170]. Scheidegger AE, *The Physics of Flow Through Porous Media*, University of Toronto Press, Toronto, 1972,

[171]. Carslaw HS and Jaeger JC, *Conduction of Heat in Solids*, 2nd Edition, Clarendo Press, Oxford, 1959.

[172]. Crank J., *Mathematics of Diffusion*, Clarendon Press, London, 1956, p148.

[173]. http://www.stml.co.uk

[174]. Law WM, Water transport in Fabric, *PhD Thesis*, Department of Textiles, University of Leeds, 1988

[175]. EDANA, Liquid wicking time, *EDANA method 10.2-96 part C,* EDANA Recommended Test Methods,1996.

[176]. Methods for determination of resistance to wicking and lateral leakage, BS3424-18 method 21, 1988.

[177]. TAPPI Routine Control Method, RC-8, TAPPI Testing method, 1950.

[178]. Cary RT, and Sproles GB, Absorbency of Terry towels: A comparative evaluation of test methods, *Text. Res. J.*, 1979, 49, p691-698.

[179]. Lichstein BM, Demand wettability, a new method for measuring absorbency characteristics of fabrics, *Proceedings of 2nd Technical Symposium, Nonwoven Product Technology,* March, 1974, INDA, p129

[180]. Laughlin RD and Davies JE, Some aspects of capillary absorption in fibrous textile wicking, *T. R. J.*, 31, p904, 1961.

[181]. Bahder TB, *Mathematica for scientists and engineers*, Reading, Addison-Wesley Pub. Co., 1995.

[182]. Aberson GM, *TAPPI*, 32, 1970.

[183]. Napier JD, *Paper Technology*, 5, p275, 1963.

[184]. Wink WA and Van den Akker J. A., *TAPPI*, 40, p528, 1957.

[185]. Arfledter AF, *TAPPI*, 1957, 40, p513.

[186]. Robinson GD, A study of the voids within the interlock structure and their influence on thermal properties of fabric, *PhD Thesis*, Department of Textile Industries, University of Leeds, 1982.

[187]. Garner W., The capillary phenomena exhibited by dye solutions and sols, *J. Soc. Dyers and Col.*, 49, p346, 1933.

[188]. Russell SJ and Mao N., Anisotropic fluid transmission in nonwoven wound dressing structures, *Proceedings of 2nd Medical Textiles Int. Confer. Bolton*, UK, *Anand, S.* (Eds.), Bolton, 1999

[189]. IST120.2 (ASTM D5736-95), Standard Test Method for thickness of Highloft Nonwoven Fabrics, *INDA Standard Test Methods*, INDA, Association of the Nonwoven Fabrics Industry, North Carolina 27513, USA, 1998.

[190]. IST10.1 (95), Standard Test Method for Absorbency Time, Absorbency Capacity, and Wicking Rate, *INDA Standard Test Methods*, INDA, Association of the Nonwoven Fabrics Industry, North Carolina 27513, USA, 1998

[191]. Standard Test Method for Absorbency Time, Absorbency Capacity, and Wicking Rate, *ASTM* , North Carolina 27513, USA, 1998.

[192]. Cobb RM and Lowe DV, *Tech. Assoc. Pap.*, 17, p213, 1933.

[193]. Swedish Textile Research Institute, *Svensk Standard, SZS 251228,* 1971.

[194]. McConnell WJ, *U.S. Pat. #4,357,827* (Nov. 9, 1982)

[195]. Miller B., Experimental Aspects of Fibre Wetting and Liquid Movement Between Fibres, *Absorbency*, (Eds.), Chatterjee, PK, Elsevier, NY, 1985.

[196]. Buras EM, et al, Measurement and theory of absorbency of cotton fabrics, *T. R. J.*, 20, p239--248, 1950.

[197]. Korner W., New Results on the Water comfort of the Absorbent Synthetic Fibre Dunoua, *Chemiefasern/Textilind*, 31, p112-116, 1981.

[198]. DeBoer JJ, The wettability of scoured and dried cotton fabrics, *T. R. J.*, 50, p624--631, 1980.

[199]. Lennox-Kerr PL, Super-absorbent Acrylic from Italy, *Textile Inst. Ind.*, 19, p83-84, 1981

[200]. Tanner D., Development of textile yarns based on customer performance, *Symposium on Yarns and Yarn Manufacturing, University of Manchester*, 1979.

[201]. Gillespie T. and Johnson T., The penetration of aqueous surfactant solutions and non-Newtonian polymer solutions into paper by capillary action, *J. Colloid. Interf. Sci.*, 36, p282—255,1971.

[202]. Montgomery SM, Miller B. and Rebenfeld L., Spatial distribution of local permeability in fibrous networks, *T. R. J.*, 62, p151-161, 1992.

[203]. Howaldt M. and Yoganathan AP, Laser-Doppler anemometry to study fluid transport in fibrous assemblies, *T. R. J*, 53, p544-551, 1983.

[204]. Hsieh YL, Liquid transport in fabric structures, *T. R. J.*, 65(5), p299-307, 1995.

[205]. Kawase T., Sekoguchi S., Fuju T. and Minagawa M., Spreading of liquids in textile assemblies, Part 3: application of an image analyser system to capillary spreading of liquids, *T. R. J.*, 58, p306, 1988.

[206]. Harrison S., et al, An apparatus to measure the water absorption properties of fabrics and fibre assemblies, *Proceedings of Medical Textiles Int. Confer. Bolton*, UK, *Ed. Anand S.*, p134—140, 1996.

[207]. Oden JT and Tinsley J., *Mechanics of elastic structures*, McGraw-Hill, London, 1967.

[208]. Golding EW and Widdis FC, (5th ed.), *Electrical measurements and measuring instruments*, Sir Issac Pitman & Sons Ltd, London, 1963.

[209]. Clive NK and Slater K., Simulation of the electric field in evenness-testing capacitors, *J. T. I.*, 65(8), p397-401, 1974.

[210]. Pelton WR and Slater K., Fringe effects in capacitance-type evenness testers, *J. T. I.*, 63(5), p295-298, 1972.

[211]. Heerens WC, Appication of capacitance techniques in sensor design, in *Current Advances in Sensors*, Jones BE. (Eds.), IOP Publishing Ltd, Bristol, 1987.

[212]. Morris AS, *The essence of measurement*, Prentice Hall, London, 1996.

[213]. Morris AS, *Principles of measurement and instrumentation,* Prentice Hall, London, 1993.

[214]. PC30F/G handbook, (see *http://www.eagle.co.za/pc30fg.html*)

[215]. EDR Software Development Kit (see *http://www.eagle.co.za/edr.html*)

[216]. Russell SJ and Mao N., Apparatus and method for the assessment of in-plane anisotropic liquid absorption in nonwoven fabrics, will be published in *AUTEX Journal*, (2), 2000 (http://www.autex.org)

[217]. General Properties of Whatman Filter Paper (see http://www.whatman.com/support/arch 4_2.html)

[218]. Moorhouse HD, Factors affecting the electrical determination of moisture content, *MSc thesis*, Department of Textile Industries, University of Leeds, 1953.

[219]. Collins RE, *Flow of Fluids through Porous Materials*, Reinhold Publishing Corporation, New York, 1961.

[220]. Muskat M., *The flow of homogenous fluids through porous media*, McGraw-Hill, , London, 1937

[221]. Chan AW, Larive DE and Morgan RJ, Anisotropic permeability of fibre preforms: Constant Flow Rate Measurement, *J. Composite Materials,* 27(10), p996, 1993.

[222]. Cuthbert D., Wood FS and Gorman JW, *Fitting Equations to Data: Computer Analysis of Multifactor Data*, Wiley, New York, 1980

223. Textiles - Test Methods for Nonwovens - Part 2: Determination of Thickness" -- *ISO 9073-2:1989(E)*.

[224]. Miao L., The gas filtration properties of needlefelts, *PhD Thesis*, Department of Textile Industries, University of Leeds, 1989.

[225] SandoClean PC, (see *http://ppp.clariant.com/chem/pre-set.htm*)

[226]. Hearle JWS and Ozsanlav V., Nonwoven fabric studies, part 5: Studies of adhesive-bonded nonwoven fabrics part 3: The determination of fibre orientation and curl, *J. T. I.*, 70, p487--497, 1979.

[227]. Kallmes OJ, Techniques for determining the fibre orientation distribution throughout the thickness of a sheet, *TAPPI*, No. 52, p482--485, 1969.

[228]. Votava A., Practical method---measuring paper asymmetry regarding fibre orientation, *TAPPI*, 65, p67, 1982.

[229]. Cowan WF and Cowdrey EJK, Evaluation of paper strength components by short span tensile analysis, *TAPPI*, 57(2), p90, 1973.

[230]. Chuleigh PW, Image formation by fibres and fibre assemblies, *T.R.J.*, 54, pp813, 1983.

[231] . Stenemur B., Method and device for monitoring fibre orientation distributions based on light diffraction phenomenon, *INDA J. Nonw. Res.*, 4, p42--45, 1992

[232]. Lee S., Effect of fibre orientation on thermal radiation in fibrous media, *J. Heat Mass Transfer,* 32(2), p311, 1989.

[233] . McGee SH and McCullough RL, Characterization of fibre orientation in short-fibre composites, *J. Appl. Phys.,* 55(1), p1394, 1983.

[234]. Orchard GA, The measurement of fibre orientation in card webs, *J.T.I.*, 44, T380, 1953.

[235]. Tsai PP and Bresse RR, Fibre orientation distribution from electrical measurements. Part1, theory, INDA *J. Nonw. Res.,* 3(3), p36, 1991.

[236]. Tsai PP and Bresse RR, Fibre orientation distribution from electrical measurements. Part2, instrument and experimental measurements, INDA *J. Nonw. Res.,* 3(4), p32, 1991.

[237]. Chaudhray MM, MSc Dissertation, University of Manchester, 1972.

[238]. Judge SM, MSc Dissertation, University of Manchester, 1973.

[239]. Prud'homme B., et al, determination of fibre orientation of cellulosic samples by X-ray diffraction, *J. Polym. Sci.,* 19, p2609, 1975.

[240]. Comparative degree of preferred orientation in nineteen wood pulps as evaluated from X-ray diffraction patterns, *TAPPI*, 33, p384, 1950.

[241]. Huang XC and Bressee RR, Characteristizing nonwoven web structure using image analysing techniques, part 2: Fibre orientation analysis in thin webs, INDA *J. Nonw. Res.*, No.2, p14-21, 1993.

[242]. Pourdeyhimi B. and Nayernouri A., Assessing fibre orientation in nonwoven fabrics, INDA *J. Nonw. Res.*, 5, p29--36, 1993.

[243]. Pouredyhimi B. and Xu B., Charaterizing pore size in nonwoven fabrics: Shape considerations, *Int. Nonwoven J.*, 6(1), p26-30, 1993.

[244]. Gong RH and Newton A., Image analysis techniques Part II: The measurement of fibre orientation in nonwoven fabrics, *T. R. J.,* 87, p371, 1996.

[245]. Britton PN, Sampson AJ, Jr. Elliot CF, Grabben HW and Gettys WE, Computer simulation of the technical properties of nonwoven fabrics, part 1: The method, *T. R. J.,* 53, p363--368, 1983.

[246]. Grindstaff TH and Hansen SM, Computer model for predicting point-bonded nonwoven fabric strength, Part 1*: T. R. J.*, 56, p383--388,1986.

[247]. Jirsak O., Lukas D. and Charrat R., A two-dimensional model of mechanical properties of textiles, *J. T. I.,* 84, p1--14, 1993.

[248]. Xu B. and Ting Y., Measuring structural characteristics of fibre segments in nonwoven fabrics, *T. R. J.,* 65, p41-48, 1995.

[249]. Pourdeyhimi B., Dent R. and Davis H., Measuring fibre orientation in nonwovens. Part 3: Fourier transform, *T. R. J.,* 67, p143--151, 1997.

[250]. Pourdeyhimi B., Ramanathan R. and Dent R., Measuring fibre orientation in nonwovens. Part 2: Direct tracking, *T. R. J.,* 66, p747--753, 1996.

[251]. Pourdeyhimi B., Ramanathan R. and Dent R., Measuring fibre orientation in nonwovens. Part 1: Simulation, *T. R. J.,* 66, pp713--722, 1996.

[252]. Pourdeyhimi B., Dent R., Measuring fibre orientation in nonwovens. Part 4: Flow field analysis, *T. R. J.*, 67, p181--187, 1997.

[253]. Komori T, Makishima K., Number of fibre-to-fibre contacts in general fibre assemblies, *T. R. J.*, 47, p13--17, 1977.

[254]. Gilmore T., et al, Tomographic approaches to nonwovens structure definition, *National Textile Centre Annual Report* , USA, Sept., 1993.

[255]. Manual of Quantimet 570, Leica Microsystems Imaging Solutions, Cambridge, UK, 1993.

[256]. Russell SJ, The effect of rubbing on the properties of woollen slubbings, *PhD Thesis*, Department of Textile Industries, University of Leeds, 1993

[257]. Simpson J. and Fiori LA, Some relationships of cotton micronaire reading and carding parameters to card loading, sliver quality and processing performance, *T. R. J.*, p691, 1971.

[258]. Townend PP, *Nep formation in Carding*, Wira, 1982.

[259]. Simpson J., Relation between 'minority' hooks and neps in the card web, *T. R. J.*, 42, p590, 1972.

[260]. Simpson J., Sliver direction, hooked ends have significant effect on the parallelization of cotton fibre, *Textile Bulletin*, 87, p39, 1974.

[261]. Hearle JWS and Sultan MAJ, A study of needled fabrics. Part 1: Experimental methods and properties. *J. T. I.*, 58, pp251-265, 1967.

[262]. Hearle JWS and Sultan MAJ, A study of needled fabrics. Part 2: Effect of needling process. *J. T. I.*, 59, p103-116, 1968

[263]. Qiao Q., The structure and mechanical properties of hydroentangled nonwoven fabrics, *PhD Thesis*, Department of Textile Industries, University of Leeds, 1999.

[264]. Smolen A., *Polypropylene*, BSc Dissertation, Department of Textile Industries, University of Leeds, 1967.

[265]. Mao N. and Russell SJ, Anisotropic characteristics of liquid absorption in nonwoven structures, *Proceedings of 80_{th} World Conference of the Textile Institute: Manchester 2000*, April, 2000.

[266] Mao N. and Russell SJ, Directional permeability in homogeneous nonwoven structures, Part 1: relationship between directional permeability and fibre orientation, accepted for publication by *J.T.I* in 8th March, 2000 and will published in 91, *J. T. I.*, Part 1, 2000.

[267]. Mao N. and Russell SJ, Directional permeability in homogeneous nonwoven structures, Part 2: permeability in idealised structures, accepted for publication by *J.T.I* in 8th March, 2000 and will published in 91, *J.T.I*, Part 1, 2000.

[268] Sullivan RR and Hertel KL, Flow of air through porous media, *J. App. Phys.*, 11, p761, 1940.

[269] Piekaar HW and Clarenburg LA, Aerosol filters: Pore size distribution in fibrous filters, *Chem. Eng. Sci.*, 22, p1399, 1967.

[270]. Dent RW, The air permeability of nonwoven fabrics, *J. Text. Inst.*, 67, p220-223, 1976.

[271]. Cox RG, The motion of long slender bodies in a viscous fluid, Part 1, *J. Fluid Mechanics*, 44, p791-810, 1970.

[272]. Sangani AS and Acrivos A., Slow flow past periodic arrays of cylinders with applications to heat transfer, *Int. J. Multiphase Flow*, 8, p193-206, 1982.

[273]. Sparrow EM, and Loeffler AL Jr., Longitudinal laminar flow between cylinders arranged in regular array, *AIChEJ.* 5, p325-330, 1959.

[274]. Drummond JE and Tahir MI, Laminar viscous flow through regular arrays of parallel solid cylinders, *Int. J. Multiphase Flow*, 10, p515-540, 1983.

[275]. Sullivan RR, Specific surface measurements on compact bundles of parallel fibres, *J. App. Phys*, 13, p725-730, 1942.

[276]. Mandel J., *The Statistical Analysis of Experimental Data*, Interscience Publishers, New York, 1963.

[277]. Jackson GW and James DF, The Permeability of Fibrous Media, *Canadian Journal of Chemical Engineering*, 64, p363, 1986.

[278]. Happel J. and Brenner H., *Low Reynolds Number Hydrodynamics*, Noordhoft International Publishing, Leyden, The Netherlands, 1973.

[279]. Wu DH, Application of image analysis in textiles, *J. China Text. Inst.*, 3(6), p23, 1993

[280]. Wan TR, Image analysis techniques for the study of structural characteristics of fibre assemblies in top manufacture. *PhD Thesis*, Department of Textile Industries, University of Leeds, U.K, 1995.

[281]. Rushton A., The analysis of textile filter media, *Separation and Filtration*, Nov./Dec., p516, 1968.

[282]. Nogai T. and Ihara M., Study on air permeability of fibre assemblies oriented unidirectionary, *J. Text. Mach. Soc. Japan*, 26, p10, 1980.